

**Contract No:**

This document was prepared in conjunction with work accomplished under Contract No. DE-AC09-08SR22470 with the U.S. Department of Energy (DOE) Office of Environmental Management (EM).

**Disclaimer:**

This work was prepared under an agreement with and funded by the U.S. Government. Neither the U. S. Government or its employees, nor any of its contractors, subcontractors or their employees, makes any express or implied:

- 1 ) warranty or assumes any legal liability for the accuracy, completeness, or for the use or results of such use of any information, product, or process disclosed; or
- 2 ) representation that such use or results of such use would not infringe privately owned rights; or
- 3) endorsement or recommendation of any specifically identified commercial product, process, or service.

Any views and opinions of authors expressed in this work do not necessarily state or reflect those of the United States Government, or its contractors, or subcontractors.

We put science to work.™



**Savannah River  
National Laboratory®**

OPERATED BY SAVANNAH RIVER NUCLEAR SOLUTIONS

A U.S. DEPARTMENT OF ENERGY NATIONAL LABORATORY • SAVANNAH RIVER SITE • AIKEN, SC

# **Hydraulic Properties Data Package for the E-Area Soils, Cementitious Materials, and Waste Zones – Update**

**R. L. Nichols**

**B. T. Butcher**

May 2020

SRNL-STI-2019-00355, Revision 1

SRNL.DOE.GOV

**DISCLAIMER**

This work was prepared under an agreement with and funded by the U.S. Government. Neither the U.S. Government or its employees, nor any of its contractors, subcontractors or their employees, makes any express or implied:

1. warranty or assumes any legal liability for the accuracy, completeness, or for the use or results of such use of any information, product, or process disclosed; or
2. representation that such use or results of such use would not infringe privately owned rights; or
3. endorsement or recommendation of any specifically identified commercial product, process, or service.

Any views and opinions of authors expressed in this work do not necessarily state or reflect those of the United States Government, or its contractors, or subcontractors.

**Printed in the United States of America**

**Prepared for  
U.S. Department of Energy**

**Keywords:** *Performance Assessment,  
Material Properties, Barriers, Disposal  
System*

**Retention:** *Permanent*

## **Hydraulic Properties Data Package for the E-Area Soils, Cementitious Materials, and Waste Zones - Update**

R. L. Nichols  
B. T. Butcher

May 2020

---

Prepared for the U.S. Department of Energy under  
contract number DE-AC09-08SR22470.



OPERATED BY SAVANNAH RIVER NUCLEAR SOLUTIONS

**REVIEWS AND APPROVALS**

**AUTHOR:**

---

R. L. Nichols, Geosciences, SRNL Date

---

B. T. Butcher, Environmental Modeling, SRNL Date

**TECHNICAL REVIEWS:**

---

L. L. Hamm, Threat Assessments, SRNL Date

**APPROVALS:**

---

D. G. Jackson, Acting Manager Date  
Environmental Sciences & Dosimetry, SRNL

---

D. A. Crowley, Manager Date  
Environmental Modeling, SRNL

---

B. D. Lee, Director Date  
Environmental Sciences, SRNL

## **ACKNOWLEDGEMENTS**

The authors gratefully acknowledge the assistance of Dr. Greg Flach in the development and review of conceptual models and data for this report. The authors would also like to recognize the contributions of Mark Phifer and Maggie Millings in the preparation of the 2006 hydraulic properties data package (Phifer et al. 2006) upon which much of the content of this report is based.

**TABLE OF CONTENTS**

**LIST OF FIGURES ..... ix**

**LIST OF TABLES ..... xii**

**LIST OF ACRONYMS AND ABBREVIATIONS ..... xv**

**1.0 EXECUTIVE SUMMARY ..... 1**

**2.0 OBJECTIVE AND SCOPE ..... 2**

**3.0 APPROACH TO DATA SELECTION ..... 3**

**4.0 BACKGROUND INFORMATION ..... 4**

**4.1 GENERAL SAVANNAH RIVER SITE DESCRIPTION ..... 4**

**4.2 E-AREA LOW-LEVEL WASTE FACILITY GENERAL DESCRIPTION..... 7**

**4.3 REGIONAL HYDROGEOLOGY ..... 11**

**4.4 E-AREA LLWF DISPOSAL UNIT TYPES ..... 15**

**4.4.1 Slit Trenches ..... 15**

**4.4.2 Engineered Trenches..... 19**

**4.4.3 Component-in-Grout (CIG) Trenches ..... 23**

**4.4.4 Low-Activity Waste Vault ..... 29**

**4.4.5 Intermediate Level (IL) Vault..... 34**

**4.4.6 Naval Reactor Component Disposal Areas ..... 40**

**5.0 SOILS DATA ..... 42**

**5.1 BACKGROUND..... 42**

**5.1.1 Goal..... 42**

**5.1.2 Data Used in Evaluation ..... 42**

**5.2 UNDISTURBED VADOSE ZONE SOIL..... 47**

**5.2.1 Grain Size..... 47**

**5.2.2 Saturated Hydraulic Conductivity ..... 49**

**5.2.3 Water Retention ..... 66**

**5.2.4 Porosity, Bulk Density, Particle Density ..... 74**

**5.2.5 Saturated Effective Diffusion Coefficient (De) ..... 74**

**5.3 CONTROLLED COMPACTED BACKFILL..... 79**

**5.3.1 Grain Size..... 79**

**5.3.2 Saturated Hydraulic Conductivity ..... 79**

**5.3.3 Water Retention ..... 80**

**5.3.4 Porosity, Bulk Density, Particle Density ..... 81**

**5.3.5 Saturated Effective Diffusion Coefficient (De)..... 81**

**5.4 OPERATIONAL SOIL COVER ..... 81**

**5.4.1 Saturated Hydraulic Conductivity ..... 81**

**5.4.2 Water Retention ..... 84**

**5.4.3 Porosity, Bulk Density, Particle Density ..... 87**

**5.4.4 Saturated Effective Diffusion Coefficient (De)..... 87**

<b>5.5 IL VAULT PERMEABLE BACKFILL &amp; GRAVEL .....</b>	<b>87</b>
<b>5.5.1 Saturated Hydraulic Conductivity .....</b>	<b>88</b>
<b>5.5.2 Water Retention .....</b>	<b>88</b>
<b>5.5.3 Porosity, Bulk Density, Particle Density .....</b>	<b>88</b>
<b>5.5.4 Saturated Effective Diffusion Coefficient (<math>D_e</math>).....</b>	<b>91</b>
<b>5.6 SATURATED ZONE .....</b>	<b>91</b>
<b>5.6.1 Saturated Zone Hydraulic Properties .....</b>	<b>91</b>
<b>5.6.2 Lower Vadose Zone Versus Saturated Zone Porosity .....</b>	<b>94</b>
<b>5.7 UNCERTAINTY ANALYSIS .....</b>	<b>98</b>
<b>5.8 COMPARISON TO OBSERVED SUCTION LEVELS IN THE FIELD .....</b>	<b>107</b>
<b>5.9 SUMMARY .....</b>	<b>107</b>
<b>6.0 CEMENTITIOUS MATERIAL DATA.....</b>	<b>111</b>
<b>6.1 EXTERNAL LITERATURE REVIEW .....</b>	<b>111</b>
<b>6.1.1 Porosity, Bulk Density, and Particle Density .....</b>	<b>111</b>
<b>6.1.2 Saturated Hydraulic Conductivity and Saturated Intrinsic Permeability .....</b>	<b>117</b>
<b>6.1.3 Characteristic Curves (Suction Head, Saturation, and Relative Permeability) .....</b>	<b>122</b>
<b>6.1.4 Saturated Effective Diffusivity .....</b>	<b>129</b>
<b>6.2 INTERNAL LITERATURE REVIEW .....</b>	<b>141</b>
<b>6.2.1 1993 Physical Properties Measurement Program (Yu et al., 1993).....</b>	<b>141</b>
<b>6.2.2 2005 Concrete Porosity, Bulk Density, and Particle Density (Sappington and Phifer, 2005) .....</b>	<b>143</b>
<b>6.2.3 2006 Component-in-Grout (CIG) Grout and Intermediate Level (IL) Vault Controlled Low Strength Material (CLSM) Testing (Dixon and Phifer, 2006) .....</b>	<b>145</b>
<b>6.2.4 2007 Cementitious Material Selection for Future Component-in-Grout Waste Disposals (Dixon and Phifer, 2007).....</b>	<b>150</b>
<b>6.2.5 2013 E-Area Vault Concrete Material Property and Vault Durability/Degradation Projection Recommendations (Phifer, 2014)...</b>	<b>151</b>
<b>6.3 E-AREA CEMENTITIOUS MATERIAL PROPERTY REPRESENTATIONS .....</b>	<b>156</b>
<b>6.3.1 Porosity, Bulk Density, and Particle Density .....</b>	<b>157</b>
<b>6.3.2 Saturated Hydraulic Conductivity .....</b>	<b>159</b>
<b>6.3.3 Water Retention Curves (Suction Head, Saturation, and Relative Permeability) .....</b>	<b>159</b>
<b>6.3.4 Saturated Effective Diffusivity .....</b>	<b>164</b>
<b>6.3.5 E-Area Cementitious Material Nominal Property Summary .....</b>	<b>167</b>
<b>6.4 E-AREA CEMENTITIOUS MATERIAL UNCERTAINTY REPRESENTATION .....</b>	<b>167</b>
<b>6.4.1 Porosity, Bulk Density, and Particle Density Uncertainty .....</b>	<b>168</b>
<b>6.4.2 Saturated Hydraulic Conductivity Uncertainty .....</b>	<b>172</b>
<b>6.4.3 Saturated Effective Diffusion Coefficient Uncertainty .....</b>	<b>175</b>
<b>6.5 E-AREA CRACKED CONCRETE REPRESENTATION.....</b>	<b>177</b>
<b>7.0 WASTE ZONE REPRESENTATION.....</b>	<b>187</b>

**7.1 SLIT TRENCH WASTE ZONE REPRESENTATION ..... 187**  
    **7.1.1 Bulk Waste Disposal Slit Trench ..... 187**  
    **7.1.2 Containerized Waste Disposal Slit Trench ..... 188**  
    **7.1.3 Hybrid Slit Trench ..... 190**  
**7.2 Engineered Trench Waste Zone Representation..... 193**  
**7.3 COMPONENT-IN-GROUT WASTE ZONE REPRESENTATION ..... 198**  
    **7.3.1 CIG Structurally and Hydraulically Intact Conditions..... 198**  
    **7.3.2 CIG Structurally Intact but Hydraulically Degraded Conditions ..... 199**  
    **7.3.3 CIG Structurally and Hydraulically Degraded Conditions ..... 199**  
**7.4 LAW VAULT WASTE ZONE REPRESENTATION..... 201**  
    **7.4.1 Prior to LAW Vault Collapse..... 201**  
    **7.4.2 After LAW Vault Collapse..... 201**  
**7.5 IL VAULT WASTE ZONE REPRESENTATION ..... 203**  
    **7.5.1 Prior to IL Vault Collapse ..... 203**  
    **7.5.2 After IL Vault Collapse ..... 203**  
**7.6 NRCDA WASTE ZONE REPRESENTATION ..... 205**  
    **7.6.1 Welded Cask ..... 205**  
    **7.6.2 Bolted Containers..... 206**  
  
**8.0 SUMMARY AND RECOMMENDATIONS..... 209**  
    **8.1 SUMMARY ..... 209**  
    **8.2 RECOMMENDATIONS ..... 210**  
  
**9.0 REFERENCES..... 211**

LIST OF FIGURES

Figure 4-1. Location of Savannah River Site and adjacent areas ..... 5

Figure 4-2. Physiographic location of Savannah River Site..... 6

Figure 4-3. Location of the General Separations Area..... 8

Figure 4-4. Location of disposal units within the E-Area LLWF, (Bagwell and Bennett, 2017) ..... 9

Figure 4-5. Inset maps showing individual LLW disposal units, (Bagwell and Bennett, 2017) ..... 10

Figure 4-6. Regional NW to SE cross section depicting generalized lithology and depositional environments for the SRS (figure from Wyatt and Harris, 2004) . 12

Figure 4-7. Comparison of lithostratigraphic and hydrostratigraphic units at SRS ..... 13

Figure 4-8. Subdivision of the UAZ by previous studies for the central SRS ..... 14

Figure 4-9. As-Built Drawing of Slit Trenches 1-4..... 17

Figure 4-10. Operational Slit Trench Photographs ..... 18

Figure 4-11. Slit and Engineered Trench closure cap configuration ..... 19

Figure 4-12. Operational Engineered Trench photographs..... 22

Figure 4-13. CIG-1 Segment 6 placement sequence ..... 28

Figure 4-14. LAWV photographs..... 30

Figure 4-15. LAWV cross-sectional view (A-A')..... 31

Figure 4-16. LAWV disposal unit closure cap configuration ..... 33

Figure 4-17. IL Vault aerial view..... 35

Figure 4-18. IL Vault interior views..... 36

Figure 4-19. E-Area ILV plan view ..... 37

Figure 4-20. E-Area ILV Section A-A..... 37

Figure 4-21. ILV disposal unit closure cap configuration..... 39

Figure 4-22. Operational NRCDA photograph..... 41

Figure 4-23. NRCDA disposal unit closure cap configuration ..... 41

Figure 5-1. Map of E-Area soils dataset locations ..... 44

Figure 5-2. Four characterization locations within the E-Area LLWF Expansion 46

Figure 5-3. Textural Triangle for E-Area and Z-Area vadose zone soils ..... 48

Figure 5-4. Original sample bulk density versus bulk density of hydraulic conductivity samples ..... 50

Figure 5-5. Percent mud vs vertical hydraulic conductivity ..... 51

Figure 5-6. Distribution of percent mud for all E-Area grain size analyses vs samples used in hydraulic conductivity evaluation..... 53

Figure 5-7. Upper and Lower Zones for EAVZCPT8..... 63

Figure 5-8. E-Area Map showing transect for cross-section, modified from Bagwell and Bennett (2017) ..... 64

Figure 5-9. Cross-section of Transect 1 in E-Area..... 65

Figure 5-10. Data and WRCs for sand samples ..... 67

Figure 5-11. WRCs for individual samples identified as sand and the resulting WRC for the representative soil type Sand ..... 68

Figure 5-12. Data and WRCs for representative soils types Clay, Clay-Sand, and Sand ..... 68

**Figure 5-13. Relative hydraulic conductivity curves for representative soil types  
 Clay, Clay-Sand, and Sand..... 69**

**Figure 5-14. Identification of representative soil types and layer thicknesses  
 comprising upper and lower vadose zone at AT-North/Megacptnorth ..... 70**

**Figure 5-15. WRCs for Upper Zone and Lower Zone..... 72**

**Figure 5-16. Relative hydraulic conductivity curve for Upper Zone and Lower  
 Zone ..... 72**

**Figure 5-17. Photomicrographs of vadose zone soils from A-Area ..... 78**

**Figure 5-18. Textural Triangle for Controlled Compacted Backfill..... 80**

**Figure 5-19. WRCs for individual samples from the Old Radioactive Waste Burial  
 Ground and the resulting data set for the Controlled Compacted Backfill ..... 81**

**Figure 5-20. Saturation vs Suction for Operational Soil Cover Before and After  
 Dynamic Compaction..... 86**

**Figure 5-21. Suction vs Relative Hydraulic Conductivity for Operational Soil  
 Cover Before and After Dynamic Compaction ..... 86**

**Figure 5-22. Saturation vs Suction for IL Vault Permeable Backfill..... 89**

**Figure 5-23. Suction vs Relative Hydraulic Conductivity for IL Vault Permeable  
 Backfill ..... 89**

**Figure 5-24. Saturation vs Suction for Gravel ..... 90**

**Figure 5-25. Suction vs Relative Hydraulic Conductivity for Gravel..... 90**

**Figure 5-26. Effective flow through a heterogeneous layered porous medium..... 96**

**Figure 5-27. Effective porosity assumptions for three combinations of layering and  
 permeability contrast ..... 96**

**Figure 5-28. Variation in Sand and Clay vertical hydraulic conductivity as a  
 function of suction head..... 97**

**Figure 5-29. Estimated effective porosity for vadose zone simulations ..... 97**

**Figure 6-1. Porosity of concrete, mortar, and cementitious paste with WCR ..... 117**

**Figure 6-2. Hanford Concrete and DSSF Grout characteristic curves (Rockhold et  
 al., 1993) ..... 123**

**Figure 6-3. Savage and Janssen (1997a) characteristic curves ..... 125**

**Figure 6-4. Baroghel-Bouny et al. (1999) characteristic curves..... 129**

**Figure 6-5. Saturated effective diffusion coefficient of concrete and mortar with  
 WCR..... 140**

**Figure 6-6. Water retention curve for Mix C-4000-8-S-2-AB based on SIMCO  
 data. .... 155**

**Figure 6-7. Old E-Area CIG Grout characteristic curves..... 161**

**Figure 6-8. Relative hydraulic conductivity curve for Old E-Area CIG grout..... 161**

**Figure 6-9. Water retention curve for new CIG grout ..... 162**

**Figure 6-10. Relative hydraulic conductivity curve for New CIG grout ..... 162**

**Figure 6-11. Water retention curve and data for E-Area CLSM..... 163**

**Figure 6-12. Relative hydraulic conductivity curve for E-Area CLSM..... 164**

**Figure 6-13. Example transitions of intact cementitious materials from intact to  
 fully-degraded conditions represented by soils: (a) concrete and (b) grout ..... 183**

**Figure 6-14. Alternative representations of a fractured medium; reproduced from  
 Altman et al. (1996), Figure 2-2 ..... 184**

<b>Figure 6-15. Alternative surrogate soils for blending to fully-degraded conditions</b>	<b>185</b>
<b>Figure 6-16. Partial blending (10.7%) to gravel representing degradation to 5 mil fractures spaced at 1 cm</b>	<b>185</b>
<b>Figure 6-17. Degradation to selected fractured conditions using fracture properties based on Or and Tuller (2000)</b>	<b>186</b>
<b>Figure 7-1. Water retention curves for Containerized Slit Trench and Hybrid Slit Trench waste zones before dynamic compaction</b>	<b>189</b>
<b>Figure 7-2. Conceptual model representing hydraulic properties of Silt Trenches and Engineered Trenches before dynamic compaction</b>	<b>194</b>
<b>Figure 7-3. Conceptual model representing hydraulic properties of Silt Trenches and Engineered Trenches after dynamic compaction</b>	<b>195</b>
<b>Figure 7-4. Conceptual model representing hydraulic properties of CIG Trench waste zone from fully intact to degraded condition for (a) Segments 1-8 and (b) Segment 9 and future</b>	<b>200</b>
<b>Figure 7-5. Conceptual model representing hydraulic properties of the Low Activity Waste Vault waste zone in (a) Intact, (b) Cracked, and (c) Collapsed states</b>	<b>202</b>
<b>Figure 7-6. Conceptual model representing hydraulic properties of the Intermediate Level Vault waste zone in (a) Intact, (b) Cracked, and (c) Collapsed states</b>	<b>204</b>
<b>Figure 7-7. Schematic of KAPL CB/TS welded cask</b>	<b>206</b>
<b>Figure 7-8. Schematic of a bolted container</b>	<b>207</b>
<b>Figure 7-9. Conceptual model representing hydraulic properties of the Naval Reactor Component Disposal Area waste zone for (a) Intact impermeable welded casks, (b) Hydraulically failed welded casks, and (c) Generic NR containerized waste</b>	<b>208</b>

LIST OF TABLES

Table 4-1. Material formulations for E-Area LLWF cementitious materials..... 26

Table 4-2. Notes on E-Area LLWF material formulations..... 27

Table 5-1. Test methods used in analyses ..... 43

Table 5-2. Datasets for E-Area and Z-Area undisturbed vadose zone soil ..... 44

Table 5-3. Datasets for E-Area and Z-Area controlled compacted soil..... 45

Table 5-4. E-Area vadose zone soils categorized by USCS ..... 49

Table 5-5. Distribution of mud fraction in E-Area vs the hydraulic conductivity dataset..... 52

Table 5-6. Upscaling parameters for hydraulic conductivity ..... 60

Table 5-7. Material properties for textural soil types in the E-Area LLWF..... 61

Table 5-8. Pump test results from the water table aquifer at TNX and D-Area .... 66

Table 5-9. Material properties for vadose zone soils in the E-Area LLWF ..... 73

Table 5-10. Summary bulk properties for vadose zone soils & Controlled Compacted Backfill..... 75

Table 5-11. Literature Values for molecular diffusion coefficient ( $D_m$ ) ..... 76

Table 5-12. Tortuosity values from literature ..... 77

Table 5-13. Calculated effective diffusion coefficients..... 79

Table 5-14. Ksat from Lambe and Whitman (1969) and calculated Ksat for the Operational Soil Cover Prior to DC ..... 82

Table 5-15. Saturated zone soils hydraulic properties ..... 94

Table 5-16. Descriptive statistics for triangular distributions describing  $p_v$  and  $p_h$  98

Table 5-17. Uncertainty Analysis summary statistics for total porosity, dry bulk density, and particle density..... 100

Table 5-18. Uncertainty analysis summary statistics for saturated hydraulic conductivity..... 103

Table 5-19. Uncertainty analysis summary statistics for saturated effective diffusion coefficient ..... 106

Table 5-20. Summary of recommended soil properties..... 108

Table 6-1. Porosity of concrete (i.e., contains cement, fine and coarse aggregate, and water) ..... 114

Table 6-2. Porosity of mortars (i.e., contains cementitious material, fine aggregate, and water) ..... 115

Table 6-3. Porosity of cementitious pastes (i.e., contains cementitious material and water)..... 116

Table 6-4. Cementitious material saturated hydraulic conductivity..... 121

Table 6-5. Hanford Concrete and DSSF Grout hydraulic properties..... 123

Table 6-6. Savage and Janssen (1997b) WCR, saturated hydraulic conductivity, and van Genuchten curve fitting parameters ..... 125

Table 6-7. Baroghel-Bouny et al. (1999) concrete mixes ..... 126

Table 6-8. Baroghel-Bouny et al. (1999) and corresponding RETC parameters and parameter values ..... 128

Table 6-9. Saturated effective diffusion coefficients of concretes (contains cement, fine and coarse aggregate, and water)..... 135

**Table 6-10. Saturated effective diffusion coefficients of mortars (contains cement, fine aggregate, and water) ..... 137**

**Table 6-11. Saturated effective diffusion coefficients of cementitious pastes (contains cementitious materials and water) ..... 138**

**Table 6-12. Summary E-Area Vault concrete properties from Core Laboratories testing (Yu et al., 1993) ..... 142**

**Table 6-13. Unsaturated intrinsic permeability from Core Laboratories testing (Yu et al., 1993) ..... 143**

**Table 6-14. Concrete porosity, bulk density, and particle density (Sappington and Phifer, 2005)..... 144**

**Table 6-15. Old CIG Grout and CLSM compressive strength..... 145**

**Table 6-16. Old CIG High-Flow Grout hydraulic and physical properties ..... 146**

**Table 6-17. Grout water retention properties as measured by GeoTesting Express, Inc. .... 148**

**Table 6-18. Grout water retention properties as measured by Idaho National Laboratory ..... 148**

**Table 6-19. CLSM hydraulic and physical properties ..... 149**

**Table 6-20. CLSM water retention properties as measured by GeoTesting Express, Inc. .... 150**

**Table 6-21. CLSM Water Retention Properties as Measured by Idaho National Laboratory ..... 150**

**Table 6-22. Hydraulic and physical properties of Mix 4000-SCC-FA-GROUT<sup>1</sup>.. 151**

**Table 6-23. van Genuchten parameters for Mix 4000-SCC-FA-GROUT ..... 151**

**Table 6-24. Hydraulic and physical properties of Mix C-4000-8-S-2-AB..... 152**

**Table 6-25. Recommended E-Area Vault Concrete uncertainty distributions..... 153**

**Table 6-26. Salts used in constant vapor pressure method for moisture retention characteristics and resulting saturation of vault concrete sample. (Phifer, 2014) ..... 155**

**Table 6-27. van Genuchten parameters for Mix C-4000-8-S-2-AB..... 155**

**Table 6-28. Recommended material properties for cementitious materials in the various E-Area LLWF Disposal Unit Types..... 158**

**Table 6-29. Cementitious material categories for assignment of representative saturated effective diffusion coefficient..... 166**

**Table 6-30. E-Area saturated effective diffusion coefficient representation summary..... 167**

**Table 6-31. Site-Specific porosity, bulk density, and particle density nominal value and standard deviation of mean..... 169**

**Table 6-32. Low, Ordinary, and High-Quality Concrete assigned standard deviation of mean for effective porosity, dry bulk density, and particle density ..... 169**

**Table 6-33. E-Area cementitious material uncertainty summary statistics for effective porosity (%)..... 170**

**Table 6-34. E-Area cementitious material uncertainty summary statistics for dry bulk density (g/cm<sup>3</sup>)..... 171**

**Table 6-35. E-Area cementitious material uncertainty summary statistics for particle density (g/cm<sup>3</sup>) ..... 171**

<b>Table 6-36. Site-Specific saturated hydraulic conductivity nominal value and standard deviation of mean .....</b>	<b>173</b>
<b>Table 6-37. Low, Ordinary, and High-Quality Concrete assigned standard deviation of mean to nominal saturated hydraulic conductivity value .....</b>	<b>173</b>
<b>Table 6-38. E-Area cementitious material uncertainty summary statistics for saturated hydraulic conductivity .....</b>	<b>174</b>
<b>Table 6-39. Log saturated effective diffusion coefficient standard deviation for concretes .....</b>	<b>176</b>
<b>Table 6-40. E-Area cementitious material uncertainty summary statistics for saturated effective diffusion coefficient.....</b>	<b>176</b>
<b>Table 7-1. Waste properties for Slit Trenches and Engineered Trenches before and after dynamic compaction .....</b>	<b>192</b>
<b>Table 7-2. Material properties for waste zones in the E-Area LLWF .....</b>	<b>196</b>

## LIST OF ACRONYMS AND ABBREVIATIONS

### ACRONYMS

ALARA	as low as reasonably achievable
bls	below land surface
CA	Composite Analysis
CIG	components-in-grout
CPT	cone penetration test
CSRA	Central Savannah River Area
DC	dynamic compaction
DWS	drinking water standard
EDE	effective dose equivalent
EMOP	E-Area Monitoring Program
ET	engineered trenches
FY	fiscal year
HLW	high-level waste
ILV	Intermediate Level Vault
ICRP	International Commission on Radiological Protection
ILNT	intermediate-level non-tritium
JCW	job control waste
LAWV	Low Activity Waste Vault
LLWF	Low-Level Waste Facility
MC	Monte Carlo
MCL	maximum contaminant level
MMI	Modified Mercalli Intensity
NCRP	National Council on Radiation Protection and Measurements
NQA	Nuclear Quality Assurance
OSR	operations/safety requirement
ORWBGCF	Old Radioactive Waste Burial Ground Common Fill Layer
ORWGLPL	Old Radioactive Waste Burial Ground Low Permeability Layer
PA	Performance Assessment
QA	quality assurance
SAR	Safety Analysis Report
SRS	Savannah River Site
ST	slit trenches
SWM	Solid Waste Management
TRU	transuranic
USCS	Unified Soil Classification System
USDA	United States Department of Agriculture
USEPA	United States Environmental Protection Agency
USGS	United States Geological Survey
VG	van Genuchten
WCR	Water-to-Cement Ratio

## ABBREVIATIONS

cm	centimeter
$\rho_b$	dry bulk density
$\rho_p$	particle density
$D_e$	saturated effective diffusion coefficient
$D_m$	molecular diffusion coefficient
ft	foot (or feet)
g	gram(s)
hr	hour
$K$	hydraulic conductivity
$K_{sat}$	saturated hydraulic conductivity
$K_h$	horizontal hydraulic conductivity
$K_r$	relative hydraulic conductivity
$K_v$	vertical hydraulic conductivity
kg	kilogram
km	kilometer
L	liter
m	meter
mL	milliliter
mrem	millirem
msl	mean sea level
$n$ or $\eta$	Porosity
pCi	picocurie
psi	pounds per square inch
s or sec	second
Sv	Sievert
yr	year

## 1.0 EXECUTIVE SUMMARY

Hydraulic property estimates for the soils, cementitious materials, and waste zones associated with the E-Area low-level radioactive waste disposal units have been provided to support the Performance Assessments (PA) for the E-Area Low-Level Waste Facility (LLWF). Nominal or “best estimate” hydraulic property values for use in the deterministic modeling are provided along with representations of the hydraulic property value uncertainty for use in sensitivity and uncertainty modeling. The hydraulic properties provided for each of the E-Area materials include: porosity ( $\eta$ ), dry bulk density ( $\rho_b$ ), particle density ( $\rho_p$ ), saturated hydraulic conductivity ( $K_{sat}$ ), characteristic curves (suction head, saturation, and relative permeability), and effective diffusion coefficient ( $D_e$ ).

A representation of the uncertainty associated with each property, except for the characteristic curves, is provided for each material, except for the E-Area waste zones. These nominal parameter values for each of the E-Area soils, cementitious materials, and waste zones, and, where indicated, parameter uncertainty representations, are based upon the following in order of priority:

- Site-specific field data,
- Site-specific laboratory data,
- Similarity to material with site-specific field or laboratory data, and
- Literature data.

Additionally, a methodology to represent long-term concrete degradation is provided. Finally, because much of the nominal hydraulic property values and uncertainty representations for the E-Area soils, cementitious materials, and waste zones are based on similarity to other materials or literature data, a methodology to prioritize additional work to better define these values and representations is outlined. Prioritization should be based on the importance of the material and/or property to the results of deterministic, sensitivity, and uncertainty modeling. This prioritization should be established through a process of sensitivity modeling. This report supersedes the previous hydraulic properties data package (Phifer et al., 2006).

Revision 1 contains clarifications, updates and corrections to text, figures and tables in a number of places in the report along with some minor editing.

## 2.0 OBJECTIVE AND SCOPE

The primary objective of this report is to provide an update to the report prepared by Phifer et al. (2006) on the hydraulic property estimates for the soils, cementitious materials, and waste zones associated with the E-Area Low-Level Waste Facility (LLWF). Phifer et al. (2006) also addressed properties for the Z-Area Saltstone Disposal Facility (SDF). Savannah River Remediation is responsible for updates to Z-Area disposal system material properties so references to Z-Area have been removed. Thus, the scope of this data package report applies only to the E-Area LLWF and this report supersedes (Phifer et al., 2006).

These hydraulic property estimates will be used as input to deterministic, sensitivity, and uncertainty modeling conducted to support the Performance Assessments (PA) for the E-Area LLWF. The hydraulic properties provided for each of the E-Area material zones include: porosity ( $\eta$ ), dry bulk density ( $\rho_b$ ), particle density ( $\rho_p$ ), saturated hydraulic conductivity ( $K_{sat}$ ), characteristic curves (suction head, saturation, and relative permeability), and effective diffusion coefficient ( $D_e$ ). Nominal or “best estimate” values are provided for use in the deterministic modeling, and representations of the value uncertainty are provided for use in sensitivity and uncertainty modeling efforts.

The updates in this report primarily pertain to replacing tables of water retention values for materials with the van Genuchten (VG) parameters describing water retention characteristics. The VG parameters mimic the values in the tables of characteristic curve values. Additionally, results from work on soils and cementitious materials related to E-Area are discussed.

This report does not provide hydraulic property estimates for the final closure cap to be installed over the disposal units but does provide minimal data for the aquifers (i.e., saturated zone). The final closure caps are described in detail and estimated material properties are provided, along with associated infiltration estimates, elsewhere (Dyer, 2019). Minimal aquifer (i.e., saturated zone) estimated material properties are provided herein, because the aquifers and their properties are described in detail elsewhere (Flach, 2018).

### 3.0 APPROACH TO DATA SELECTION

The property values assigned for the porosity ( $\eta$ ), dry bulk density ( $\rho_b$ ), particle density ( $\rho_p$ ), saturated hydraulic conductivity ( $K_{sat}$ ), characteristic curves (suction head, saturation, and relative permeability), and effective diffusion coefficient ( $D_e$ ) for each of the E-Area soils, cementitious materials, and waste zones are based upon the following in order of priority:

- Site-specific field data,
- Site-specific laboratory data,
- Similarity to material with site-specific field or laboratory data, and
- Literature data.

## 4.0 BACKGROUND INFORMATION

### 4.1 GENERAL SAVANNAH RIVER SITE DESCRIPTION

The Savannah River Site (SRS) occupies about 300 square miles (780 km<sup>2</sup>) in Aiken, Barnwell, and Allendale Counties on the Upper Atlantic Coastal Plain of southwestern South Carolina (Figure 4-1). The center of the SRS is approximately 22 miles (36 km) southeast of Augusta, GA; 20 miles (32 km) south of Aiken, SC; 100 miles (160 km) from the Atlantic Coast; and is bounded on the southwest by the Savannah River for about 17 miles (28 km). The Fall Line, which separates the Atlantic Coastal Plain physiographic province from the Piedmont physiographic province, is approximately (50 km) northwest of the central SRS (Figure 4-2).

The elevation of the SRS ranges from 80 ft above mean sea level (msl) (24 m msl) at the Savannah River to about 400 ft-msl (122 m msl) in the upper northwest portion of the site (USGS, 1987). The Pleistocene Coastal terraces and the Aiken Plateau form two distinct physiographic subregions at the SRS (McAllister et al., 1996). The Pleistocene Coastal terraces are below 270 ft-msl (82 m msl) in elevation, with the lowest terrace constituting the present flood plain along the Savannah River and the higher terraces characterized by gently rolling terrain. The relatively flat Aiken Plateau occurs above 270 ft-msl (82 m msl) and is dissected by local streams.

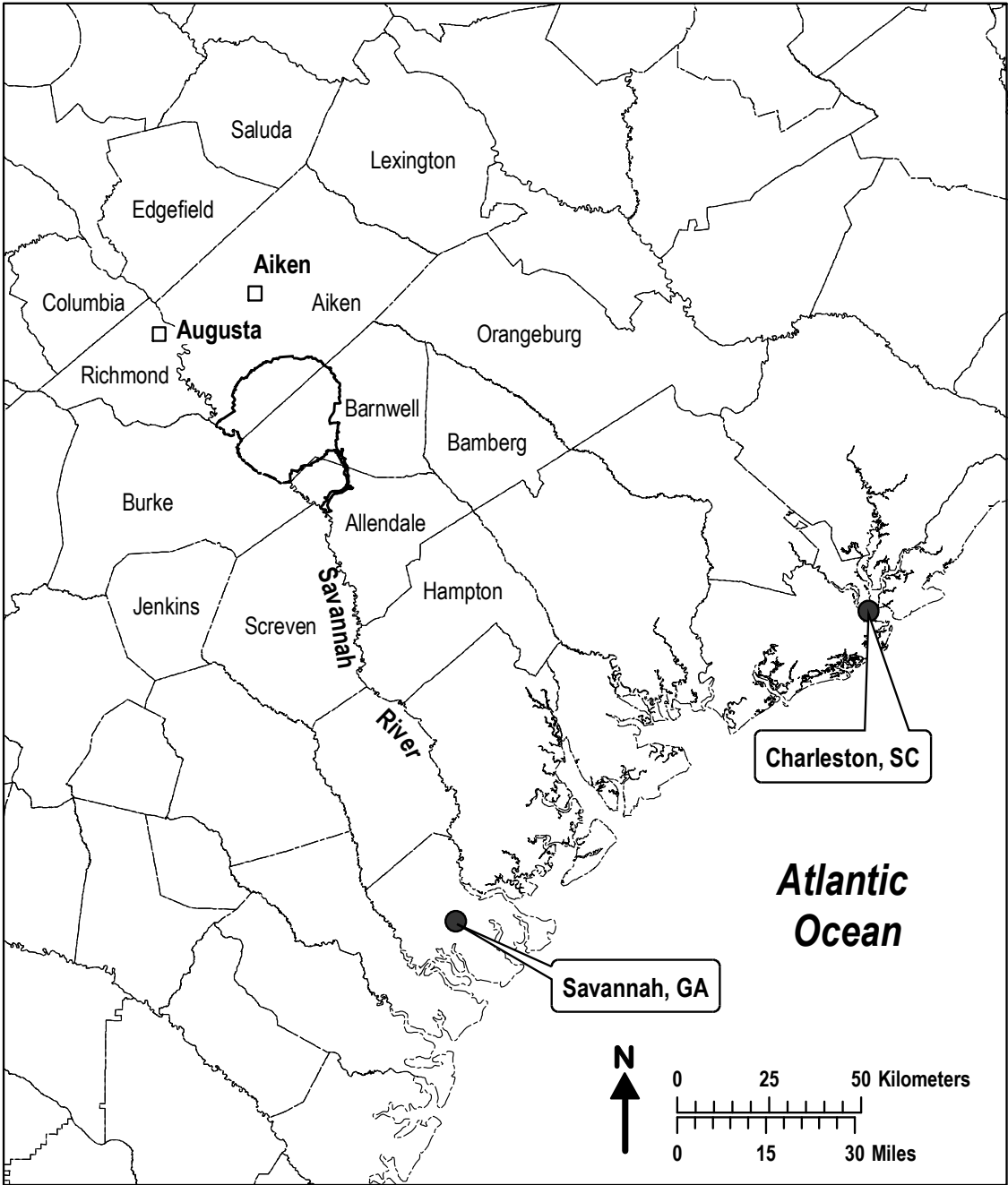


Figure 4-1. Location of Savannah River Site and adjacent areas

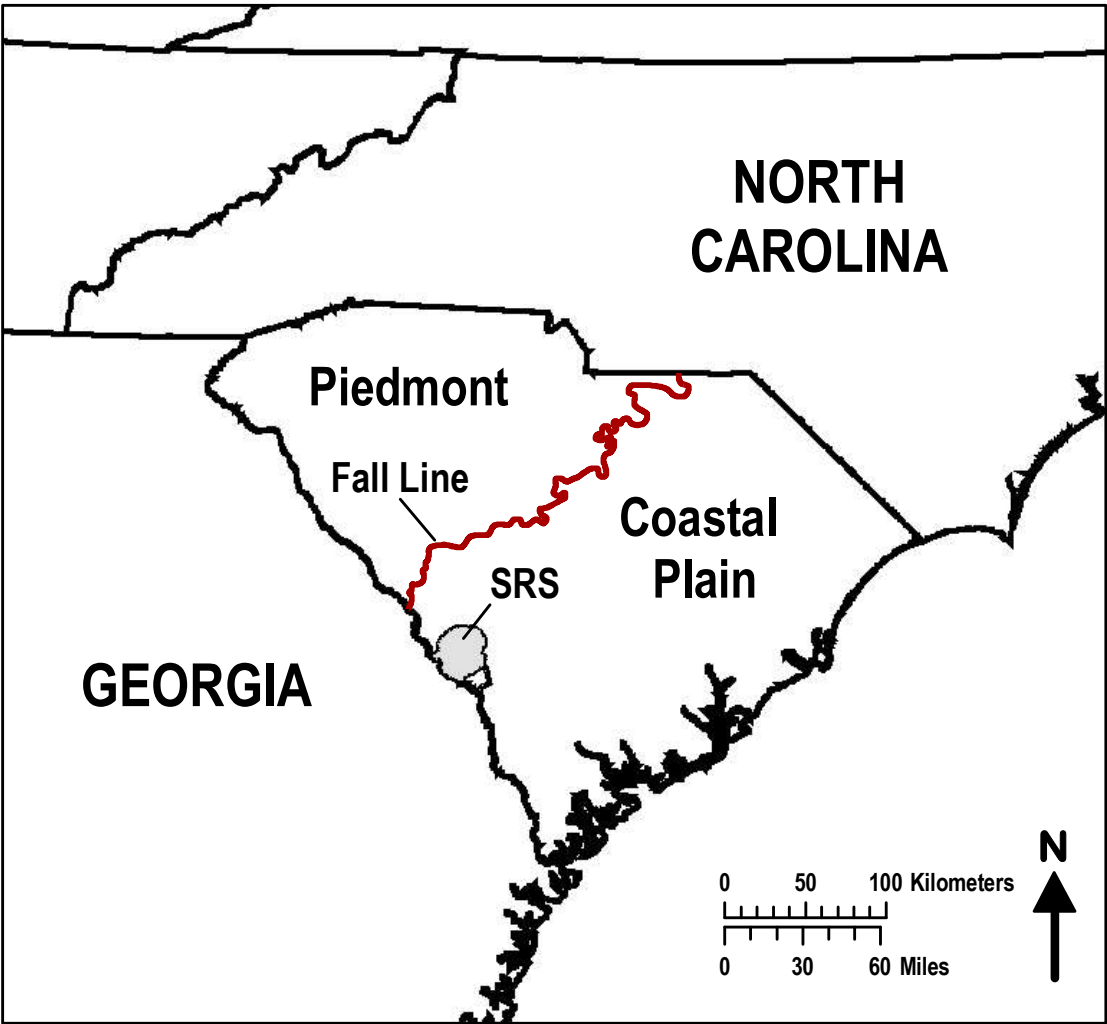


Figure 4-2. Physiographic location of Savannah River Site

## 4.2 E-AREA LOW-LEVEL WASTE FACILITY GENERAL DESCRIPTION

The E-Area Low Level Waste Facility is in the central region of the SRS known as the General Separations Area (GSA) (Figure 4-3). Radiological operations at the E-Area LLWF began in 1994. The current E-Area LLWF area developed for disposal consists of approximately 100 acres (0.4 km<sup>2</sup>). It is an elbow-shaped, cleared area, which curves to the northwest, situated immediately north of the Mixed Waste Management Facility (MWMF) (Figure 4-3).

The E-Area LLWF is located on an interfluvial plateau, which is drained by several perennial streams (Figure 4-3). The natural topography of the site slopes from an elevation of about 290 ft-msl (88 m-msl) in the southernmost corner to an elevation of 250 ft-msl (76 m-msl) in the northernmost corner. The site is bordered by three streams with several intermittent streams present within the area boundary. Runoff is to the north toward Upper Three Runs Creek, to the east toward Crouch Branch, and to the west toward an unnamed branch. Upper Three Runs is approximately 2,500 ft (760 m) north of the facility boundary. The nearest perennial stream is approximately 1,200 (370 m) northeast of the boundary.

Disposal units within the current footprint of the E-Area LLWF include the Slit Trenches (STs), Engineered Trenches (ETs), Component-In-Grout (CIG) Trenches, the Low Activity Waste Vault (LAWV), the Intermediate Level Vault (ILV), and the Naval Reactor Component Disposal Areas (NRCDAs) (Figure 4-4 and inset A and B Figure 4-5). Solid Waste Management (SWM) identified additional plots (6-9) for future development (Millings et al., 2011). Plots 6 and 8 proposed for future development are hereafter referred to as Expansion E-Area LLWF, see inset C Figure 4-5.

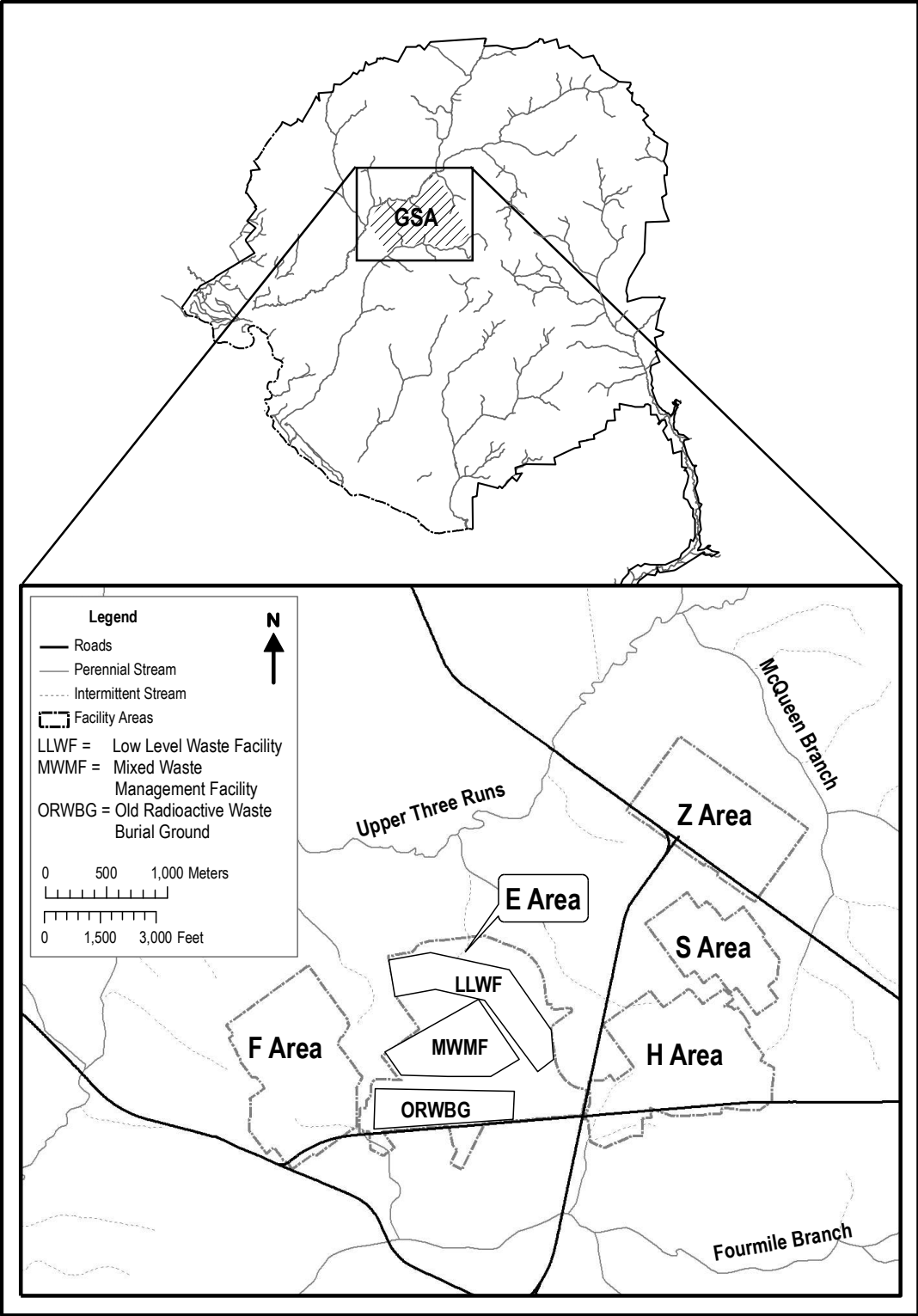
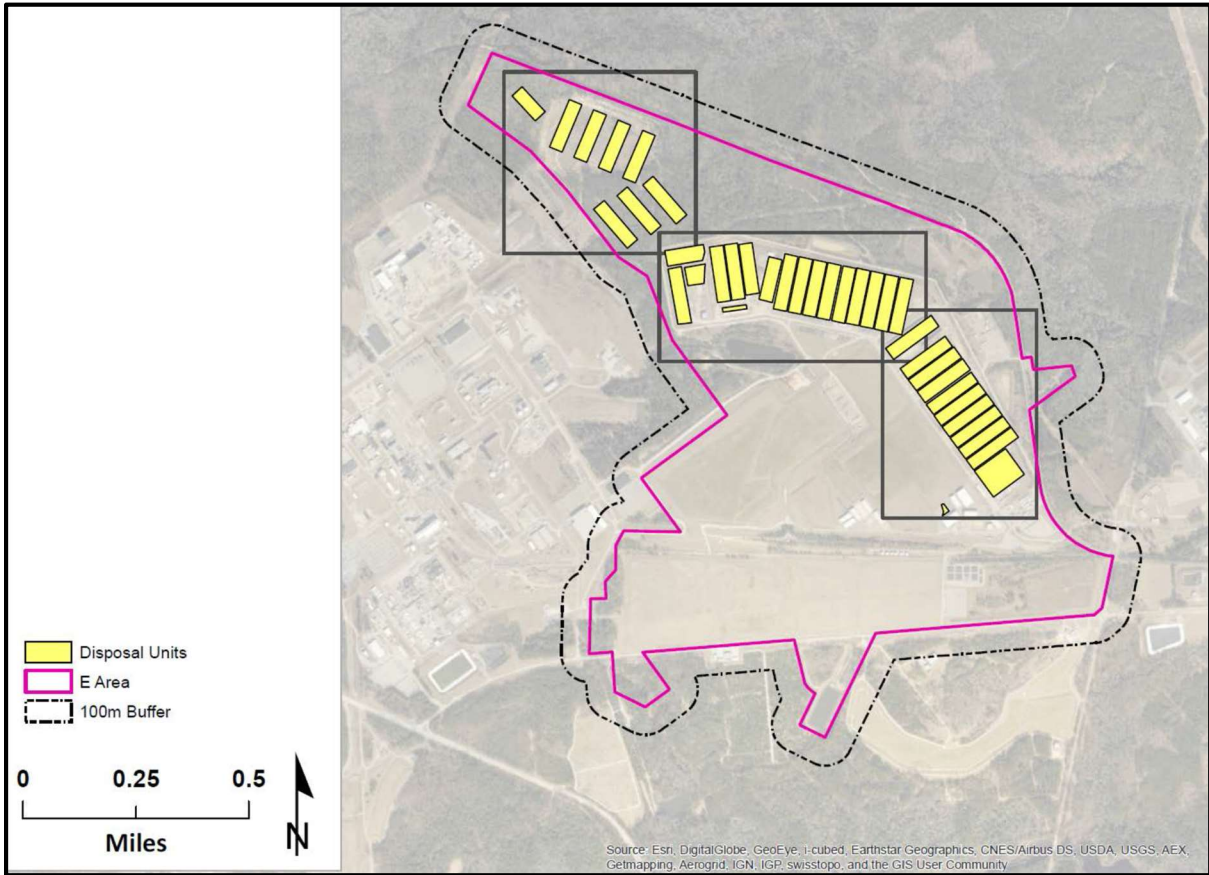


Figure 4-3. Location of the General Separations Area



**Figure 4-4. Location of disposal units within the E-Area LLWF, (Bagwell and Bennett, 2017)**

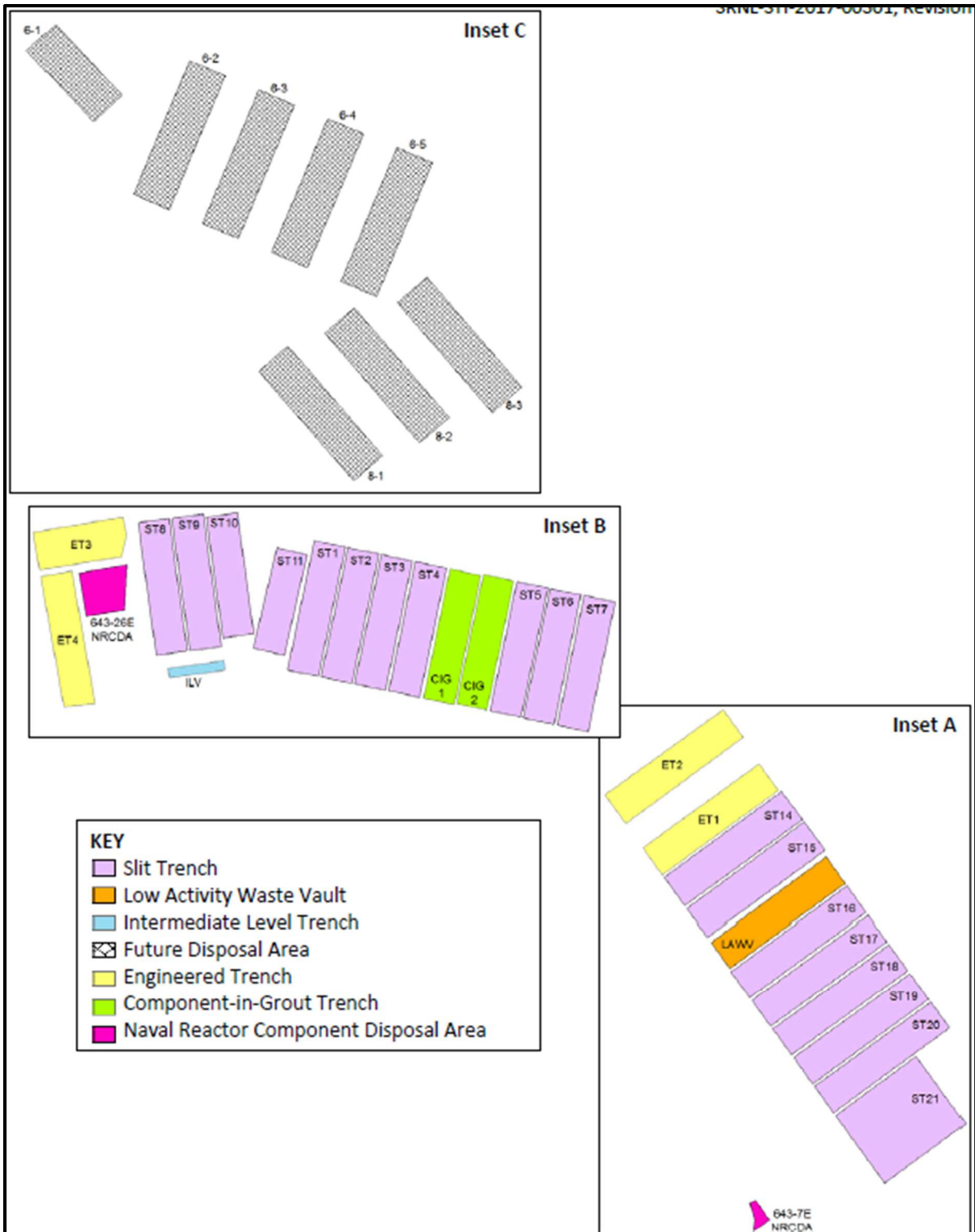


Figure 4-5. Inset maps showing individual LLW disposal units, (Bagwell and Bennett, 2017)

### 4.3 REGIONAL HYDROGEOLOGY

The Atlantic Coastal Plain consists of a southeast-dipping wedge of unconsolidated and semi-consolidated sediment, which extends from its contact with the Piedmont Province at the Fall Line to the continental shelf edge. Sediments range in geologic age from Late Cretaceous to Recent and include sands, clays, limestones and gravels. This sedimentary sequence ranges in thickness from essentially zero at the Fall Line to more than 4,000 feet (1,219 meters) at the Atlantic Coast (Siple, 1967). Figure 4-6 shows a generalized cross section of the sedimentary strata and their corresponding depositional environments for the Upper Coastal Plain down-dip through the SRS into the Lower Coastal Plain. At the SRS, coastal plain sediments thicken from about 690 ft (210 m) at the northwestern border of the site to about 1,400 ft (430 m) at the southeastern border of the site (Fallaw and Price, 1995). More detailed descriptions of the geology of the SRS and GSA can be found in several historical and recent reports (Aadland et al., 1995; Aadland et al., 1991; Colquhoun et al., 1983; Dennehy et al., 1989; Fallaw and Price, 1995; Fallaw et al., 1990; Logan and Euler, 1989; Siple, 1967; Wyatt and Harris, 2004).

This report focuses on the Tertiary age sediments of the Upland Unit and the Tobacco Road Sand. These sediments are part of the Upper Aquifer Zone (UAZ) of the Upper Three Runs Aquifer. Figure 4-7 shows the regional lithologic units and their corresponding hydrostratigraphic units.

The UAZ includes the Upland Unit, the Tobacco Road Sand and part of the Dry Branch Formation. Massive beds of sand and clayey sand with minor clay interbeds typically characterize the UAZ. The Upland unit commonly consists of very dense, clayey sediments and gravelly sands. The top of the UAZ is defined by the water table. The water table typically mimics topography, but with subdued relief relative to topography.

In past studies the UAZ for the central SRS has been subdivided into hydrostratigraphic intervals based on characteristic piezocone penetration test (CPT) logs (Flach et al., 1999) (Flach et al., 2005b). The vadose zone sediments evaluated in the present report are interpreted as being correlative to the “A” and “uu” intervals identified and described in these past studies (Figure 4-8). These studies described the “A” interval as correlative with the upper parts of the Tobacco Road Sand. This section is characterized by a relatively stable and low friction ratio curve, which is indicative of a more massively bedded unit with somewhat higher permeability than the units above and below it. The uppermost subdivision, “uu”, corresponds to the fluvial sediments of the Upland Unit, recent alluvial material deposited by active streams, and any local soil horizons that have formed in-situ from the lithostratigraphic units. This unit is characterized by a higher and more irregular friction ratio curve (Flach et al., 1999).

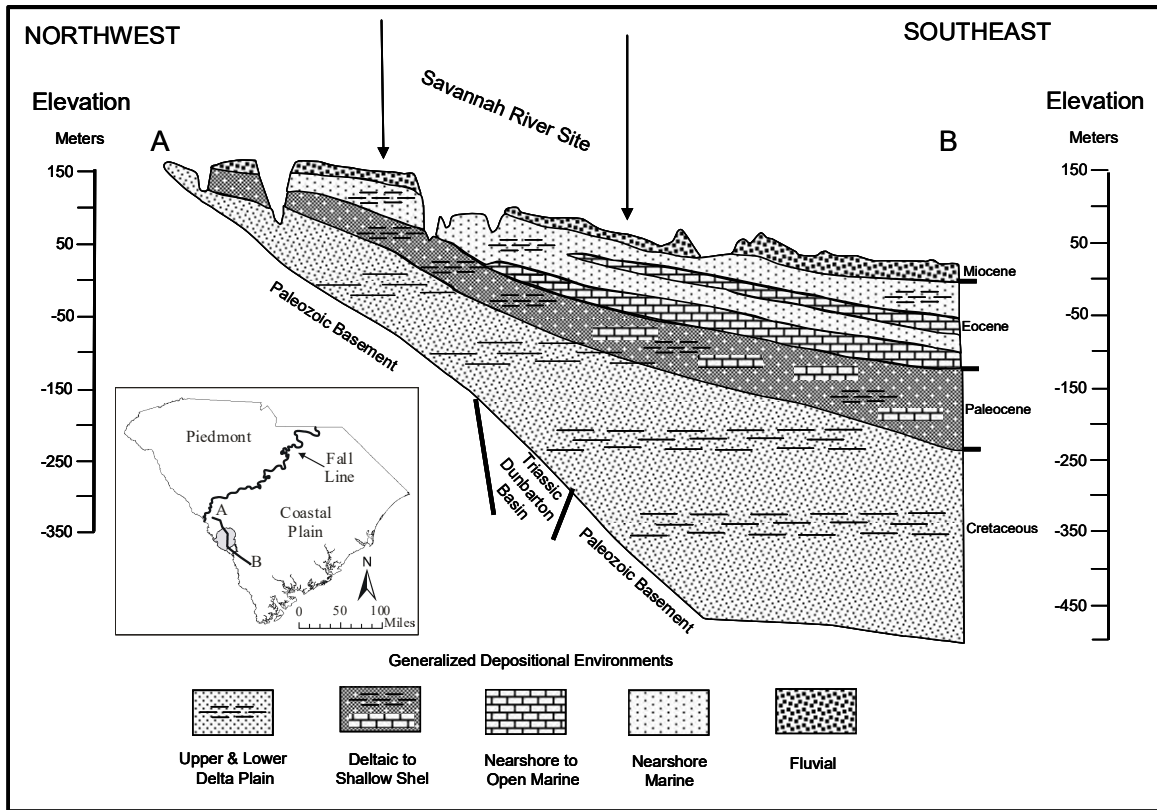
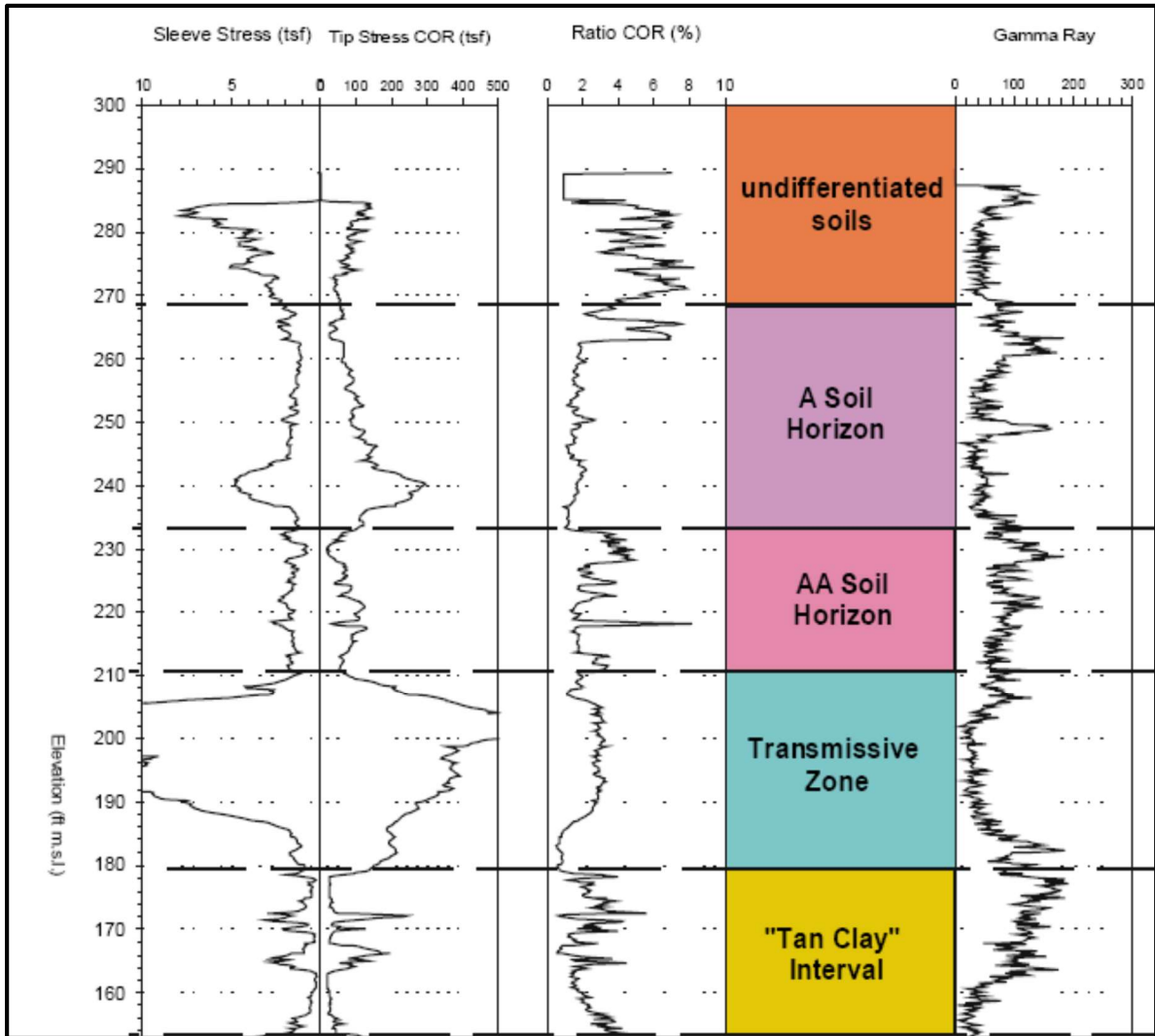


Figure 4-6. Regional NW to SE cross section depicting generalized lithology and depositional environments for the SRS (figure from Wyatt and Harris, 2004)

CHRONOSTRATIGRAPHIC UNITS			LITHOSTRATIGRAPHIC UNITS (Modified from Fallaw and Price, 1995)		HYDROSTRATIGRAPHIC UNITS (Modified from Aadland et al., 1995)				
Era	System	Series	Group	Formation					
CENOZOIC	Tertiary	Miocene(?)		"upland" unit					
		Eocene	Upper	Barnwell Group	Tobacco Road Sand	Upper Aquifer Zone (UAZ)			
					Dry Branch Formation	Twiggs Clay Member	Tan Clay Confining Zone (TCCZ)		Upper Three Runs Aquifer
						Griffins Landing Member			
						Irwinton Sand Member			
		Clinchfield Formation	Lower Aquifer Zone (LAZ)						
		Middle	Orangeburg Group	Santee Formation					
				Warley Hill Formation	Gordon Confining Unit				
				Congaree Formation	Gordon Aquifer				
		Lower	Black Mingo Group	Fourmile Branch Formation					
		Paleocene		Upper	Snapp Formation				
				Lower	Lang Syne Formation				
					Sawdust Landing Formation	Meyers Branch Confining Unit			

Figure 4-7. Comparison of lithostratigraphic and hydrostratigraphic units at SRS



**Figure 4-8. Subdivision of the UAZ by previous studies for the central SRS**

Figure 4-8 is modified from Figure 2-22 from Flach et al. (1999). Sleeve stress, tip stress and ratio are from CPT (piezocone penetration test) measurements that reflect the physical properties of sediment and can be used to infer sediment type; gamma ray is a logging tool that measures the natural radioactivity in sediments and can be used to infer sediment type. Elevation is in feet from mean sea level; sleeve stress and tip stress in tons per square feet; ratio incorporates sleeve stress/tip stress in %; and gamma ray in API units (American Petroleum Institute).

## 4.4 E-AREA LLWF DISPOSAL UNIT TYPES

As discussed in Section 4.2 and shown on Figure 4-4, the E-Area LLWF contains the following six types of disposal units including Slit Trenches, Engineered Trenches, Component-In-Grout Trenches, the Low Activity Waste Vault, the Intermediate Level Vault, and the Naval Reactor Component Disposal Areas. The following sections (4.4.1 through 4.4.6) provide a description of each type of disposal unit. The information was primarily extracted from the 2008 E-Area LLWF PA (WSRC 2008) and 2009 E-Area LLWF closure plan (Phifer et al. 2009). References in addition to these are noted in the applicable sections.

### 4.4.1 Slit Trenches

Slit Trenches are below-grade earthen disposal units with vertical side slopes making them inaccessible by vehicle. Each Slit Trench is generally laid out in a series of five narrow parallel trench rows. Exceptions to this typical design have been employed such as the construction of Slit Trench #9 which was excavated in a terraced fashion to permit vehicle entry for disposal of failed reactor vessel heat exchangers. In the typical design, each trench row is generally 20 feet (6.1 m) deep, 20 feet (6.1 m) wide, and 656 feet (200 m) long with ten feet (3 m) to 14 feet (4.3 m) of undisturbed soil separating each parallel trench row. A set of five, 20-foot (6.1 m) wide trench rows, are grouped together within a 157-foot (48 m) wide by 656-foot (200 m) long footprint forming a single Slit Trench. Ten Slit Trenches, designated STs 1-9 and ST 14, have been placed in operation, starting with ST 1 in 1995. ST's 1-5 are now operationally closed. Nine additional Slit Trenches have been designated for future disposals. Figure 4-5 provides the layout of the ten existing and nine future Slit Trench footprints relative to other E-Area LLWF disposal unit types. Figure 4-9 is an as-built drawing of ST's 1-4 showing the layout of trench rows within each Slit Trench.

Low-level waste consisting of soil, debris, rubble, wood, concrete, equipment, and job control waste is disposed within the Slit Trenches. Job control waste consists of potentially contaminated protective clothing (plastic suits, shoe covers, lab coats, etc.), plastic sheeting, etc. Slit Trench waste may be disposed in bulk form (e.g., demolition waste delivered in roll-off pans) or contained within B-25 boxes, B-12 boxes, 55-gallon drums, SeaLand containers, and other metal containers. A section of a trench row, referred to as a trench "unit", is typically opened at one end as needed to meet near term disposal needs with operations proceeding to the other end of the trench as space is utilized. Figure 4-9 shows the actual layout of units within ST's 1-4. The excavated soil from trench construction is stockpiled for later placement over disposed waste. Additional units of trench space are not excavated until needed in order to minimize the area of open trench and the time trench units remain open. Waste placement typically begins at one end of the open trench unit and proceeds toward the other end. Bulk waste is bulldozed into the trench while containerized waste and large equipment are typically crane-lifted into place. Eventually, containerized waste areas of the trench are filled in with either bulk waste or clean soil to fill the voids between adjacent containers and the trench wall. Slit Trenches are typically filled to within four feet of the top of the trench with waste and daily cover, if required. Figure 4-10 provides operational photographs of Slit Trenches being filled with containerized and bulk waste.

Operational closure of the Slit Trenches is being conducted in stages. Once a unit of the Slit Trench is filled with waste, stockpiled clean soil is bulldozed in a single lift over that section

of trench to produce a minimum 4-foot (1.2 m) thick clean soil layer over the waste (i.e., operational soil cover). The operational soil cover is graded to provide positive drainage off and away from the disposal operation. Subsequent trench units are filled with waste, covered with an operational soil cover, and graded to promote positive drainage until the entire Slit Trench is filled and covered. Once a Slit Trench (i.e., the 157-foot (47.8 m) wide by 656-foot (200 m) long footprint) is filled, completely covered with the 4-foot (1.2 m) soil cover, and a vegetative cover of shallow rooted grass is established, it is ready for a low-permeability stormwater runoff cover. This low-permeability cover will be installed over the entire Slit Trench to promote runoff and minimize infiltration into the underlying buried waste (Collard and Hamm 2008). A single operational stormwater runoff cover with a lengthwise crest may cover a single or multiple Slit Trenches.

Installation of the operational stormwater runoff covers involves the placement of grading fill and structural fill soil layers over the operational soil cover, which will be graded to promote even greater drainage off the trenches. The runoff cover will consist of a low-permeability, geosynthetic material or another water shedding material. The runoff cover will span the closed Slit Trenches and will be connected to adjacent concrete drainage ditches to promote positive drainage. It will extend a minimum of 10 feet (3.0 m) beyond the edge of all sides of the trenches. The first such operational stormwater runoff covers were installed over ST's 1-4 and ST 5 in 2010-11. After installation of the operational stormwater runoff cover, a Slit Trench is considered operationally closed (Phifer 2004; Collard and Hamm 2008; USEPA 2008).

After operational closure, the subsidence potential of Slit Trenches is highly variable due to waste variability. The only mechanical compaction that the soil and waste in the trench receives is from the bulldozer and other heavy equipment moving over the top of a completely backfilled trench. The subsidence potential could range from zero for bulk waste to 13.5 feet for B-25 boxes containing low-density waste. Additionally, to minimize future subsidence of the final closure cap, limits on the disposal of containers with significant void space that are considered non-crushable (i.e., typically thick-walled containers that will not be stabilized by dynamic compaction) have been imposed. (Hang et al., 2005; Swingle and Phifer, 2006)

At the end of the operational period for the entire facility, currently projected to be year 2065 (Sink 2016), a low-permeability interim runoff cover will be installed and maintained during the 100-year institutional control period (i.e., interim closure). The interim runoff cover will consist of the surface application of a geomembrane or other water-shedding material designed to maximize runoff. Based on a recent parametric study (Hang and Flach 2016), the interim runoff cover will need to extend a minimum of 10 ft (3.0 m) beyond the edge of all sides of the trenches to minimize lateral infiltration through the sides of the trench. The operational stormwater runoff cover overlying the Slit Trenches will be integrated with adjacent interim runoff covers from either Engineered Trenches and/or CIG Trenches. The pre-existing operational stormwater runoff cover over an individual Slit Trench or group of Slit Trenches may transition into the interim runoff cover if the cover material is deemed serviceable for continued sustained performance after technical evaluation. These runoff covers will be maintained during the 100-year institutional control period, including the repair of any subsidence-induced damage.

Final closure of the Slit Trenches and the entire E-Area LLWF, will take place at the end of the 100-year institutional control period, projected to be year 2165. Static surcharging and/or dynamic compaction of the Slit Trenches will be conducted at the end of the 100-year institutional control period, when the effectiveness of the subsidence treatment will be greater due to corrosion and loss of structural integrity of metal containers. Dynamic compaction will not be carried out over any Slit Trench unit that has been designated as containing special wastes for which container or waste form credit is taken to slow contaminant release (such as those containing M-Area glass and ETP Carbon Columns). It is assumed that this subsidence treatment essentially eliminates future subsidence potential except in those areas designated not to undergo dynamic compaction or containing non-crushable containers with significant void space. Final closure will consist of a multilayer soil-geomembrane closure cap installed over all the disposal units integrated with a drainage system to carry away runoff to nearby sediment basins. Figure 4-11 provides the anticipated Slit Trench closure cap configuration. This integrated closure system will minimize moisture contact with the waste and provide an intruder deterrent.

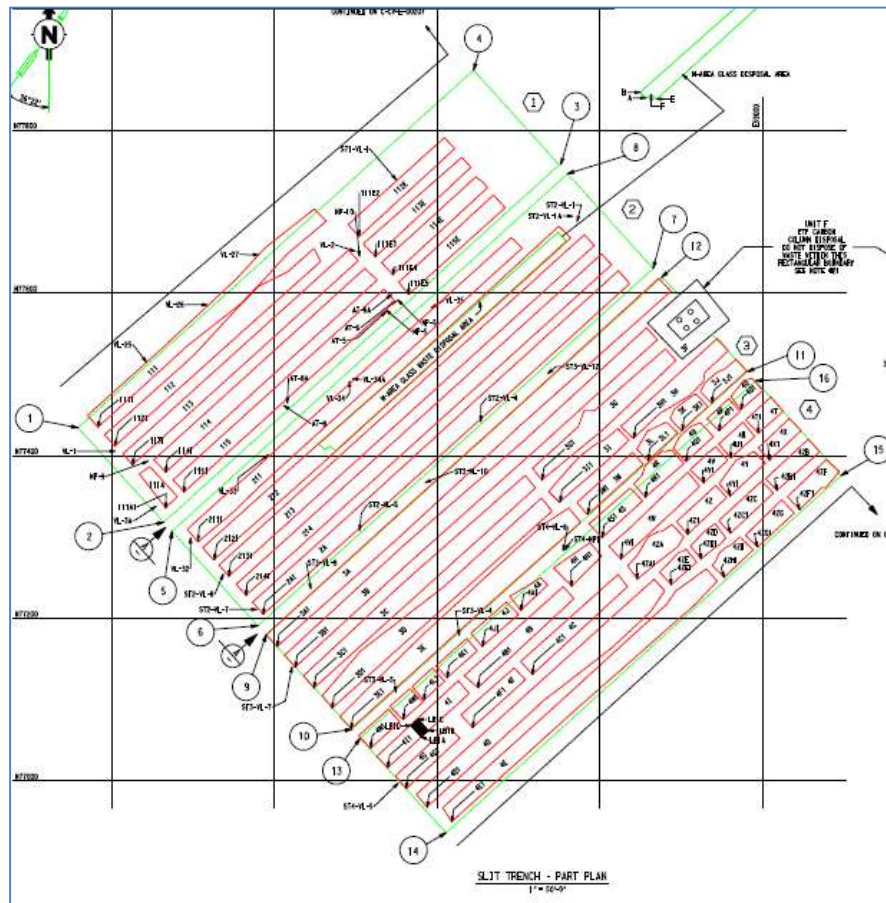
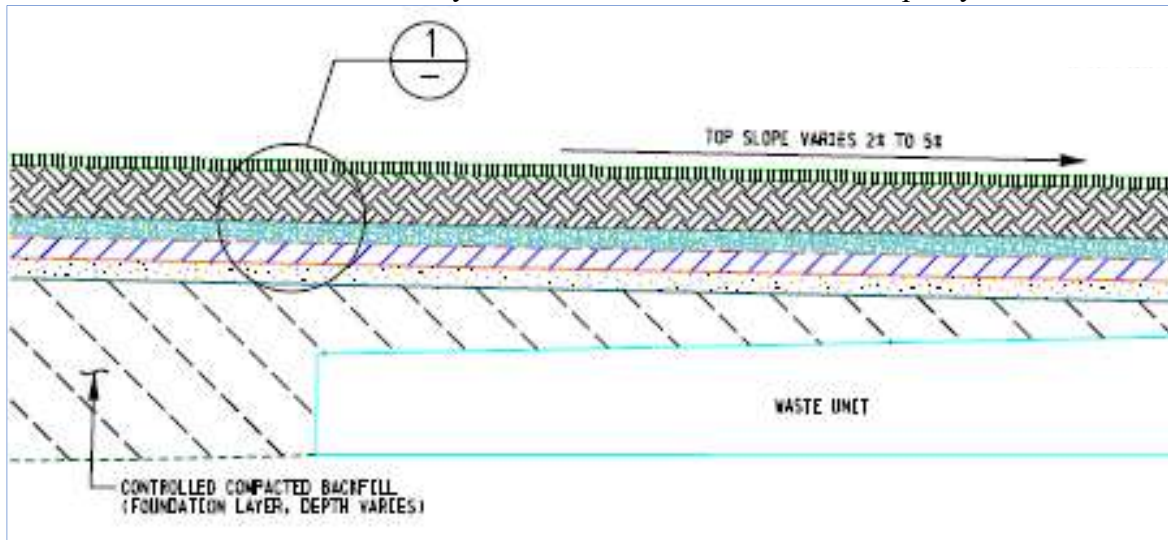


Figure 4-9. As-Built Drawing of Slit Trenches 1-4



**Figure 4-10. Operational Slit Trench Photographs**

E-Area LLWF Multilayer Soil-Geomembrane Closure Cap Layers



Detail 1

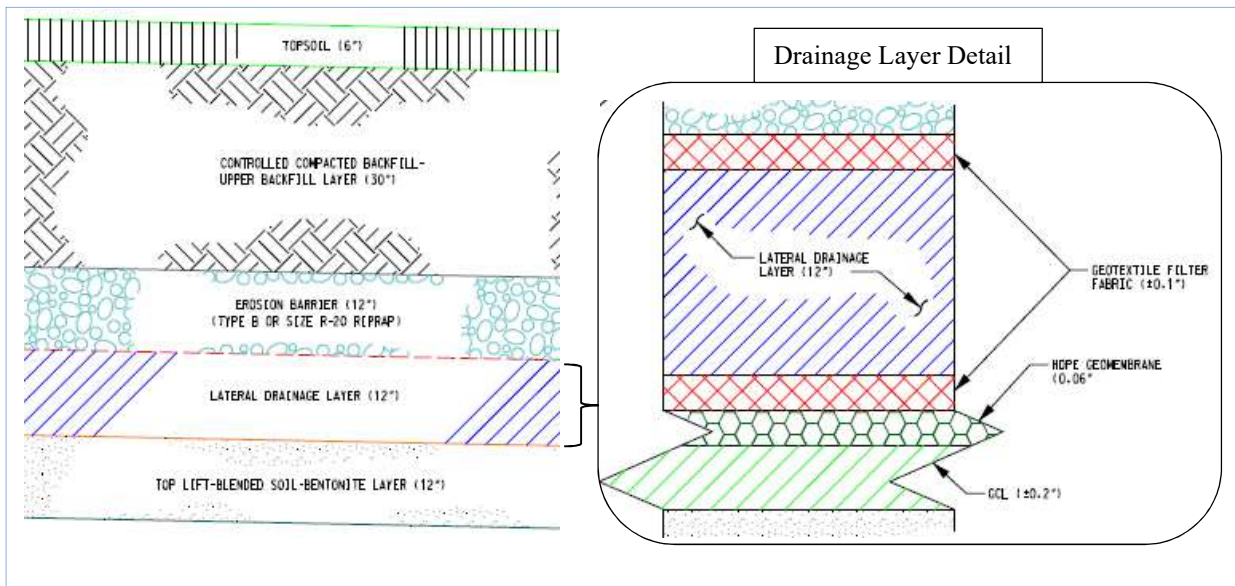


Figure 4-11. Slit and Engineered Trench closure cap configuration

4.4.2 Engineered Trenches

The Engineered Trenches (ETs) are below grade earthen disposal units. There are currently three Engineered Trenches in the E-Area LLWF with a fourth planned in the next few years. Figure 4-5 provides the layout of the first four ETs relative to other E-Area LLWF disposal unit types. Each Engineered Trench is a vehicle-accessible, open trench design that allows stacking of containerized waste primarily packaged in B-25 boxes and SeaLand containers. Engineered Trenches consist of the following common design elements:

- A berm around the top on the sides where the local terrain slopes toward the trench
- Side slopes range from 1.25:1 (horizontal:vertical) to 1.5:1 and generally covered with an erosion control matting and seeded
- A vehicle access ramp to the bottom
- A bottom consisting of compacted soil, a geotextile filter fabric, and approximately 6 inches of granite crusher run (from bottom to top) sloped to a sump or low point for collection of surface runoff within the interior of the trench (ET #1 and #2 only)
- A sump (ET #1 and #2 only) with 1-to-1 side slopes and a geotextile fabric and a polyethylene geoweb slope cover, infilled with either 4,000-psi concrete covering the sump side slopes and sump bottom (ET #1) or riprap (ET #2)

Engineered Trench #1, which is operationally closed, is approximately 650 feet (198 m) long by 150 feet (46 m) wide (bottom dimensions) and varies in depth from 16 to 25 feet (4.9 to 7.6 m). It is designed to contain approximately 12,000 B-25 boxes of waste. As part of closure, the concrete in the floor of the ET #1 sump was broken up to promote drainage that is essentially equivalent to that of the surrounding native soil and the sump backfilled with typical E-Area soil (Wilhite et al., 2009).

Engineered Trench #2 is approximately 656 feet (200 m) long by 160 feet (49 m) wide (bottom dimensions) and varies in depth from 14 to 23 feet (4.3 to 7.0 m). It is also designed to contain approximately 12,000 B-25 boxes of waste. ET #2 is essentially identical to ET #1 except for sump details. The bottom of ET #2 was formerly sloped to a low point where a 24 inch (0.6 m) steel pipe took water from ET#2 to the ET #1 sump (Swingle and Phifer, 2006). In 2009 as a part of ET #1 closure, the pipe connecting ET #2 to the ET #1 sump was sealed to prevent flow between trenches. A new un-lined sump was installed in ET #2.

Engineered Trench #3 is approximately 455 feet (139 m) long by 182 feet (55 m) wide (bottom dimensions) and approximately 22 feet (6.7 m) deep. The long axis of ET #3 is oriented perpendicular to the neighboring trench units. It will hold between 9,000 to 10,000 B-25 boxes. There are no plans for a sump in ET #3. The trench floor is sloped to a low point for collection of surface runoff within the interior of the trench.

During the operational period, low-level waste contained within B-25 boxes, B-12 boxes, 55-gallon drums, SeaLand containers, components, and/or other metal containers are stacked by forklift or placed by crane within the Engineered Trench. B-25 boxes are the predominant disposal containers utilized. The B-25 boxes are stacked in rows four high (approximately 17 feet high) with a forklift, typically beginning at the end of the trench opposite the access ramp. The stacks of B-25 boxes are generally placed immediately adjacent to one another with as little void space as possible between the stacks. Figure 4-12 provides operational photographs of ET #1, ET #2 and ET #3.

Operational closure of the Engineered Trenches is being conducted in stages. Excavated soil from trench construction is stockpiled for later placement over disposed waste. As a sufficient number of B-25 rows are placed, the stockpiled clean soil is bulldozed in a single lift over some of the completed rows to produce a minimum 4-foot-thick (1.2 m) clean soil layer over them (i.e., operational soil cover). Where the depth of an ET is less than the height of a stack of 4 B-25 boxes (e.g., at the west ends of ET #1 and ET #2) soil is mounded

above the original grade to provide adequate operational soil cover. This operational soil cover is only applied to that portion of the completed rows that allows for maintenance of a safe distance from the working face (i.e., where new boxes are placed in the stack) within the trench (see Figure 4-12). The operational soil cover is graded to provide positive drainage off the trench and away from the working face.

Placement of the B-25 boxes continues until the trench is filled with boxes. At that point, the minimum 4 feet (1.2 m) of operational soil cover is placed over the remaining portion of the trench, the entire area is graded to provide positive drainage off the trench, a vegetative cover of shallow rooted grass is established, and it is considered operationally closed. Unlike Slit Trenches, Engineered Trenches do not receive a low-permeability cover at the operational closure stage. This difference results from a regulatory agreement applying only to Slit Trenches which receive offsite CERCLA waste. After operational closure, the subsidence potential of Engineered Trenches has been estimated as 13.5 feet due to stacked B-25 boxes containing low-density waste (Phifer and Wilhite, 2001). Additionally, to minimize future subsidence of the final closure cap, limits on the disposal of containers with significant void space that are considered non-crushable (i.e., containers that will not be stabilized by dynamic compaction) have been imposed (Swingle and Phifer, 2006).

At the end of the operational period for E-Area, currently projected to be year 2065 (Sink 2016), a low-permeability interim runoff cover will be installed and maintained during the 100-year institutional control period (i.e., interim closure). The interim runoff cover will involve the placement of up to an additional 2-foot of soil over the Engineered Trenches, that is graded to promote even greater drainage off the trenches. The interim runoff cover will consist of the surface application of a high-density polyethylene (HDPE) geomembrane or other appropriate material. The runoff cover will extend a minimum of 10 ft (3 m) beyond the edge of all sides of the trenches to minimize lateral infiltration through the sides of the trench.

Final closure of the Engineered Trenches and the entire E-Area LLWF will take place at the end of the 100-year institutional control period. Static surcharging and/or dynamic compaction of the Engineered Trenches will be conducted at the end of the 100-year institutional control period, when the effectiveness of the subsidence treatment will be greater due to corrosion and loss of structural integrity of metal containers. It is assumed that this subsidence treatment essentially eliminates future subsidence potential except in those areas containing non-crushable containers with significant void space. (Swingle and Phifer, 2006) Final closure will consist of a multilayer soil-geomembrane closure cap installed over all the disposal units integrated with a drainage system to carry away runoff to nearby sediment basins. Figure 4-11 provides the anticipated Slit and Engineered Trench closure cap configuration. This integrated closure system will minimize moisture contact with the waste and provide an intruder deterrent.

Engineered Trench #1 and Engineered Trench #2 Aerial View (2-2-2011)



Engineered Trench #3 Aerial View (2-18-2016)



Engineered Trench #3 View from Berm (3-15-2016)



Figure 4-12. Operational Engineered Trench photographs

#### 4.4.3 Component-in-Grout (CIG) Trenches

Component-In-Grout (CIG) disposal units are below-grade earthen trenches with essentially vertical side slopes that contain grout encapsulated waste components providing a greater degree of waste isolation than Slit or Engineered Trenches. CIG Trenches are contained within 157-foot-wide (48 m) by 656-foot-long (200 m) footprints. Two such CIG Trench footprints, designated CIG-1 and CIG-2, were originally planned for E-Area with each CIG footprint laid out in five parallel, nominally 20-foot-wide (6.1 m) by 650-foot-long (198 m), trenches separated by 10 feet (3.0 m) of undisturbed soil. Figure 4-5 provides the layout of the two CIG footprints relative to other E-Area LLWF disposal unit types.

Since approval of the 2008 PA, CIG Trenches have been underutilized and have no waste forecasted through the end of E-Area operations. Consequently, the remaining unused portion of CIG-1 and future location of CIG-2 will be repurposed as Slit or Engineered Trenches in the next PA revision. CIG Trench modeling will be updated and integrated with Slit or Engineered Trench models to produce a new PA baseline in which the existing nine CIG-1 Trench disposal segments will be treated as ST special waste forms. The following facility description and material properties will be used for that update.

Components disposed within the CIG Trenches consist of large radioactively contaminated equipment and other smaller waste forms such as B-25 boxes to fill in the space around and above the large equipment. Components to date consist of tankers, radioactive sources in a concrete culvert filled with grout, SeaLands, B-25s, B-12s, flat bed trailers, tanks, high integrity containers, columns, etc.

CIG Trench excavation has been conducted on an as-needed basis and only to that depth, width, and length (i.e., trench segment) required for disposal of a particular component(s) to minimize the area of open trench, the time the trench section is open, and to minimize grout costs. The depth and width of each unit can vary greatly depending upon the size of the component(s) being disposed. The existing units within a CIG Trench footprint are numbered in order of placement. The excavated soil is stockpiled for later use. Six feet (1.8 m) of undisturbed soil separates each unit within an individual trench row.

The bottom of a unit is filled with high-flow grout to a minimum one-foot thickness and allowed to solidify. The component(s) are then placed on the one-foot base grout layer with a crane and additional grout is poured around, between, and over the component(s) for encapsulation. Additional layers of component(s) and grout may be placed on top of previous layers until a trench segment is filled to a height of approximately 16 feet (4.9 m). The grouting operation is conducted to achieve a minimum one foot of grout below, between and above components and surrounding undisturbed soil and soil cover for complete encapsulation.

Three hundred years of structural integrity is ensured after disposal in one of three ways: 1) components are filled with grout or controlled low strength material (CLSM), 2) components are determined to be in and of themselves structurally sound for 300 years after burial through a structural-corrosion evaluation, or 3) the encapsulated CIG trench segment is overlaid with a 20-inch steel-reinforced 3000 psi concrete mat with CLSM between the top of the grout and bottom of the concrete slab. A 20-inch thick concrete mat can support a

12.5-foot soil overburden from the final closure cap (Peregoy, 2006a). Employing these stabilization measures minimizes subsidence potential of CIG trench units during the initial 300-years following burial under the cap design evaluated by the 2008 E-Area PA (WSRC, 2008). The impact of the new conceptual closure cap design on the durability of the concrete mat will be evaluated by the next PA. Following this initial intact period, the subsidence potential ranges from zero for segments containing component(s) filled with grout or CLSM to an estimated maximum of 10 feet for segments containing component(s) that are not filled or containing predominately B-25 boxes with low density waste. (Jones et al., 2004; Peregoy, 2006b; Phifer, 2004)

After the top grout has solidified, a 4-foot-thick clean layer of material (described below) is placed over the grout encapsulated waste components. On top of this 4-foot-thick clean layer is placed an overlying soil, which is graded to provide positive drainage off and away from the CIG Trenches. This process continues until the entire trench is filled and completely covered with 4 feet of clean material. The 4-foot-thick clean layer consists of one of the following:

- A minimum 4-foot layer of clean soil from the excavation stockpile placed in a single lift with a bulldozer (i.e., operational soil cover), or
- A combination from bottom to top of a nominal 1.33-foot layer of CLSM, a minimum 20-inch thick concrete mat, and a nominal 1-foot layer of clean soil from the excavation stockpile is placed over the grout encapsulated waste components for a minimum 4-foot thickness. The reinforced concrete mat utilizes minimum 3000 psi concrete, is a minimum 20-inch thick, extends 1-foot beyond the aerial dimensions of the grout on all sides, includes #8 rebar at 6-inch spacing across the width of the trench and #4 rebar at 6-inch spacing along the length of the trench tied to the #8 rebar, and the rebar is placed at the bottom of the mat and has a minimum concrete cover of 3 inches. (Peregoy, 2006a)

In addition, an operational stormwater runoff cover will be installed within 3 months after each CIG Segment has been emplaced. The operational runoff cover will be maintained during the operational period and incorporated into or replaced by the interim runoff cover during the following 100-year institutional control period. The interim runoff cover will involve the placement of up to an additional 2-foot of soil over the existing CIG units, that is graded to promote even greater drainage off the trench. The interim runoff cover will consist of the surface application of a high-density polyethylene (HDPE) geomembrane or geotextile fabric with spray on asphalt emulsion or some other appropriate material. It will extend a minimum of 10 feet beyond the edge of all sides of each unit.

Final closure of the CIG Trenches and the entire E-Area LLWF will take place at the end of the 100-year institutional control period. Dynamic compaction of the CIG Trench units will not be conducted. Final closure will consist of a multilayer soil-geomembrane closure cap installed over all the disposal units integrated with a drainage system to carry away runoff to nearby sediment basins. Figure 4-11 provides the anticipated CIG Trench closure cap configuration which, as stated earlier, is to be converted to either a Slit or Engineered Trench for the remaining unused space. This integrated closure system will minimize moisture contact with the waste and provide an intruder deterrent.

Currently waste has been placed within CIG Trench footprint CIG-1 within units 1 through 8. The following provides information on these existing units:

- CIG-1 units 1 through 3: The interiors of the components within segments 1 through 3 were filled with grout or CLSM; therefore, there is essentially no significant void space within these units. These units are covered with an operational stormwater runoff cover.
- CIG-1 units 4 through 7 and 9: Many of the components and other wastes within units 4, 5, 6, 7 and 9 consist of low strength containers such as B-25 boxes, Tankers, and SeaLands with significant interior void space. These units are covered with an operational stormwater runoff cover. Installation of a reinforced concrete mat over these units is planned prior to installation of the E-Area LLWF final closure cap, which will occur at the end of the 100-year institutional control period. The timing of the reinforced concrete mat installation is yet to be determined.
- CIG-1 unit 8: This unit has been overlaid with CLSM, an 18-inch thick reinforced concrete mat, and clean soil. This 18-inch thick concrete mat can support an 11.4-foot soil overburden from the final closure cap. This unit is covered with an operational stormwater runoff cover.

Formulation of the original high flow grout (used for units 1 through 8), CLSM, and 3000 psi concrete are provided in Table 4-1 and Table 4-2. Also shown is a new grout used for unit 9 (and any future CIG trench segments if needed) as recommended in Dixon and Phifer (2007). This grout has a lower saturated hydraulic conductivity than the original CIG grout. Also presented in Table 4-1 and Table 4-2 are the cementitious material formulations for the E-Area ILV and LAWV, discussed later in sections 4.4.4 and 4.4.5, respectively.

Figure 4-13 provides photographs of the placement sequence for existing CIG-1 Segment 6.

**Table 4-1. Material formulations for E-Area LLWF cementitious materials.**

Material	Mix Id	Cement <sup>1</sup> (lb/yd <sup>3</sup> )	Fly Ash <sup>2</sup> (lb/yd <sup>3</sup> )	Blast Furnace Slag <sup>3</sup> (lb/yd <sup>3</sup> )	Water (gal/yd <sup>3</sup> )	Sand <sup>4</sup> (lb/yd <sup>3</sup> )	Aggregate <sup>5</sup> (lb/yd <sup>3</sup> )	Set Regulator <sup>6</sup> (oz/yd <sup>3</sup> )	HRWR <sup>7</sup> (oz/yd <sup>3</sup> )
Old CIG High Flow Grout	A2000-X-0-0-AB	618	-	-	71	2283	-	-	-
CLSM	EXE-X-P-0-X	50	600	-	66	2515	-	-	-
CIG Segment 8 Concrete Mat	B-3000-6-0-2-A	400	70	-	35	1149	1900	-	-
CIG Concrete Mat	B-3000-6-0-2-A+	520	-	-	35.5	1172	1850	-	-
New CIG Grout	4000-SCC-FA-Grout	600	600	-	59.7	1743	-	36	48
Vault Concrete	C-4000-8-S-2-AB	120	135	275	28.8	1270	1750	-	-

<sup>1</sup> ASTM C150, <sup>2</sup> ASTM 618, <sup>3</sup> Grade 120 ASTM C989, <sup>4</sup> ASTM C33, <sup>5</sup> ASTM C33, <sup>6</sup> Set Regulator = Recover, <sup>7</sup> High Range Water Reducing Admixture (HRWR) = Adva 380

**Table 4-2. Notes on E-Area LLWF material formulations.**

Mix ID	Specification	Maximum WCR	Minimum Compressive Strength, psi @ 28 days	Reference	Note
A2000-X-0-0-AB	C-SPS-G-00085, Rev. 5	0.96	2000	(WSRC, 2004)	Grout is simply poured into the trench with no consolidation or curing requirements
EXE-X-P-0-X	C-SPS-G-00085, Rev.5	0.85	150	(WSRC, 2004)	CLSM is simply poured into the trench or IL Vault with no consolidation or curing requirements
B-3000-6-0-2-A	C-SPS-G-00085 Rev.5	0.62	3000	(WSRC, 2004)	Concrete mats are placed with standard field construction practices and are not built to the same level of quality control as major projects
B-3000-6-0-2-A+	C-SPS-G-00085, Rev. 5	0.57	3000	(WSRC, 2006)	
4000-SCC-FA-Grout	C-SPS-G-00085, Rev.6	0.83	4680	(Dixon and Phifer, 2007)	Grout is simply poured into the trench with no consolidation or curing requirements
C-4000-8-S-2-AB	C-SPS-G-00041	0.45	4000	(WSRC, 1994)	High quality workmanship was implemented for placement of this concrete

Note: WCR = water-to-cement ratio.

Emplacement of Bottom Foot of Grout



Component Emplacement



Grouting Sides of Segment



Initial Waste Layer Encapsulated



Top of Grout



4-Foot of Clean Soil Cover



Figure 4-13. CIG-1 Segment 6 placement sequence

#### 4.4.4 Low-Activity Waste Vault

The Low-Activity Waste Vault (LAWV) is an above-grade, reinforced concrete vault. It is approximately 643 feet (196 m) long, 145 feet (44 m) wide, and 27 feet (8.2 m) high at the roof crest. It is divided into 3 modules along its length, which are approximately 214 feet (65 m) long and contain 4 cells each. The modules share a common footer but have a 2-inch gap between their adjacent walls. The 12-cell total is designed to contain more than 12,000 B-25 boxes of waste. Figure 4-5 provides the layout of the LAWV relative to other E-Area LLWF disposal unit types. Figure 4-14 provides photographs of the LAWV and Figure 4-15 provides a cross-sectional view (A-A'). The LAWV consists of the following:

- Controlled compacted backfill soil base
- Geotextile Filter Fabric
- 1-foot 3-inch (0.38 m) graded stone sub-drainage system to collect water from under and around the vault and route it to manhole drains
- Crusher run stone base
- 30-inch (0.76 m) continuous footer under all interior and exterior walls
- 1-foot (0.3 m) thick, cast-in-place, reinforced concrete floor slab sloped to an interior collection trench, which drains to an external sump
- 2-foot (0.6 m) thick, cast-in-place, reinforced, interior and exterior concrete walls that are structurally mated to the footer (the exterior end walls of modules 1 and 3 are 2-foot 6-inches thick (0.76 m))
- Exterior and interior personnel openings with doors, 36 inch (0.9 m) square exterior fan openings, and exterior forklift access openings
- AASHTO Type IV bridge beams to support the concrete roof
- 3-½ inch (9 cm) thick precast deck panels overlain by 12-½ inch (31.7 cm) thick cast-in-place, reinforced concrete slab for a total 16 inch (40.6 cm) thick concrete roof.
- A bonded-in-place layer of fiberboard insulation and a layer of waterproof membrane roofing on top of the roof slab
- A gutter/downspout system to drain the roof

The formulation of the concrete utilized in the LAWV is provided in Table 4-1. This concrete formulation was utilized for the continuous footer, floor slab, interior and exterior walls, and the cast-in-place roof slab. This formulation was not utilized for the AASHTO Type IV bridge beams and precast deck panels.

During the operational period low-activity containerized waste (predominately B-25 boxes and B-12 boxes) are stacked by forklift within the vault. B-25 (approximately 4-foot high by 6-foot long by 4-foot wide) and/or equivalent pairs of B-12 (approximately 2-foot high by 6-foot long by 4-foot wide) boxes are stacked four high. The waste within the containers typically includes job control waste, scrap metal, and contaminated soil and rubble. Job control waste consists of potentially contaminated protective clothing (plastic suits, shoe covers, lab coats, etc.), plastic sheeting, etc. The scrap metal consists of contaminated tools, process equipment and piping, and laboratory equipment. Soil and rubble are generated from demolition activities.

Arial View



View of a Vault Cell Opening



Figure 4-14. LAWV photographs

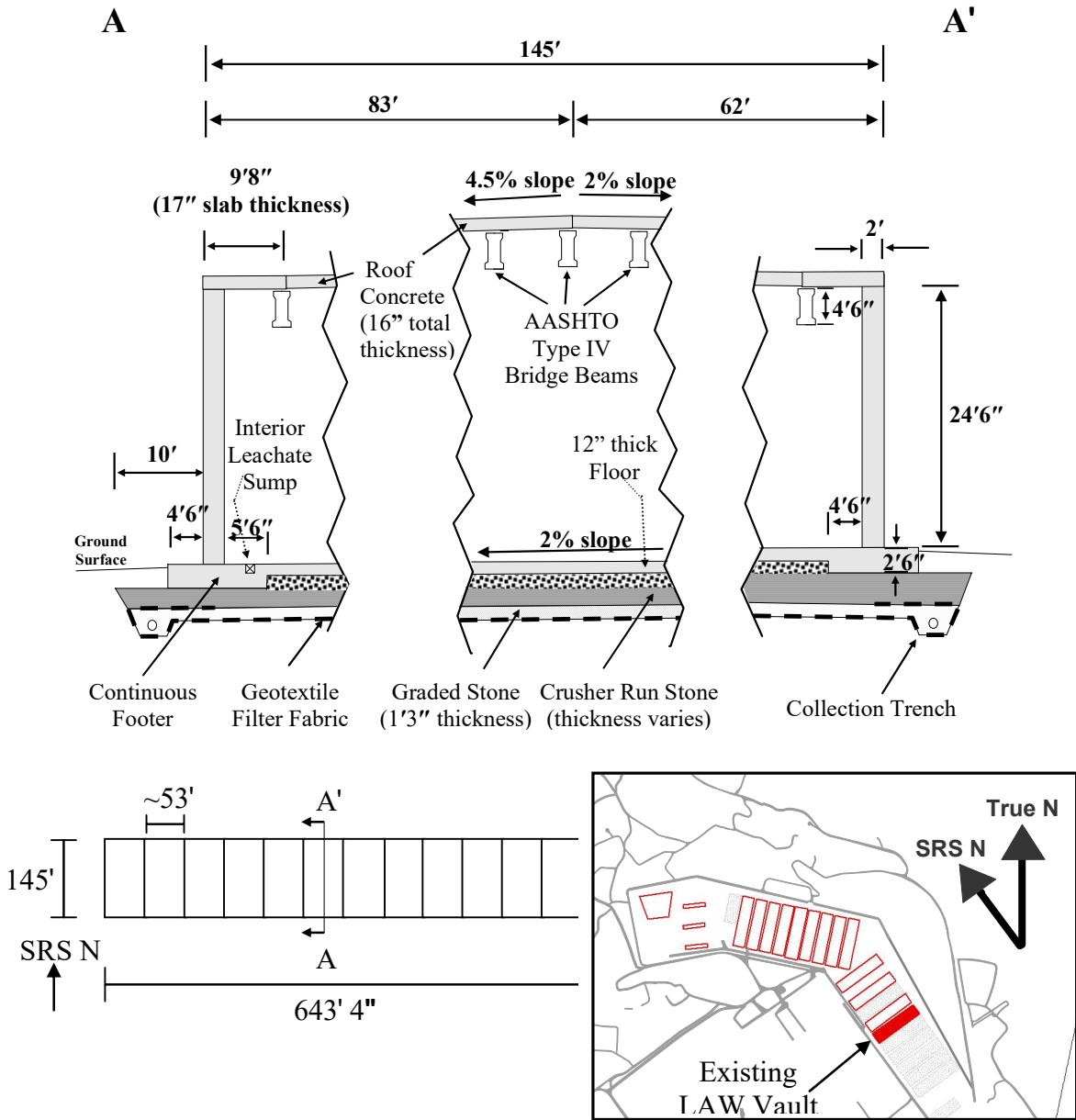


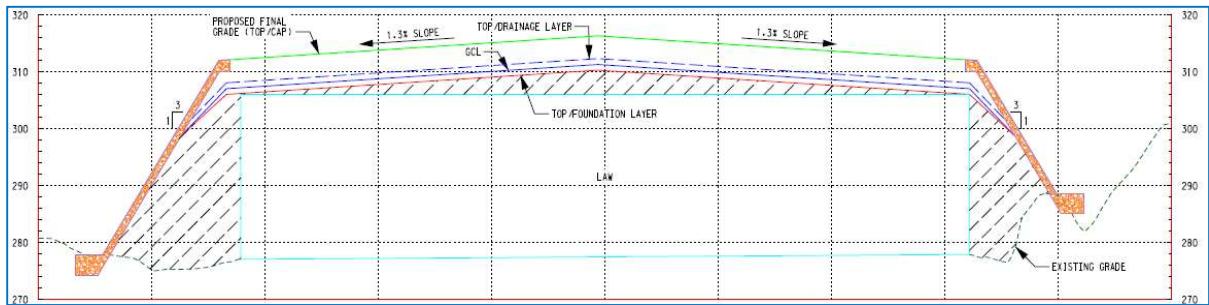
Figure 4-15. LAWV cross-sectional view (A-A')

The average waste density within the containers has been estimated at  $0.1785 \text{ g/cm}^3$  (Phifer and Wilhite, 2001), which along with the vault dimensions results in a subsidence potential of approximately 21 feet (Jones and Phifer, 2006).

Operational closure of the LAWV will be conducted in stages. Individual cells will be closed as they are filled with stacks of containerized waste (metal and/or concrete containers) and the entire vault will be closed after it is filled. Such operational closure includes filling the interior collection trench and exterior sump with grout and sealing exterior vault openings, including those between modules, with reinforced concrete equivalent to that utilized within the vault floor, walls and roof. The reinforcing steel will be tied into the reinforcing steel of the vault itself, forming a unified structure with continuous walls. No additional closure actions are anticipated beyond that of operational closure for the LAWV during the 100-year institutional control period (i.e., interim closure).

Final closure of the LAWV will take place at final closure of the entire E-Area LLWF, at the end of the 100-year institutional control period. Final closure will consist of the installation of an integrated closure system designed to minimize moisture contact with the waste and to provide an intruder deterrent. The integrated closure system will consist of a multilayer soil-geomembrane closure cap installed over all the disposal units and a drainage system. Figure 4-16 provides the anticipated closure cap configuration above the LAWV. The crest lines of the closure cap will be approximately centered over the long and short axes of the vault and slope a minimum 1.3% away from the apex in order to minimize the overburden loads on the vault and maximize runoff and lateral drainage from the overlying closure cap.

LAWV cross-section through long axis of the vault



Closure cap detail

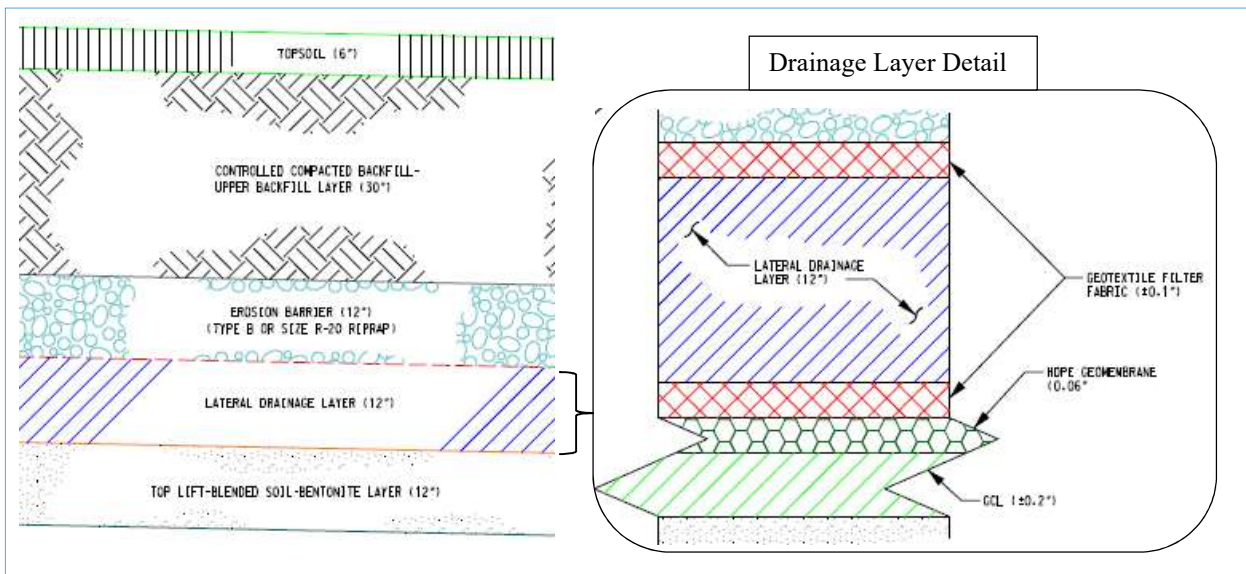


Figure 4-16. LAWV disposal unit closure cap configuration

#### 4.4.5 Intermediate Level (IL) Vault

The Intermediate Level (IL) Vault is a below-grade, reinforced concrete vault. It consists of two modules, which together encompass a 279-foot (85 m) by 48-foot (15 m) area. The Intermediate Level Tritium (ILT) module contains two cells, whose inside dimensions are 25-foot (7.6 m) by 44-foot (13 m) by 26-foot (7.9 m) deep. ILT Cell #1 contains 144, 20-inch (51 cm) diameter by 20-foot (6.1 m) long vertical silos. The Intermediate Level Non-Tritium (ILNT) module contains seven identical cells, whose inside dimensions are 25-foot (7.6 m) by 44-foot (13 m) by 28-foot (8.7 m) deep. The area between the two modules provides manhole access to the subdrain system. Figure 4-5 provides the layout of the IL Vault relative to other E-Area LLWF disposal unit types. Figure 4-17 provides a photograph of the exterior view of the IL Vault, Figure 4-18 shows interior views of the IL Vault, Figure 4-19 provides a plan view of the operational vault, and Figure 4-20 provides a cross-section of the operationally closed vault. The IL Vault consists of the following:

- Controlled compacted backfill soil base
- Graded stone sub-drainage system to collect and drain any water under the vault to a dry well
- Crusher Run stone base
- 30-inch (0.76 m) thick, reinforced concrete, base slab, which extends 2 feet (0.6 m) beyond the exterior walls
- The floor of each cell slopes to a drain which runs to a sump in the base slab of each cell, and it is overlain by a minimum 14-inch (0.36 m) graded stone drainage layer
- 30-inch (0.76 m) thick, reinforced concrete, exterior end walls and 24-inch (0.61 m) thick, reinforced concrete, exterior side walls; and 18-inch (0.46 m) thick, reinforced concrete, interior walls; all of which are structurally mated to the base slab and have no horizontal joints
- Exterior wall surfaces are coated with a tar-based waterproofing and interior wall surfaces have a drainage net attached.
- Continuous waterstop seals at all concrete joints
- 1.5-foot (0.46 m) thick, reinforced concrete, shielding tees available when necessary for radiation shielding over all bulk cells (the silo cell utilizes individual shielding plugs for each silo)
- Sloped rain covers, consisting of a roofing membrane on metal deck on steel framing installed over each cell, to direct rainwater onto the ground for runoff (used during operations only and will be replaced with a permanent concrete roof after cessation of operations)

The formulation of the concrete utilized for all concrete in the IL Vault is provided in Table 4-1.

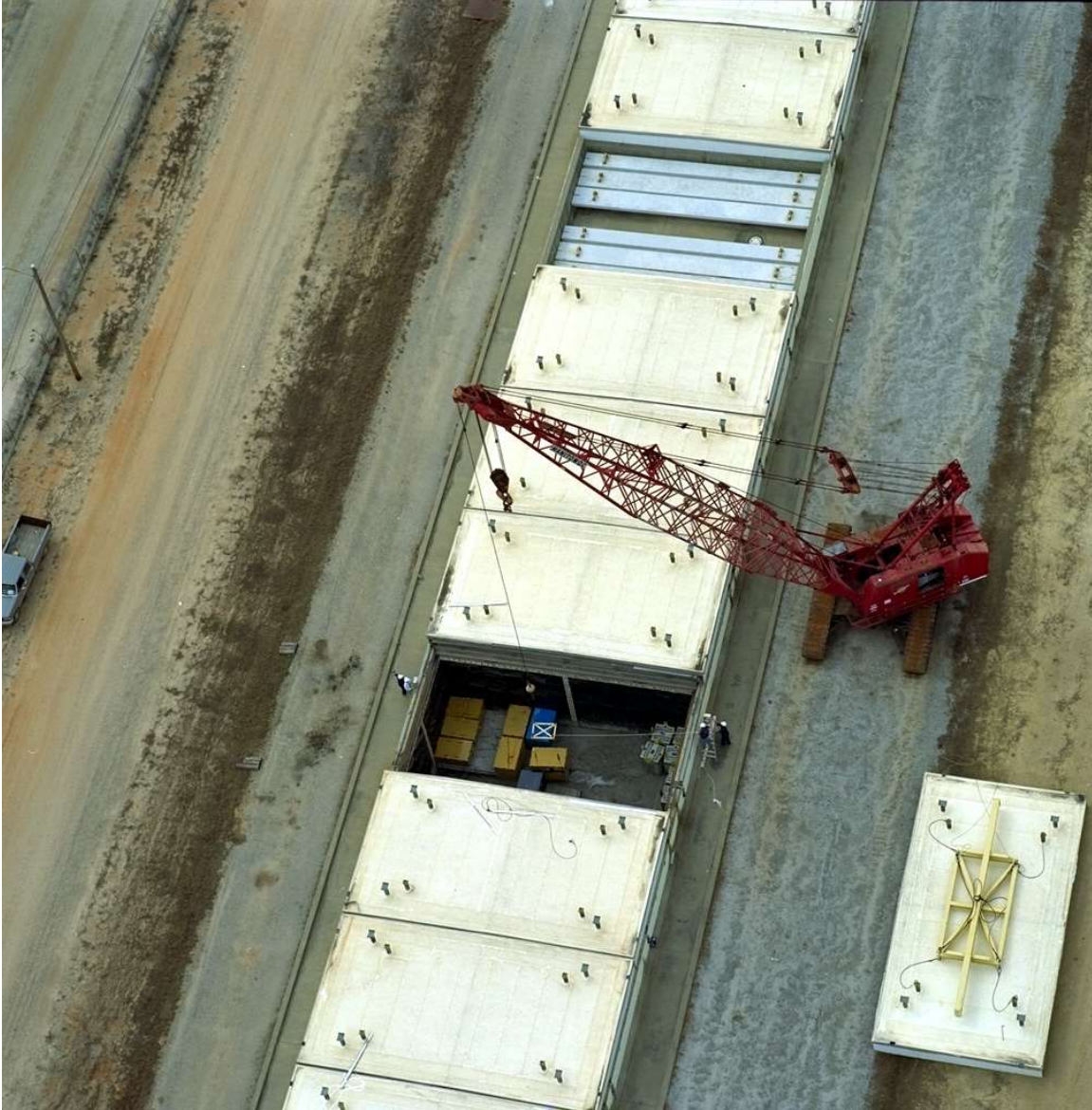
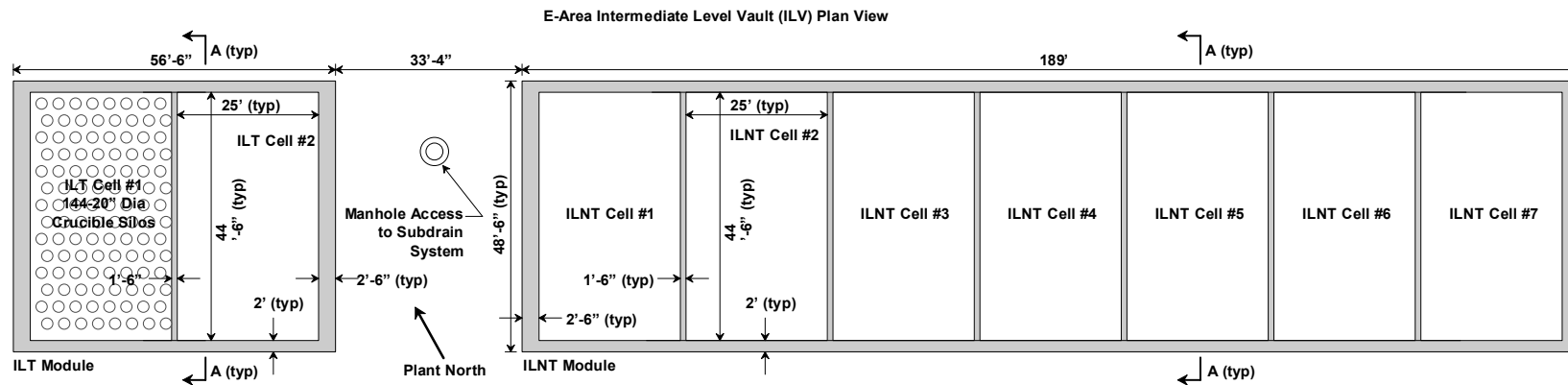


Figure 4-17. IL Vault aerial view

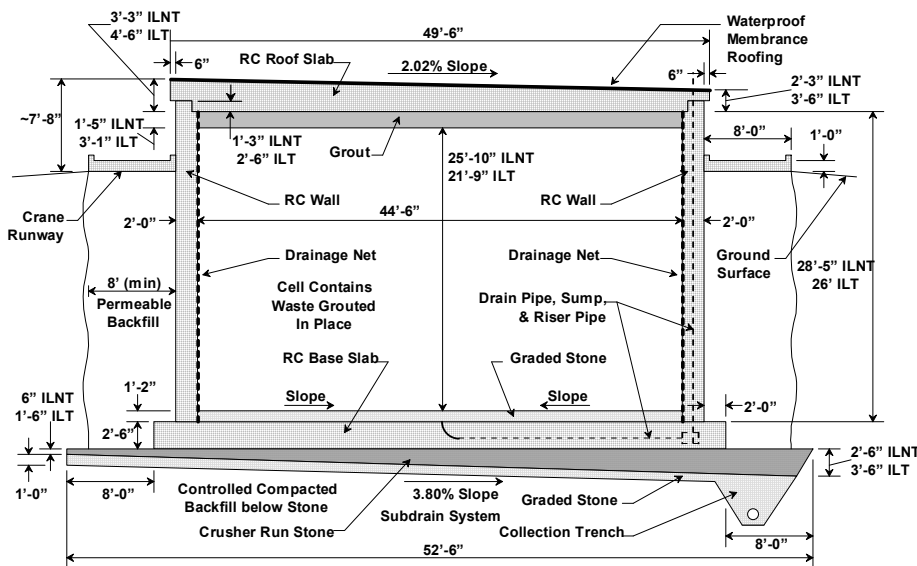


Figure 4-18. IL Vault interior views



Note:  
 - RC Base Slab, which extends 2 feet beyond the exterior walls all around is not shown  
 - The top of the interior ILT wall is 2'-6" lower than exterior ILT walls  
 - The top of interior INLT walls are 1'-3" lower than exterior INLT walls

Figure 4-19. E-Area ILV plan view



- Notes to Figure 4-20:
- ILNT = Intermediate Level Non-Tritium
  - ILT = Intermediate Level Tritium
  - Crucible Silos in ILT Cell #1 not shown
  - Permeable backfill is sand with maximum 10% passing #200 sieve compacted to 90% minimum
  - Interior graded stone is ASTM D488-88 No. 57 and it is 1'-2" thick at walls and 1'-5" thick in cell center at drain; the top 6" of the stone is underlain by a geotextile fabric to prevent intrusion of grout into the bottom 8" of the stone
  - RC base slab is 2'-6" at walls and 2'-3" in cell center at drain
  - Crusher run stone is Georgia 25
  - Exterior graded stone is ASTM D488-88 No. 57 or 67

Figure 4-20. E-Area ILV Section A-A

During the operational period small containers of tritium waste are placed in ILT Cell #1 as follows:

- The waste is placed in individual silos.
- A shielding plug is placed over each silo containing waste.

During the operational period intermediate-activity waste is placed in ILT Cell #2 and ILNT Cells #1 through #7 as follows:

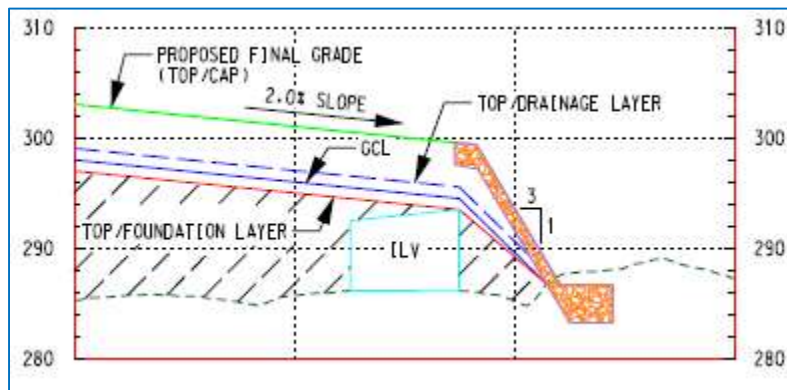
- The first layer of waste is placed within each cell directly on top of the graded stone drainage layer.
- The first layer of waste is encapsulated in grout which forms the surface for the placement of the next layer of waste.
- Subsequent layers of waste are placed directly on top of the previous encapsulated waste, however subsequent layers may be encapsulated with controlled low strength material (CLSM) rather than grout.

The waste placed within ILT Cell #2 and ILNT Cells #1 through #7 typically consists of job control waste, scrap hardware, and contaminated soil and rubble. Containers predominately include drums, B-12 boxes, B-25 boxes, and other metal containers. Job control waste primarily consists of highly contaminated protective clothing (plastic suits, shoe covers, lab coats, etc.), plastic sheeting, etc. The scrap hardware consists of reactor hardware, reactor fuel and target fittings, jumpers, and used canyon and tank farm equipment. Soil and rubble is generated from demolition activities (Dixon and Phifer, 2008). Average waste density within the ILV containers has not been estimated, however with the assumption that the waste has a density similar to that of waste within the LAWV (i.e., 0.1785 g/cm<sup>3</sup>) (Phifer and Wilhite, 2001), a maximum subsidence potential of 19 feet is estimated. The grout and CLSM formulations utilized in the IL Vault are provided in Table 4-1 and Table 4-2.

Operational closure of the IL Vault will be conducted in stages. ILT Cell #1 will be operationally closed by placing a final layer of grout level with the top of the interior vault wall, with installed silo shielding plugs remaining in place within the final grout layer. ILT Cell #2 and ILNT Cells #1 through #7 will be operationally closed as they are filled with waste by removing any shielding tees and placing a final layer of grout level with the top of the interior vault walls. The final grout layer over the ILT cells will be 3-foot 1-inch (0.94 m) thick, and over the ILNT cells, it will be 1-foot 5-inches (0.43 m) thick. After the entire ILT module has been filled, it will be operationally closed, by installing a 3-foot 6-inch (1.07 m) to 4-foot 6 inch (1.37 m) permanent reinforced concrete roof slab and overlying bonded-in-place fiberboard insulation and waterproof membrane roofing over the entire module. After the entire ILNT module has been filled, it will be operationally closed, by installing a 2-foot 3-inch (0.69 m) to 3-foot 3 inch (0.99 m) permanent reinforced concrete roof slab and overlying bonded-in-place fiberboard insulation and waterproof membrane roofing over the entire module. The rain covers, shielding tees, and unused shielding plugs will no longer be required after installation of the permanent roof slab. No additional closure actions are anticipated beyond that of operational closure for the IL Vault during the 100-year institutional control period (i.e., interim closure).

Final closure of the IL Vaults will take place at final closure of the entire E-Area LLWF, at the end of the 100-year institutional control period. Final closure will consist of the installation of an integrated closure system designed to minimize moisture contact with the waste and to provide an intruder deterrent. The integrated closure system will consist of a multilayer soil-geomembrane closure cap installed over all the disposal units and a drainage system. Figure 4-21 provides the IL Vault closure cap configuration. The closure cap will have a 2% slope perpendicular to the long axis of the IL vault, in order to minimize the overburden loads on the vault and maximize runoff and lateral drainage from the overlying closure cap.

IL Vault cross-section through short axis of the vault



Closure cap detail

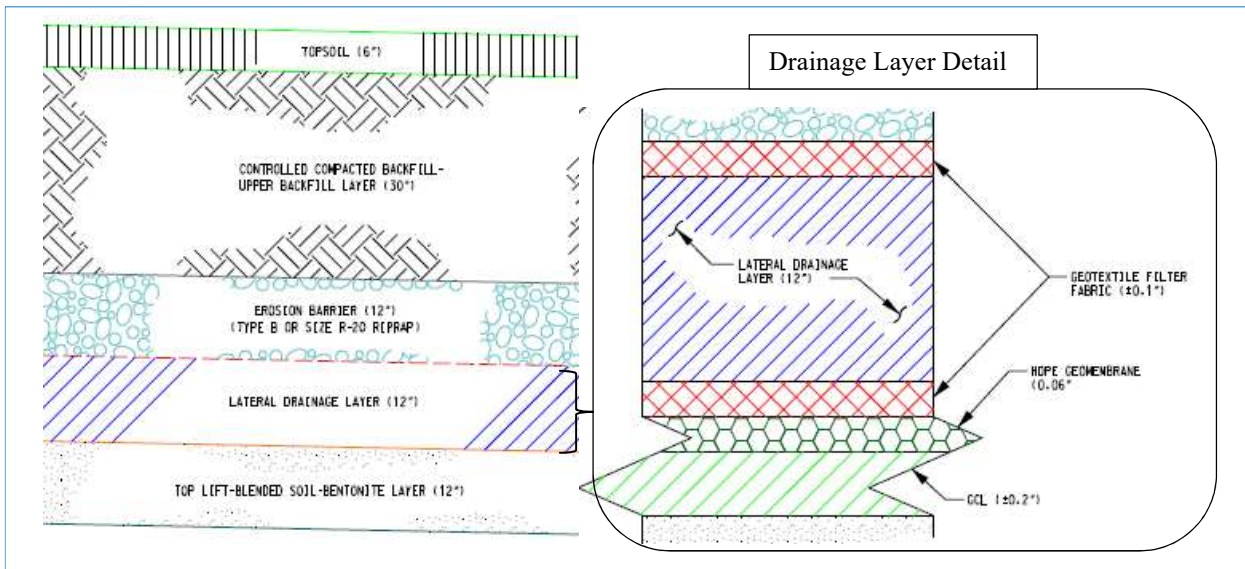


Figure 4-21. ILV disposal unit closure cap configuration

#### 4.4.6 Naval Reactor Component Disposal Areas

Naval Reactor Component Disposal Areas (NRCDA) are above grade gravel pads for the disposal of Naval Reactor Waste Shipping/Disposal Casks containing waste naval reactor (NR) components as well as less robust containers of other auxiliary equipment. Two NRCDA are associated with the E-Area LLWF. The 643-7E NRCDA contains approximately 41 casks, is a trapezoidal area consisting of approximately 0.13 acres (546 m<sup>2</sup>) and is closed to future receipts. It has an interim soil cover in place. The 643-26E NRCDA is currently in operation, is an irregularly shaped area consisting of approximately 1.1 acres (4,430 m<sup>2</sup>) and is expected to receive approximately 33 welded casks and 380 bolted casks for disposal through the year FY2040. Figure 4-5 provides the layout of the two NRCDA relative to other E-Area LLWF disposal unit types.

During the operational period waste naval reactor components and associated equipment contained within welded casks and bolted containers are placed on the NRCDA. NR components have historically consisted of core barrels, adapter flanges, closure heads, pumps, and other similar equipment from the Navy. A new surface contaminated waste form in the last several years has been the shear block which is part of a new shielding system. Due to the variety of NR waste components and levels of contamination, there is no standard NR waste container. Detailed configurational descriptions of the NR waste components are not available because of the classified nature of this information. According to unclassified data supplied by the NR program, a representative type of activated metal component is the KAPL core barrel/thermal shield (CB/TS) in a heavily shielded, welded cask, and a representative type of surface-contaminated component (from activated corrosion products) is the KAPL Closure Head in a thinner-walled bolted container. The steel casks and bolted containers have thick walls, are closed with a gasket or welds, and are considered water and air tight. Figure 4-22 provides an operational photograph of the 643-26E NRCDA that shows the offloading of a welded cask.

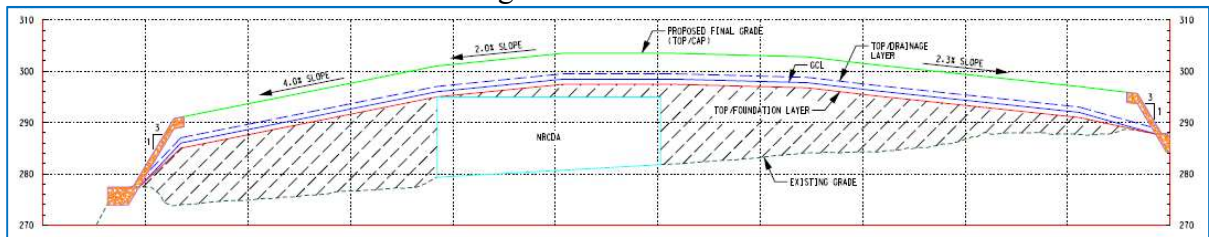
No additional operational closure or interim closure beyond simply placing containers on the NRCDA is necessitated due to the water and air-tight nature of the casks and bolted containers. However, if radiation shielding is required for personnel protection during the operational or institutional control period, the casks may be surrounded with a structurally suitable material that will be capable of supporting the final closure cap without resulting in differential subsidence at the time the cap is installed.

Final closure of the NRCDA will take place at final closure of the entire E-Area LLWF, at the end of the 100-year institutional control period. Prior to final closure, the space around, between, and over the casks will have to be filled with a structurally suitable material that will support the final closure cap without resulting in differential subsidence. Dynamic compaction of the NRCDA will not be conducted. Final closure will consist of installation of an integrated closure system designed to minimize moisture contact with the waste and to provide an intruder deterrent. The integrated closure system will consist of a multilayer soil-geomembrane closure cap installed over all the disposal units and a drainage system. Figure 4-23 provides the NRCDA closure cap configuration for the 643-26E NRCDA pad. The closure cap over both pads will have a minimum 2% slope and identical closure cap profile in order to minimize the overburden loads on the components and maximize runoff and lateral drainage from the overlying closure cap.



Figure 4-22. Operational NRCDA photograph

643-26E NRCDA cross-section looking east



Closure cap detail

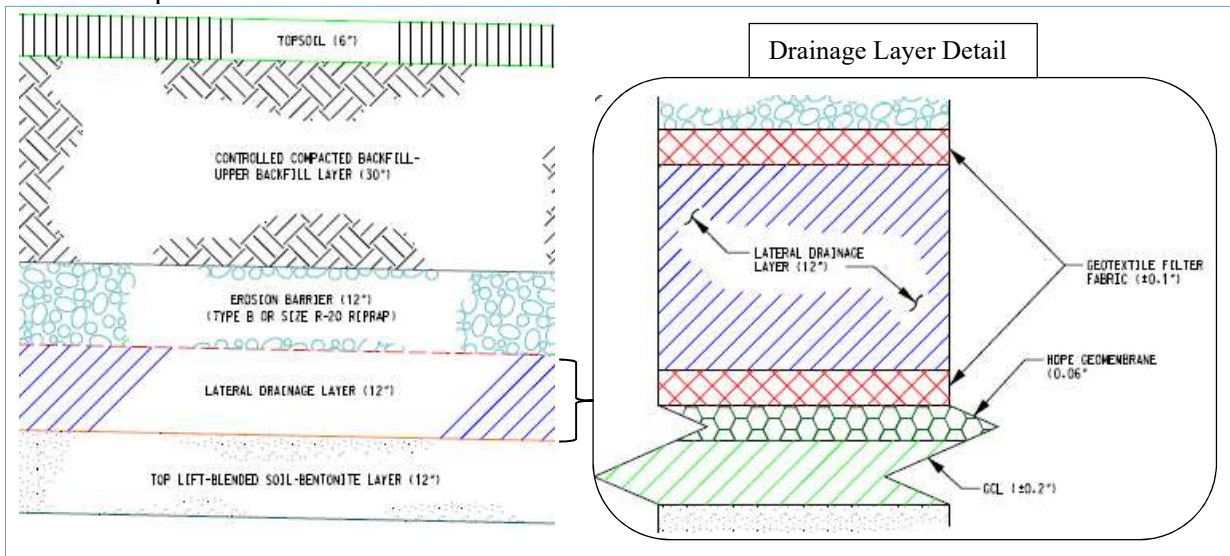


Figure 4-23. NRCDA disposal unit closure cap configuration

## 5.0 SOILS DATA

### 5.1 BACKGROUND

#### 5.1.1 Goal

The purpose of this soils evaluation is to provide estimates of porosity ( $n$ ), dry bulk density ( $\rho_b$ ), particle density ( $\rho_p$ ), saturated hydraulic conductivity ( $K_{sat}$ ), characteristic curves (suction head, saturation, and relative permeability), and effective diffusion coefficient ( $D_e$ ) for input to E-Area PA models. Estimates are provided for the following materials:

- undisturbed vadose zone soils
- controlled compacted backfill
- 4-ft operational soil cover (before and after dynamic compaction)
- permeable backfill for the Intermediate Level Vault
- a generic “gravel”

Material properties for undisturbed vadose zone soils, controlled compacted backfill, operational soil cover, and permeable backfill for the IL Vault were derived by compositing properties for individual samples. The method of compositing varies depending on the specific material being represented by the composited results. Each compositing method is described in this section of the report.

#### 5.1.2 Data Used in Evaluation

Existing soils data from the General Separations Area were gathered from databases, SRS documents, and laboratory reports. The primary types of soils data for this evaluation included:

- grain size (sieve analyses)
- hydraulic property datasets (laboratory measurements of vertical hydraulic conductivity and water retention)
- bulk property measurements (bulk density and porosity)
- piezocone penetration test or CPT (cone penetration test) logs
- continuous core descriptions/geophysical logs

##### *5.1.2.1 Grain Size, Hydraulic Property, Bulk Property Datasets*

Undisturbed vadose zone samples have been collected using Shelby tubes for grain size, hydraulic property, and bulk property measurement. Sampling was conducted during various projects in E-Area and Z-Area from the mid-1980s through May 2005. Sampling protocols used by the various labs in conducting these analyses are provided in Table 5-1.

**Table 5-1. Test methods used in analyses**

Parameter	Test Method
Grain Size	ASTM D422/D1140, D2217
Bulk Density	ASTM D4531
Porosity	EM1110-2-1906
Saturated Hydraulic Conductivity	ASTM D5084
Water Retention	ASTM D2325

**5.1.2.2 Piezocone Penetration Test (CPT) Logs**

Cone penetration tests (CPT) provide subsurface vertical profiles that can be indicative of soil types. Because it is considered a low-cost and reliable characterization tool, numerous CPT locations have been completed across E-Area. As the tool is pushed into the subsurface, measurements are compiled relating to the resistance and pore pressure of the sediments. Friction ratio is a measurement that represents the tool’s sleeve resistance divided by tip resistance. As sleeve resistance increases, the fines content typically increases (Lunne et al., 1997). CPT logs have been regarded as predictions of soil behavior rather than exact soil type. Some studies have produced methodologies for calibrating CPT measurements in order to predict mud content (Syms et al., 2001). However, for this evaluation, the CPT data were used qualitatively in conjunction with grain size data and continuous core descriptions to define soil type.

**5.1.2.3 Continuous Core Descriptions/Geophysical Logs**

Core descriptions and geophysical logs are available for several locations in E-Area. These borings and wells were completed primarily in the 1980s using mud rotary and split spoon sampling techniques. Geophysical logs include gamma ray, spontaneous potential, and resistivity. Foot-by-foot core descriptions in addition to field log descriptions are available for several of the locations. The usefulness of these descriptions for evaluating the upper vadose zone is limited because the upper 10 ft of the holes were typically drilled out (resulting in no core to describe).

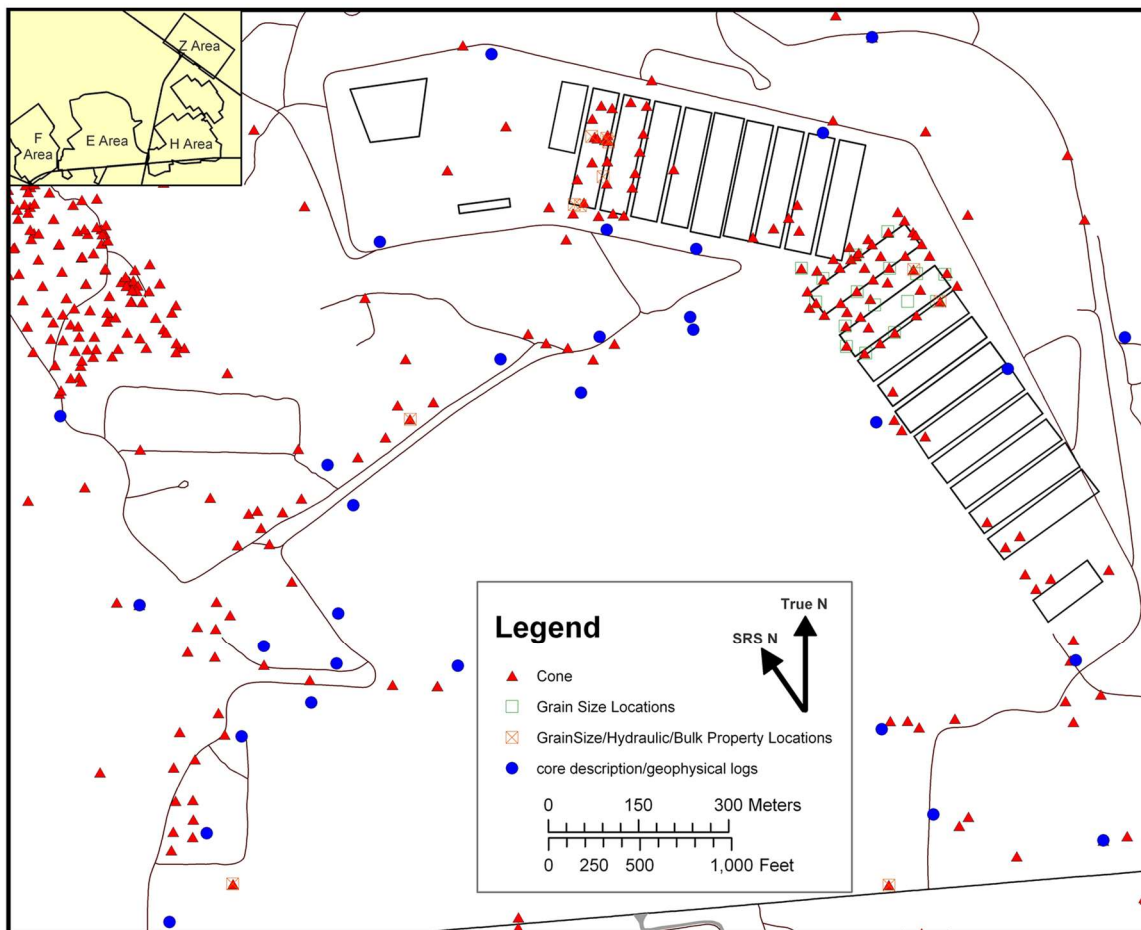
**5.1.2.4 Vadose Zone Soil**

Table 5-2 provides the approximate number of each data type for E-Area and Z-Area undisturbed vadose zone soils. Figure 5-1 shows the location of the various data types in E-Area.

The number of samples and locations identified for hydraulic property datasets in Table 5-2 reflect the data that were collected. Samples may not have been included in this evaluation if the samples were suspected to be of poor quality (or non-representative). Data quality for hydraulic properties will be further discussed in Section 5.2.2 Saturated Hydraulic Conductivity for undisturbed vadose zone soil.

**Table 5-2. Datasets for E-Area and Z-Area undisturbed vadose zone soil**

Data Type	E-Area	Z-Area
Grain Size Analyses	92 samples (25 locations)	373 samples (39 locations)
Hydraulic & bulk property	64 samples (11 locations)	4 samples (2 locations)
CPT logs	90 locations in vicinity of future and existing disposal units	31 locations in vicinity of future and existing vaults
Continuous core descriptions/geophysical logs	8 locations in vicinity of future and existing disposal units	7 locations in vicinity of future and existing vaults



**Figure 5-1. Map of E-Area soils dataset locations**

**5.1.2.5 Controlled Compacted Backfill**

Because the disposal units have not been closed and controlled compacted backfill does not yet exist, no analytical data for this material are available. Samples from the Old Radioactive Waste Burial Ground and compacted composite samples from Z-Area were used in this evaluation to represent the controlled compacted backfill soil. Table 5-3 provides an approximate number of each data type.

**Table 5-3. Datasets for E-Area and Z-Area controlled compacted soil**

<b>Data Type</b>	<b>E-Area</b>	<b>Z-Area</b>
Grain Size Analyses	41 samples (27 locations)	2 samples (2 locations)
Hydraulic & bulk property	14 samples (14 locations)	8 samples (2 locations)

Samples from the Old Radioactive Waste Burial Ground consisted of borrow pit material that had been placed on top of the Burial Ground to increase runoff. The tested material consisted primarily of sandy clay soils and was typical of controlled compacted backfill material. Sampling and analysis took place in 2001.

Z-Area samples were collected in May 2005 from the upper 12 feet of vadose zone soil in Z-Area. More specifically, samples were collected from two locations at 4, 6, 8, 10, and 12 feet. For each location, the soil from the various depths was mixed together to form a composite. Samples were remolded in the laboratory and prepared at different moisture contents (allowing moisture to vary 1.5% above and below the optimum moisture content). Additionally, samples were compacted to a minimum of 95% of the maximum dry density (modified proctor).

The number of samples and locations identified for hydraulic property datasets in Table 5-3 reflect the data that were collected. Samples may not have been included in this evaluation if the samples were suspected to be of poor quality (or non-representative). Data quality for hydraulic properties will be further discussed in Section 5.3.2 Saturated Hydraulic Conductivity for controlled compacted backfill.

**5.1.2.6 4-ft Operational Soil Cover**

No samples have been collected and analyzed for the 4-ft operational soil cover. Soil property estimates provided in this report are based on the properties of the undisturbed vadose zone samples. Further information regarding the estimates for the operational soil cover is provided in Section 5.4 Operational Soil Cover.

**5.1.2.7 Permeable Backfill for the Intermediate Level (IL) Vault**

According to engineered drawings for the IL Vault, the vault was constructed using a permeable backfill with <15% mud. The backfill likely came from local borrow pits and therefore vadose zone soils data were used to estimate the properties of the backfill. Two samples (VL-1, 44-46' bls and VL-1, 13-14' bls from E-Area) were used in this evaluation.

### 5.1.2.8 Generic Gravel

Soil properties were estimated for a generic “gravel” layer based on literature and reported laboratory results for gravel utilized in the construction of some of the vaults in the area. The reported data includes water retention and relative permeability for two gravel samples (GL-1 and GL-2) (Yu et al., 1993).

### 5.1.2.9 E-Area LLWF Expansion

Millings et al. (2011) present the results of a characterization program undertaken in 2011 to collect site specific data for the vadose zone lying beneath the adjacent undeveloped portions of the E-Area LLWF comprising an additional 100-acres. This characterization program consisted of collecting cone penetrometer logs (CPT) and individual soil samples. The CPT logs contain tip resistance, sleeve resistance, friction ratio, pore pressure and electrical resistivity. Individual soil samples were tested to determine grain size distribution, dry bulk density, porosity, saturated hydraulic conductivity, water retention characteristics, mineralogy, elemental composition, and organic content. Figure 5-2 shows the four locations where completion of eight soil borings, four geophysical logs, and the collection of 522 feet of core and 33 Shelby tubes from ECP plots 6, 7, 8 and 9 took place.

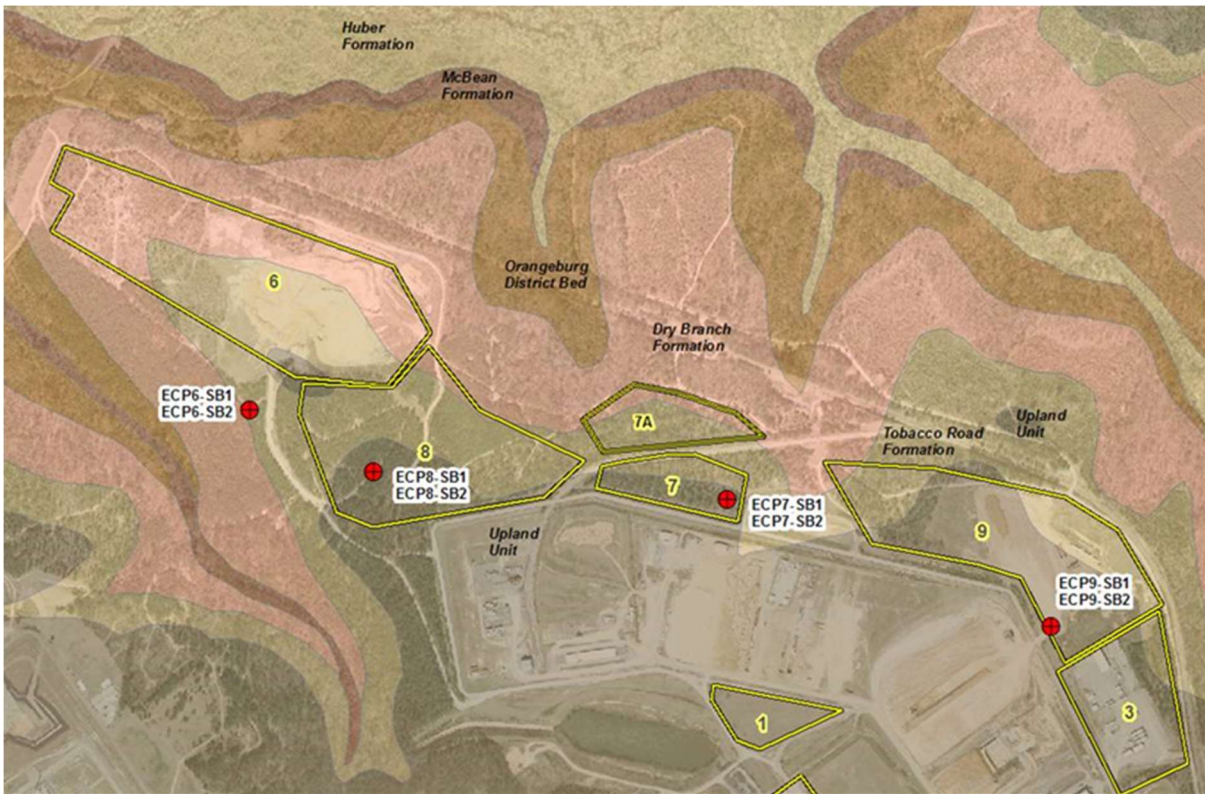


Figure 5-2. Four characterization locations within the E-Area LLWF Expansion

## 5.2 UNDISTURBED VADOSE ZONE SOIL

### 5.2.1 Grain Size

Soil texture can be classified using an agricultural approach developed by the U. S. Department of Agriculture (USDA) or by an engineering methodology known as the Unified Soil Classification System (USCS). The USDA system defines 12 basic textural groups, which can be shown in graphical form on a textural triangle. Only soil with grains less than 2 mm (passing through No. 10 sieve) is considered in this classification system. Sand represents particles between 0.05 and 2.0 mm in size; silt consists of particles 0.002 and 0.05 mm; and clay comprises particles smaller than 0.002 mm in size.

The USCS classifies soils based on how soils would behave as engineering construction material. Unlike the USDA system, the USCS includes all particle sizes. Moreover, it defines sand as particles between 0.074 mm (No. 200 sieve) and 4.76 mm (No. 4 sieve), and silts and clays particles less than 0.074 mm. Classification under this system also involves measurements of liquid limit and plastic limit (Atterberg Limits). The liquid limit represents the moisture content above which the soil flows as a viscous liquid and below which it is plastic. The plastic limit is the moisture at which the soil will start to crumble when rolled in the palm of the hand. The plasticity index relates these two limits and is defined as the difference between the liquid limit and plastic limit.

There is no easy method for correlating between the two soil classification systems. For this evaluation, both were used to the extent possible to describe the soils. Much of the recent laboratory grain size analyses were performed according to the USCS methodology; however, some analyses vary slightly in the particle size limits for sand, silt and clay and not all analyses include the Atterberg Limits (liquid and plasticity limits).

A textural triangle based on the USDA system is provided in Figure 5-3. Available E-Area (n = 44) and Z-Area (n = 29) data are plotted for comparison. Because much of the laboratory data did not use the USDA particle size designations, the location of data points may vary from their actual USDA classification (had the grain size analyses been performed using the USDA particle size limits). All of the grain size data plotted in Figure 5-3 come from the LAW, AT&E, or GTE laboratories, which used similar particle size bounds for sand, silt, and clay. The data may be biased toward the sand textural class because for these analyses sand included particle sizes up to 4.75 mm. Silt included 0.074 mm to 0.005 mm (as opposed to the USDA limits of 0.05 mm to 0.002 mm) and clay consisted of particles less than 0.005 mm (USDA label of less than 0.002 mm). Despite these differences in particle size limits, the figure does provide a general view of soil texture (the relative amounts of % sand, % silt, and % clay) for comparison of samples. E-Area and Z-Area samples tend to be very similar in terms of percent sand, silt and clay. E-Area samples also include samples with significant amounts of clay.

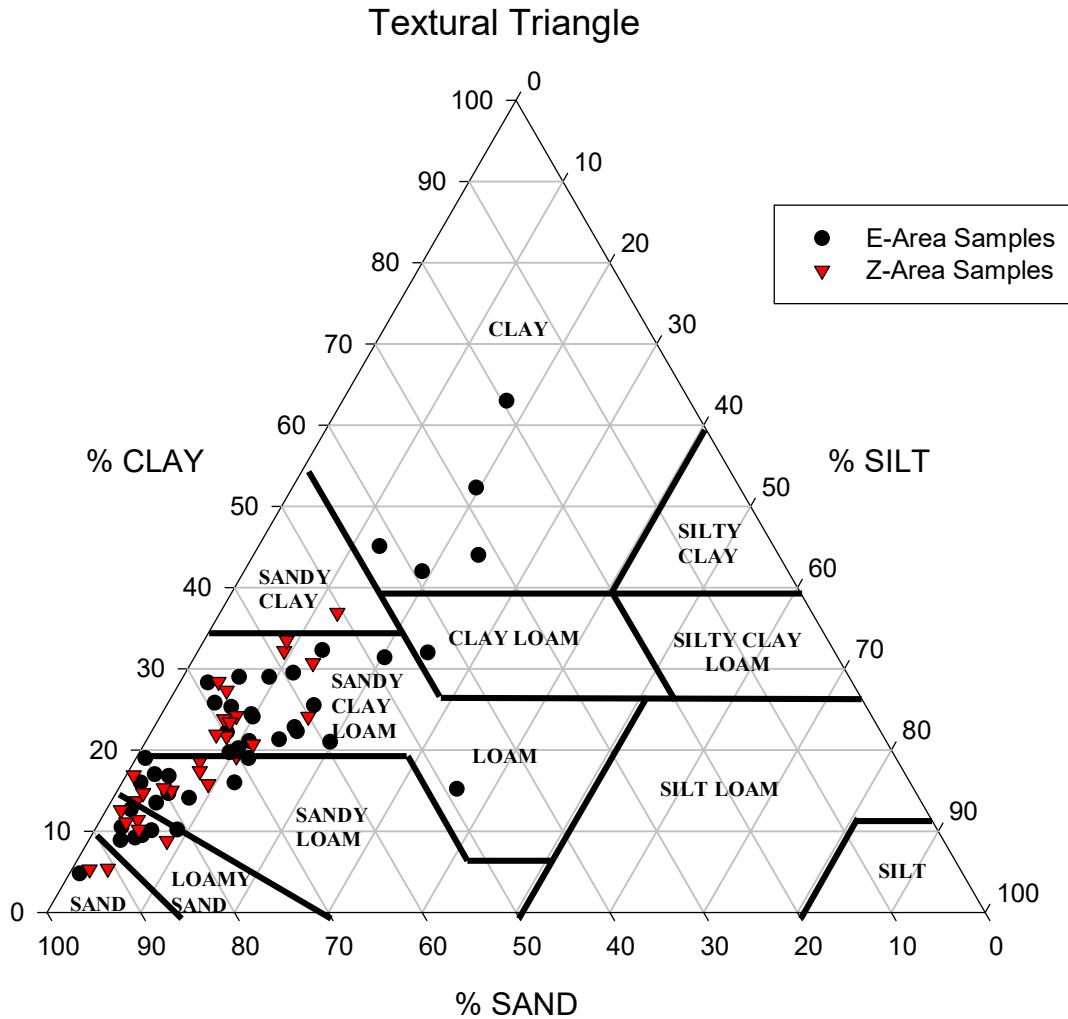


**Figure 5-3. Textural Triangle for E-Area and Z-Area vadose zone soils**

Out of the E-Area and Z-Area samples that have been classified using the USCS, most were designated as “SC” (clayey sands or sand-clay mixture). Table 5-4 provides a list of USCS classifications and the number of samples from E-Area classified in each category. Three materials were selected to represent the unsaturated zone materials in E-Area using grain size to differentiate the materials. These materials are “Sand” which consists of sediments with <25% Mud (silt + clay), “Clay Sand” which consists of sediments with >25% and <50% mud, and “Clay” which consists of >50% mud.

The unsaturated zone was divided into two zones, the Upper and Lower Zone, based on textural properties for purposes of representing the hydrologic processes that regulate groundwater flow. The Upper Zone consists of Clay and Clay-Sand and the Lower Zone consists of Clay-Sand and Sand.

**Table 5-4. E-Area vadose zone soils categorized by USCS**

Symbol	Classification Description <sup>1</sup>		# of Samples <sup>2</sup>
CH	>50% of material is smaller than #200 sieve (0.074 mm)	Inorganic clays of high plasticity; fat clays	2
SC	>50% of material is LARGER than #200 sieve (0.074 mm)	Clayey sands, sand-clay mixtures; more than ½ of coarse fraction is smaller than #4 sieve size	10
SM	>50% of material is LARGER than #200 sieve (0.074 mm)	Silty sands, sand-silt mixtures; more than ½ of coarse fraction is smaller than #4 sieve size	1

<sup>1</sup> from AGI Data Sheets (Dutro et al., 1989)

<sup>2</sup> includes only laboratory data where USCS classification was specified

In addition to describing the soils according to the USDA and USCS classifications systems, grain size data were further used to help evaluate hydraulic conductivity data as described in the next section.

## 5.2.2 Saturated Hydraulic Conductivity

### 5.2.2.1 Review of Data Quality

In the laboratory, sub-samples are typically collected from the original Shelby tube sample for vertical saturated hydraulic conductivity measurements. This process of sub-sampling can disturb the sample resulting in a hydraulic conductivity measurement unrepresentative of the original sample collected from the field. For this evaluation, bulk density measurements from the hydraulic conductivity samples were compared to the bulk density measurements of the original sample to validate that the sub-sample used in the laboratory test was similar to the original field sample. Hydraulic conductivity samples that had a bulk density within 5% of the original sample's bulk density were considered the most reliable. Figure 5-4 shows a comparison of the bulk density measurements with middle line representing a one-to-one relationship (measurements are the same) and the dashed outer lines representing 5% boundary. Four data points fall on or outside the 5% boundary (indicated by orange circles on the graph). Three of the four data points were removed from the dataset.

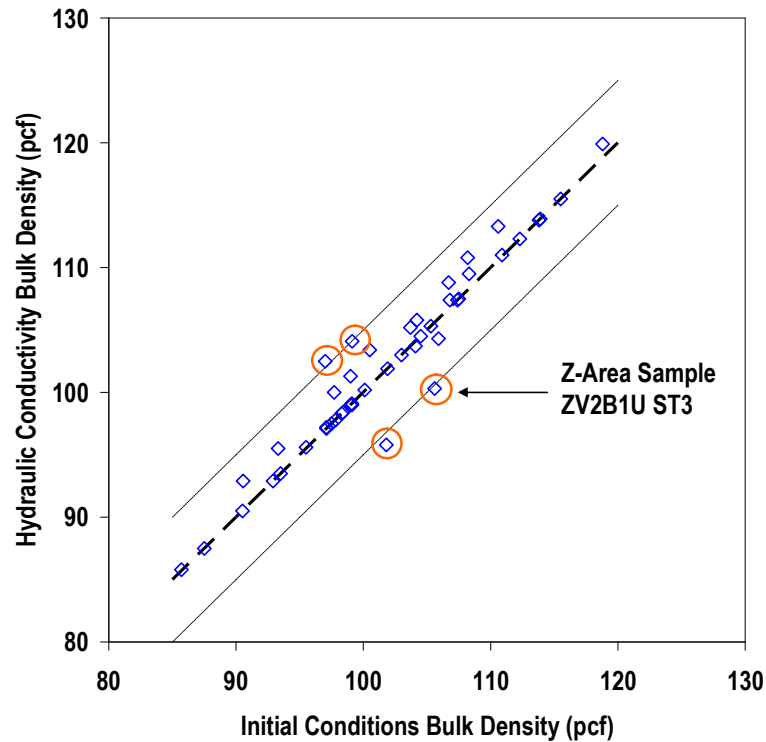


**Figure 5-4. Original sample bulk density versus bulk density of hydraulic conductivity samples**

The percent saturation and effective stress were also noted where the laboratory had provided data. Samples analyzed at saturations less than 90% were removed from the dataset. Because of the scarcity of data, samples in which the laboratory reports did not specify saturation were assumed to have been analyzed near or at saturation. The effective stress exerted on these laboratory samples during the hydraulic conductivity testing ideally would be low in order to represent typical field conditions. Because the samples come from the vadose in E- and Z-Area, there would be little overburden (or low effective stress). The BGST samples were measured at higher effective stresses than other samples in the dataset and higher than the stresses most likely to be encountered in the field. However, the BGST samples were included in this evaluation because of the scarcity of data and because their hydraulic conductivity measurements fell within the range of measurements for the other samples. Though samples from both E-Area and Z-Area were used in this data quality review, the discussion that follows focuses on the comparison of the E-Area grain size analyses with the hydraulic conductivity dataset.

Because the grain size analyses are more widespread and numerous than the hydraulic property datasets and percent mud is typically considered to have a controlling effect on hydraulic conductivity, the statistical distribution of percent mud was used to aid in determining whether samples analyzed for hydraulic properties were representative of area soils. Percent mud reflects the clay and silt size fraction from grain size analyses and includes the sediment fraction less than 0.074 mm in size (or 0.062 mm for a few of the labs).

As shown in Figure 5-5, a relationship is evident between percent mud and vertical saturated hydraulic conductivity for the samples used in this evaluation. As percent mud increases, the vertical saturated hydraulic conductivity decreases.

Logarithmic or arithmetic probability graphs have often been used in earth sciences to depict statistical distributions of various types of data (Sinclair, 1976). The probability plots in this report show the number of standard deviations across the top axis with “0” corresponding to the mean value of the graphed population. The cumulative percentage is given at the bottom of the graphs. The “y” axis provides the data (in this case, percent mud) on a logarithmic scale. On a probability plot with an arithmetic “y” axis, a normal population will plot as a straight line. On a probability plot with a logarithmic “y” axis, a log-normal population will plot as a straight line.

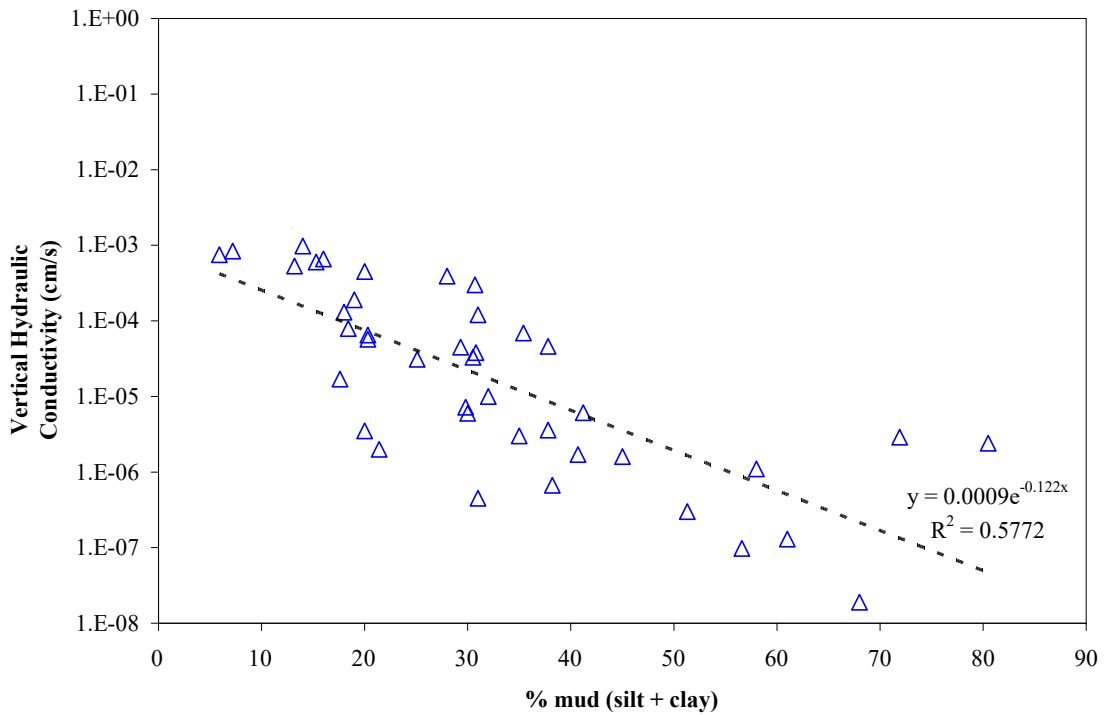


Figure 5-5. Percent mud vs vertical hydraulic conductivity

In general, the sample populations of percent mud in this study are log-normal. Figure 5-6 shows the cumulative distribution for percent mud for all of the samples in E-Area versus the percent mud in the samples analyzed for hydraulic conductivity. From the available data, the hydraulic conductivity samples appear to be representative of all E-Area grain size samples. However, it is important to note that most of the additional grain size data (samples collected where no hydraulic properties data were measured) predominately come from the engineered trenches and slit trenches rather than being distributed throughout E-Area. Table 5-5 provides percentages of the mud fraction for the E-Area sample population in relation to the samples used in this evaluation for hydraulic conductivity.

Because only four hydraulic conductivity measurements are available for Z-Area, these measurements were included with the E-Area dataset. Although the distribution of percent mud indicates there may be a difference in the grain sizes in E-Area versus Z-Area, there is currently not enough hydraulic conductivity data to differentiate hydraulic properties of the two areas.

**Table 5-5. Distribution of mud fraction in E-Area vs the hydraulic conductivity dataset**

<b>Mud fraction</b>	<b>All E-Area Data</b>	<b>Hydraulic Conductivity Dataset</b>
> 50% mud	14%	17%
25-50% mud	47%	46%
< 25% mud	39%	37%
Total	100%	100%

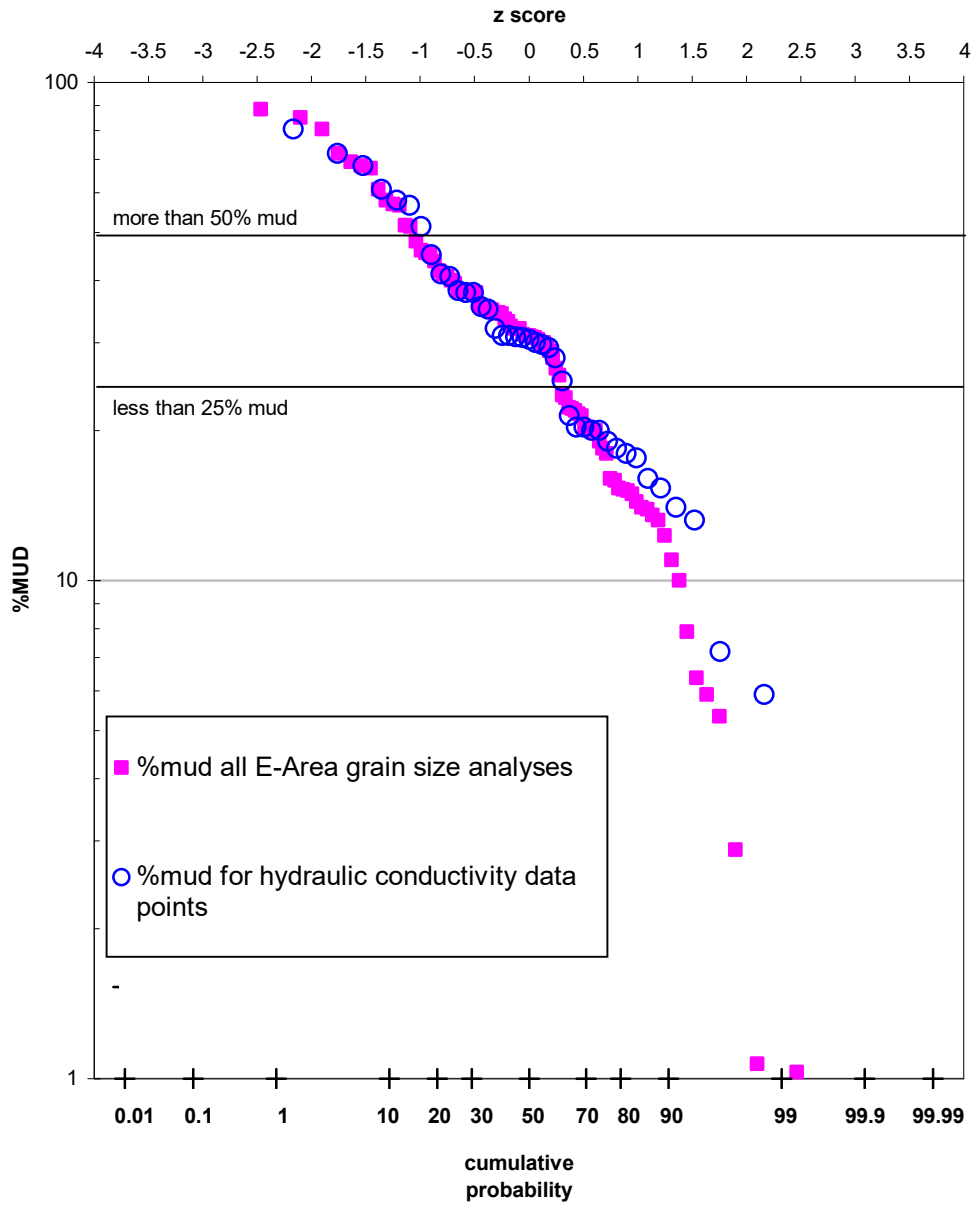


**Figure 5-6. Distribution of percent mud for all E-Area grain size analyses vs samples used in hydraulic conductivity evaluation**

### 5.2.2.2 Upscaling Methods

Atlantic Coastal Plain sediment deposits are naturally heterogeneous at multiple scales, and characterization data are invariably sparse. Adequately accounting for spatial variability in permeability is a challenge, and several modeling approaches have been developed. A common method is to generate upscaled conductivities for the horizontal and vertical directions based on stochastic methods, and use these values to define a homogeneous, but anisotropic, hydraulic conductivity field in numerical flow and transport modeling (Dagan and Neuman, 1997; Gelhar, 1993; Zhang, 2002). The goal of this approach is to reproduce the average flow behavior of the heterogeneous system. The effect of heterogeneity on solute transport, specifically field-scale dispersion, is captured through appropriate dispersivity settings in a Fickian dispersion model (Gelhar, 1997), or mobile fraction and mass transfer coefficient values in a dual-domain formulation (Fehley et al., 2000; Flach et al., 2004; Harvey and Gorelick, 2000).

Many concepts of geologic heterogeneity have been presented (Anderson, 1997). For the geologic setting at the Savannah River Site, a mixture of discrete and continuous representations of permeability variability is appropriate for dealing with multi-scale heterogeneity. The approach is to capture larger scale heterogeneity in the form of discrete formations and facies, and view conductivity as a distinct continuous statistical distribution within each facies (Brannan and Haselow, 1993; Jean et al., 2004; Webb and Anderson, 1996). Stochastic analysis can be used to derive upscaled conductivity values within each region of continuous permeability variation.

Upscaling refers to the process of replacing a heterogeneous conductivity field within a particular finite volume with a single, “equivalent”, conductivity value. The equivalent conductivity is defined as the value that reproduces some average behavior of the block, such as mean flow for a given head difference. A closely related problem is that of determining the “effective” conductivity of a heterogeneous media. The distinction is stated by Sanchez-Vila et al. (1995) as, “effective parameters are defined as representative values of the mean behavior through an ensemble of realizations, while equivalent parameters are associated with a certain geometry and defined as spatial averages computed on a single realization. These two definitions should converge to the same value for very large geometries and under the assumption of ergodicity.”

The stochastic approach is based on an assumed statistical distribution of small-scale or “point” values of conductivity ( $K$ ), and a spatial correlation model. Although not without shortcomings, hydraulic conductivity is often assumed to have a stationary log-normal distribution and a single correlation scale, on the basis of supporting characterization data (Freeze and Cherry, 1979) and partly for analytical convenience. Log-normal means that the natural logarithm of conductivity,  $\ln(K)$ , has a normal distribution. Stationary means that the statistical properties of the medium (mean, variance, spatial correlation) do not change with location within the region of interest. These assumptions are most reasonable in the context of a single facie, but can be applied to a formation with further approximation. Sarris and Paleologos (2004) have shown that log-normality is preserved as conductivity is upscaled, which supports the assumption regardless of scale of data observation (support scale).

Gelhar and Axness (1983) derived analytical expressions for the effective conductivity tensor of an infinite, ergodic, anisotropically-correlated medium with log-normally distributed conductivity, subjected to a uniform mean flow. The three-dimensional anisotropy of the heterogeneous medium is defined in terms an exponential covariance function with distinct correlation scales for each coordinate direction,  $\lambda_1$ ,  $\lambda_2$  and  $\lambda_3$

$$C(r_1, r_2, r_3) = \sigma^2 \exp \left[ - \left( \frac{r_1^2}{\lambda_1^2} + \frac{r_2^2}{\lambda_2^2} + \frac{r_3^2}{\lambda_3^2} \right)^{1/2} \right] \quad (1)$$

where

$C$   $\equiv$  covariance

$\sigma^2$   $\equiv$  variance of the natural logarithm of point conductivities

$r_i$   $\equiv$  distance between points in direction  $i$

$\lambda_i$   $\equiv$  integral scale for direction  $i$

As explained by Sarris and Paleologos (2004), the integral scale  $\lambda_i$  is the “length over which the value of the covariance function decreases by a factor of  $e^{-1}$  in direction  $i$ .” When the mean flow is aligned with the bedding plane ( $\lambda_1 = \lambda_2 > \lambda_3$ ), the non-zero components of the conductivity tensor are:

$$\overline{K_{11}} = \overline{K_{22}} = \overline{K_h} = K_g \left[ 1 + \sigma^2 \left( \frac{1}{2} - g_{11} \right) \right] = \quad (2)$$

$$\overline{K_{33}} = \overline{K_v} = K_g \left[ 1 + \sigma^2 \left( \frac{1}{2} - g_{33} \right) \right] \quad (3)$$

where:

$\overline{K_h}$   $\equiv$  effective horizontal conductivity

$\overline{K_v}$   $\equiv$  effective vertical conductivity

$K_g$   $\equiv$  geometric mean of point conductivity field = median =  $\exp(\mu)$ , where  $\mu$  is the mean of  $\ln(K)$

$\sigma^2$   $\equiv$  variance of the natural logarithm of point conductivities,  $\ln(K)$

and  $g_{11}$  and  $g_{33}$  are functions of the correlation scales. For case being considered here, they are defined in terms of the ratio of horizontal to vertical correlation,  $\rho = \lambda_h / \lambda_v > 1$ , as follows:

$$g_{11} = \frac{1}{2} \frac{1}{\rho^2 - 1} \left[ \frac{\rho^2}{(\rho^2 - 1)^{1/2}} \tan^{-1}(\rho^2 - 1)^{1/2} - 1 \right] \quad (4)$$

$$g_{33} = \frac{\rho^2}{\rho^2 - 1} \left[ 1 - \frac{1}{(\rho^2 - 1)^{1/2}} \tan^{-1}(\rho^2 - 1)^{1/2} \right] \quad (5)$$

The above analytical results are based on a first-order perturbation analysis, and strictly speaking, only exact in the limit as the variance approaches zero. Accurate results can be expected for small variances. For large variances, the predictions may become increasingly inaccurate, or even nonphysical. For example,  $\bar{K}_v$  is negative when  $\rho = \lambda_h / \lambda_v \rightarrow \infty$  and the variance of  $\ln(K)$  exceeds 2. To remedy such nonphysical results and hopefully extend the range of applicability of effective conductivity predictions, Gelhar and Axness (1983) proposed the following generalization of equations (2) and (3):

$$\bar{K}_h = K_g \exp \left[ \sigma^2 \left( \frac{1}{2} - g_{11} \right) \right] \quad (6)$$

$$\bar{K}_v = K_g \exp \left[ \sigma^2 \left( \frac{1}{2} - g_{33} \right) \right] \quad (7)$$

The generalization is motivated by the observation that a Taylor series expansion of equations (6) and (7) contains equations (2) and (3), respectively, as the first two terms. Subsequent comparison of equation (2) to numerical simulations indicates that the exponential generalization is accurate for isotropic systems and variances up to 7, but over predicts effective horizontal conductivity for anisotropic systems (Gelhar, 1997; Sarris and Paleologos, 2004).

Ababou and Wood (1990) note that equations such as (6) and (7) can alternatively be written in terms of a “p-norm” defined by

$$K_p \stackrel{\text{def}}{=} \left[ \frac{1}{N} \sum_i (K_i)^p \right]^{1/p} = (\bar{K}^p)^{1/p} \quad (8)$$

because

$$K_p = K_g \exp \left( \frac{p\sigma^2}{2} \right) \quad (9)$$

Comparing equations (6) and (7) with (9), one finds

$$p_h = 1 - 2g_{11} \quad (10)$$

$$p_v = 1 - 2g_{33} \quad (11)$$

where  $p_h$  and  $p_v$  are the averaging exponents associated with horizontal and vertical effective conductivity. That is, equations (6) and (7) are exactly equivalent to

$$\overline{K}_h = (\overline{K^{p_h}})^{1/p_h} \quad (12)$$

and

$$\overline{K}_v = (\overline{K^{p_v}})^{1/p_v} \quad (13)$$

As explained by Ababou and Wood (1990), the p-norm encompasses the familiar averages of arithmetic ( $p = 1$ ), geometric ( $p \rightarrow 0$ ), and harmonic ( $p = -1$ ) as well as any blend in between. In more recent years, numerous authors have developed expressions for effective conductivity based on less restrictive assumptions than those adopted by Gelhar and Axness (1983), such as bounded media with various boundary conditions, gradually varying mean flow, non-stationary conductivity, and radial flow. Frequently the effective conductivity is formulated as a power-average (8) with the power  $p$  having been determined from numerical simulations or a combined numerical-analytical approach (Sanchez-Vila et al., 1995).

The ratio of upscaled horizontal to vertical conductivity ( $R$ ) can be computed directly from:

$$R = \frac{\overline{K}_h}{\overline{K}_v} = \frac{(\overline{K^{p_h}})^{1/p_h}}{(\overline{K^{p_v}})^{1/p_v}} = \frac{K_g \exp\left[\sigma^2 \frac{p_h}{2}\right]}{K_g \exp\left[\sigma^2 \frac{p_v}{2}\right]} = \exp\left[\left(\frac{p_h - p_v}{2}\right) \sigma^2\right] \quad (14)$$

Note that the final result depends only on power-averaging exponents and the variance of point conductivity.

The related problem of determining “equivalent” block conductivities has received less attention in literature but is of great practical importance because "effective" conductivity estimates are strictly valid only for regions that span at least 10 or 100 times the integral correlation scale (Kitanidis, 1997). Frequently model blocks, and even the entire model domain, are not significantly larger than the scale of heterogeneity. This observation is especially supported by recent research that suggests variability exists at all scales without bound and motivates the use of fractal models. However, the concern can be alleviated by confining the continuous statistical model of permeability to a single facies (Anderson, 1991).

Sanchez-Vila et al. (1995) summarize and compare upscaling approaches proposed to-date. Two out of the four approaches reviewed by Sanchez-Vila et al. (1995) are practical in that a mechanism for computing block conductivity from point values was provided by the author(s). Of these approaches, Desbarats (1992) is particularly appealing because of its simplicity. Desbarats (1992) conjectured that equivalent block conductivities can be formulated as a power-average, a reasonable hypothesis considering the successful use of p-norms in defining effective conductivity. Desbarats (1992) empirically determined the appropriate power through numerical experimentation. For cubic blocks and an isotropic conductivity field, the optimal averaging exponent was determined to be  $p = 1/3$ . Interestingly, this is the same power as is appropriate for the effective conductivity of an infinite domain, as can be seen from equations (4) and (10). As Desbarats (1992) notes, this observation further supports the empirical result.

For an anisotropic media with  $\lambda_h/\lambda_v = 10$  and block dimensions of  $L_h/\lambda_h = L_v/\lambda_v = 3$ , the optimal averaging exponents were found through numerical experimentation to be  $p_h = 0.59$  and  $p_v = -0.33$ . Unlike the isotropic case, these results differ from the averaging exponents for effective conductivity of an infinite medium with  $\lambda_h/\lambda_v = 10$ . The latter results are  $p_h = 0.86$  and  $p_v = -0.72$  (see equations (4), (5), (10) and (11)). The discrepancy may be a reflection of equation (2) already over predicting  $K_h$  in infinite anisotropic media for large variances, as previously stated. Desbarats (1992) recommends that numerical calibration experiments be used to define the power exponents for the specific combination of block geometry and correlation scales of interest. However as Desbarats (1992) notes, equations such as (10) and (11) give the correct values for the limiting cases of an isotropic or perfectly stratified medium, and “provide a convenient alternative to tedious numerical experiments”.

Sarris and Paleologos (2004) performed a similar numerical investigation as Desbarats (1992) over a larger range of conditions. For an anisotropic media with  $\lambda_h/\lambda_v = 10$  and block dimensions of  $L_h/\lambda_h = L_v/\lambda_v = 8$ , the optimal averaging exponents were found to be  $p_h = 0.40$  and  $p_v = 0.05$ . Table 5-6 summarizes the power-average exponents estimated from the three studies discussed. Sarris and Paleologos (2004) and Desbarats (1992) considered different block sizes ( $L/\lambda$ ), which presumably explains the difference between their results.

The stochastic analyses described above can be used to interpret small-scale permeability data as follows. For each formation:

- Develop a statistical distribution of small-scale or “point” conductivities ( $K$ ) from laboratory measurements of permeability and other information. A log-normal distribution with mean ( $\mu$ ) and variance ( $\sigma^2$ ) for  $\ln(K)$  is presumed to adequately represent reality.

- Estimate the degree of spatial continuity in the horizontal and vertical directions. Spatial correlation is presumed to be adequately defined by an exponential covariance model, where anisotropy is specified by the ratio of horizontal to vertical correlation lengths ( $\lambda_h / \lambda_v$ ) for point conductivities.
- Calculate upscaled horizontal and vertical conductivities using equation (9) and appropriate power-average exponents ( $p_h, p_v$ ). Table 5-6 is a likely source for the latter. Anisotropy in upscaled conductivity can be computed from equation (14).
- Alternatively, compute upscaled conductivities directly from permeability data using equation (8) and appropriate power-average exponents. In this case, the first step above can be omitted, as the power-average exponents depend only on  $\lambda_h / \lambda_v$ .

Atlantic Coastal Plain sediments are clearly stratified and imply anisotropic correlation scales,  $\lambda_h$  and  $\lambda_v$ . Judgment based on knowledge of the depositional environment and visual inspection of outcrops suggests a reasonable ratio is roughly  $\lambda_h / \lambda_v = 10$ . Values for this level of anisotropy have been presented in Table 5-6 for regions of varying size ( $L/\lambda$ ). If upscaled conductivities are desired for the entire thickness and a large horizontal extent of a formation, then  $L/\lambda$  could be considered large within the context of the assumed geostatistical model, which incorporates a single correlation scale. However, a stationary log-normal geostatistical model applied to a formation does not incorporate larger scale heterogeneity or spatial continuity, as stated earlier. This recognition suggests a much lower assumption for  $L/\lambda$ .

Gelhar and Axness (1983) provide values for an infinite extent, but these values are biased toward the end members of  $p_h = 1$  and presumably  $p_v = -1$ , when variance is high. As block size decreases, the exponents contract toward  $p = 0$  with  $L/\lambda = 8$ , but the trend reverses in going to  $L/\lambda = 3$ . The optimal choice for the present application is not obvious. The values reported by Desbarats (1992) of  $p_h = +0.59$  and  $p_v = -0.33$  are in the middle of those presented in Table 5-6, and were chosen for this application.

Laboratory measurements for vertical hydraulic conductivity were assumed to reflect horizontal hydraulic conductivity for upscaling purposes. This assumption is thought to be valid because the laboratory sample sizes are small and thus the measurements likely reflect a homogeneous hydraulic conductivity. If there is significant preferential deposition or weathering of minerals, this assumption may be slightly biased.

**Table 5-6. Upscaling parameters for hydraulic conductivity**

Values	Conductivity $K$	Method	Block Size $L/\lambda$	Anisotropy $\lambda_h / \lambda_v$	Horizontal exponent $p_h$	Vertical exponent $p_v$
Gelhar and Axness (1983)	Effective	Analytical	Infinite	10	+0.86	-0.72
Desbarats (1992)	Equivalent	Numerical	3	10	+0.59	-0.33
Sarris and Paleologos (2004)	Equivalent	Numerical	8	10	+0.40	+0.05
Selected for SRS application	-	-	-	-	+0.59	-0.33

**5.2.2.3 Saturated Hydraulic Conductivity Calculations**

Using the described upscaling method, horizontal ( $K_h$ ) and vertical ( $K_v$ ) conductivities were calculated for the undisturbed vadose zone soils. Laboratory data were subdivided according to the following textural properties:

- >50% mud (generalized as “clay”)
- 25-50% mud (generalized as “clay-sand”)
- <25% mud (generalized as “sand”)

$K_h$ , and  $K_h/K_v$  for these textural classes are provided in Table 5-7. Also included in this table are water retention parameters, bulk properties and saturated effective diffusion coefficients for these materials which are discussed later in sections 5.2.3, 5.2.4 and 5.2.5, respectively.

**Table 5-7. Material properties for textural soil types in the E-Area LLWF**

Property	Material		
	Sand	Clay-Sand	Clay
$K_{sat}$ , cm/sec <sup>1</sup>	2.8E-4	3.5E-5	7.2E-7
$K_h/K_v$ <sup>1</sup>	4.3	4.8	3.4
# of samples used in $K_h/K_v$ calculations	15	19	7
Porosity, $n$	0.383	0.374	0.433
Dry bulk density, $\rho_b$ , gm/cm <sup>3</sup>	1.65	1.68	1.52
Particle density, $\rho_p$ , gm/cm <sup>3</sup>	2.67	2.69	2.68
# of sample data points used in vG parameter estimation	30	30	15
$\theta_s$	0.383000	0.374000	0.433000
$\theta_r$	0.082137	0.057974	0.278156
$\alpha$	0.199006	0.035465	0.009832
$n$	1.241769	1.140621	1.287965
$m$	0.194697	0.123285	0.223581
Tortuosity, $\tau$	2.0	3.0	4.0
Effective Diffusion Coefficient, $D_e$	8.0E-6	5.3E-6	4.0E-6

<sup>1</sup> These are initial  $K_{sat}$  values & ratios for the textural soil types based on the data sample mean. Final  $K_{sat}$  values found in Table 5-9 were estimated based on a +2-sigma adjustment to obtain better agreement with field monitoring data. See Section 5.8 and Table 5-18 for explanation

Saturated hydraulic conductivities have also been estimated for upper and lower vadose zone hydrostratigraphic units in E-Area. Grain size data, visual core descriptions and CPT logs indicate that the upper and lower vadose zone have different textural properties. Figure 5-7, which shows the CPT logs from a location near the Slit Trenches, illustrates this difference. Using the CPT logs and grain size analyses, hydraulic laboratory data were lumped into an upper zone and lower zone. These data were then upscaled using the methods in Section 5.2.2.2 (where  $p_h = +0.59$  and  $p_v = -0.33$ ) to generate  $K_h$  and  $K_v$  for the upper vadose zone and lower vadose zone.  $K_h$ , and  $K_h/K_v$  for these vadose zone units are provided in Table 5-9. Results show that the upper zone has a lower  $K_h$  and  $K_v$  than the lower zone reflecting the greater abundance of fine-grained sediments and heterogeneity in the upper zone. Also included in this table are water retention parameters, bulk properties and saturated effective diffusion coefficients for these hydrostratigraphic units which are discussed later in sections 5.2.3, 5.2.4 and 5.2.5, respectively.

Using available CPT logs, visual core descriptions and grain size analyses, the boundaries of the upper and lower zone was defined across E-Area (Bagwell and Bennett, 2017). Bagwell and Bennett (2017) identified the top and bottom of the primary hydrogeologic units beneath the center of each of the waste units in the E-Area LLWF. Figure 5-9 is a cross-section

along the transect shown in Figure 5-8 (red line) illustrating the various hydrogeologic units beneath each waste unit. It is important to note that the Upper Zone is absent in the western part of the E-Area LLWF and the lower zone crosses below the Tan Clay in the west as well due to a declining water table.

Calculated  $K_h$  and  $K_v$  values using the described approach is within the range of  $K_h$  and  $K_v$  measured from pump tests for the water table aquifer near TNX and D-Area. Although the measurements reflect the saturated zone, the water table aquifer at TNX and D-Area is similar to the vadose zone in E-Area. At TNX and D-Area, the water table aquifer is approximately 40 to 60 ft in thickness and consists of a highly layered system of fine sands, silts and clays. The vadose zone at E-Area has a similar thickness and is likewise comprised of layers of sands, silts and clays. Data from the TNX and D-Area pump tests (Phifer et al. 2000) were used for comparative purposes to confirm that the  $K_h$  and  $K_v$  calculated in this evaluation are reasonable estimates.

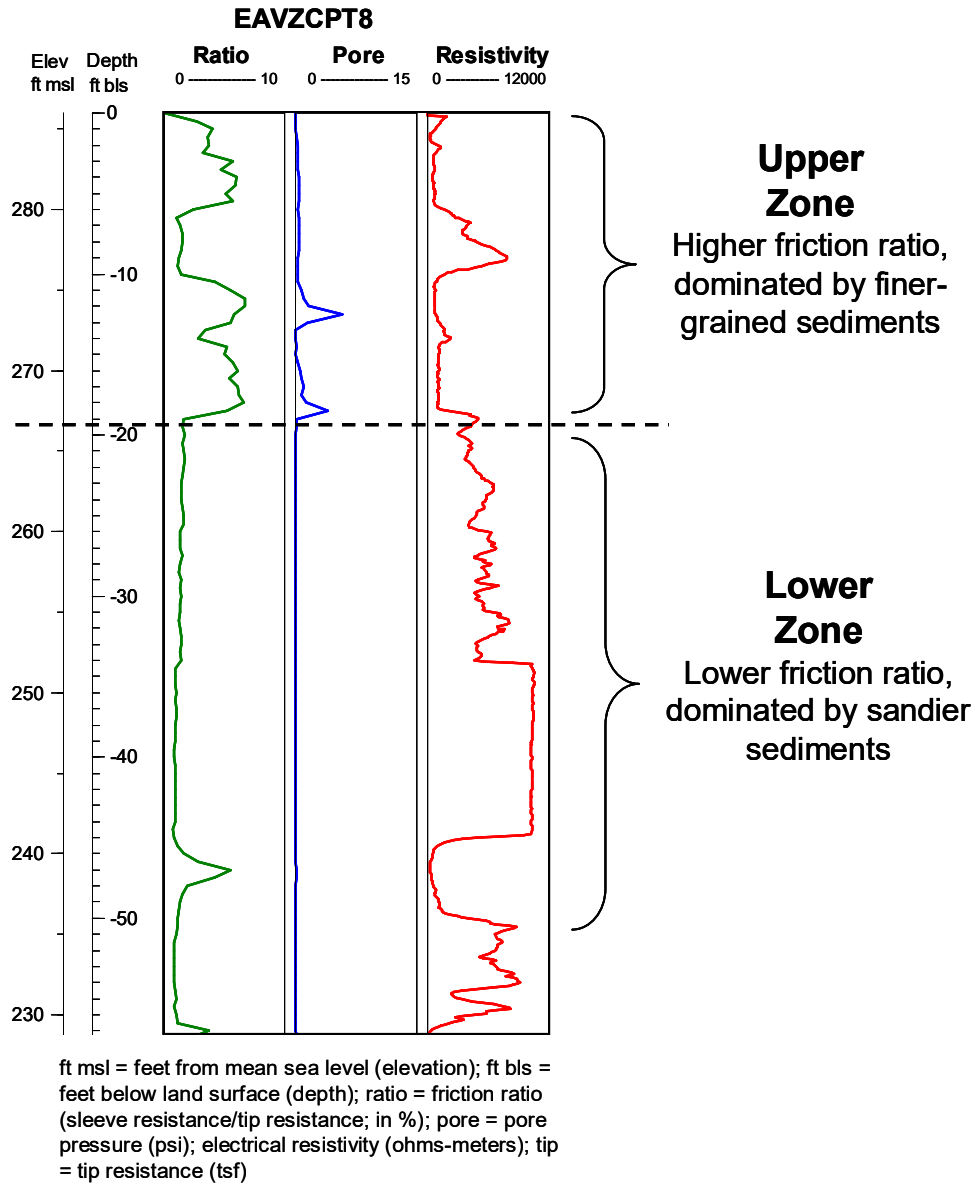


**Figure 5-7. Upper and Lower Zones for EAVZCPT8**

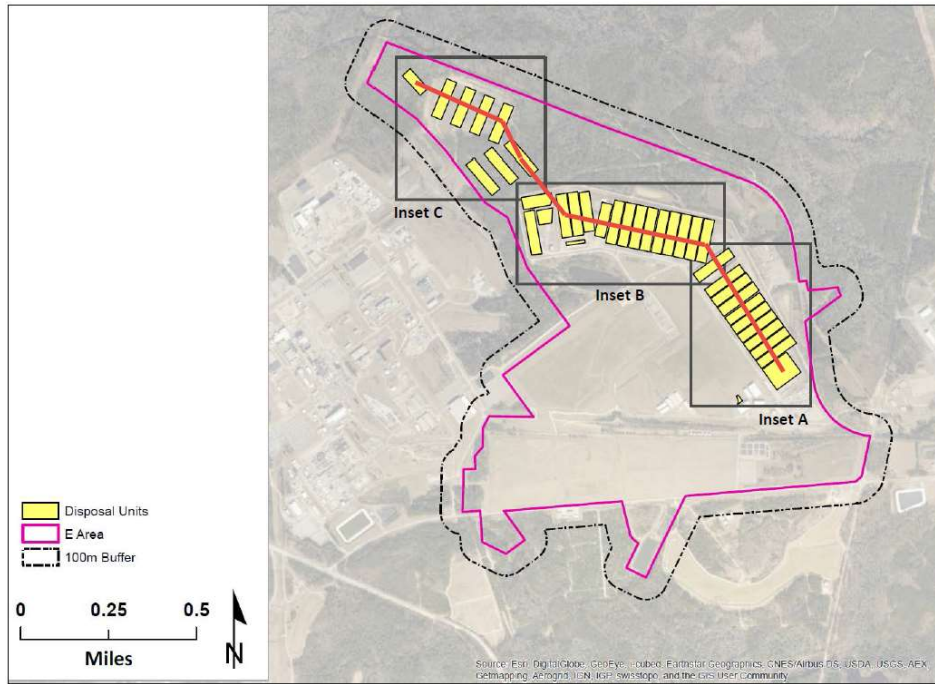


**Figure 5-8. E-Area Map showing transect for cross-section, modified from Bagwell and Bennett (2017)**

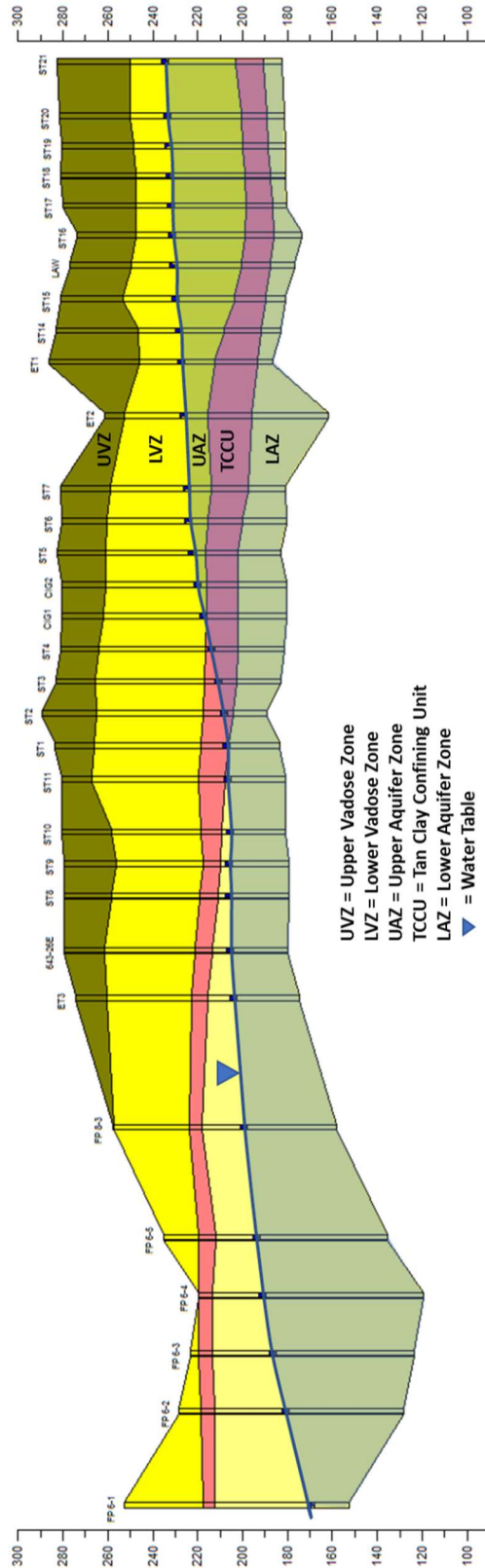


Figure 5-9. Cross-section of Transect 1 in E-Area

Table 5-8 provides data from these pump tests.  $K_h$  measurements at TNX and D-Area vary between 5.9E-5 cm/sec (0.17 ft/day) and 1.1E-2 cm/sec (30.6 ft/day).  $K_v$  measurements vary between 9.4E-6 cm/sec (0.03 ft/day) and 7.1E-4 cm/sec (2.0 ft/day).  $K_h/K_v$  varies between 2 and 42.

**Table 5-8. Pump test results from the water table aquifer at TNX and D-Area**

Well ID	Area	$K_h$ (cm/s)	$K_v$ (cm/s)	$K_h/K_v$	Analysis Method	Aquifer Thickness (ft)	Source
DCB-8	D-Area	4.0E-04	9.4E-06	42.1	Neuman	64.0	Phifer et al, 2000
DGP-17	D-Area	5.5E-04	5.9E-05	9.3	Neuman	64.0	Phifer et al, 2000
DCB-2A	D-Area	8.1E-04	3.8E-05	21.4	Quick Neuman	64.5	Phifer et al, 2000
TCM-2	TNX	1.1E-02	4.6E-04	23.5	Neuman	42.0	Phifer et al, 1998
TCM-1	TNX	6.6E-03	7.1E-04	9.4	Neuman	42.0	Phifer et al, 1998
TNX-11D	TNX	3.2E-03	2.4E-04	13.7	Neuman	42.0	Phifer et al, 1998
DCB-24A	D-Area	5.9E-05	2.8E-05	2.1	Neuman	48.5	Phifer et al, 1996
DCB-24B	D-Area	3.4E-04	3.2E-05	10.6	Neuman	48.5	Phifer et al, 1996
DCB-24C	D-Area	1.1E-03	9.1E-05	12.1	Neuman	48.5	Phifer et al, 1996

### 5.2.3 Water Retention

The water retention characteristics of sediments are commonly represented by water retention curves (WRCs) based on a closed form equation published by van Genuchten (1980). The van Genuchten equation relates water content ( $\theta$ ) [and thus water saturation ( $S$ )] to pressure head ( $\psi$ ) which can be used with laboratory data to determine the van Genuchten (VG) parameters for a water retention curve, equations (15) and (16).

$$S_e = [1 + |\alpha\psi|^n]^{-m} \quad (15)$$

$$S_e = \frac{\theta - \theta_r}{\theta_s - \theta_r} \quad (16)$$

$S_e$  = effective water saturation

$\alpha$  and  $n$  are fitting parameters (i.e., shape factors)

$\psi$  = pressure head

$m = 1 - 1/n$  (constraint to yield close form permeability expressions)

$\theta$  = water content

$\theta_s$  = total porosity

$\theta_r$  = residual water content

WRCs for individual samples of the vadose zone were developed by determining VG parameters using a least squares regression method to fit the data. An unweighted least-squares fit method was implemented using the SOLVER routine in MS Excel. Figure 5-10 shows an example of the results from fitting laboratory data for six sand samples with the VG equation to develop VG parameters for a WRC. Circles represent laboratory data and lines represent the WRCs for each of the samples considered.

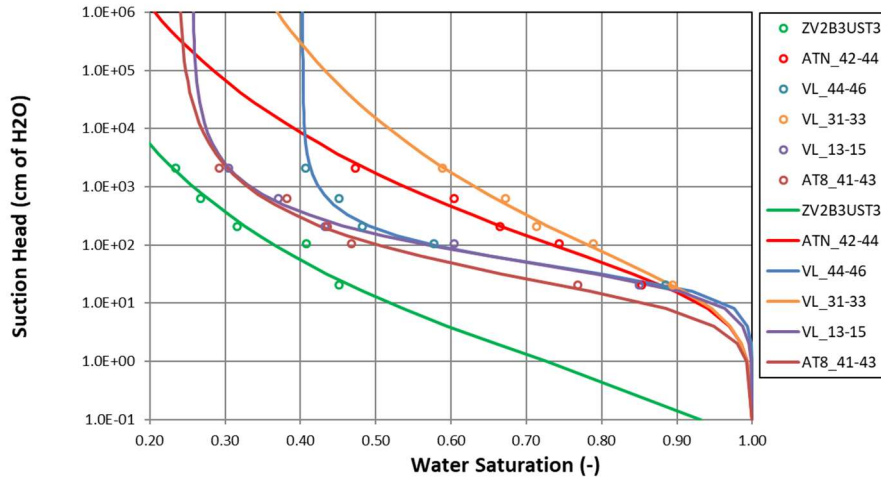


**Figure 5-10. Data and WRCs for sand samples**

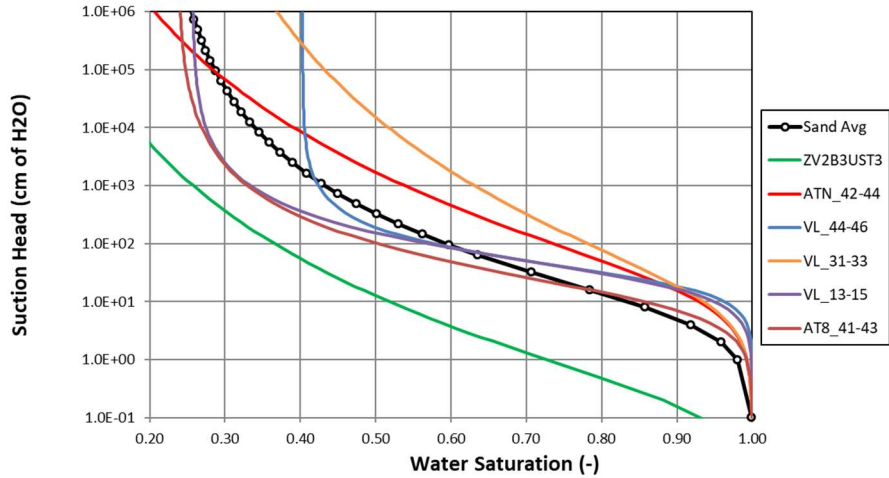
Once WRCs were developed for individual soil samples they were grouped by previously identified textural classes to produce representative soil types. The WRCs in each textural class were then composited to develop a WRC and VG parameters for the representative soil type (i.e., “sand”, “clay-sand”, and “clay”, see Table 5-7). Suction head at five different water contents were measured for each soil sample. Six, six, and three soil samples were considered for the “sand”, “clay-sand”, and “clay” soil types, respectively. Individual samples were composited in a class by averaging the water content ( $\theta$ ) for each sample ( $i$ ) at selected suction heads ( $\psi$ ), equation (17).

$$\overline{s_{\psi_j}} = \frac{1}{n} \sum_{i=1}^n s_i(\psi_j) \quad (17)$$

$s_i$  = Saturation at suction ( $\psi_j$ ) for material  $i$   
 $n$  = total number of samples for specific soil type

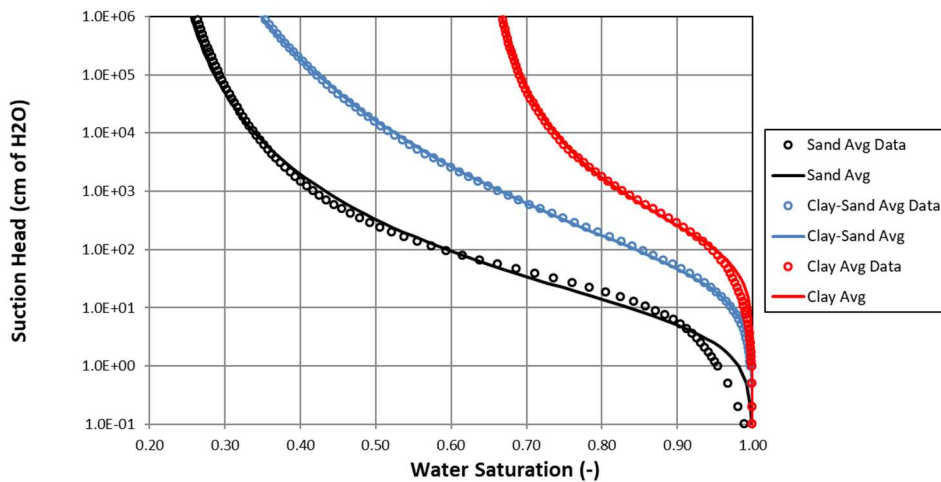
Uniform weighting of the composite soil type was employed.

Figure 5-11 shows the WRC for individual samples identified as sand and the resulting data set for the representative soil type Sand WRC.



**Figure 5-11. WRCs for individual samples identified as sand and the resulting WRC for the representative soil type Sand**

The resulting composited data sets for each of the 3 representative soil types were fit to the VG equation to determine VG parameters using the previously described least squares method. Figure 5-12 shows the composite data set and WRC curve for each of the representative soil types.



**Figure 5-12. Data and WRCs for representative soils types Clay, Clay-Sand, and Sand**

van Genuchten (1980) published a closed form equation (18) for predicting the relative hydraulic conductivity ( $K_{rel}$ ) of soils relating  $K_{rel}$  to  $\Psi$  that uses the VG parameters derived from  $S_e, \psi$  data described above.

$$K_{rel} = S_e^L \left[ 1 - \left( 1 - S_e^{1/m} \right)^m \right]^2 \quad (18)$$

Relative hydraulic conductivity curves for each of the representative soil types can be calculated using the MvG equation (18) are presented in Figure 5-13.

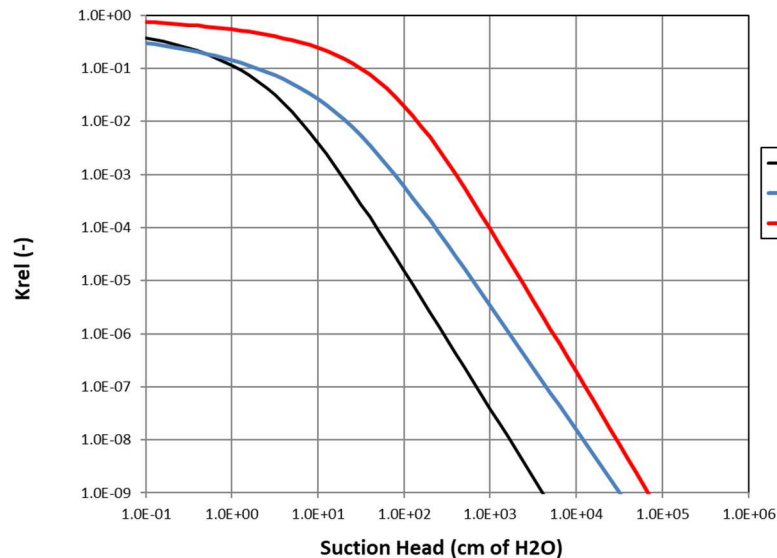


**Figure 5-13. Relative hydraulic conductivity curves for representative soil types Clay, Clay-Sand, and Sand**

For a representative location (AT-North/Megacptnorth), data were categorized into an Upper Zone and Lower Zone, and thicknesses of the representative soil types (“sand”, “clay-sand” and “clay”) were determined using CPT logs, visual core descriptions and grain size analyses.

Figure 5-14 shows the representative soil types and layer thicknesses comprising the upper and lower vadose zone at this location. Using these thicknesses, a proportion (or percentage) of the textural categories was computed for the upper and lower zones. For example, the 21.5-foot thick upper zone consisted of approximately 81% “clay-sand” and 19% “clay”. The soil moisture profiles for the “clay”, “clay-sand” and “sand” were then combined into one curve based on the proportion of each textural category. The method of using a representative location, textural properties and layer thicknesses appeared to provide curves that were representative of the “average” conditions for the Upper and Lower zones and less influenced by outlier samples compared to averaging data for each zone with no account for thicknesses of the various soil types.

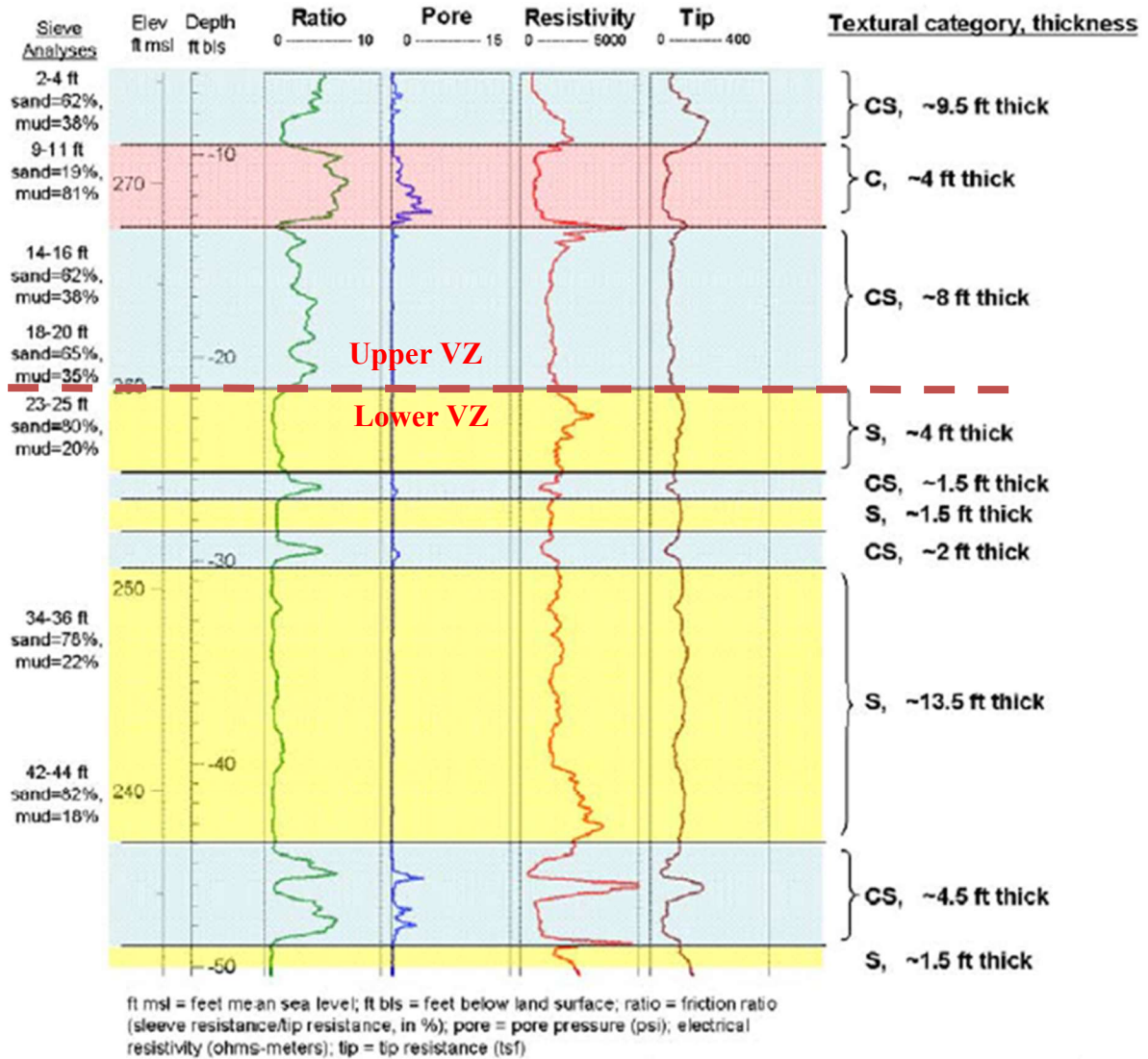


Figure 5-14. Identification of representative soil types and layer thicknesses comprising upper and lower vadose zone at AT-North/Megacptnorth

VG parameters were calculated for the Upper Vadose Zone (UVZ) and Lower Vadose Zone (LVZ) by compositing the appropriate representative soil types. The UVZ is represented by 81 % Clay-Sand and 19 % Clay. WRCs for these two representative soil types were composited to develop a data set for the Upper Zone using equation (19) The resulting data set was then analyzed using previously described method to determine VG parameters for the Upper Zone.

$$S_{UZ}(\psi_i) = 0.81 * S_{ClSd}(\psi_i) + 0.19 * S_{Cl}(\psi_i) \quad (19)$$

The LVZ is represented by 72 % Sand and 28 % Clay-Sand. WRCs for these two representative soil types were composited to develop a data set for the LVZ using equation (20). The resulting data set was then analyzed using the previously described method to determine VG parameters for the Lower Zone.

$$S_{LZ}(\psi_i) = 0.72 * S_{Sd}(\psi_i) + 0.28 * S_{ClSd}(\psi_i) \quad (20)$$

Figure 5-15 and Figure 5-16 show the WRC and  $K_{rel}$  curves for the Upper and Lower Zone respectively.

VG parameters for all vadose zone soil categories (i.e., undisturbed and disturbed soils) are provided in Table 5-9 along with saturated hydraulic conductivity values, bulk properties and saturated effective diffusion coefficients for these materials. Derivations of these property values for Controlled Compacted Backfill (CCB), Operational Soil Cover (OSC), IL Vault Permeable Backfill (PB) and Gravel are discussed later in sections 5.3, 5.4 and 5.5, respectively.

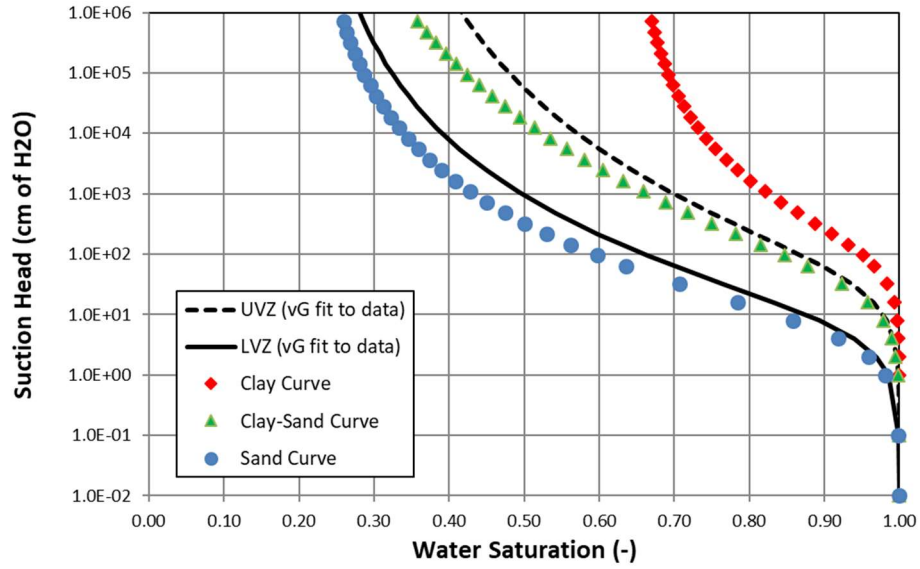


Figure 5-15. WRCs for Upper Zone and Lower Zone

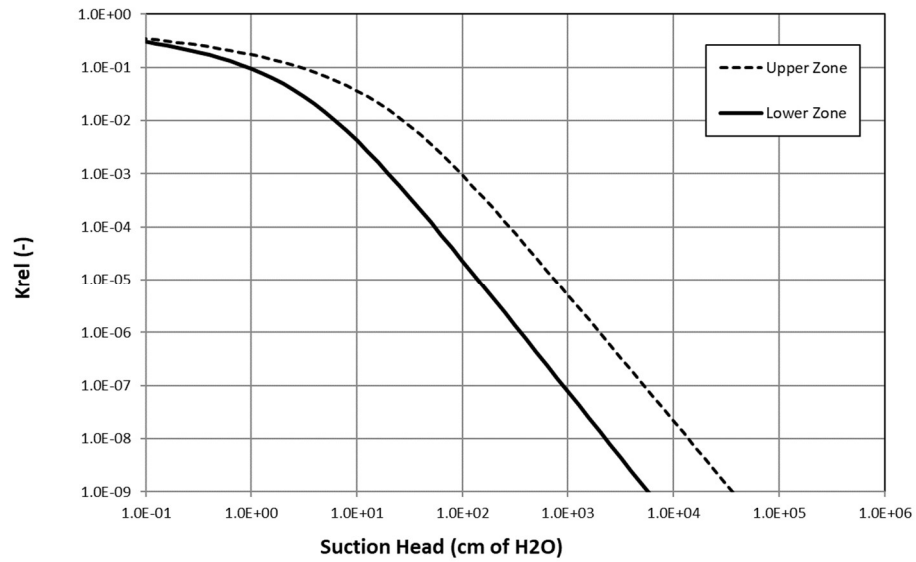


Figure 5-16. Relative hydraulic conductivity curve for Upper Zone and Lower Zone

Table 5-9. Material properties for vadose zone soils in the E-Area LLWF

Property	Material						
	Undisturbed Vadose Zone Soils		Disturbed Soils				
	Upper Zone (UZ)	Lower Zone (LZ)	Operational Soil Cover			IL Vault Permeable Backfill (PB)	Gravel (G1)
			Controlled Compacted Backfill (CCB)	Before Dynamic Compaction (OSC1)	After Dynamic Compaction (OSC2)		
$K_{sat}$ , cm/sec	3.2E-5 <sup>1</sup>	1.8E-4 <sup>1</sup>	7.6E-5	1.2E-4	1.4E-5	1.4E-3	1.0E-2
$K_h/K_v$	22 <sup>1</sup>	4.5 <sup>1</sup>	1.9	1	1	1.9	1
Porosity, $n$	0.385 <sup>2</sup>	0.380 <sup>2</sup>	0.355	0.456	0.275	0.415	0.300
Dry bulk density, $\rho_b$ , gm/cm <sup>3</sup>	1.65 <sup>2</sup>	1.66 <sup>2</sup>	1.71	1.44	1.92	1.56	1.82
Particle density, $\rho_p$ , gm/cm <sup>3</sup>	2.69 <sup>2</sup>	2.67 <sup>2</sup>	2.65	2.65	2.65	2.67	2.60
$\theta_s$	0.385000	0.380000	0.355000	0.456000	0.275000	0.415000	0.300000
$\theta_r$	0.102446	0.077849	0.198349	0.121330	0.073171	0.136697	0.021000
$\alpha$	0.030177	0.167698	0.037124	0.040416	0.018263	0.037919	0.137676
$n$	1.153676	1.195226	1.463642	1.153656	1.153659	1.724947	1.479624
$m$	0.133205	0.163338	0.316773	0.133191	0.133193	0.420272	0.324153
Effective Diffusion Coefficient, $D_e$	5.3E-6	5.3E-6	5.3E-06	5.3E-06	4.0E-06	8.0E-06	9.4E-06

<sup>1</sup> These are initial  $K_{sat}$  values & ratios for undisturbed VZ soils based on the data sample mean. Final  $K_{sat}$  values found in Table 5-9 were estimated based on a +2-sigma adjustment to obtain better agreement with field monitoring data. See Section 5.8 and Table 5-18 for explanation.

<sup>2</sup> For consistency with water retention calculations, bulk material properties (total porosity, dry bulk density and particle density) for the UVZ and LVZ are based on the weighted volume fraction of sand, clayey-sand and clay in each zone at a single E-Area representative sample location (AT-North/Megacptnorth, Figure 5-14) and not the average of the overall dataset.

#### 5.2.4 Porosity, Bulk Density, Particle Density

Porosity values reflect laboratory measurements of the total volume of pore space in the soil samples. Because samples were collected from the vadose zone, where flow primarily occurs in the vertical direction perpendicular to strata, the total porosity was assumed to be roughly equivalent to the effective porosity. Bulk density corresponds to the dry bulk density or the total mass of dry soil per unit volume of material (including pore spaces). Particle density reflects the mass of dry soil particles per unit volume of soil particles (not including pore space). Particle density was calculated using laboratory measurements of porosity and dry bulk density according to:

$$\rho_p = \frac{\rho_b}{(1 - \eta)} \quad (21)$$

where  $\rho_p$  = particle density,  $\rho_b$  = dry bulk density, and  $\eta$  = porosity (Hillel, 1982).

Total porosity, bulk density, and particle density were calculated for the UVZ and the LVZ. Calculations for these categories entailed arithmetic averaging of laboratory data. Estimates for the textural property categories (i.e., “clay”, “clay-sand” and “sand”) included all samples for which corresponding grain size data were available. All available laboratory data were lumped into either the upper or lower vadose zone using CPT logs and visual core descriptions and arithmetically averaged. Table 5-10 provides ranges of the laboratory data along with the calculated averages. Porosity measurements ranged from 29% to 48%; dry bulk density ranged from 1.37 g/cm<sup>3</sup> to 1.90 g/cm<sup>3</sup>; and particle density varied from 2.61 g/cm<sup>3</sup> to 2.81 g/cm<sup>3</sup>.

#### 5.2.5 Saturated Effective Diffusion Coefficient ( $D_e$ )

For this evaluation, the effective diffusion coefficient ( $D_e$ ) is defined as the molecular diffusion coefficient ( $D_m$ ) divided by the porous medium tortuosity ( $\tau$ )

$$D_e = \frac{D_m}{\tau} \quad (22)$$

Note that  $D_e$  does not include the effects of sorption or porosity.  $D_m$  is the aqueous diffusion coefficient of a chemical species in open or pure water. Because no measured effective diffusion data were available from laboratory data or literature for soils typical of E-Area and Z-Area, generic literature values for  $D_m$  and  $\tau$  were used to calculate  $D_e$ .

**Table 5-10. Summary bulk properties for vadose zone soils & Controlled Compacted Backfill**

Material Description	Porosity (unitless)			Bulk Density g/cm <sup>3</sup>			Particle Density <sup>1</sup> g/cm <sup>3</sup>		
	min	max	avg	min	max	avg	min	max	avg
Upper Vadose Zone (Above 264 ft-msl in E-Area) <sup>2</sup>	0.290	0.480	0.385	1.40	1.90	1.65	2.63	2.73	2.69
Lower Vadose Zone (Below 264 ft-msl in E-Area) <sup>2</sup>	0.330	0.480	0.380	1.37	1.80	1.66	2.61	2.81	2.67
Sand (<25% Mud)	0.330	0.430	0.383	1.50	1.80	1.65	2.63	2.72	2.67
Clay-Sand (25-50% Mud)	0.290	0.470	0.374	1.49	1.90	1.68	2.61	2.81	2.69
Clay (>50% Mud)	0.360	0.480	0.433	1.37	1.72	1.52	2.64	2.73	2.68
Controlled Compacted Backfill	0.290	0.420	0.355	1.55	1.86	1.71	2.62	2.68	2.65

<sup>1</sup> Particle density calculated; particle density = dry bulk density/(1-porosity) (from Hillel, 1982)

<sup>2</sup> Average values for bulk properties obtained from samples used in estimating the weighted volume fraction of sand, clayey-sand and clay in each zone at a single E-Area representative sample location (AT-North/Megacptnorth, Figure 5-14). Min and max values taken from the overall sample dataset.

Table 5-11 provides molecular diffusion coefficient values ( $D_m$ ) from the literature for several inorganic compounds and ions. Overall, the  $D_m$  values range from 8.5E-6 to 2.0E-5 cm<sup>2</sup>/s (Bruins, 2003; Faure, 1991; Robinson and Stokes, 1955). A  $D_m$  value of 1.6E-5 cm<sup>2</sup>/s was used for the  $D_e$  calculations. This value is based on measurements of sodium chloride (NaCl) in a dilute solution. In high concentration solutions, the movement of the solvent molecules will affect the movement of the solute molecules or ions. However, in dilute solutions, the diffusion coefficients are considered to represent the motion of the solute molecules or ions through a stationary solvent.

Tortuosity ( $\tau$ ) corrects for the geometry of the pore space in the sediments. It is often defined as:

$$\tau = \left(\frac{l_e}{l}\right)^2 \quad (23)$$

where  $\tau$  = tortuosity or tortuosity factor,  $l_e$  = the true or effective path length, and  $l$  = the shortest distance through a porous medium (or the direct path from higher concentration to lower concentration) (Boving and Grathwohl, 2001; Dykhuizen and Casey, 1989; Maerki et al., 2004; Thibodeau, 1979).

In general, tortuosities range from 2 to 6 for silica gel, alumina, and other porous materials (Perry and Green, 1997; Thibodeau, 1979). Tortuosity has been measured by diffusion or resistivity experiments for various materials and rocks (Boving and Grathwohl, 2001; Dykhuizen and Casey, 1989; Greskovich et al., 1975; Maerki et al., 2004). Studies have also shown the existence of empirical relationships between tortuosity and porosity (Boudreau, 1996; Dykhuizen and Casey, 1989; Maerki et al., 2004). Several factors such as pore size distribution, the number and shape of pore intersections, and the number of dead-end pores affect the tortuosity of a material making it a difficult parameter to determine (Dykhuizen and Casey, 1989).

Table 5-12 provides experimental values from the literature and values assumed for this evaluation. Based on theoretical relationships, tortuosity generally decreases as porosity increases but this relationship assumes an idealized system with connectivity among pores.

**Table 5-11. Literature Values for molecular diffusion coefficient ( $D_m$ )**

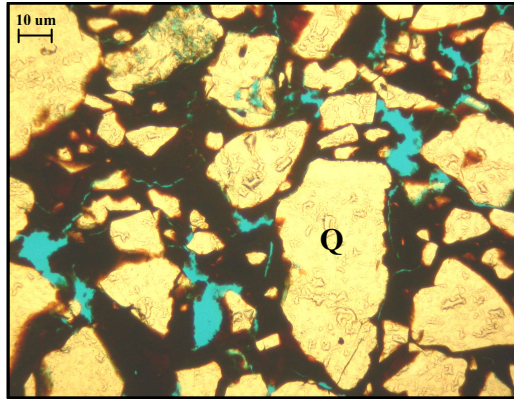
Compound/Ion	Diffusivity in Open Water (cm <sup>2</sup> /sec)		Reference
NaCl	1.61E-05	at 25°C, dilute solution	Robinson & Stokes, 1955
NaCl	1.30E-05	at 20°C, dilute solution	Bruins, 2003
NaCl	1.60E-05	at 25°C, dilute solution	Bruins, 2003
KCl	2.00E-05	at 25°C, dilute solution	Robinson & Stokes, 1955
KCl	1.60E-05	at 20°C, 1 molar solution	Bruins, 2003
MgCl	1.10E-05	at 20°C, 1 molar solution	Bruins, 2003
MgCl	1.40E-05	at 30°C, 1 molar solution	Bruins, 2003
NH <sub>4</sub> Cl	1.60E-05	at 20°C, 1 molar solution	Bruins, 2003
CaCl <sub>2</sub>	1.34E-05	at 25°C, dilute solution	Robinson & Stokes, 1955
CaCl <sub>2</sub>	1.10E-05	at 20°C, 1 molar solution	Bruins, 2003
KNO <sub>3</sub>	1.93E-05	at 25°C, dilute solution	Robinson & Stokes, 1955
KNO <sub>3</sub>	1.54E-05	at 24°C, 1 molar solution	Bruins, 2003
NH <sub>4</sub> NO <sub>3</sub>	1.93E-05	at 25°C, dilute solution	Robinson & Stokes, 1955
MgSO <sub>4</sub>	8.49E-06	at 25°C, dilute solution	Robinson & Stokes, 1955
K <sub>2</sub> SO <sub>4</sub>	9.00E-06	at 20°C, 1 molar solution	Bruins, 2003
Br <sup>-</sup>	2.01E-05	at 25°C, dilute solution	Faure, 1991
Cl <sup>-</sup>	2.03E-05	at 25°C, dilute solution	Faure, 1991
NO <sub>3</sub> <sup>-</sup>	1.90E-05	at 25°C, dilute solution	Faure, 1991
HCO <sub>3</sub> <sup>-</sup>	1.18E-05	at 25°C, dilute solution	Faure, 1991

**Table 5-12. Tortuosity values from literature**

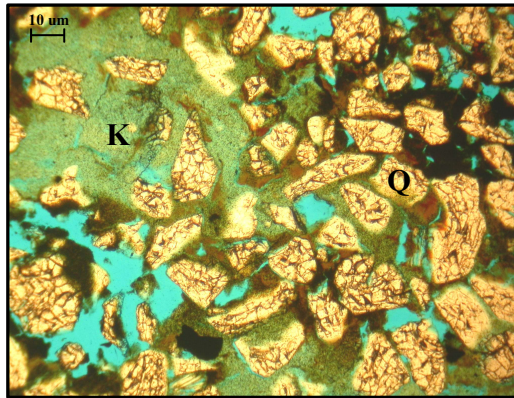
Material Description	Porosity (unitless)	Tortuosity	Reference
Sand, unconsolidated, 0.147-0.208 mm (fine sand)	0.49	1.4	Greskovich et al, 1975
Sand, unconsolidated, 0.208-0.295 mm (fine-medium sand)	0.51	1.5	Greskovich et al, 1975
Sand, unconsolidated, 0.417-0.589 mm (medium-coarse sand)	0.51	1.4	Greskovich et al, 1975
Limestone mud, consolidated (chalk) (Ch')	0.426	3.1	Boving and Grathwohl, 2001
Limestone mud, consolidated (chalk) (Ch'')	0.427	2.8	Boving and Grathwohl, 2001
Limestone mud, consolidated (chalk) (KL2')	0.229	3.7	Boving and Grathwohl, 2001
Limestone mud, consolidated (chalk) (KL2'')	0.24	6.1	Boving and Grathwohl, 2001

For this evaluation, the average porosities among the soils were fairly similar (near 0.40 with a range of 0.29 to 0.48). The “clay” and “clay-sand” categories were assumed to have higher tortuosities because of their poor sorting and greater amount of fine-grained matrix. Sorting refers to the range of grain sizes in the samples and poor sorting implies a large range of grain sizes. Note that the textural category names (“clay”, “clay-sand”, and “sand”) reflect the general amount of mud (silt and clay sized particles) in the samples. A greater presence of silt and clay-sized particles was assumed to restrict pore connectivity and increase tortuosity.

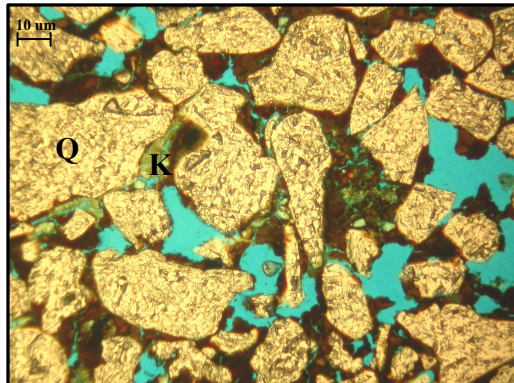
Figure 5-17 provides several photomicrographs of vadose zone soils from a shallow soil boring in A-Area. The photomicrographs show examples of fine-grained matrix (silt and clay-size fraction) and its relationship to porosity (in blue in the photomicrographs). To make the petrographic thin sections (slides), undisturbed core samples were epoxy impregnated, mounted on a glass slide, ground to 30 microns and polished. Although vacuum impregnation may disturb loosely bound material (e.g. loose sands in the photomicrograph from 24 ft), the porosity of these samples relative to each other is still evident. The fine-grained matrix in these samples is composed of iron oxides and kaolinite, a type of clay, and is typical of vadose zone soils at SRS. Porosity is evident by the blue epoxy. As shown in these photomicrographs, the amount and distribution of the fine-grained matrix can affect the amount of porosity and connectivity among pores.



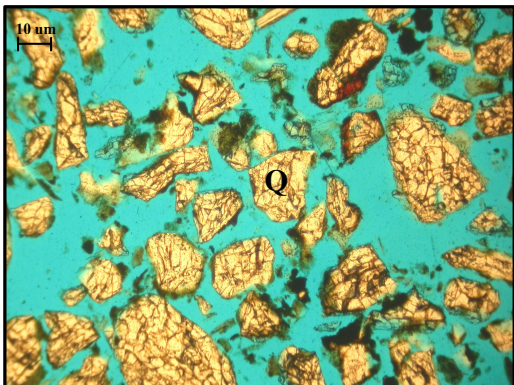
13-15 feet below land surface; blue epoxy = pore space; "Q" = quartz sand grains; dark reddish-brown to black = iron oxides.  
Note: iron oxides nearly block some pores.



~25 feet below land surface; blue epoxy = pore space; "Q" = quartz sand grains; dark reddish-brown to black = iron oxides; "K" = kaolinite.  
Note: iron oxides and kaolinite nearly block some pores.



~18 feet below land surface; blue epoxy = pore space; "Q" = quartz sand grains; dark reddish-brown to black = iron oxides; "K" = kaolinite.  
Note: some pores blocked or restricted by kaolinite and iron oxides



~24 feet below land surface; blue epoxy = pore space; "Q" = quartz sand grains; dark reddish-brown to black = iron oxides.  
Note: relatively little matrix material (iron oxides and kaolinite)

Figure 5-17. Photomicrographs of vadose zone soils from A-Area

Using literature based molecular diffusivity and tortuosity values,  $D_e$  was calculated for each of the textural categories and the upper and lower zone, Table 5-7 and Table 5-9.

**Table 5-13. Calculated effective diffusion coefficients**

Material	Tortuosity	$D_e$
"Sand"	2	8.0E-06
"Clay-Sand"	3	5.3E-06
"Clay"	4	4.0E-06
Upper Zone	3	5.3E-06
Lower Zone	3	5.3E-06

### 5.3 CONTROLLED COMPACTED BACKFILL

#### 5.3.1 Grain Size

Grain size analyses for the samples used to represent the controlled compacted backfill (CCB) are presented on a textural triangle in Figure 5-18. The data include samples from the Old Radioactive Waste Burial Ground and compacted composite samples from Z-Area. Samples were analyzed by LAW and GTE laboratories, which have similar particle size limits for sand, silt, and clay. As discussed in Section 5.2.1, Grain Size for undisturbed vadose zone soil, data may be biased toward the sand class because sand included particle sizes up to 4.75 mm. Nevertheless, all the data cluster together in the sandy clay loam category. Samples evaluated according to the USCS were classified as “SC” (clayey sands or sand-clay mixtures) or “SM” (silty sands, sand-silt mixtures).

#### 5.3.2 Saturated Hydraulic Conductivity

The criteria used in determining the reliability of the vadose zone soil samples consisted of comparing the bulk density of the initial sample with the sub-sample used in the hydraulic conductivity analyses. These criteria could not be applied to the laboratory samples for the controlled compacted backfill soils because for many of the samples, an initial bulk density was not measured in the laboratory. Out of the 34 hydraulic conductivity samples available from E-Area and Z-Area, 32 samples were used in this evaluation. The results from two samples were not used. These samples were duplicates of other samples but were analyzed at a higher effective stress and had significantly lower vertical saturated hydraulic conductivity values.

The upscaling methodology used for the vadose zone soil was applied to the data for the controlled compacted soils to include heterogeneity and spatial continuity. Using a  $p_h = +0.59$  and  $p_v = -0.33$ , the calculated horizontal saturated hydraulic conductivity ( $K_h$ ) was  $7.6E-5$  cm/sec and the vertical saturated hydraulic conductivity ( $K_v$ ) was  $4.1E-5$  cm/sec.

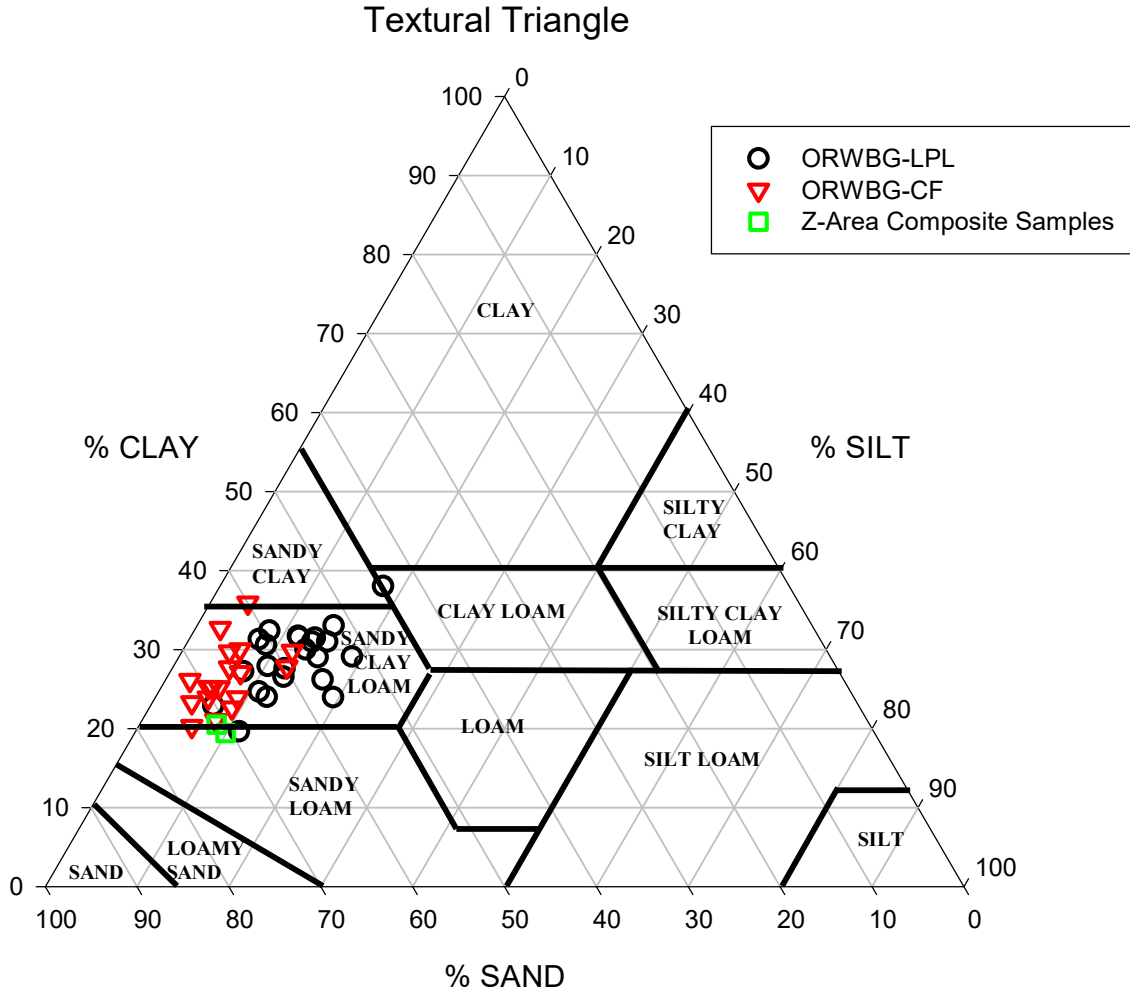


**Figure 5-18. Textural Triangle for Controlled Compacted Backfill**

### 5.3.3 Water Retention

As previously mentioned in Section 5.1.2.5 none of the disposal units have been closed and the controlled compacted backfill (CCB) does not yet exist and as a result there are no water retention data. Water retention data collected on samples from the Old Radioactive Waste Burial Ground (ORWBG) were used to develop the VG parameters for CCB. The same approach for determining VG parameters for representative soil types described in section 5.2.3 was used for the CCB. VG parameters for CCB are presented in Table 5-9. Figure 5-19 shows the WRCs for individual ORWBG samples and the CBB. The samples used in this evaluation are only representative of the controlled compacted backfill (and are not true samples of the future controlled compacted backfill). Therefore, soil moisture curves should be considered as rough estimates for the potential properties of the controlled compacted backfill.

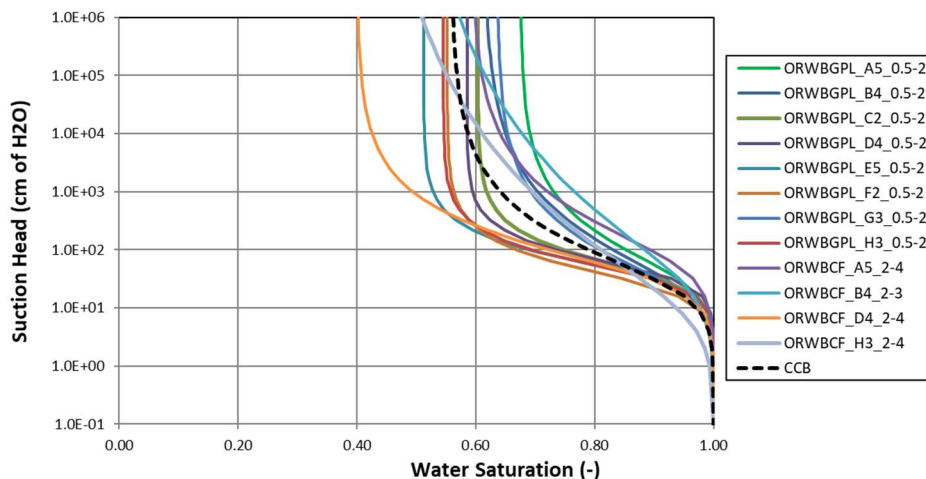


**Figure 5-19. WRCs for individual samples from the Old Radioactive Waste Burial Ground and the resulting data set for the Controlled Compacted Backfill**

### 5.3.4 Porosity, Bulk Density, Particle Density

Only 19 of the 32 samples used in the hydraulic conductivity evaluation had laboratory measurements of porosity and dry bulk density. Calculations for these categories entailed arithmetic averaging of laboratory data. Table 5-10 provides a summary of the bulk properties. Samples representing the controlled compacted backfill had an average porosity of 35%, an average bulk density of 1.71 g/cm<sup>3</sup>, and a calculated particle density of 2.65 g/cm<sup>3</sup>.

### 5.3.5 Saturated Effective Diffusion Coefficient ( $D_e$ )

No laboratory measurements of  $D_e$ ,  $D_m$ , or  $\tau$  are available for the controlled compacted backfill samples. Because the controlled compacted soil will come from the vadose zone, a  $D_e$  of 5.3E-6 cm<sup>2</sup>/s was chosen, the same value as assigned to upper vadose zone and lower zone, the single zone, and the “clay-sand” category.

## 5.4 OPERATIONAL SOIL COVER

No samples have been collected and analyzed for the operational soil cover. However, because the operational soil cover will be derived from the upper vadose zone soils, properties from the upper vadose zone soils can be used to estimate the operational soil cover properties before dynamic compaction (OSC1) and after dynamic compaction (OSC2).

### 5.4.1 Saturated Hydraulic Conductivity

#### 5.4.1.1 Prior to Dynamic Compaction

Several methods were employed to estimate the hydraulic conductivity of the operational soil cover prior to dynamic compaction (DC). These methods included using data from Lambe and Whitman (1969), data from SRS M-Area soils, and the Kozeny-Carman equation. All of these methods were also used in a prior evaluation of the operational soil cover in the “Preliminary Closure Analysis for Slit Trenches #1 and #2” (Flach et al., 2005a).

1. Lambe and Whitman (1969) provide  $K_{sat}$  data for various soils versus the void ratio ( $e$ ) in their Figure 19.5. A void ratio was calculated for the operational soil cover and UVZ soils.  $K_{sat}$  values were read from the graph Figure 19.5 in Lambe and Whitman (1969) at these two void ratios ( $e$ ) for unconsolidated sediments. The ratio of the  $K_{sat}$  values at the two void ratios ( $e$ ) from Lamb and Whitman together with the upper zone horizontal  $K_{sat}$  value was used to estimate a  $K_{sat}$  for the operational soil cover. The calculations are presented below.

Porosity is related to void ratio by way of the following equation (Hillel, 1982)

$$e = \frac{n}{(1 - n)} \quad (24)$$

The porosity of the operational soil cover was estimated based on assumed bulk density of 90 pcf ( $1.44 \text{ g/cm}^3$ ) (Phifer and Wilhite, 2001) and particle density of  $2.65 \text{ g/cm}^3$  (Hillel, 1982). Porosity ( $n$ ) is related to bulk density ( $\rho_b$ ) and particle density ( $\rho_p$ ):

$$n = 1 - \frac{\rho_b}{\rho_p} \quad (25)$$

The calculated porosity for the operational soil cover equaled 0.456.

A void ratio ( $e$ ) of 0.838 was calculated for the operational soil cover based on a computed porosity of 0.456 and a bulk density of 90 pcf. A void ratio ( $e$ ) of 0.639 was calculated for the UVZ soil based on an average laboratory porosity of 0.385 and an average laboratory bulk density of 102.82 pcf (or  $1.65 \text{ g/cm}^3$ ).

Table 5-14 provides the  $K_{sat}$  values from Lambe and Whitman (1969) along with the calculated value for the operational soil cover. This method yielded a high hydraulic conductivity relative to the other methods and higher than what would be expected in the field.

**Table 5-14. Ksat from Lambe and Whitman (1969) and calculated Ksat for the Operational Soil Cover Prior to DC**

Soil type	Ksat at e=0.613 (cm/s)	Ksat at e=0.838 (cm/s)	Ksat with e=0.838/ Ksat with e=0.613
21 Silt - North Carolina	5.5E-07	2.0E-05	36.4
22 Sand - from dike	1.4E-04	4.0E-04	2.9
		average	19.61
		estimated Ksat	1.2E-03

2. Another method of estimating hydraulic conductivity employed soil samples collected from M-Area. Samples were tested by LAW Engineering (Jackson, 2000) at 5 psi and 10 psi. The difference in hydraulic conductivity at 5 psi versus 10 psi was assumed to roughly represent the difference in porosity of the operational soil cover versus the native vadose zone soil. The average ratio (vertical hydraulic conductivity at 5 psi/vertical hydraulic conductivity at 10 psi) for the M-Area soils is 1.94 (Phifer, 2005). Therefore, it was estimated that the operational soil cover had a hydraulic conductivity approximately 1.94 times as high as the upper vadose zone (6.2E-5 cm/sec).

$$K_{sat} = 1.94 \times 6.2E-5 \text{ cm/sec} = 1.2E-4 \text{ cm/sec}$$

3. The third method of estimating hydraulic conductivity involved the Kozeny-Carman equation as described in Freeze and Cherry (1979). This equation relates  $K_{sat}$  to mean particle diameter and the shape and packing of grains. Porosity is used to represent the shape and packing of grains.

$$K_{sat} = \left( \frac{\rho g}{\mu} \right) \left[ \frac{n^3}{(1-n)^2} \right] \left( \frac{d_m^2}{180} \right) \quad (26)$$

where  $\rho$  = fluid density,  $g$  = acceleration due to gravity,  $\mu$  = fluid viscosity,  $n$  = porosity, and  $d_m^2$  = mean particle size squared.

It was assumed that the particle size distribution of the operational soil cover and upper vadose zone (native soil) are approximately the same because they are the same soils (with different densities). Therefore, the parameter  $d_m$  remained constant in the equations. Using the laboratory measured porosity and hydraulic conductivity for the upper zone soils and the estimated porosity of the operational soil cover, saturated hydraulic conductivity can be determined for the operation soil cover.

$$\frac{K_{sat-OSC1}}{K_{sat-}} = \frac{\left[ \frac{n_2^3}{(1-n_2)^2} \right]}{\left[ \frac{n_1^3}{(1-n_1)^2} \right]} = \frac{\left[ \frac{(0.456)^3}{(1-0.456)^2} \right]}{\left[ \frac{(0.385)^3}{(1-0.385)^2} \right]} \quad (27)$$

$$K_{sat-OSC1} = 2.123 * K_{sat-UZ}$$

$$\text{or } 2.123 \times 6.2E-5 \text{ cm/sec} = 1.3E-4 \text{ cm/sec}$$

Methods #2 and #3 suggest that the hydraulic conductivity for the operational soil cover before DC is approximately two times the hydraulic conductivity of the UVZ soils (a ratio of 1.94 for method #2 and a ratio of 2.123 for method #3). For this evaluation, the operational soil cover prior to DC was assumed to be 2.123 times the UVZ horizontal hydraulic conductivity (i.e., 1.3E-4 cm/sec).

The vertical hydraulic conductivity for the operational soil cover was assigned the same value as the horizontal hydraulic conductivity. The operational soil cover consists of excavated soil from the upper vadose zone. The soil is stockpiled until later placement over the waste using a bulldozer. These operational techniques are assumed to have grossly homogenized the UVZ soil (i.e. eliminating most large-scale layering), which would create loosely packed soils with similar vertical and horizontal hydraulic conductivities.

#### 5.4.1.2 After Dynamic Compaction

Using the Kozeny-Carman equation (described above), a saturated hydraulic conductivity was approximated for the operational soil cover after DC (OSC2). Porosity was calculated using equation (25) where ( $\rho_p$ ) or particle density was assumed to be 2.65 g/cm<sup>3</sup> (Hillel, 1982) and  $\rho_b$  or bulk density was estimated at 120 pcf (or 1.92 g/cm<sup>3</sup>) (Phifer and Wilhite, 2001). Using this equation, the porosity for the operational soil cover after DC was estimated as 0.275.

Saturated hydraulic conductivity was calculated according to:

$$\frac{K_{sat-OSC2}}{K_{sat-UZ}} = \frac{\left[ \frac{(0.275)^3}{(1 - 0.275)^2} \right]}{\left[ \frac{(0.385)^3}{(1 - 0.385)^2} \right]} \quad (28)$$

$$K_{sat-OSC2} = 0.261 * K_{sat-}$$

$$\text{or } 0.261 \times 6.2\text{E-}5 \text{ cm/sec} = 1.6\text{E-}5 \text{ cm/sec}$$

The vertical and horizontal hydraulic conductivity for the operational soil cover after DC was assumed to be the same.

#### 5.4.2 Water Retention

Estimations of water retention and unsaturated hydraulic conductivity curves for the operational soil cover entailed using Leverett scaling and the sample data for the upper zone. Leverett scaling consists of adjusting capillary pressure based on permeability. Leverett observed that for similar unconsolidated sands that for any member ( $i$ ) of a group (Bear, 1972):

$$\frac{P_c}{\sigma} \left[ \frac{K_i}{n_i} \right]^{1/2} = J(S_w) \quad (29)$$

where  $P_c$  is capillary pressure,  $\sigma$  is related to interfacial tension,  $K$  reflects the material's permeability,  $n$  corresponds to porosity, and  $S_w$  is water saturation.

The Leverett function ( $J$ ) is the same for all materials in a class.  $P_c$  is defined as:

$$P_c = \frac{\rho g}{\sigma} * \psi \quad (30)$$

where  $\rho$  is fluid density,  $g$  is reflects acceleration due to gravity and  $\psi$  reflects the water pressure head.

Comparing materials of two similar classes (e.g., upper vadose zone and the operational soil cover) at the same saturation shows that:

$$\frac{\rho g}{\sigma} * \psi_1 * \left[ \frac{K_1}{n_1} \right]^{1/2} = \frac{\rho g}{\sigma} * \psi_2 * \left[ \frac{K_2}{n_2} \right]^{1/2} \quad (31)$$

Rearranging the equation and canceling like variables yields the following for the same saturation value:

$$\psi_2 = \left[ \frac{K_1 n_2}{K_2 n_1} \right]^{1/2} * \psi_1 \quad (32)$$

where subscripts 1 and 2 refer to two different media.

The unknown suction head ( $\psi_2$ ) at a particular saturation in medium 2 can be approximated on the basis of the corresponding (known) suction head ( $\psi_1$ ) at the same saturation in medium 1 and the hydraulic conductivity ( $K_1/K_2$ ) and porosity ( $n_2/n_1$ ) ratios. Using equation (32) along with estimates of hydraulic conductivity and porosity for the operational soil cover, and values for the upper vadose zone soils, the water retention curves for the operational soil cover were estimated. Saturation versus suction curves for the operational soil cover before and after dynamic compaction are shown in Figure 5-20. For a particular suction value, the operational soil cover prior to DC has a lower saturation than the upper vadose zone soil and the operational soil cover after DC. Suction versus relative hydraulic conductivity ( $K_r$ ) curves are presented in Figure 5-21. At a given suction, the relative hydraulic conductivity ( $K_r$ ) for the operational soil cover prior to DC is lower than the  $K_r$  for the upper vadose zone soil and operational soil after DC.

$$\psi_{OSC1} = 0.747 * \psi_{UZ} \quad (33)$$

$$\psi_{OSC2} = 1.653 * \psi_{UZ} \quad (34)$$

Equation (33) and (34) were used to generate data for a WRC so VG parameters for OSC1 and OSC2 could be developed. The resulting WRC data sets for OSC1 and OSC2 were fit to the VG equation to determine VG parameters using the previously described least squares method. Figure 5-20 and Figure 5-21 show the WRC and  $K_{rel}$  curves for OSC1 and OSC2 and Table 5-9 contains the calculated VG parameter values.

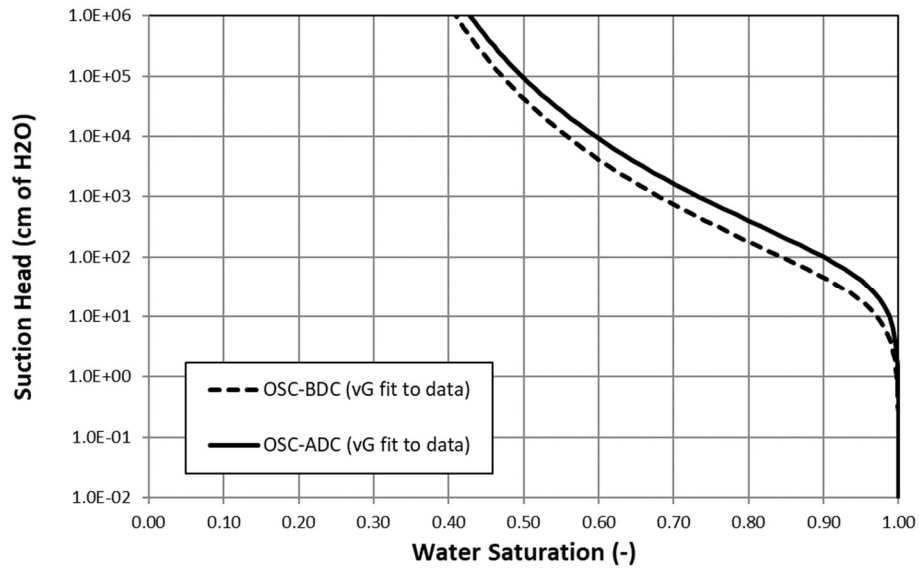


**Figure 5-20. Saturation vs Suction for Operational Soil Cover Before and After Dynamic Compaction**

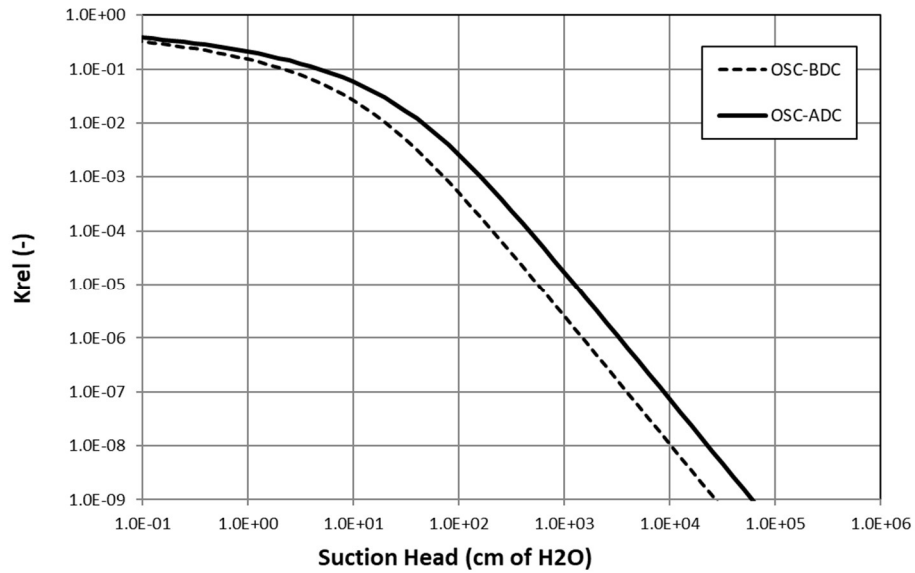


**Figure 5-21. Suction vs Relative Hydraulic Conductivity for Operational Soil Cover Before and After Dynamic Compaction**

### 5.4.3 Porosity, Bulk Density, Particle Density

#### 5.4.3.1 Prior to Dynamic Compaction

The porosity of the operational soil cover was estimated based on an assumed bulk density of 90 pcf (1.442 g/cm<sup>3</sup>) (Phifer and Wilhite, 2001) and a particle density of 2.65 g/cm<sup>3</sup> (Hillel, 1982). Using the equation from Hillel (1982), a porosity of 0.456 (or 45.6%) was calculated for the operational soil cover before DC.

#### 5.4.3.2 After Dynamic Compaction

Porosity was calculated using an assumed particle density of 2.65 g/cm<sup>3</sup> (Hillel, 1982) and an estimated bulk density of 120 pcf (or 1.92 g/cm<sup>3</sup>) (Phifer and Wilhite, 2001). Using the relationship between particle density and bulk density given by equation 25, a porosity of 0.27 (or 27%) was computed for the operational soil cover after DC.

### 5.4.4 Saturated Effective Diffusion Coefficient ( $D_e$ )

The  $D_e$  for the operational soil cover before DC was assumed to be similar to the vadose zone soils. Therefore, a  $D_e$  of 5.3E-6 cm<sup>2</sup>/s was chosen, the same value as assigned to upper vadose zone and lower zone, the single zone, and the “clay-sand” category. The operational soil cover after DC would likely possess a lower  $D_e$  than the soil before DC due to decreasing pore space and tighter packing of grains from the dynamic compaction. These changes in pore structure would potentially increase tortuosity. Therefore, the operational soil cover after DC was assigned a  $D_e$  of 4.0E-6 cm<sup>2</sup>/s.

## 5.5 IL VAULT PERMEABLE BACKFILL & GRAVEL

According to the engineered drawings for the IL Vault, a permeable backfill (PB) was used that had less than 15% mud. Because the backfill likely came from local sources, vadose zone soil sample properties were used to estimate hydraulic conductivity, water retention, and bulk material properties for this evaluation. Only two of the vadose zone soil samples (VL-1, 13-15' and VL-1, 44-46') had grain size distributions with <15% mud and hydraulic conductivity measurements that are considered reliable (see section 5.2.2.1, Review of Data Quality). Therefore, these two samples were used to determine the estimates.

Data for the generic “gravel” came from both literature and laboratory results. In particular, laboratory data was used to estimate hydraulic conductivity and water retention properties (Yu et al., 1993). Two samples (GL-1 and GL-2) representing gravel used in the area were collected in 1992 and analyzed by Core Laboratories for a previous evaluation. Porosity and particle density values for this evaluation were based primarily on literature. The gravel properties reported in this evaluation are intended to provide generic gravel properties based on data currently available.

## 5.5.1 Saturated Hydraulic Conductivity

### 5.5.1.1 IL Vault Permeable Backfill

The arithmetic average of the laboratory measured vertical hydraulic conductivity for the two VL-1 samples was 7.6E-4 cm/sec. The backfill was given a  $K_h$  to  $K_v$  ratio of 1.9, the same as the controlled compacted backfill, because it is assumed to have undergone similar handling and operational processes during installation. Using this ratio, the  $K_h$  was computed to be 1.4E-3 cm/sec.

### 5.5.1.2 Gravel

The arithmetic average of the laboratory measured saturated hydraulic conductivity for the two gravel samples (GL) was 1.5E-1 cm/sec. The gravel was assumed to have a  $K_h$  to  $K_v$  ratio of 1.0 and therefore the same hydraulic conductivity for  $K_h$  and  $K_v$ .

## 5.5.2 Water Retention

### 5.5.2.1 IL Vault Permeable Backfill

Water retention data collected on 2 vadose zone samples VL-1, 13-15' and VL-1, 44-46 were used to develop the VG parameters for PB. The same approach for determining VG parameters for representative soil types described in section 5.2.3 was used for the PB. Figure 5-22 shows the saturation versus suction curve and Figure 5-23 shows suction versus relative hydraulic conductivity ( $K_r$ ) curve based on an average of the laboratory data for VL-1, 13-15' and VL-1, 44-46'.

### 5.5.2.2 Gravel

Soil moisture data for two gravel samples (GL-1 and GL-2) were used to develop the VG parameters for G1. The same approach for determining VG parameters for representative soil types described in section 5.2.3 was used for the G1. Figure 5-24 shows the saturation versus suction curve and Figure 5-25 shows suction versus relative hydraulic conductivity ( $K_r$ ) curve based on an average of the laboratory data.

## 5.5.3 Porosity, Bulk Density, Particle Density

### 5.5.3.1 IL Vault Permeable Backfill

The laboratory measured porosity of the two VL-1 samples (i.e., samples VL\_13-15 and VL\_44-46) averaged 0.415. Dry bulk density measured in the laboratory averaged 1.56 g/cm<sup>3</sup>. A particle density of 2.67 g/cm<sup>3</sup> was calculated using equation (25).

### 5.5.3.2 Gravel

Freeze and Cherry (1979) provide a range of porosity values of 0.25 to 0.40 for unconsolidated gravel deposits. Fredlund and H.Rahardjo (1993) also give a wide range of porosities from 0.12 to 0.46 for a well-graded silty sand and gravel mixture. The average porosity of the two gravel samples (GL-1 and GL-2) analyzed by Core Laboratories was 0.383. For this evaluation, the generic gravel was assigned a porosity of 0.300.

Bulk density and particle density were not measured for the two gravel samples (GL-1 and GL-2) submitted in 1992 to Core Laboratories. Granite, which often comprises gravel, has a

general particle density ranging from 2.5 to 2.7 g/cm<sup>3</sup> (Dutro et al., 1989). For this evaluation, a particle density of 2.60 g/cm<sup>3</sup> was chosen for the generic gravel.

Using equation (25) relating porosity ( $n$ ) to particle density ( $\rho_p$ ) and bulk density ( $\rho_b$ ), a bulk density of 1.82 g/cm<sup>3</sup> was computed for the gravel.

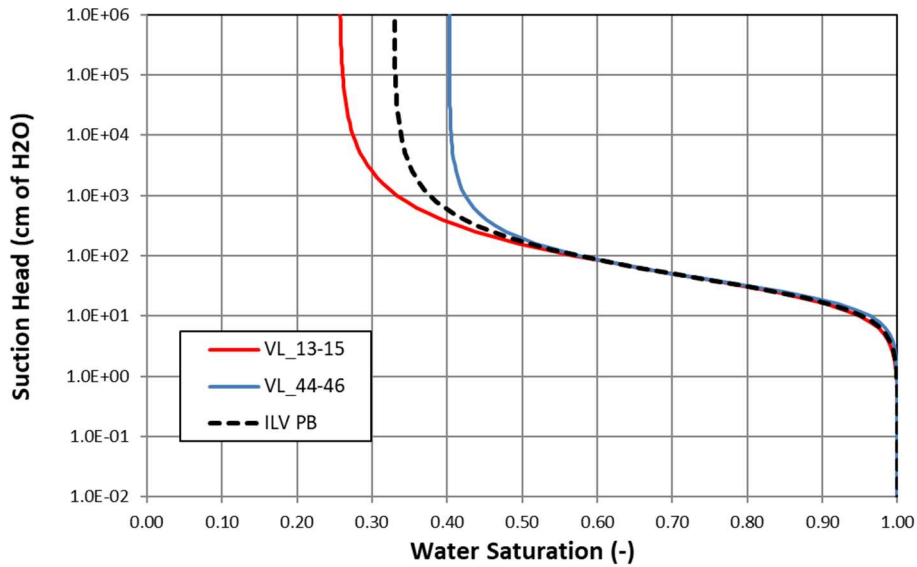


Figure 5-22. Saturation vs Suction for IL Vault Permeable Backfill

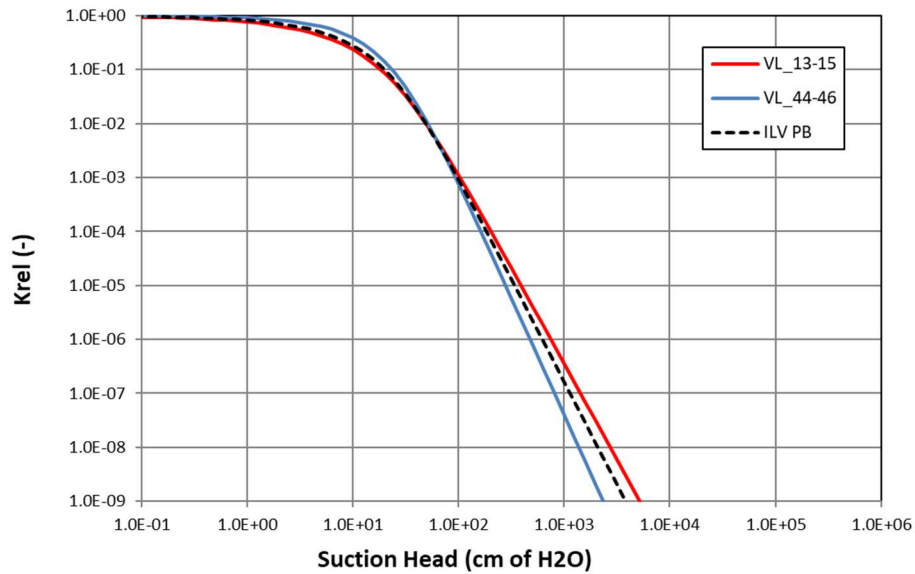


Figure 5-23. Suction vs Relative Hydraulic Conductivity for IL Vault Permeable Backfill

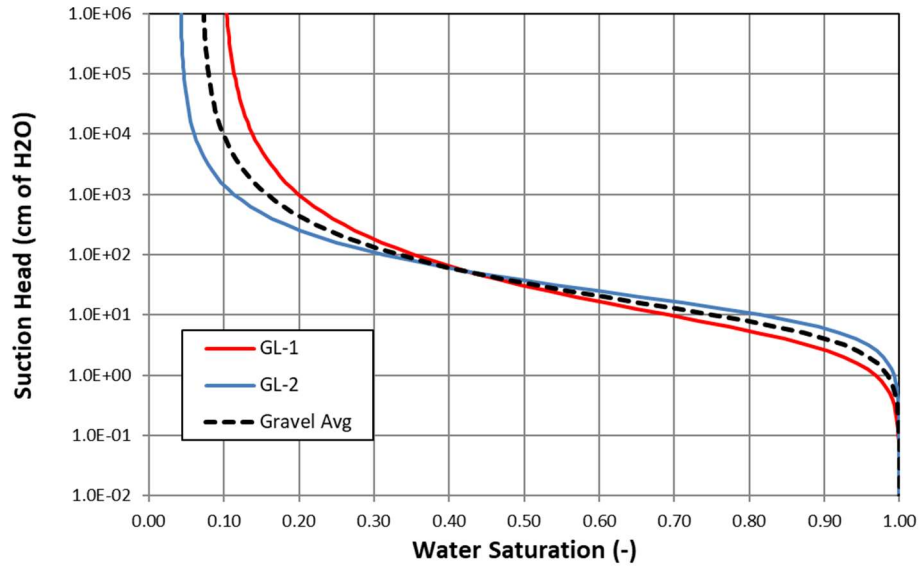


Figure 5-24. Saturation vs Suction for Gravel

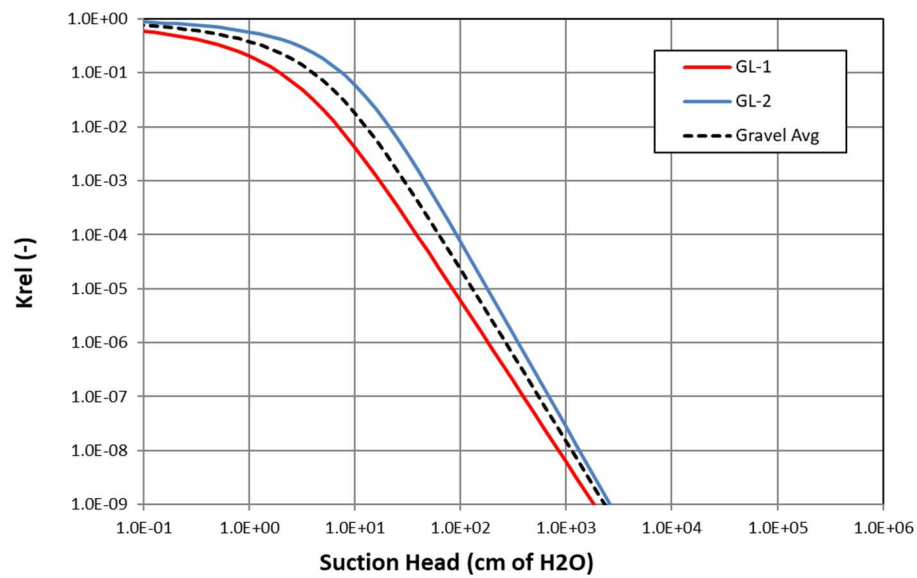


Figure 5-25. Suction vs Relative Hydraulic Conductivity for Gravel

#### 5.5.4 Saturated Effective Diffusion Coefficient ( $D_e$ )

The same molecular diffusion coefficient ( $D_m$ ) value of  $1.6E-5$  cm<sup>2</sup>/sec used for the vadose zone soils was applied for the  $D_e$  calculations for the IL Vault permeable backfill and generic gravel. As with the vadose zone soil evaluation,  $D_e$  was calculated using equation (22). The molecular diffusion coefficient ( $D_m$ ) and tortuosity ( $\tau$ ) values are based on literature values. No experimental data for these materials are available.

##### 5.5.4.1 IL Vault Permeable Backfill

The IL Vault permeable backfill was assigned a tortuosity ( $\tau$ ) value of 2, the same value used for the “sand” category. This particular  $\tau$  was chosen because the two VL-1 samples representing the IL Vault permeable backfill were categorized as “sand” in the initial vadose zone soils evaluation. With the same  $D_m$  and  $\tau$ , the IL Vault permeable backfill had the same  $D_e$  as the “sand” ( $8.0E-6$  cm<sup>2</sup>/s).

##### 5.5.4.2 Gravel

The gravel is thought to have a lower tortuosity than the values assigned to the vadose zone soils. A tortuosity ( $\tau$ ) value of 1.7 was chosen based on a hypothetical three-dimensional diffusion path with the pore making a 45° angle with the vertical (y) direction as described by Thibodeaux (1979). This  $\tau$  value resulted in a calculated  $D_e$  of  $9.4E-6$  cm<sup>2</sup>/s.

### 5.6 SATURATED ZONE

The General Separations Area groundwater flow model as described by Flach (2019) will form the basis of the groundwater flow and transport modeling updates to be performed for the E-Area LLWF, Z-Area SDF and F&H Tank Closure Performance Assessments (PA).

#### 5.6.1 Saturated Zone Hydraulic Properties

Of the parameters evaluated herein [i.e. porosity, dry bulk density, particle density, saturated hydraulic conductivity, characteristic curves (suction head, saturation, and relative permeability), and effective diffusion coefficient], the GSA groundwater flow model addresses porosity, saturated hydraulic conductivity, and characteristic curves for the saturated zone. Relative to porosity Flach and Harris (1996) state the following:

*“Aadland and others (1995, Tables 3 and 7) estimate the average porosity of the Upper Three Runs and Gordon aquifers to be about 35%. Regions of relatively immobile water, ranging from grain-sized “dead-end” pores to macro-scale clay intervals, do not effectively participate in contaminant transport. Therefore an “effective” porosity value, smaller than the total porosity, is commonly used for transport simulations and particle tracing related to contaminant migration. An effective porosity value of 25% is assumed uniformly in the GSA model for computing a pore velocity field that may be used later for particle tracing. The assumed porosity value is consistent with the general recommendation of Looney and others (1987, p. 39).”*

Based upon this recommendation by Flach and Harris (1996) which has been retained for the updated GSA\_2018 model (Flach, 2019), an effective porosity of 25% will be assigned to all saturated zone soils. Within the Porflow model, the effective, total, and diffusive porosities are all set equal to 25%.

Flach (2019) discusses the assignment of saturated hydraulic conductivity within the GSA groundwater flow model in detail. The saturated hydraulic conductivity fields developed within the GSA groundwater flow model are incorporated into this effort by reference. For the saturated zone the characteristic curves are not applicable because under saturated conditions both the saturation and relative permeability are equal to one.

For the groundwater flow modeling described by Flach (2019), the dry bulk density, particle density, and effective diffusion coefficient of the soil materials are not specifically incorporated in the modeling. However, for combined flow and transport modeling as conducted within the PA, these parameters are required along with the “solute-solid distribution coefficient”,  $K_d$ . The distribution coefficient,  $K_d$ , is addressed separately by Kaplan (2016). The Upper Three Runs and Gordon aquifer unit characteristics are similar to the lower vadose zone as described in Section 5.2. As outlined in Section 5.2 the lower vadose zone has an average porosity, dry bulk density, and particle density of 39%, 1.62 g/cm<sup>3</sup>, and 2.66 g/cm<sup>3</sup>, respectively.

Because an effective porosity of 25% rather than the total porosity of 39% has been assigned to these materials, the lower vadose zone particle density of 2.66 g/cm<sup>3</sup> cannot be assigned to these materials (Bechtel-SAIC, 2005; Flach, 2012). Because porosity is in the denominator of the retardation factor,  $R$ , equation, assignment of a particle density of 2.66 g/cm<sup>3</sup> would result in an artificially greater contaminant retardation within the model:

$$R = 1 + \frac{\rho_b K_d}{\eta_T} \quad (35)$$

where  $R$  = retardation factor;  $\rho_b$  = dry bulk density;  $K_d$  = distribution coefficient;  $\eta_T$  = total porosity (Freeze and Cherry, 1979) and

$$\rho_b = \rho_p (1 - \eta_T) \quad (36)$$

where  $\rho_p$  = particle density (Hillel 1982)

$$R = 1 + \frac{\rho_p (1 - \eta_T) K_d}{\eta_T} \quad (37)$$

As seen in equation (37), to decrease the porosity from a total of 39% to an effective of 25% and still maintain a consistent retardation factor an effective particle density less than the lower vadose zone particle density of 2.66 g/cm<sup>3</sup> will be required based upon the above equation. This can be derived using equivalent retardation factors as follows:

$$\begin{aligned}
 R_1 &= R_2 \\
 1 + \frac{\rho_{pT}(1 - \eta_T)K_d}{\eta_T} &= 1 + \frac{\rho_{pe}(1 - \eta_e)K_d}{\eta_e} \\
 \frac{\rho_{pT}(1 - \eta_T)K_d}{\eta_T} &= \frac{\rho_{pe}(1 - \eta_e)K_d}{\eta_e} \\
 \rho_{pe} &= \frac{\rho_{pT}(1 - \eta_T)\eta_e}{(1 - \eta_e)\eta_T} \tag{38}
 \end{aligned}$$

Substitute values into the equation:

$$\begin{aligned}
 \rho_{pe} &= \frac{2.66 \text{ g/cm}^3 (1 - 0.39)0.25}{(1 - 0.25)0.39} \\
 \rho_{pe} &= 1.39 \text{ g/cm}^3
 \end{aligned}$$

where  $\rho_{pT}$  = particle density based upon total porosity = 2.66 g/cm<sup>3</sup>;  $\eta_T$  = total porosity = 0.39;  $K_d$  = distribution coefficient (same on both sides of the equation);  $\rho_{pe}$  = particle density based upon effective porosity;  $\eta_e$  = effective porosity = 0.25.

The dry bulk density ( $\rho_{be}$ ) associated with effective porosity of 25% determined from the following equation:

$$\rho_{be} = \rho_{pe}(1 - \eta_e) \tag{39}$$

where  $\rho_{pe}$  = particle density based upon effective porosity = 1.39 g/cm<sup>3</sup>;  $\eta_e$  = effective porosity = 0.25 (Hillel 1982) is  $\rho_{be} = 1.04 \text{ g/cm}^3$ .

An alternative derivation of Equation set (38) is presented by Flach (2012). Bechtel-SAIC (2005), Equation 6-3, alternatively defined an effective distribution coefficient  $K_d$  instead of an effective bulk density, using the same adjustment factor as Flach (2012) and embedded in Equation set (38), but the net effect on retardation  $R$  is the same.

Within the GSA 2018 (Flach, 2019) model soils with a saturated hydraulic conductivity greater than 1.0E-07 cm/s are defined as sand and those with a saturated hydraulic conductivity less than 1.0E-07 cm/s are defined as clay for the purpose of defining transport properties (i.e.,  $K_d$  and  $D_e$ ). For consistency with the vadose zone soils described in Section 5.2, the saturated zone soils within the GSA model that are defined as sandy will be assigned the effective diffusion coefficient of the lower vadose zone (i.e., 5.3E-06 cm<sup>2</sup>/s) and those defined as clay will be assigned that of the vadose zone clay (i.e., 4.0E-06 cm<sup>2</sup>/s).

Table 5-15 provides a summary of the saturated zone soils hydraulic properties.

**Table 5-15. Saturated zone soils hydraulic properties**

Saturated Hydraulic Conductivity	Water Retention	Effective Porosity (unitless)	Effective Dry Bulk Density (g/cm <sup>3</sup> )	Effective Particle Density (g/cm <sup>3</sup> )	Saturated Effective Diffusion Coefficient (cm <sup>2</sup> /s)
See Flach and Harris (1996) and Flach et al. (2004)	Not applicable	0.250	1.04	1.39	Sand: 5.3E-06 Clay: 4.0E-06

### 5.6.2 Lower Vadose Zone Versus Saturated Zone Porosity

As discussed above current PA analyses of aquifer flow and transport (i.e., saturated zone soils) assume an effective porosity of 0.25, which is lower than the total porosity of 0.39 used for the lower vadose zone soil. Use of a lower value than total porosity for saturated flow and transport is common modeling practice (Fetter, 1993) and defines the effective area/volume through which porous-medium flow occurs. In the context of numerical field-scale transport simulations, an effective porosity partially addresses the effects of unresolved physical heterogeneity at the sub-grid scale. In the context of sedimentary geologic systems, a computational block contains strata of varying permeability with essentially no flow occurring in a fraction of strata with sufficiently low permeability. Figure 5-26 illustrates the concept for a layered system comprising two distinct materials.

Although the vadose and saturated zones exhibit similar physical heterogeneity, total porosity is currently assumed in vadose zone PA models because of markedly different flow conditions. Vadose zone flow is predominantly perpendicular to strata, rather than parallel to layering in the aquifer. Also, unsaturated conditions in the vadose zone significantly reduce the permeability contrast between coarse- and fine-grained materials, in comparison to saturated conditions in the aquifer. Both phenomena significantly reduce the extent to which flow can effectively bypass portions of the porous medium, as shown schematically in Figure 5-27.

The left image is a reproduction of Figure A, which represents typical aquifer heterogeneity and flow orientation to strata and justifies a lower porosity setting in modeling ( $\eta = 0.25$ ). Sand and clay properties from Section 5.2 are used to define the conductivity (K) contrast under saturated conditions (Figure 5-28). The extent of horizontal layering is assumed to be consistent with a 10:1 ratio of spatial correlation length ( $\lambda$ ).

The right images show two end member cases for which porosity should not be reduced from the total ( $\eta = 0.39$ ). The upper image depicts a uniform permeability field, that is, when the permeability contrast is zero. The lower image shows perfect layering perpendicular to the hydraulic gradient, forcing flow to go through both materials. In both cases, flow would pass

through the entire porous volume rather than bypassing a portion. As the conductivity contrast decreases and/or anisotropy in horizontal to vertical correlation length decreases, the porosity value assumed for transport simulations should increase relative to aquifer conditions and approach total porosity.

An appropriate porosity setting for vadose simulations can be estimated through a double interpolation approach summarized in Figure 5-29. PA simulations indicate a typical soil suction level of 100-200 cm in E-area (see Section 5.8). The permeability contrast between sand and clay in this suction range is approximately 1.5 orders of magnitude. Assuming similar layering in the aquifer and vadose zones, but 90-degree different mean flow direction, produces a vadose zone anisotropy ratio of 1:10. Linear interpolation of log K contrast (ratio) between aquifer conditions and the homogeneous end member can be used to estimate effective porosity for the vadose zone, considering only K contrast effects:

$$\frac{\eta - 0.39}{\log(K_1/K_2) - 0} = \frac{0.25 - 0.39}{2.7 - 0} \quad (40)$$

For the assumed vadose properties, the result is  $\eta = 0.31$ . A second interpolation can be used to estimate the added effect of flow orientation to strata:

$$\frac{\eta - 0.39}{\log(\lambda_1/\lambda_2) - (-3)} = \frac{0.25 - 0.39}{1 - (-3)} \quad (41)$$

For the assumed vadose properties, the final result is  $\eta = 0.35$ .

This estimate is only 10% lower than the total porosity value, and represents a small perturbation compared to uncertainty in unsaturated soil properties. The latter control the saturation level, which along with porosity, define flow area/volume under unsaturated conditions in the vadose zone. Specifically, pore velocity ( $v$ ) is computed from Darcy velocity ( $U$ ) as:

$$v = \frac{U}{\eta * S} \quad (42)$$

where S is saturation.

Uncertainty in saturation is significantly larger than uncertainty in (effective) porosity. Given the approximate nature of the preceding analysis and considering uncertainties in various parameters, a total porosity value is appropriate for vadose zone modeling.

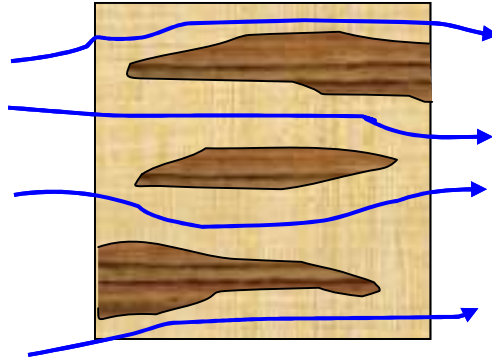


**Figure 5-26. Effective flow through a heterogeneous layered porous medium**

Note: Little or no flow occurs through the low permeability layers (dark brown). Flow predominantly occurs through higher permeability layers (tan).

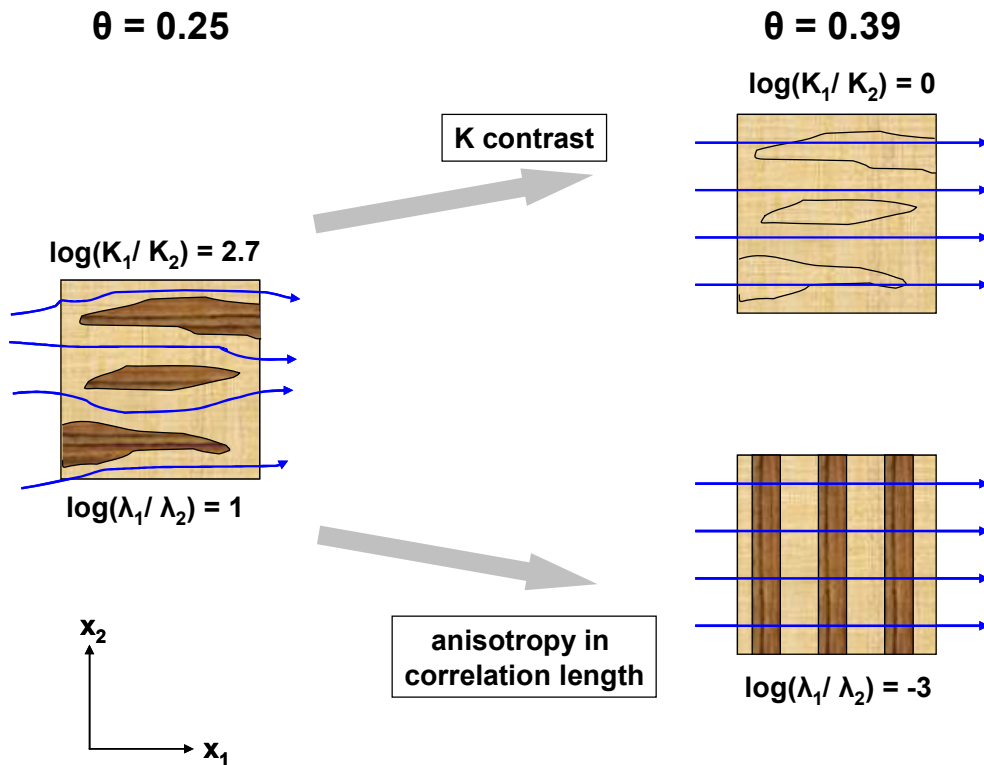


**Figure 5-27. Effective porosity assumptions for three combinations of layering and permeability contrast**

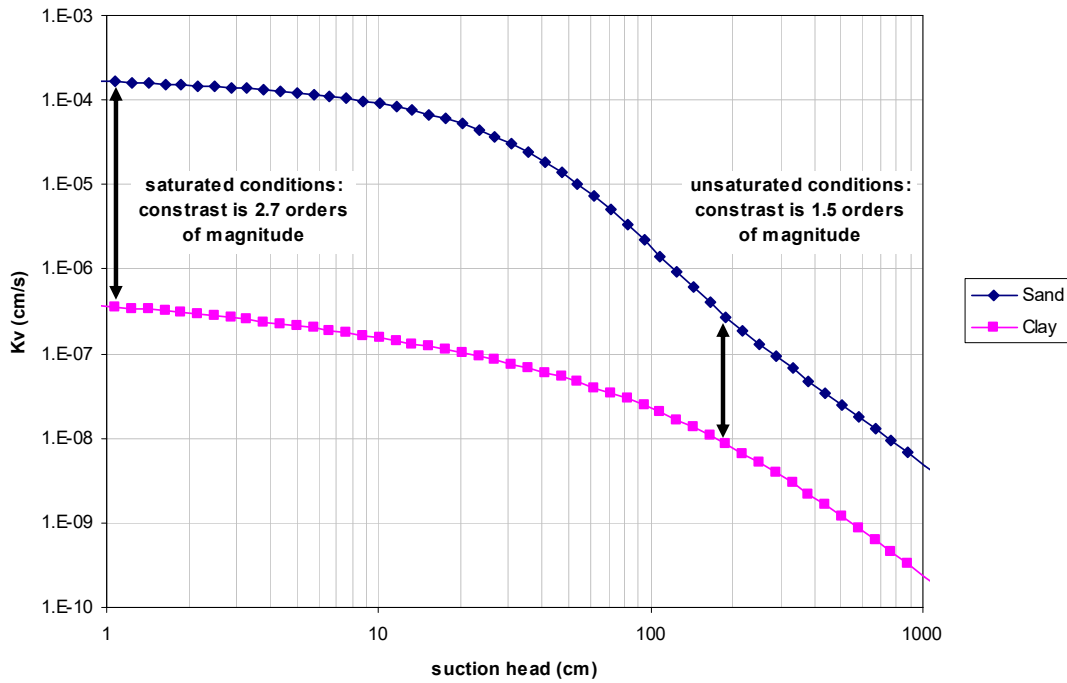


Figure 5-28. Variation in Sand and Clay vertical hydraulic conductivity as a function of suction head

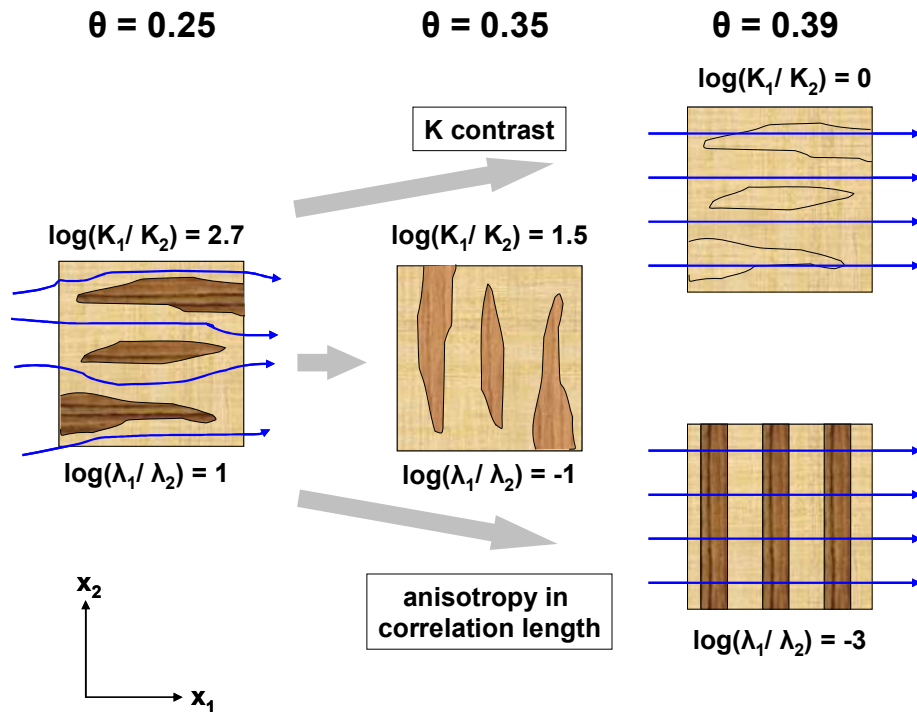


Figure 5-29. Estimated effective porosity for vadose zone simulations

## 5.7 UNCERTAINTY ANALYSIS

Uncertainty values are defined here for porosity ( $n$ ), dry bulk density ( $\rho_b$ ), particle density ( $\rho_p$ ), saturated hydraulic conductivity ( $K_{sat}$ ) and effective diffusion coefficient ( $D_e$ ), but not for the characteristic curves (suction head, saturation, and relative permeability). Uncertainty in the property values derived through arithmetic averaging was estimated using the well-known expression (e.g., (Walpole and Meyers, 1978):

$$s_{mean} = \frac{s}{\sqrt{n}} \quad (43)$$

where  $s_{mean}$  is the estimated standard deviation of the (arithmetic) sample mean,  $s$  is the estimated standard deviation of the population, and  $n$  is the number of samples.

$s_{mean}$  is sometimes referred to as the standard error of the mean. This value represents the uncertainty in the mean soil property values. Summary statistics are provided in Table 5-17 for total porosity, dry bulk density, and particle density.

Uncertainty in recommended nominal values derived through non-linear averaging processes ( $K_{sat}$ ) or solely from literature-based values ( $D_e$ ) was estimated using Monte Carlo simulation. In Monte Carlo simulation (MC), numerous realizations are generated by randomly sampling the statistical distributions of input parameters and computing sample statistics from the corresponding output values. In this study, 10,000 realizations were generated in each MC simulation so that the sample statistics would be sufficiently reliable. MC simulations were performed using GoldSim 9.20 (GoldSim Technology Group LLC, Issaquah, WA, [www.goldsim.com](http://www.goldsim.com)).

Uncertainty in the sample of small-scale conductivity measurements was addressed using a bootstrapping technique (Efron, 1982). In the bootstrap approach, the data sample is used as a surrogate for the true underlying population. Sample realizations are generated by randomly re-sampling the actual sample, with replacement. For effective horizontal and vertical conductivity, uncertain inputs to the analysis are the averaging exponents,  $p_h$  and  $p_v$ , and the sample of small-scale or "point" conductivity measurements. Based on summary Table 5-6, triangular distributions were developed. Parameters for the triangular distributions for  $p_h$  and  $p_v$  are listed in Table 5-16.

**Table 5-16. Descriptive statistics for triangular distributions describing  $p_v$  and  $p_h$**

Statistic	$p_h$	$p_v$
Min	0.34	-0.73
Peak	0.59	-0.33
Max	0.84	0.07

Table 5-18 summarizes the sample statistics derived through MC simulation. Log-normal distributions were observed to be reasonable representations of the MC probability distributions for the saturated effective diffusion coefficient and hydraulic conductivities. The mean values for hydraulic conductivity are very close, if not identical to, the deterministic values in Table 5-7, suggesting that 10,000 MC realizations are sufficient to produce reliable uncertainty statistics.

For effective diffusion coefficient, the molecular diffusion coefficient was assumed to be well known and only tortuosity was randomly varied in MC simulations. Uncertainty in each tortuosity was represented by a truncated normal distribution with a mean value defined by Table 5-19, a standard deviation of 0.5, and truncation limits at  $\pm 1.5$  (3 sigma) about the mean.

**Table 5-17. Uncertainty Analysis summary statistics for total porosity, dry bulk density, and particle density**

Total Porosity (unitless)										
Material	Upper Zone	Lower Zone	"SAND"	"CLAY-SAND"	"CLAY"	Operational Soil Cover (prior to DC) <sup>1</sup>	Operational Soil Cover (after DC) <sup>1</sup>	Controlled Compacted Backfill	ILV Permeable Backfill <sup>2</sup>	Gravel <sup>3</sup>
Type of Distribution	Normal	Normal	Normal	Normal	Normal	Normal	Normal	Normal	Normal	Normal
Min (3sigma)	0.23	0.27	0.29	0.23	0.31	0.31	0.12	0.24	0.32	0.21
Max (3sigma)	0.54	0.52	0.47	0.52	0.56	0.61	0.42	0.47	0.50	0.39
Variance of Sample Mean	2.54E-03	1.69E-03	9.22E-04	2.43E-03	1.78E-03	2.54E-03	2.54E-03	1.40E-03	9.22E-04	9.22E-04
Standard Deviation of Sample Mean	5.04E-02	4.11E-02	3.04E-02	4.93E-02	4.21E-02	5.04E-02	5.04E-02	3.75E-02	3.04E-02	3.04E-02
Mean	0.39	0.39	0.38	0.37	0.43	0.46	0.27	0.35	0.41	0.30
Count	23	21	15	19	7	n/a	n/a	19	n/a	n/a

**Table 5-17. Uncertainty Analysis summary statistics for total porosity, dry bulk density, and particle density – continued**

Bulk Density

Material	Upper Zone	Lower Zone	"SAND"	"CLAY-SAND"	"CLAY"	Operational Soil Cover (prior to DC) <sup>1</sup>	Operational Soil Cover (after DC) <sup>1</sup>	Controlled Compacted Backfill	ILV Permeable Backfill <sup>2</sup>	Gravel <sup>3</sup>
Type of Distribution	Normal	Normal	Normal	Normal	Normal	Normal	Normal	Normal	Normal	Normal
Min (3sigma)	1.24	1.31	1.40	1.32	1.16	1.03	1.51	1.42	1.31	1.57
Max (3sigma)	2.06	1.92	1.90	2.05	1.89	1.85	2.33	2.00	1.81	2.07
Variance of Sample Mean	1.88E-02	1.04E-02	6.95E-03	1.48E-02	1.48E-02	1.88E-02	1.88E-02	9.43E-03	6.95E-03	6.95E-03
Standard Deviation of Sample Mean	1.37E-01	1.02E-01	8.34E-02	1.22E-01	1.22E-01	1.37E-01	1.37E-01	9.71E-02	8.34E-02	8.34E-02
Mean	1.65	1.62	1.65	1.68	1.52	1.44	1.92	1.71	1.56	1.82
Count	23	21	15	19	7	n/a	n/a	19	n/a	n/a

**Table 5-17. Uncertainty Analysis summary statistics for total porosity, dry bulk density, and particle density – continued**

Particle Density

Material	Upper Zone	Lower Zone	"SAND"	"CLAY-SAND"	"CLAY"	Operational Soil Cover (prior to DC) <sup>1</sup>	Operational Soil Cover (after DC) <sup>1</sup>	Controlled Compacted Backfill	ILV Permeable Backfill <sup>2</sup>	Gravel <sup>3</sup>
Type of Distribution	Normal	Normal	Normal	Normal	Normal	Normal	Normal	Normal	Normal	Normal
Min (3sigma)	2.60	2.55	2.60	2.56	2.58	2.57	2.57	2.60	2.57	2.53
Max (3sigma)	2.76	2.80	2.74	2.81	2.78	2.73	2.73	2.70	2.71	2.67
Variance of Sample Mean	7.43E-04	1.75E-03	5.57E-04	1.74E-03	1.14E-03	7.43E-04	7.43E-04	2.88E-04	5.57E-04	5.57E-04
Standard Deviation of Sample Mean	2.73E-02	4.19E-02	2.36E-02	4.17E-02	3.37E-02	2.73E-02	2.73E-02	1.70E-02	2.36E-02	2.36E-02
Mean	2.68	2.68	2.67	2.69	2.68	2.65	2.65	2.65	2.64	2.60
Count	23	21	15	19	7	n/a	n/a	19	n/a	n/a

<sup>1</sup> no data is available for the operational soil cover; assumed to have same standard deviation as upper zone; DC=dynamic compaction

<sup>2</sup> mean value based on 2 measurements; type of distribution, variance, and standard deviation are assumed to be same as "sand"

<sup>3</sup> little data are available for the gravel; assumed to have same standard deviation as "sand"

**Table 5-18. Uncertainty analysis summary statistics for saturated hydraulic conductivity**

Statistical Results from Bootstrapping Technique (based on sample data)  
 $\log K_h^1$

Material	Upper Zone	Lower Zone	"SAND"	"CLAY-SAND"	"CLAY"	Operational Soil Cover (prior to DC) <sup>2,3</sup>	Operational Soil Cover (after DC) <sup>2,3</sup>	Controlled Compacted Backfill	ILV Permeable Backfill <sup>4</sup>	Gravel <sup>5</sup>
Type of Distribution	normal	normal	normal	normal	normal	normal	normal	normal	normal	normal
Min (3sigma)	-5.21	-4.13	-4.00	-5.08	-6.94	-4.52	-5.45	-4.40	-3.54	-1.24
Max (3sigma)	-4.01	-3.35	-3.16	-3.88	-5.44	-3.32	-4.25	-3.86	-2.70	-0.40
Variance of Sample Mean	4.00E-02	1.69E-02	1.96E-02	4.00E-02	6.25E-02	4.00E-02	4.00E-02	7.92E-03	1.96E-02	1.96E-02
Standard Deviation of Sample Mean	2.00E-01	1.30E-01	1.40E-01	2.00E-01	2.50E-01	2.00E-01	2.00E-01	8.90E-02	1.40E-01	1.40E-01
Mean <sup>6</sup>	-4.61	-3.74	-3.58	-4.48	-6.19	-3.92	-4.85	-4.13	-3.12	-0.82
	2.5E-05	1.8E-04	2.6E-04	3.3E-05	6.5E-07	1.2E-04	1.4E-05	7.4E-05	4.6E-04	1.5E-01
Count	3	7	15	19	7	n/a	n/a	32	n/a	n/a

**Table 5-18. Uncertainty analysis summary statistics for saturated hydraulic – continued**

Statistical Results from Bootstrapping Technique (based on sample data)

$\log K_v^1$

Material	Upper Zone	Lower Zone	"SAND"	"CLAY-SAND"	"CLAY"	Operational Soil Cover (prior to DC) <sup>2,3</sup>	Operational Soil Cover (after DC) <sup>2,3</sup>	Controlled Compacted Backfill	ILV Permeable Backfill <sup>4</sup>	Gravel <sup>5</sup>
Type of Distribution	normal	normal	normal	normal	normal	normal	normal	normal	normal	normal
Min (3sigma)	-6.36	-5.24	-5.10	-5.78	-7.57	-4.70	-5.63	-4.71	-4.56	-1.75
Max (3sigma)	-4.80	-3.80	-3.24	-4.46	-5.71	-3.14	-4.07	-4.05	-2.70	0.11
Variance of Sample Mean	6.76E-02	5.76E-02	9.61E-02	4.84E-02	9.61E-02	6.76E-02	6.76E-02	1.21E-02	9.61E-02	9.61E-02
Standard Deviation of Sample Mean	2.60E-01	2.40E-01	3.10E-01	2.20E-01	3.10E-01	2.60E-01	2.60E-01	1.10E-01	3.10E-01	3.10E-01
Mean <sup>6</sup>	-5.58 2.6E-06	-4.52 3.0E-05	-4.17 6.8E-05	-5.12 7.6E-06	-6.64 2.3E-07	-3.92 1.2E-4	-4.85 1.4E-5	-4.38 4.2E-05	-3.63 3.1E-01	-0.82 1.5E-1
Count	3	7	15	19	7	n/a	n/a	32	n/a	n/a

<sup>1</sup> note that  $K_h$  and  $K_v$  are log normally distributed

<sup>2</sup> no data is available for the operational soil cover; hydraulic conductivity estimated based on upper zone properties; assumed to have same standard deviation as upper zone; DC=dynamic compaction

<sup>3</sup> the three ET's planned for Plot 8 are assumed to be backfilled with LVZ soils due to the absence of a UVZ in this vicinity; therefore, will need to use the same analysis (Kozeny-Carman equation) described in Section 5.4.1 for estimating mean hydraulic conductivity for Plot 8 OSC before and after DC applying the modified statistics from Table 5-18; this will result in a different set of summary statistics than for OSC obtained from UVZ material.

<sup>4</sup> mean value based on 2 measurements; type of distribution, variance, and standard deviation are assumed to be same as "sand"

<sup>5</sup> little hydraulic conductivity data available; assumed to have same standard deviation as "sand"

<sup>6</sup> top number is the log of the mean; bottom number is the mean

**Table 5-18. Uncertainty analysis summary statistics for saturated hydraulic – continued**

Modified Statistics Using Adjusted Saturated Hydraulic Conductivities (based on  $+2\sigma$ )

$\log K_h^1$

Material	Upper Zone	Lower Zone	"SAND"	"CLAY-SAND"	"CLAY"
Type of Distribution	normal	normal	normal	normal	normal
Min (3sigma)	-4.81	-3.87	-3.72	-4.68	-6.45
Max (3sigma)	-3.61	-3.09	-2.88	-3.48	-4.95
Variance of Sample Mean	4.00E-02	1.69E-02	1.96E-02	4.00E-02	6.25E-02
Standard Deviation of Sample Mean <sup>1</sup>	2.00E-01	1.30E-01	1.40E-01	2.00E-01	2.50E-01
Recommended Value <sup>2</sup>	-4.21	-3.48	-3.30	-4.08	-5.70
	6.2E-05	3.3E-04	5.0E-04	8.3E-05	2.0E-06
Count	3	7	15	19	7

$\log K_v^1$

Material	Upper Zone	Lower Zone	"SAND"	"CLAY-SAND"	"CLAY"
Type of Distribution	normal	normal	normal	normal	normal
Min (3sigma)	-5.84	-4.76	-4.48	-5.34	-6.95
Max (3sigma)	-4.28	-3.32	-2.62	-4.02	-5.09
Variance of Sample Mean	6.76E-02	5.76E-02	9.61E-02	4.84E-02	9.61E-02
Standard Deviation of Sample Mean <sup>1</sup>	2.60E-01	2.40E-01	3.10E-01	2.20E-01	3.10E-01
Recommended Value <sup>2</sup>	-5.06	-4.04	-3.55	-4.68	-6.02
	8.7E-06	9.1E-05	2.8E-04	2.1E-05	9.5E-07
Count	3	7	15	19	7

<sup>1</sup> standard deviation of sample mean comes from statistical results from bootstrapping technique (see above tables)

<sup>2</sup> top number is the log of the recommended value; bottom number is the recommended value

**Table 5-19. Uncertainty analysis summary statistics for saturated effective diffusion coefficient**

log De <sup>1</sup>										
Material	Upper Zone	Lower Zone	"SAND"	"CLAY-SAND"	"CLAY"	Operational Soil Cover (prior to DC)	Operational Soil Cover (after DC)	Controlled Compacted Backfill	ILV Permeable Backfill <sup>2</sup>	Gravel
Type of Distribution	normal	normal	normal	normal	normal	normal	normal	normal	normal	normal
Min (3sigma)	-5.49	-5.49	-5.44	-5.49	-5.55	-5.49	-5.55	-5.49	-4.75	-5.39
Max (3sigma)	-5.05	-5.05	-4.72	-5.05	-5.23	-5.05	-5.23	-5.05	-4.84	-4.67
Variance of Sample Mean	5.18E-03	5.18E-03	1.44E-02	5.18E-03	2.81E-03	5.18E-03	2.81E-03	5.18E-03	1.44E-02	1.44E-02
Standard Deviation of Sample Mean	0.072	0.072	0.12	0.072	0.053	0.072	0.053	0.072	0.12	0.12
Mean <sup>3</sup>	-5.27 5.4E-06	-5.27 5.4E-06	-5.08 8.3E-06	-5.27 5.4E-06	-5.39 4.1E-06	-5.27 5.4E-06	-5.39 4.1E-06	-5.27 5.4E-06	-4.79 1.6E-05	-5.03 9.4E-06

<sup>1</sup> note that De was assumed to be log normally distributed; no data available so assumptions were made based on literature values

<sup>2</sup> mean value based on 2 measurements; type of distribution, variance, and standard deviation are assumed to be same as "sand"

<sup>3</sup> top number is the log of the mean; bottom number is the mean

## 5.8 COMPARISON TO OBSERVED SUCTION LEVELS IN THE FIELD

Figure 3-5 in Nichols et al. (2000) reported field pore pressure readings from the Vadose Zone Monitoring System (VZMS) in E-area at three locations and 4 depths per location over an 8-month period. The field measurements indicate average suction levels in the approximate range of 50 to 200 cm. Water content ranged from roughly 0.15 to 0.30, suggesting saturation levels between 35% and 75%. Infiltration over the local area is estimated to be 30 cm/yr (12 in/yr). These data provide an opportunity to compare simulated pressure head and saturation, using the estimated upper and lower vadose zone properties established in the preceding sections, to field observations.

PORFLOW numerical simulations using the mean property values produced suction head and saturation values of 17 cm and 98% in the upper vadose zone, and 100 cm and 78% in the lower vadose zone. In comparison to the field data, these values indicate excessive water holdup in the model simulation. The apparently low unsaturated hydraulic conductivity values could be a result of bias in the saturated conductivity estimate and/or the soil characteristic curves. Because uncertainty has been estimated for saturated hydraulic conductivity, a convenient adjustment can be made by increasing saturated conductivities to the higher end (+2-sigma) of their uncertainty range, while leaving other properties undisturbed.

With this modification, PORFLOW numerical simulations produced suction head and saturation values of 83 cm and 91% in the upper vadose zone, and 170 cm and 72% in the lower vadose zone. These values are in better agreement with the field monitoring data. Hence, the recommended values for the undisturbed soils (upper, lower, and single zone) for use in the modeling are based on +2-sigma of the calculated saturated hydraulic conductivity. In addition, saturated hydraulic conductivity values for the textural categories (sand, clay-sand, and clay) were approximated using the +2-sigma adjustment. For uncertainty analysis, we suggest retaining the variance/standard deviation values shown Table 5-18 for association with the adjusted conductivity recommendations. The bottom of Table 5-18 (“Modified Statistics Using Adjusted Saturated Hydraulic Conductivities (based on +2-sigma)”) provides the recommended means (which incorporate the increase in saturated conductivities) together with the variance/standard deviation values determined from the bootstrapping technique.

## 5.9 SUMMARY

Table 5-20 provides a summary of the soil properties recommended for the modeling with designations (in a column labeled “source”) to specify from where the data came from. This report primarily evaluates available soil property data for the vicinity near the E-Area disposal units. In some cases, data from Z-Area were also incorporated into the evaluation.

**Table 5-20. Summary of recommended soil properties**

Material	Saturated Hydraulic Conductivity				Bulk Properties					
	$K_h$ (cm/s)	$K_v$ (cm/s)	$K_h/K_v$	Source	Saturated Effective Diffusion Coefficient, $D_e$ (cm <sup>2</sup> /s)	Source	Total Porosity (unitless)	Dry Bulk Density (g/cm <sup>3</sup> )	Particle Density (g/cm <sup>3</sup> )	Source
Upper Vadose Zone (Above 264 ft-msl in E-Area)	6.2E-05	8.7E-06	7.1	<i>a</i>	5.3E-06	<i>k</i>	0.385	1.65	2.68	<i>h</i>
Lower Vadose Zone (Below 264 ft-msl in E-Area)	3.3E-04	9.1E-05	3.6	<i>a</i>	5.3E-06	<i>k</i>	0.395	1.62	2.68	<i>h</i>
E-Area Operational Soil Cover Prior to Dynamic Compaction	1.2E-04	1.2E-04	1.0	<i>d</i>	5.3E-06	<i>k</i>	0.46	1.44	2.65	<i>i</i>
E-Area Operational Soil Cover after Dynamic Compaction	1.4E-05	1.4E-05	1.0	<i>f</i>	4.0E-06	<i>k</i>	0.27	1.92	2.65	<i>i</i>
Controlled Compacted Backfill	7.6E-05	4.1E-05	1.9	<i>c</i>	5.3E-06	<i>k</i>	0.35	1.71	2.65	<i>h</i>
IL Vault Permeable Backfill	1.4E-03	7.6E-04	1.9	<i>g</i>	8.0E-06	<i>k</i>	0.41	1.56	2.64	<i>g</i>
Sand (<25% Mud)	5.0E-04	2.8E-04	1.8	<i>b</i>	8.0E-06	<i>k</i>	0.383	1.65	2.67	<i>h</i>
Clay-Sand (25-50% Mud)	8.3E-05	2.1E-05	4.0	<i>b</i>	5.3E-06	<i>k</i>	0.374	1.68	2.69	<i>h</i>
Clay (>50% Mud)	2.0E-06	9.5E-07	2.1	<i>b</i>	4.0E-06	<i>k</i>	0.433	1.52	2.68	<i>h</i>
Gravel	1.5E-01	1.5E-01	1.0	<i>e</i>	9.4E-06	<i>k</i>	0.30	1.82	2.6	<i>j</i>
Saturated Zone Soils	--	--	--	<i>o</i>	Sand: 5.3E-06 Clay: 4.0E-06	<i>p</i>	0.25	1.04	1.39	<i>p</i>

Table 5-20. Summary of recommended soil properties - Continued

Material	Water Retention					Source
	$\theta_s$	$\theta_r$	$\alpha$	$n$	$m$	
Upper Vadose Zone (Above 264 ft-msl in E-Area)	0.385000	0.102446	0.030177	1.153676	0.133205	<i>l</i>
Lower Vadose Zone (Below 264 ft-msl in E-Area)	0.380000	0.077849	0.167698	1.195226	0.163338	<i>l</i>
E-Area Operational Soil Cover Prior to Dynamic Compaction	0.456000	0.121330	0.040416	1.153656	0.133191	<i>n</i>
E-Area Operational Soil Cover after Dynamic Compaction	0.275000	0.073171	0.018263	1.153659	0.133193	<i>n</i>
Controlled Compacted Backfill	0.355000	0.198349	0.037124	1.463642	0.316773	<i>m</i>
IL Vault Permeable Backfill	0.415000	0.136697	0.037919	1.724947	0.420272	<i>m</i>
Sand (<25% Mud)	0.383000	0.082137	0.199006	1.241769	0.194697	<i>m</i>
Clay-Sand (25-50% Mud)	0.374000	0.057974	0.035465	1.140621	0.123285	<i>m</i>
Clay (>50% Mud)	0.433000	0.278156	0.009832	1.287965	0.223581	<i>m</i>
Gravel	0.300000	0.021000	0.137676	1.479624	0.324153	<i>m</i>
Saturated Zone Soils	--	--	--	--	--	<i>n/a</i>

Notes to Table 5-20:

*a* - based on 2 sigma of MegacptN/ATN location and sample; using CPT to define thickness and textural properties; averaging based on textural properties ("clay", "clay-sand", "sand) and thickness and using combination of arithmetic and geometric averaging ( $p_v = -0.33$  and  $p_h = 0.59$ )

*b* - based on 2 sigma; uses "most reliable" data (based on comparing bulk density); averaging uses combination of arithmetic and geometric averaging ( $p_v = -0.33$  and  $p_h = 0.59$ )

*c* - uses all samples from Old Radioactive Waste Burial Ground and Z-Area composite samples; averaging uses combination of arithmetic and geometric averaging ( $p_v = -0.33$  and  $p_h = 0.59$ )

*d* - based on Kozeny-Carman equation, Upper Zone porosity and hydraulic conductivity, assumed bulk density of operational soil cover of 90 pcf and bulk density of 2.65 g/cm<sup>3</sup> (calculated porosity of 0.456); the three ET's planned for Plot 8 are assumed to be backfilled with LVZ soils due to the absence of a UVZ in this vicinity; therefore, will need to use the same analysis (Kozeny-Carman equation) described in Section 5.4.1 for estimating hydraulic conductivity for Plot 8 OSC before DC

*e* - based on straight arithmetic average of two samples (GL-1 and GL-2 from WSRC-RP-93-894)

*f* - based on Kozeny-Carman equation, Upper Zone porosity and hydraulic conductivity, assumed bulk density of operational soil cover of 120 pcf and bulk density of 2.65 g/cm<sup>3</sup> (calculated porosity of .27); the three ET's planned for Plot 8 are assumed to be backfilled with LVZ soils due to the absence of a UVZ in this vicinity; therefore, will need to use the same analysis (Kozeny-Carman equation) described in Section 5.4.1 for estimating hydraulic conductivity for Plot 8 OSC after DC

*g* - based on straight arithmetic average of two samples (VL-1 44-46 and VL-1 13-15; samples with < 15% mud) with  $K_h/K_v$  of 1.9 (based upon controlled compacted backfill)

*h* - based on straight arithmetic average of all samples (used most reliable from hydraulic conductivity standpoint)

*i* - used WSRC-RP-2001-00613 (Phifer and Wilhite 2001) as reference for bulk density of operational cover before (90pcf) and after dynamic compaction (120pcf); particle density is based on Hillel, 1982

*j* - used Freeze and Cherry (Groundwater) and Dutro, Dietrich and Foose (AGI Data Sheets) to come up with estimate of porosity and particle density (calculated bulk density from these values)

*k* - based on literature values of tortuosity and molecular diffusion coefficients

*l* - used CPT to define thickness and textural properties at MegacptN/ATN location; averaged textural property curves ("clay", "clay-sand", "sand) based on the proportion of each in the upper zone, lower zone, and single zone

*m* - averaging of all reliable samples; samples for the controlled compacted backfill come from Old Radioactive Waste Burial Ground and Z-Area composite samples; gravel samples include GL-1 and GL-2 curves (WSRC-RP-93-894); IL Vault permeable backfill includes VL-1 44-46 and VL-1 13-15

*n* - used Upper Zone and adjusted suction head based on estimated porosity and estimated hydraulic conductivity (Leverett scaling)

*o* - refer to Flach and Harris (1996) and Flach (2004)

*p* - refer to discussion in Section 5.6 Saturated Zone; porosity, dry bulk density, and particle density values are the "effective" values

## 6.0 CEMENTITIOUS MATERIAL DATA

### 6.1 EXTERNAL LITERATURE REVIEW

#### 6.1.1 Porosity, Bulk Density, and Particle Density

The porosity of fully hydrated cement paste (i.e., cementitious material and water) can be classified into the following categories (Clifton and Knab, 1989; Helms, 1966; Popovics, 1992):

- Gel pores:  $<5E-07$  to  $1E-05$  mm
- Capillary pores:  $1E-05$  to  $0.01$  mm
- Entrained air:  $0.025$  to  $0.050$  mm
- Air voids due to incomplete consolidation:  $0.1$  to  $2.0$  mm

Cement paste pore-size distribution is a broad and continuous spectrum of pore sizes with separate peaks representing gel and capillary pores. Gel pores are the small pores formed within the fully hydrated cement paste that constitute about 28 percent of the paste volume. Capillary porosity results when the volume of cement gel is not sufficient to completely fill all the original water filled space in the cement paste. Therefore, capillary porosity increases rapidly with an increase in the water-to-cementitious material ratio (WCR). Capillary pores constitute a negligible volume for fully hydrated cement paste with a WCR between 0.35 and 0.40 or less and up to about 30 percent with a WCR of 0.70. A WCR between 0.35 and 0.40 is the minimum WCR for attaining complete hydration of the cementitious materials. In addition, increases in the WCR result in an increase in the gel and capillary pore size and greater pore system continuity. Fully hydrated cement paste with a WCR of 0.7 or less may produce a relatively discontinuous capillary pore system, however this does not destroy the continuity of the pore system as a whole, because water flow can occur through the gel pores. (Beaudoin and Marchand, 2001; Neville, 1973; Popovics, 1992)

In addition to porosity within the cement paste itself, the porosity of concrete (cementitious material, fine and coarse aggregate, and water) is also influenced by porosity resulting from air voids and those due to the fine and coarse aggregate. Air voids within concrete are produced due to purposeful air entrainment and due to incomplete consolidation of the concrete. Air voids (due to both air entrainment and incomplete consolidation) can make up 1 to 10 percent of the concrete by volume. Concrete is made up of about 75 percent by volume fine and coarse aggregate. Therefore, the characteristics of the aggregate greatly influence the porosity of the concrete. Aggregate porosity ranges from nearly 0 to as much as 20 percent by volume (most commonly about 1 to 5 percent). Pores size also varies greatly among different aggregates. In very dense aggregates, such as granite, the aggregate pores are in the intermediate capillary pore size range and frequently they are in the largest capillary pore size range. Additionally, the aggregate-paste interface can exhibit separation and microcracking thus adding to the porosity of the cement.

The following are factors that have been found to reduce concrete porosity:

- Low WCR (increased unit cementitious material content and reduced unit water content that can be facilitated by the use of high-range water reducers)(ACI, 201.2R-01; Clifton and Knab, 1989; Walton et al., 1990)
- Use of blast furnace slag, fly ash, and silica fume as cementitious material replacements for the cement content(ACI, 201.2R-01, 232.2R-03, 233R-03, 234R-96; Popovics, 1992; Soroushian and Alhozaimy, 1995)
- Proper mix proportioning (i.e., water, cementitious material, fine aggregate, and coarse aggregate proportioning) to produce a dense homogeneous concrete
- Air entrainment(ACI, 201.2R-01)
- Properly placed and well consolidated concrete (minimizes segregation and honeycombing)(ACI, 201.2R-01)
- Effectively cured concrete (minimizes cracking and maximizes cementitious material hydration) (ACI, 201.2R-01; Beaudoin and Marchand, 2001; Neville, 1973; Walton et al., 1990)

As can be seen it is not only the concrete mix properties that influence the porosity of concrete but also its field placement, consolidation, and curing. For properly placed, consolidated and cured concrete the WCR is the most important factor in controlling porosity. (Clifton and Knab, 1989) The use of blast furnace slag, fly ash, and silica fume as cementitious material replacements for the cement content is probably the second most important factor in controlling porosity. Calcium hydroxide and other soluble alkalis are released during Portland cement hydration. The water-soluble calcium hydroxide and other alkalis are very easily leached out of the concrete matrix, which increases the concrete porosity and overall size of pores. Blast furnace slag, fly ash, and silica fume react with soluble calcium hydroxide and other alkalis to produce calcium silicate hydrate (C-S-H), which is much less soluble. Concrete pores, which would have normally contained calcium hydroxide, are, in part, filled with C-S-H instead, thus reducing the porosity and refining the pore structure.(ACI, 232.2R-03, 233R-03, 234R-96; Soroushian and Alhozaimy, 1995) Effective curing is very important to concrete pore structure, because the cementitious material hydration products (i.e., gel) are approximately 2.1 times the volume of the unhydrated cementitious material. Therefore, with curing, the gel gradually fills some of the original water-filled space. (Beaudoin and Marchand, 2001; Neville, 1973; Popovics, 1992)

There are two primary methods of measuring the porosity of concrete: gravimetric and mercury intrusion porosimetry (MIP). The gravimetric method of measuring concrete porosity involves determination of effective porosity (i.e., inter-connected porosity which is available to water flow or water intrudeable porosity) from measurements of the concrete sample saturated weight, concrete sample oven dried weight, and concrete sample volume (ASTM, C 642 – 97; Flint, 2002a). The MIP of measuring concrete porosity involves determination of effective porosity (i.e., inter-connected porosity which is available to mercury flow or mercury intrudeable porosity) from the measurement of the volume of liquid mercury forced into a concrete sample under incrementally increasing pressures (ASTM, D 4404-84).

Table 6-1, Table 6-2, and Table 6-3 provide the measured effective porosities of concrete (i.e., contains cement, fine and coarse aggregate, and water), mortar (i.e., contains cementitious material, fine aggregate, and water), and cementitious paste (i.e., contains cementitious material and water), respectively, obtained from various literature sources that used MIP or gravimetric means to measure the porosity. Total porosity, which also includes dead pores (i.e., those that are not interconnected), is not measured by these two methods. Figure 6-1 provides the effective porosity of concrete, mortar, and cementitious paste with WCR, based upon the data from these literature sources. From these data, the porosity of concrete, mortar, and cementitious paste, that do not contain blast furnace slag, fly ash, and silica fume, is seen to range from 9.6 to 18.4 (Table 6-1), from 7.5 to 20.8 (Table 6-2), and from 8.7 to 22.2 (Table 6-3), respectively. In general, it is seen that porosity increases with increasing WCR (Table 6-1). As seen in Table 6-2 the porosity of mortars containing silica fume are significantly less than those that do not. From this data the porosity of cementitious paste that contains silica fume is shown to range from 4.0 to 22.5 (Table 6-2), and it is not clear whether cementitious paste containing silica fume has a porosity different from that of pastes that do not contain silica fume. Figure 6-1 also provides WCR-porosity relationships developed from these data for concrete, mortar, paste, and paste with silica fume.

The bulk density of normal weight concrete ranges from 120 to 165 lbs/ft<sup>3</sup> (from 1.92 to 2.64 g/cm<sup>3</sup>). (Helms, 1966) The bulk density of concrete is typically determined by the same gravimetric method utilized to determine effective porosity. (ASTM, C 642 – 97) The particle density of concrete is typically determined by calculation from porosity and bulk density as follows in equation (44); (Flint, 2002b):

$$\rho_p = \frac{\rho_b}{(1 - \eta)} \quad (44)$$

where  $\rho_p$  = particle density;  $\rho_b$  = dry bulk density;  $\eta$  = porosity

The particle density of concrete can also be directly measured as a specific gravity of the concrete solids (USACE, 1970).

**Table 6-1. Porosity of concrete (i.e., contains cement, fine and coarse aggregate, and water)**

WCR	Cement	Fly Ash	BFS	SF	Sand	Aggregate	Cure Time	Porosity (%)	Method	Source
0.38	1 part/dry material	0	0	0	1.1 part/dry material	2.7 part/dry material	27 days	9.6	MIP	Kumar and Bhattacharjee 2003
0.42	1 part/dry material	0	0	0	1.3 part/dry material	3.2 part/dry material	27 days	11.7	MIP	Kumar and Bhattacharjee 2003
0.46	1 part/dry material	0	0	0	1.5 part/dry material	3.6 part/dry material	27 days	12.4	MIP	Kumar and Bhattacharjee 2003
0.5	410 kg/m <sup>3</sup>	0	0	0	558 kg/m <sup>3</sup>	1171.8 kg/m <sup>3</sup>	28 days	~15	G	Safiuddin and Hearn 2005
0.51	1 part/dry material	0	0	0	1.8 part/dry material	3.9 part/dry material	27 days	11.6	MIP	Kumar and Bhattacharjee 2003
0.56	1 part/dry material	0	0	0	2.2 part/dry material	4.2 part/dry material	27 days	12.0	MIP	Kumar and Bhattacharjee 2003
0.6	342 kg/m <sup>3</sup>	0	0	0	643.5 kg/m <sup>3</sup>	1171.8 kg/m <sup>3</sup>	28 days	~18.4	G	Safiuddin and Hearn 2005
0.65	1 part/dry material	0	0	0	2.5 part/dry material	5.1 part/dry material	27 days	12.1	MIP	Kumar and Bhattacharjee 2003

BFS = blast furnace slag; SF = silica fume; MIP = mercury intrusion porosimetry; G = gravimetric

**Table 6-2. Porosity of mortars (i.e., contains cementitious material, fine aggregate, and water)**

WCR	Cement	Fly Ash	BFS	SF	Sand	Aggregate	Cure Time	Porosity (%)	Method	Source
0.25	100 wt% CM	0	0	0	50 total vol%	0	3 months	7.5	MIP	Delagrave et al. 1998
0.3	639 kg/m <sup>3</sup>	0	0	0	1380 kg/m <sup>3</sup>	0	28 days	8.0	G	Lafhaj et al. 2005
0.35	639 kg/m <sup>3</sup>	0	0	0	1380 kg/m <sup>3</sup>	0	28 days	10.2	G	Lafhaj et al. 2005
0.40	639 kg/m <sup>3</sup>	0	0	0	1380 kg/m <sup>3</sup>	0	28 days	12.0	G	Lafhaj et al. 2005
0.45	100 wt% CM	0	0	0	50 total vol%	0	3 months	12.2	MIP	Delagrave et al. 1998
0.45	639 kg/m <sup>3</sup>	0	0	0	1380 kg/m <sup>3</sup>	0	28 days	12.2	G	Lafhaj et al. 2005
0.45	Yes	0	0	0	Yes	0	Unknown	16.0	MIP	Hernandez et al. 2000
0.5	639 kg/m <sup>3</sup>	0	0	0	1380 kg/m <sup>3</sup>	0	28 days	13.2	G	Lafhaj et al. 2005
0.50	Yes	0	0	0	Yes	0	Unknown	19.0	MIP	Hernandez et al. 2000
0.55	639 kg/m <sup>3</sup>	0	0	0	1380 kg/m <sup>3</sup>	0	28 days	13.4	G	Lafhaj et al. 2005
0.55	Yes	0	0	0	Yes	0	Unknown	19.9	MIP	Hernandez et al. 2000
0.60	639 kg/m <sup>3</sup>	0	0	0	1380 kg/m <sup>3</sup>	0	28 days	13.6	G	Lafhaj et al. 2005
0.60	Yes	0	0	0	Yes	0	Unknown	20.8	MIP	Hernandez et al. 2000
0.25	94 wt% CM	0	0	6 wt% CM	50 total vol%	0	3 months	4.6	MIP	Delagrave et al. 1998
0.45	94 wt% CM	0	0	6 wt% CM	50 total vol%	0	3 months	11.7	MIP	Delagrave et al. 1998

BFS = blast furnace slag; SF = silica fume; MIP = mercury intrusion porosimetry; G = gravimetric; wt% = weight percent; CM = cementitious materials; Vol% = volume percent

**Table 6-3. Porosity of cementitious pastes (i.e., contains cementitious material and water)**

WCR	Cement	Fly Ash	BFS	SF	Sand	Aggregate	Cure Time	Porosity (%)	Method	Source
0.25	100 wt%	0	0	0	0	0	3 months	8.7	MIP	Delagrave et al. 1998
0.25	100 wt%	0	0	0	0	0	56 days	11.3	MIP	Johnson and Wilmont 1992
0.35	100 wt%	0	0	0	0	0	56 days	18.1	MIP	Johnson and Wilmont 1992
0.45	100 wt% CM	0	0	0	0	0	3 months	22.2	MIP	Delagrave et al. 1998
0.25	94 wt%	0	0	6 wt%	0	0	3 months	4.0	MIP	Delagrave et al. 1998
0.25	90 wt%	0	0	10 wt%	0	0	56 days	14.2	MIP	Johnson and Wilmont 1992
0.25	85 wt%	0	0	15 wt%	0	0	56 days	13.0	MIP	Johnson and Wilmont 1992
0.35	90 wt%	0	0	10 wt%	0	0	56 days	22.5	MIP	Johnson and Wilmont 1992
0.35	85 wt%	0	0	15 wt%	0	0	56 days	19.8	MIP	Johnson and Wilmont 1992
0.45	94 wt% CM	0	0	6 wt% CM	0	0	3 months	18.6	MIP	Delagrave et al. 1998

BFS = blast furnace slag; SF = silica fume; MIP = mercury intrusion porosimetry; wt% = weight percent; CM = cementitious materials

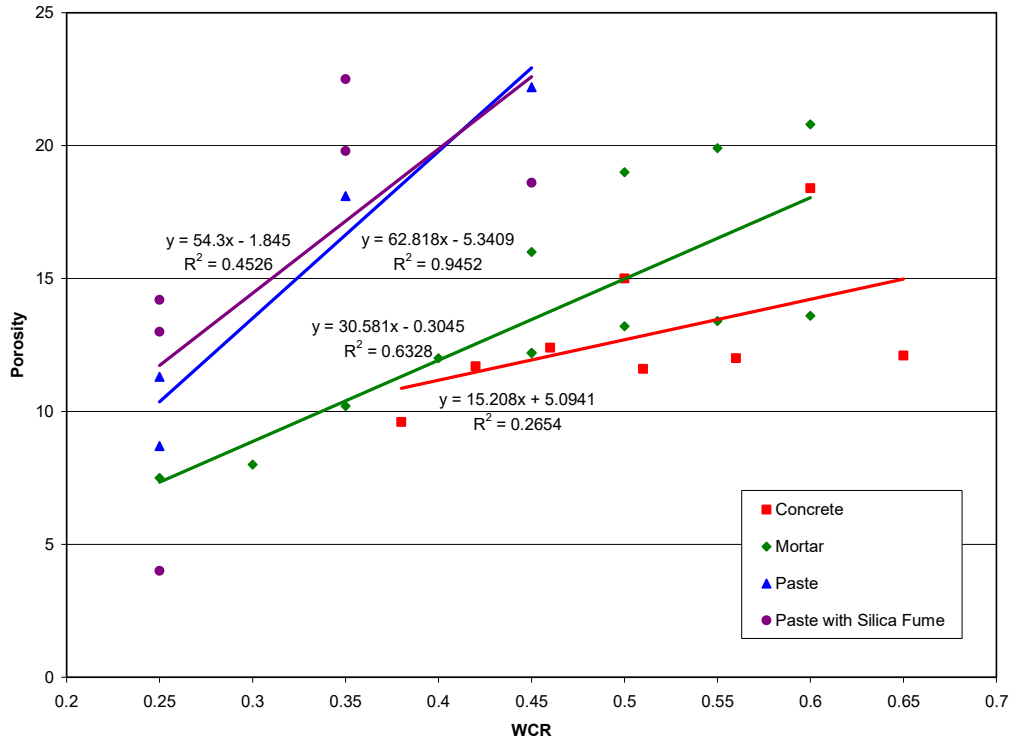


**Figure 6-1. Porosity of concrete, mortar, and cementitious paste with WCR**

### 6.1.2 Saturated Hydraulic Conductivity and Saturated Intrinsic Permeability

Saturated hydraulic conductivity,  $K$ , is a function of both the porous media and permeating fluid. Based upon Darcy’s Law the hydraulic conductivity is defined as follows (Freeze and Cherry, 1979):

$$K = \frac{Q * \Delta L}{A * \Delta h} \quad (45)$$

where  $K$  = length/time (typically cm/s);  $Q$  = flow rate (typically cm<sup>3</sup>/s);  $\Delta L$  = flow distance (cm);  $A$  = area (typically cm<sup>2</sup>);  $\Delta h$  = change in fluid head over the flow distance (typically cm of water).

Saturated intrinsic permeability,  $k_i$ , or just permeability is a function of the porous media alone. Permeability is related to hydraulic conductivity as follows (Freeze and Cherry, 1979):

$$k_i = K \left( \frac{u}{\rho * g} \right) \quad (46)$$

where  $k_i$  = length<sup>2</sup> (typically cm<sup>2</sup>);  $K$  = length/time (typically cm/s);  $u$  = fluid dynamic viscosity (typically cp = 0.01 P = 0.01 g/cm·s);  $\rho$  = fluid density (typically g/cm<sup>3</sup>);  $g$  = acceleration of gravity (980.6 cm/s<sup>2</sup>)

This leads to the following equation for intrinsic permeability (Freeze and Cherry, 1979):

$$k_i = \frac{Q * \Delta L * u}{A * \Delta h * \rho * g} \quad (47)$$

where  $k_i$  = length<sup>2</sup> (typically cm<sup>2</sup>);  $Q$  = flow rate (typically cm<sup>3</sup>/s);  $\Delta L$  = flow distance (cm);  $u$  = fluid dynamic viscosity (typically cp = 0.01 P = 0.01 g/cm·s);  $A$  = area (typically cm<sup>2</sup>);  $\Delta h$  = change in fluid head over flow distance (typically cm of water) ;  $\rho$  = fluid density (typically g/cm<sup>3</sup>);  $g$  = acceleration of gravity (980.6 cm/s<sup>2</sup>)

Typically, within the literature the term concrete permeability is used to refer to both saturated hydraulic conductivity and saturated intrinsic permeability, and the only way to determine which is actually being referenced is by the units utilized. The typical units of concrete saturated hydraulic conductivity used in the literature are cm/s. The typical units of saturated intrinsic permeability used in the literature are cm<sup>2</sup> and darcy. A darcy “is defined as the permeability that will lead to a specific discharge of 1 cm/s for a fluid with a viscosity of 1 cp under a hydraulic gradient that makes the term  $\rho g \Delta h / \Delta L$  equal to 1 atm/cm (Freeze and Cherry, 1979):

$$1 \text{ darcy} = 9.87E - 09 \text{ cm}^2$$

In the following generic discussion of cementitious materials, the term permeability refers to both saturated hydraulic conductivity and saturated intrinsic permeability.

The permeability of a cementitious material is a function of its pore structure characteristics (i.e., porosity, pore size distribution, connectivity of pores, and extent of separation and microcracking at aggregate-paste interfaces). The permeability of a cementitious material increases with increases in porosity, greater distribution of larger sized pores, greater pore connectivity, and increased separation and microcracking at the aggregate-paste interface. (Clifton and Knab, 1989; Neville, 1973; Soroushian and Alhozaimy, 1995)

Although gel pores (<5E-07 to 1E-05 mm) of fully hydrated cement paste constitute about 28 percent of the paste volume, the permeability of cement paste with only gel pores is only about 7.0E-14 cm/s. Capillary porosity (1E-05 to 0.01 mm) results when the volume of cement gel is not sufficient to completely fill all the original water filled space in the cement paste. Negligible capillary porosity exists in fully hydrated cement paste with a WCR between 0.35 and 0.40, but it increases rapidly as the WCR increases. For cement paste with a WCR of 0.70, the capillary porosity increases to about 30 percent. Additionally, increases in the WCR result in an increase in the gel and capillary pore size and greater pore system connectivity. The permeability of cement paste with significant capillary porosity is 20 to 1000 times that of cement paste with only gel pores. (Beaudoin and Marchand, 2001; Neville, 1973; Popovics, 1992; Verbeck, 1966)

Porosity resulting from purposeful air entrainment (0.025 to 0.050 mm) actually decreases the permeability of concrete by producing air filled bubbles within the concrete that do not form part of the interconnected porosity. (ACI, 201.2R-01; Popovics, 1992).

However, air voids resulting from incomplete consolidation (0.1 to 2.0 mm) typically produce increased interconnected porosity, particularly at the aggregate-paste interface, resulting in increased permeability. (Soroushian and Alhozaimy, 1995; Verbeck, 1966)

Because concrete is made up of about 75 percent by volume fine and coarse aggregate, the aggregate can influence the permeability of concrete. Aggregate porosity typically ranges from 1 to 5 percent, and in very dense aggregates, such as granite, the aggregate pores are in the intermediate capillary pore size range and frequently they are in the largest capillary pore size range. The permeability of granite has been measured at  $1.56E-8$  and  $5.35E-9$  cm/s, and that of quartz has been measured at  $8.24E-12$  cm/s. The influence of the aggregate on the permeability of well-consolidated concrete, however, is generally small, because the cement paste encases the aggregate, requiring flow through the paste. Under these conditions it is the paste permeability that has the greatest effect on the overall concrete permeability. However, the aggregate can either decrease or increase the permeability of concrete.

Low permeability aggregate in well-consolidated concrete decreases the effective area over which flow can occur and provides a more torturous flow path both of which decrease the permeability. High permeability aggregate will increase concrete permeability. Concrete that has not been well-consolidated can result in increased separation and microcracking at the aggregate-paste interface and honeycombing, which can also increase the concrete permeability. (Neville, 1973; Soroushian and Alhozaimy, 1995; Verbeck, 1966)

As indicated, the cementitious material's pore structure characteristics (i.e., porosity, pore size distribution, connectivity of pores, and extent of separation and microcracking at aggregate-paste interfaces) essentially determine the permeability of the cementitious material. Therefore, the same factors which have been shown to reduce concrete porosity also reduce its permeability:

- Low WCR (increased unit cementitious material content and reduced unit water content that can be facilitated by the use of high-range water reducers) (ACI, 201.2R-01; Clifton and Knab, 1989; Snyder, 2003; Verbeck, 1966; Walton et al., 1990)
- Use of blast furnace slag, fly ash, and silica fume as cementitious material replacements for the cement content (ACI, 201.2R-01, 232.2R-03, 233R-03, 234R-96; Clifton and Knab, 1989; Popovics, 1992; Soroushian and Alhozaimy, 1995)
- Proper mix proportioning (i.e., water, cementitious material, fine aggregate, and coarse aggregate proportioning) to produce a dense homogeneous concrete
- Air entrainment (ACI, 201.2R-01; Popovics, 1992)
- Properly placed and well consolidated (minimizes segregation and honeycombing) (ACI, 201.2R-01; Clifton and Knab, 1989)
- Effectively cured (minimizes cracking and maximizes cementitious material hydration) (ACI, 201.2R-01; Beaudoin and Marchand, 2001; Clifton and Knab, 1989; Neville, 1973; Popovics, 1992; Soroushian and Alhozaimy, 1995; Walton et al., 1990)

As can be seen, it is not only the concrete mix properties that influence the permeability of concrete but also its field placement, consolidation, and curing. For properly placed, consolidated and cured concrete, the WCR is the most important factor in controlling permeability. (Clifton and Knab, 1989) However, while the permeability of concrete is a function of WCR, the measured permeability of various concretes at a fixed WCR can still vary over orders of magnitude due to the other factors that influence permeability. (Snyder, 2003) The use of blast furnace slag, fly ash, and silica fume as cementitious material replacements for the cement content is probably the second most important factor in controlling permeability. (ACI, 232.2R-03, 233R-03, 234R-96; Soroushian and Alhozaimy, 1995) See Section 6.1.1 for additional detail on the impact of blast furnace slag, fly ash, and silica fume on decreasing porosity and permeability.

The following are other items of note in association with concrete permeability:

- Permeability decreases as hydration continues because the volume of gel is approximately 2.1 times that of unhydrated cement. (Neville, 1973; Popovics, 1992)
- In general the greater the strength of concrete the lower its permeability. (Neville, 1973)

There are two predominant methods of measuring the saturated hydraulic conductivity or saturated intrinsic permeability of cementitious materials: permeameter and centrifuge methods. The permeameter methods basically involve the establishment of a hydraulic gradient across the sample and measuring the volume of fluid passed through the sample with time from which the saturated hydraulic conductivity can be calculated. Typical methods for conducting permeameter tests of cementitious materials are found in USACE (1992) and ASTM (D 5084-10). The centrifuge method basically involves the application of a steady-state centrifugal force and constant water flux to a sample from which the saturated hydraulic conductivity can be calculated. The methods for conducting centrifuge tests of cementitious materials are found in ASTM (6527-00) and Nimmo et al. (2002).

Table 6-4 provides literature values of saturated hydraulic conductivity for various cementitious materials. As seen the saturated hydraulic conductivity of concrete is stated to range from  $\sim 1.0\text{E}-14$  to  $1.0\text{E}-07$  cm/s (but more typically the range is reported as from  $1.0\text{E}-13$  to  $1.0\text{E}-08$  cm/s) with typical concrete in the range of  $1.0\text{E}-09$  to  $1.0\text{E}-08$  cm/s and low WCR concrete (approximately 0.45 and less) less than  $1.0\text{E}-10$  cm/s. A significant fraction of the literature values of saturated hydraulic conductivity for concrete are in the E-11 range. Aged and field concrete have a saturated hydraulic conductivity range of  $2.0\text{E}-11$  to  $1.0\text{E}-07$  cm/s. Cement pastes have a saturated hydraulic conductivity range of  $1.0\text{E}-13$  to  $4.0\text{E}-08$  cm/s. Controlled Low Strength Material (CLSM) or Flowable Fill has a saturated hydraulic conductivity range of  $3.3\text{E}-07$  to  $1.0\text{E}-04$  cm/s.

**Table 6-4. Cementitious material saturated hydraulic conductivity**

Sample Description	Saturated Hydraulic Conductivity (cm/s)	Reference
Concrete	$K_{sat}$ ranges from 1.0E-14 to 1.0E-09	Basheer 2001
Concrete	$K_{sat}$ ranges from 1.0E-13 to 1.0E-08	Clifton and Knab 1989
Typical concrete	$K_{sat}$ ranges from ~1.0E-09 to ~1.0E-08	Snyder 2003
Concrete with low WCR	<1.0E-10	Walton et al. 1990
12 concretes with WCR from 0.28 to 0.9; a range of aggregate, sand and cementitious ingredients including silica fume and superplasticizers (Lowest w/c not directly related to lowest K measurement.)	$K_{sat}$ ranges from 2.8E-11 to 6.1E-11	El-Dieb and Hooton 1994
Concrete with WCR = 0.35; Air content = 4.0 vol%; Compressive Strength = 33.1 MPa	3.7E-12	Basheer 2001
Concrete with WCR = 0.45; Air content = 5.8 vol%; Compressive Strength = 26.1 MPa	1.3E-11	Basheer 2001
Concrete with WCR = 0.45; 3 inch aggregate (Values for concretes with 1.5 inch aggregate are slightly less than for 3 inch aggregate at corresponding WCR)	~ 9.7 E-11	USDOI 1981
Concrete with WCR = 0.5; 3 inch aggregate (Values for concretes with 1.5 inch aggregate are slightly less than for 3 inch aggregate at corresponding WCR)	~ 2.9E-10	USDOI 1981
Concrete cured for about 700 hours with WCR = 0.51	1.0E-11	Hearn et al. 1994
Concrete with WCR = 0.55; Air content = 7.3 vol%; Compressive Strength = 20.0 MPa	4.7E-11	Basheer 2001
Concrete with WCR = 0.56	$K_{sat}$ ranges from ~3.0E-12 to ~7.0E-10	Hearn and Figg 2001
Concrete with WCR = 0.65; Air content = 6.8 vol%; Compressive Strength = 16.6 MPa	8.1E-11	Basheer 2001
Concrete with WCR = 0.75; Air content = 6.5 vol%; Compressive Strength = 10.6 MPa	1.1E-10	Basheer 2001
Ten concrete cores from structures in the Midlands of England	$K_{sat}$ ranges from 4.9E-11 to 1.1E-07	Osborne 1989
Ten concrete cores from structures in North East England	$K_{sat}$ ranges from 1.7E-10 to 5.4E-08	Osborne 1989
26 year old concrete with WCR = 0.9; porosity = 0.19	$K_{sat}$ ranges from 4.0E-11 to 2.0E-10	Hearn et al. 1994
26 year old concrete with WCR = 0.9	$K_{sat}$ ranges from 1.0E-10 to 2.2E-10	Hearn 1990
26 year old concrete with WCR = 0.9; dried and re-saturated	$K_{sat}$ ranges from 2.0E-11 to 2.2 E-10	Hearn 1990
26 year old concrete with WCR = 0.9; oven dried and re-saturated	$K_{sat}$ ranges from <9.8E-12 to 1.8E-09	Hearn 1990

**Table 6-4. Cementitious material saturated hydraulic conductivity - continued**

Sample Description	Saturated Hydraulic Conductivity (cm/s)	Reference
Hardened cement pastes	$K_{sat}$ ranges from 1.0E-11 to 4.0E-08	Luping and Nilsson 1992
Mature cement paste with w/c ratio of 0.3	1.0E-13	Powers et al. 1954; Powers et al. 1955
Mature cement paste with w/c ratio of 0.38	3.0E-13	Powers et al. 1954; Powers et al. 1955
Mature cement past with w/c ratio of 0.7	1.0E-10	Powers et al. 1954; Powers et al. 1955
Controlled low strength material (CLSM) or Flowable fill or Flowable Slurry	$K_{sat}$ ranges from 3.3E-07 to 1.0E-04	Naik et al. 2001
CLSM with a WCR = 0.60; 47 kg/m <sup>3</sup> Type I cement, 451 kg/m <sup>3</sup> Class F fly ash, 1105 kg/m <sup>3</sup> sand	~1.3E-05	Naik et al. 2001
CLSM with a WCR = 0.70; 35 kg/m <sup>3</sup> Type I cement, 482 kg/m <sup>3</sup> Class F fly ash, 1149 kg/m <sup>3</sup> sand	~1.3E-05	Naik et al. 2001
CLSM with a WCR = 1.12; 44 kg/m <sup>3</sup> Type I cement, 242 kg/m <sup>3</sup> Class F fly ash, 1461 kg/m <sup>3</sup> sand	7.5E-05	Naik et al. 2001
CLSM with a WCR = 1.25; 46 kg/m <sup>3</sup> Type I cement, 244 kg/m <sup>3</sup> Class F fly ash, 1274 kg/m <sup>3</sup> sand	6.9E-05	Naik et al. 2001

Note: modified from Table 5-1, WSRC 2005b

### 6.1.3 Characteristic Curves (Suction Head, Saturation, and Relative Permeability)

Rockhold et al. (1993) estimated the hydraulic properties for a concrete and the double-shell slurry feed (DSSF) grout (i.e., grouted waste form) for use within a Performance Assessment (PA) for the disposal of grouted double-shell tank waste at Hanford (WHC, 1993). A 7.5-cm-diameter by 15-mm-long concrete cylinder was obtained from the U.S. Army Waterways Experiment Station and cut into six subsamples for testing. The mix formulation of the concrete is not provided by Rockhold et al. (1993). Core samples were taken from a simulated DSSF grout waste form that was poured in 1988. The simulated DSSF grout consisted of 8-9 pounds of dry cementitious material per gallon of simulated salt waste solution mixed together. The dry cementitious material consisted of 6% type I/II Portland cement, 47% blast furnace slag, and 47% fly ash. The salt waste solution contains about 25 to 27 wt% salts, consisting primarily of sodium, nitrate, nitrite, and hydroxide ions (WHC, 1993).

Rockhold et al. (1993) determined the dry bulk density, total porosity, particle density, saturated hydraulic conductivity, and water retention data for the concrete and DSSF grout. The water retention data was utilized with the RETC program to determine the van Genuchten curve fitting parameters for both the concrete and DSSF grout so that their respective characteristic curves could be produced (i.e., suction head, saturation, and relative permeability). See Section 5.3.3, Water Retention, for a discussion of this methodology. Table 6-5 provides the dry bulk density, total porosity, particle density, saturated hydraulic conductivity, and the van Genuchten curve fitting parameters for both

the concrete and DSSF grout, and Figure 6-2 provides the resulting characteristic curves for the concrete and DSSF grout.

**Table 6-5. Hanford Concrete and DSSF Grout hydraulic properties**

Parameter	Hanford Concrete	DSSF Grout
$\rho_b$ (g/cm <sup>3</sup> )	1.99	1.10
$\eta$	0.2258	0.5781
$\rho_p$ (g/cm <sup>3</sup> )	2.59	2.61
$K_{sat}$ (cm/s)	3.75E-10	1.47E-08
$\theta_r$	0.0	0.0
$\theta_s$	0.2258	0.5781
$\alpha$ (cm <sup>-1</sup> of H <sub>2</sub> O) <sup>1</sup>	7.61E-06	1.08E-05
$n$	1.393	1.650
$m = 1 - \frac{1}{n}$	0.282	0.394

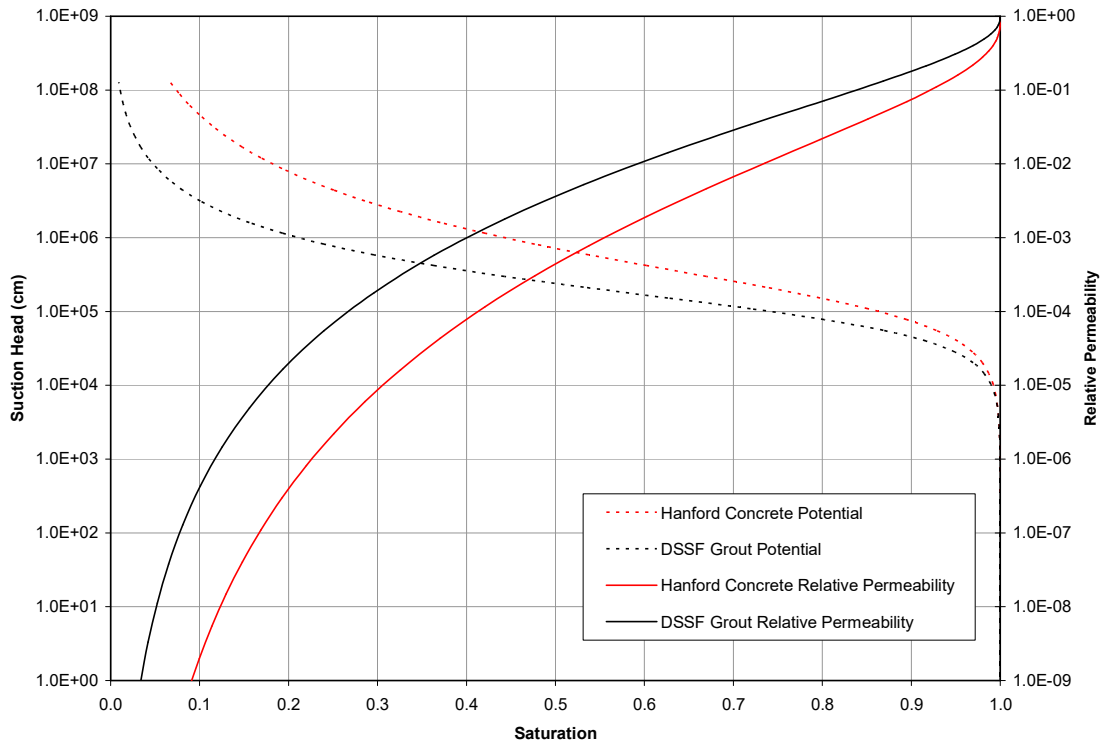


**Figure 6-2. Hanford Concrete and DSSF Grout characteristic curves (Rockhold et al., 1993)**

Savage and Janssen (1997b) conducted saturated hydraulic conductivity tests and drainage experiments on four different concrete mixtures. The saturated hydraulic conductivity of two 152-mm-diameter by 89-mm-thick disks for each concrete mixture was determined using low-gradient falling head permeameters (total of eight samples). The one-dimensional drainage in the axial direction of three saturated 152-mm-diameter by 32-mm-thick disks for each concrete mixture was determined within each of four constant relative humidity chambers (total of 48 samples). The drainage was recorded as moisture content with time until equilibrium conditions were reached. Each constant relative humidity chamber was set at different constant relative humidity to include the humidities of 97, 75, 53, and 31 percent. After the samples in the 97% relative humidity chamber had reached equilibrium, equilibrium conditions were determined and they were placed in a 92% relative humidity chamber.

The moisture content at equilibrium for each relative humidity (97, 92, 75, 53, and 31 percent) was converted into suction head versus volumetric moisture content by use of the Schofield equation. This suction head versus volumetric moisture content data was utilized to estimate van Genuchten curve fitting parameters for use in determining the characteristic curves (i.e., suction head, saturation, and relative permeability relationships) for each of the four concrete mixtures (see Section 5.3.3, Water Retention, for a discussion of this methodology). Table 6-6 provides the estimated van Genuchten curve fitting parameters along with the WCR and saturated hydraulic conductivity for each of the concrete mixtures. Figure 6-3 provides the resulting characteristic curves (i.e., suction head, saturation, and relative permeability relationships) for each of the four concrete mixtures. (Savage and Janssen, 1997b)

**Table 6-6. Savage and Janssen (1997b) WCR, saturated hydraulic conductivity, and van Genuchten curve fitting parameters**

Parameter	Concrete Mix			
	M60	M64	M69	M87
WCR	0.40	0.40	0.45	0.40
$K_{sat}$ (cm/s)	8.5E-10	5.6E-10	3.4E-10	3.8E-10
$\theta_r$	0.006	0.009	0.000	0.005
$\theta_s$	0.111	0.122	0.119	0.124
$\alpha$ (cm <sup>-1</sup> of H <sub>2</sub> O) <sup>1</sup>	2.47E-06	2.27E-06	2.89E-06	2.36E-06
n	1.723	1.750	1.666	1.739
m	0.420	0.429	0.400	0.425

WCR = water-to-cement ratio;  $K_{sat}$  = saturated hydraulic conductivity;  $\theta_r$  = residue volumetric moisture content;  $\theta_s$  = saturated volumetric moisture content;  $\alpha$  = constant related to air-entry pressure; n = a measure of the pore-size distribution; m = 1-1/n

<sup>1</sup> The  $\alpha$  exponent was incorrect within Savage and Janssen (1997b) Table 3, Moisture-related parameters and variables, as determined by the Savage and Janssen (1997b) Figure 3, Moisture characteristic curve. The exponent in meters<sup>-1</sup> of H<sub>2</sub>O should have been E-04 rather than E8, as shown in the table, in order to produce the Savage and Janssen (1997b) Figure 3 curve.

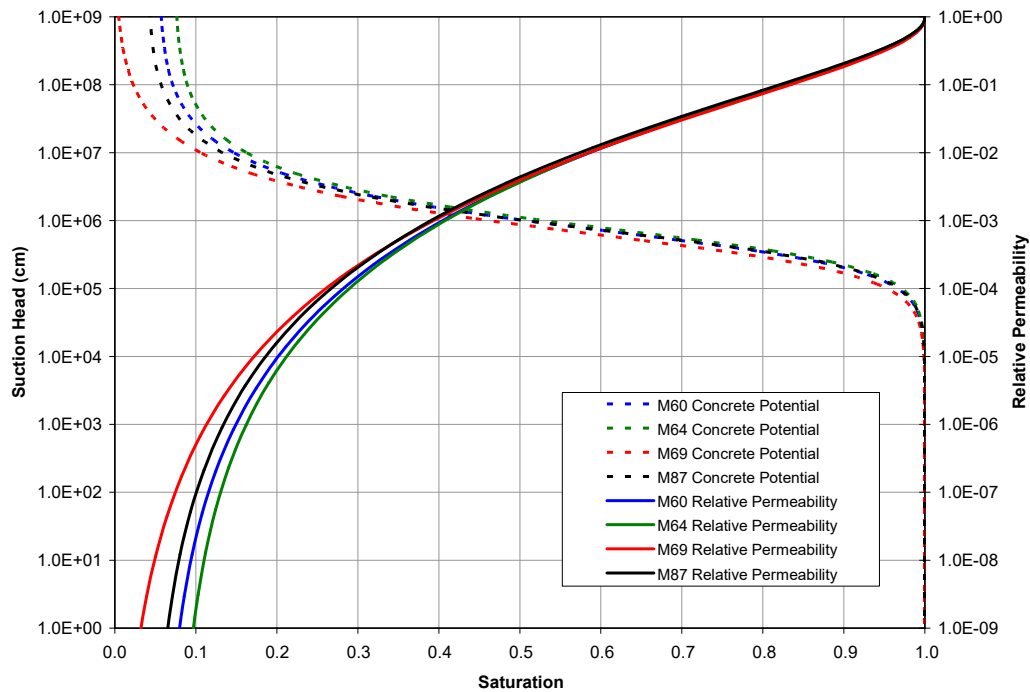


**Figure 6-3. Savage and Janssen (1997a) characteristic curves**

Additionally Savage and Janssen (1997b) utilized the saturated hydraulic conductivity and characteristic curves produced from the van Genuchten curve fitting parameters for each of the concrete mixtures to obtain unsaturated hydraulic conductivities. From this information equations (i.e., a model) were developed to quantitatively predict the drainage (moisture content versus time) for each of the concrete mixes. The drainage models produced based upon soil physics principles were able to accurately predict the unsaturated moisture movement within the concrete samples (i.e., the actual measured drainage). In the words of the authors, “the applicability of soil physics principles” (i.e., van Genuchten method) “to unsaturated moisture movement in PPC” (Portland cement concrete) “capillary pores has been clearly established.”

Baroghel-Bouny et al. (1999) conducted water vapor desorption and adsorption experiments (i.e., water content versus relative humidity) on 90-mm-diameter by 3-mm-thick disks of the two concrete mixes described in Table 6-7. The experiments included the measurement of sample diameter and thickness with relative humidity and the moisture content distribution of drying samples by gamma-ray measurements. The data produced from these experiments were utilized to produce water vapor desorption and adsorption isotherms, a model of shrinkage due to drying, and a model of the isothermal drying process.

**Table 6-7. Baroghel-Bouny et al. (1999) concrete mixes**

Mix Property	Ordinary Concrete (Mix BO)	High Performance Concrete (Mix BH)
WCR	0.48	0.26
Cement	Type I	Type I
Silica fume/cement ratio	0	0.1
Aggregate/cement ratio	5.48	4.55
Sand/gravel ratio	0.62	0.51
28-day Compressive Strength (MPa)	49.4	115.5

As part of the effort to develop a model of the isothermal drying process, Baroghel-Bouny et al. (1999) determined the total porosity and intrinsic permeability and performed curve fitting to determine the best fit values for parameters  $a$  and  $b$  of each mix for the following capillary curve equation:

$$p_c(S_i) = a(S_i^{-b})^{1-1/b} \quad (48)$$

where  $p_c(S_i)$  = capillary pressure in MPa at given liquid water saturation;  $S_i$  = given liquid water saturation

The above equation utilized by Baroghel-Bouny et al. (1999) is a variant of the following RETC equation for effective saturation (or reduced water content),  $S_e$ :

$$S_e = [1 + |\alpha\psi|^n]^{-m} \quad (49)$$

See Section 5.2.3, Water Retention, for a definition of terms

The following relationships exist among the RETC and Baroghel-Bouny et al. (1999) parameters:

$$\begin{aligned}
 k_{iSat} &= K_{sat} \left( \frac{\mu}{\rho * g} \right) \\
 \theta_s &= \eta \\
 \alpha &= \frac{\rho * g}{a} \\
 n &= \frac{1}{1 - 1/b} \\
 m &= \frac{1}{b} = 1 - 1/n
 \end{aligned}
 \tag{50}$$

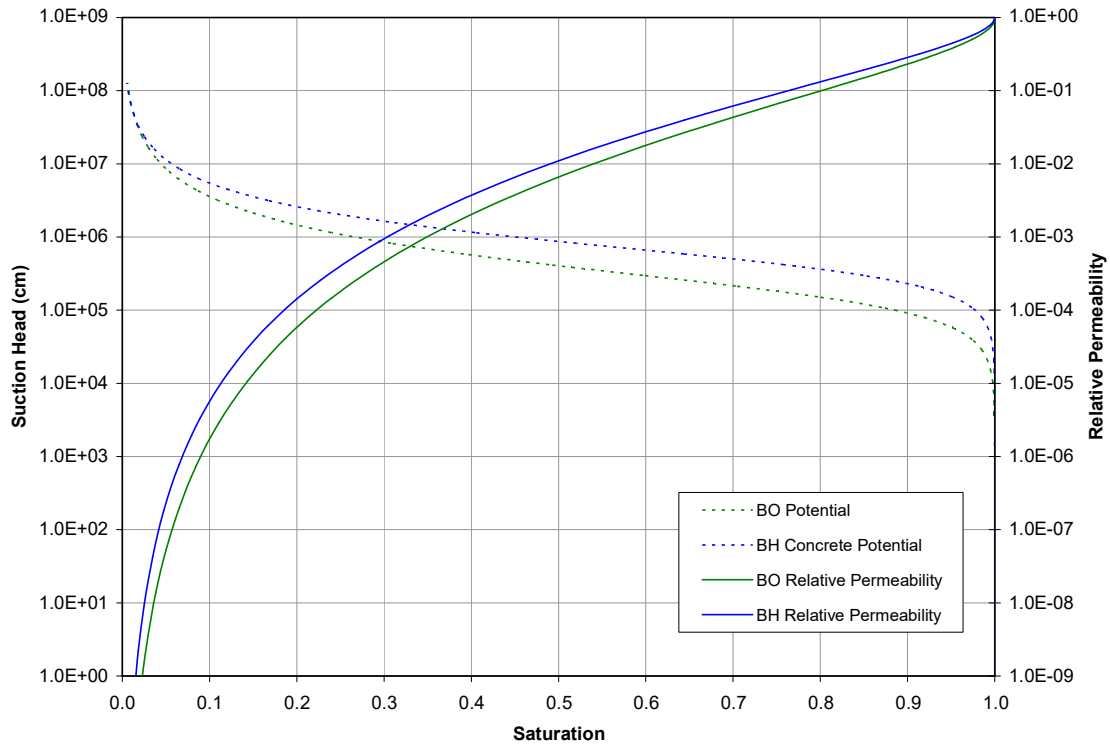
where  $k_i$  = saturated intrinsic permeability (typically  $m^2$ );  $K_{Sat}$  = saturated hydraulic conductivity (typically  $cm/s$ );  $\mu$  = fluid dynamic viscosity;  $\rho$  = fluid density (water);  $g$  = acceleration of gravity,  $\theta_s$  = saturated volumetric moisture content;  $\eta$  = porosity

Table 6-8 provides the parameters and values developed by Baroghel-Bouny et al. (1999) and the corresponding RETC values based upon the above relationships. Figure 6-4 provides the resulting characteristic curves (i.e., suction head, saturation, and relative permeability relationships) for each of the concrete mixtures based upon the RETC parameters and use of the Mualem-van Genuchten type function for the relative permeability (See Section 5.3.3, Water Retention, for the equation).

**Table 6-8. Baroghel-Bouny et al. (1999) and corresponding RETC parameters and parameter values**

<b>Ordinary Concrete (Mix BO)</b>			
<b>Baroghel-Bouny et al. (1999)</b>		<b>RETC</b>	
<b>Parameter</b>	<b>Value</b>	<b>Parameter</b>	<b>Value</b>
$K_{i\ Sat}$	3.0E-21 m <sup>2</sup>	$K_{sat}$	2.92E-12 cm/s
no corresponding parameter		$\theta_r$	0 (assumed)
$\eta$	0.122	$\theta_s$	0.122
a	18.6237 MPa	$\alpha$	5.2562E-06 cm <sup>-1</sup> of H <sub>2</sub> O
b	2.2748	n	1.7844
b	2.2748	m	0.4396
<b>High Performance Concrete (Mix BH)</b>			
<b>Baroghel-Bouny et al. (1999)</b>		<b>RETC</b>	
<b>Parameter</b>	<b>Value</b>	<b>Parameter</b>	<b>Value</b>
$K_{i\ Sat}$	5.0E-22 m <sup>2</sup>	$K_{sat}$	4.87E-13 cm/s
no corresponding parameter		$\theta_r$	0 (assumed)
$\eta$	0.082	$\theta_s$	0.082
a	46.9364 MPa	$\alpha$	2.0856E-06 cm <sup>-1</sup> of H <sub>2</sub> O
b	2.0601	n	1.9433
b	2.0601	m	0.4854

A comparison of all the cementitious characteristic curves produced by Rockhold et al. (1993) (Figure 6-2), Savage and Janssen (1997b) (Figure 6-3), and Baroghel-Bouny et al. (1999) (Figure 6-4) shows that all the curves are very similar. A comparison of these cementitious characteristic curves to the soil characteristic curves in Figure 5-12 shows a substantial difference, particularly in the suction head at which drainage begins.



**Figure 6-4. Baroghel-Bouny et al. (1999) characteristic curves**

### 6.1.4 Saturated Effective Diffusivity

Various methods have been utilized to evaluate the diffusion of ionic species through cementitious materials. The following are some of the more common methods found in the literature (Basheer, 2001):

- The rapid chloride permeability test or coulomb test (AASHTO, T 277-05; ASTM, C 1202-05) provides a measure of the electrical charge that can be passed through a concrete specimen over a set period of time (typically 6 hours). This electrical charge measurement provides an indirect, qualitative measure of the diffusivity of the concrete specimen and not a direct measurement of the specimen’s diffusion coefficient. Therefore, results from these types of tests will not receive further consideration herein.
- The chloride penetration tests (AASHTO, T 259-02; ASTM, C 1556-04) provide a measure of the one-dimensional penetration of chloride into concrete specimens over a set period of time (typically 35 to 90 days). From the measured chloride penetration depth or chloride penetration profile, a diffusion coefficient for the specimen can be determined using Fick’s second law of diffusion. Due to the test conditions, it is assumed that the calculated diffusion coefficient represents that under saturated conditions.

- Solidified waste leach tests (ANS, ANSI/ANS-16.1-2003; ASTM, C 1308-95) provide a measure of the cumulative fraction of a waste constituent leached from a solidified waste form in a water bath over a set period of time (typically 11 to 90 days). From the measure of the cumulative fraction of a waste constituent leached, a diffusion coefficient for the specimen can be determined. Due to the test conditions, it is assumed that the calculated diffusion coefficient represents that under saturated conditions.
- Steady-state natural diffusion tests (Basheer, 2001) provide a measure of the steady-state flux of an ionic species through a saturated cementitious material, which is subjected to a constant concentration gradient. It can take weeks to months to reach steady-state conditions. From the measured steady-state flux of an ionic species, a diffusion coefficient for the specimen can be determined using Fick's first law of diffusion. A standardized test procedure for this method has not been developed.
- Steady-state migration tests (Basheer, 2001) provide a measure of the steady-state flux of an ionic species through a saturated cementitious material, which is subjected to both a constant concentration gradient and an applied voltage. Steady-state conditions are achieved much sooner for this test than for the steady-state natural diffusion tests due to the addition of the applied voltage. From the measured steady-state flux of an ionic species, a diffusion coefficient for the specimen can be determined using the Nernst-Planck equation, which can account for flux due to diffusion and migration due to applied voltage. A standardized test procedure for this method has not been developed, however the test may be conducted utilizing the applied voltage cell utilized for the rapid chloride permeability test (AASHTO, T 277-05; ASTM, C 1202-05).

Diffusion tests which are conducted to steady-state conditions (i.e., steady-state natural diffusion and steady-state migration tests) produce results which have eliminated sorption or binding of the ionic species to the cementitious matrix (i.e., sorption, precipitation, and other such effects that retard the transport of the species prior to reaching steady-state conditions). Tests that are not conducted to steady-state conditions produce results that include the effects of sorption or binding of the ionic species to the cementitious matrix if the ionic species is non-conservative in this respect. Chloride, which is often used in the diffusion tests listed above, is a non-conservative species that sorbs or binds to cementitious materials. Non-steady-state tests that utilize conservative species (i.e., those that do not sorb or bind to cementitious materials) do not include the effects of sorption or binding. (Atkinson et al., 1984; Basheer, 2001; Castellote et al., 2001b; Truc et al., 2000)

Within the literature, four different types of diffusion coefficients are typically utilized. However, the nomenclature utilized within the literature is inconsistent. Therefore the following definitions of diffusion coefficient have been made in order to classify the various values of diffusion coefficient found within the literature (Seitz and Walton, 1993; Walton et al., 1990):

- The molecular diffusion coefficient,  $D_m$ , is the diffusion coefficient of a species in open water. “This term assumes saturation and does not include tortuosity or sorption due to a porous media.”
- The effective diffusion coefficient,  $D_e$ , is the diffusion coefficient of a species through a saturated porous medium taken over the pore area of the medium through which diffusion occurs under steady-state conditions. That is,  $D_e$ , includes the effects of tortuosity, but not the effects of sorption and porosity. It is defined as the molecular diffusion coefficient,  $D_m$ , divided by the porous medium tortuosity,  $\tau$ , ( $D_e = D_m/\tau$ ) and can be determined as follows under steady-state conditions:

$$D_e = \frac{J}{\eta A (\partial c / \partial x)} \quad 51$$

where  $J$  = flux in mols/s

$\eta$  = porosity

$A$  = surface area

$\partial c / \partial x$  = change in concentration with change in distance

The effective diffusion coefficient,  $D_e$ , is the form of the diffusion coefficient used in transport equations such as those utilized by the PORFLOW model.

- The intrinsic diffusion coefficient,  $D_i$ , is the diffusion coefficient of a species through a saturated porous medium taken over the total surface area of the medium through which diffusion occurs under steady-state conditions. That is  $D_i$ , includes the effects of tortuosity and porosity, but not sorption.  $D_i$  is the diffusion coefficient typically determined from steady-state natural diffusion and steady-state migration tests across a thin slice of porous media. It is defined as the porosity,  $\eta$ , times the molecular diffusion coefficient,  $D_m$ , divided by the porous medium tortuosity,  $\tau$ , ( $D_i = \eta D_m / \tau$ ) and can be determined as follows under steady-state conditions:

$$D_i = \frac{J}{A (\partial c / \partial x)} \quad 52$$

Where:  $J$  = flux in mols/s

$\eta$  = porosity

$A$  = surface area

$\partial c / \partial x$  = change in concentration with change in distance

In summary,  $\eta D_m / \tau = \eta D_E = D_i$ , therefore the effective diffusion coefficient,  $D_e$ , can be determined from the intrinsic diffusion coefficient,  $D_i$ , through the following relationship:

$$D_e = D_i / \eta \quad 53$$

where  $\eta$  = porosity

- The apparent diffusion coefficient,  $D_a$ , is the diffusion coefficient of a species into or out of a porous medium taken over the surface area of the medium through which diffusion occurs under potentially non-steady-state conditions.  $D_a$  includes the effects of tortuosity, porosity, and sorption or binding (i.e., sorption, precipitation, and other such effects that retard the transport of the species prior to reaching steady-state conditions).  $D_a$  is the diffusion coefficient typically determined from chloride penetration tests (AASHTO, T 259-02; ASTM, C 1556-04) and solidified waste leach tests (ANSI/ANS-16.1-2003; ASTM, C 1308-95). It is typically assumed that the  $D_a$  produced from these tests represents saturated conditions due to the testing conditions. For conservative species (i.e., non-sorbing species) the  $D_a$  produced from these tests is essentially equivalent to the intrinsic diffusion coefficient,  $D_i$ . Chloride penetration tests (AASHTO, T 259-02; ASTM, C 1556-04) are typically only applied to the diffusion of chloride under non-steady-state conditions. Because chloride is a non-conservative species in cementitious materials under non-steady-state conditions, data from such tests cannot be utilized in order to determine the effective diffusion coefficient,  $D_e$ . Consequently, results from these types of tests will not receive further consideration herein.

Based upon this classification of diffusion coefficients found within the literature, the saturated intrinsic diffusion coefficients,  $D_i$ , produced from steady-state natural diffusion and steady-state migration tests in addition to saturated apparent diffusion coefficients,  $D_a$ , produced for conservative species from solidified waste leach tests (ANSI/ANS-16.1-2003; ASTM, C 1308-95) are considered satisfactory in determining the saturated effective diffusion coefficient,  $D_e$ , for modeling input. Additionally comparative testing of steady-state natural diffusion tests and steady-state migration tests have demonstrated that these tests produce similar saturated intrinsic chloride diffusion coefficients. (Castellote et al., 2001a; Castellote et al., 2001b)

As indicated above, the material properties which affect diffusion are the material's porosity and tortuosity; in other words, diffusion is affected by the characteristics of the material's porosity (i.e., effective porosity and size, distribution, and continuity of pores (i.e., tortuosity)). Therefore, the same factors that have been shown to reduce concrete porosity also reduce its diffusion coefficient:

- Low WCR (increased unit cementitious material content and reduced unit water content that can be facilitated by the use of high-range water reducers) (ACI, 201.2R-01; Ampadu et al., 1999; Atkinson et al., 1984; Clifton and Knab, 1989; Delagrave et al., 1998; Leng et al., 2000; Walton et al., 1990)
- Use of blast furnace slag, fly ash, and silica fume as cementitious material replacements for the cement content (ACI, 201.2R-01, 232.2R-03, 233R-03, 234R-96; Ampadu et al., 1999; Beaudoin and Marchand, 2001; Delagrave et al., 1998; Johnston and Wilmot, 1992; Leng et al., 2000; Popovics, 1992; Soroushian and Alhozaimy, 1995; Stanish and Thomas, 2003)
- Proper mix proportioning (i.e., water, cementitious material, fine aggregate, and coarse aggregate proportioning) to produce a dense homogeneous concrete

- Air entrainment(ACI, 201.2R-01)
- Properly placed and well consolidated (minimizes segregation and honeycombing)(ACI, 201.2R-01)
- Effectively cured (minimizes cracking and maximizes cementitious material hydration)(ACI, 201.2R-01; Ampadu et al., 1999; Beaudoin and Marchand, 2001; Neville, 1973; Stanish and Thomas, 2003; Walton et al., 1990)

Additionally, it has been noted that the aggregates within concrete can produce a reduction in the diffusion coefficient over that in cementitious paste alone by increasing the tortuosity of the matrix and reducing area available for diffusion. However the presence of significant porous interfacial transition zones (ITZ) between the aggregate and paste, particularly if they are interconnected, probably facilitates diffusion. (Delagrave et al., 1998)

It has also been noted that intrinsic diffusion coefficients of concrete vary directly with permeability as shown by the following results reported by Basheer (2001) for steady state natural diffusion tests of chloride through concretes of various permeabilities:

Concrete Permeability	Intrinsic Diffusion Coefficients
High	>5E-08 cm <sup>2</sup> /s
Average	1 to 5E-08 cm <sup>2</sup> /s
Low	<1E-08 cm <sup>2</sup> /s

Table 6-9, Table 6-10, and Table 6-11 provide the measured saturated intrinsic diffusion coefficients of various species through concrete (i.e., contains cement, fine and coarse aggregate, and water), mortar (i.e., contains cementitious material, fine aggregate, and water), and cementitious paste (i.e., contains cementitious material and water), respectively, obtained from various literature sources. These tables provide the results of tests conducted with chloride (Cl<sup>-</sup>), nitrite (NO<sub>2</sub><sup>-</sup>), tritiated water (T3), and oxygen (O<sub>2</sub>) as the diffusing ion or molecule. Atkinson et al. (1984) state that the intrinsic diffusion coefficient does not appear to be sensitive to the specific diffusing ion or molecule similar to that in free water, and therefore concludes that an intrinsic diffusion coefficient value for any single ion or molecule can fairly well approximate that of another.

The intrinsic diffusion coefficients of Table 6-9, Table 6-10, and Table 6-11 have been converted to effective diffusion coefficients by dividing the intrinsic diffusion coefficients by the respective porosities. Where the porosities were not provided in the literature an estimated porosity was determined based upon WCR-porosity relationships developed within Section 6.1.1 (see Figure 6-1). Figure 6-5 provides the saturated effective diffusion coefficients of concrete, concrete with fly ash, concrete with blast furnace slag, mortar, and mortar with silica fume with WCR, based upon the data from these literature sources. The saturated effective diffusion coefficients of cementitious materials from Table 6-9, Table 6-10, and Table 6-11 is seen to range from

approximately  $1.0\text{E-}08$  to  $5.0\text{E-}07$   $\text{cm}^2/\text{s}$ . This is a relatively narrow range at just over one order of magnitude, particularly in comparison to the range of saturated hydraulic conductivities for cementitious materials. These data clearly show that the effective diffusion coefficient decreases with decreasing WCR and with the addition of fly ash, blast furnace slag, and silica fume.

Table 6-9. Saturated effective diffusion coefficients of concretes (contains cement, fine and coarse aggregate, and water)

WCR	Cement (kg/m <sup>3</sup> )	Fly Ash (kg/m <sup>3</sup> )	BFS (kg/m <sup>3</sup> )	Sand (kg/m <sup>3</sup> )	Aggregate (kg/m <sup>3</sup> )	Cure Time (days)	Species	Intrinsic Diffusion Coefficient, $D_i$ (cm <sup>2</sup> /s)	Assumed Porosity, $\eta^1$ (%)	Effective Diffusion Coefficient, $D_e = D_i/\eta$ (cm <sup>2</sup> /s)	Source
0.26	600	0	0	620	1100	28	Cl <sup>-</sup>	2.4E-09	9.0	2.67E-08	Leng et al. (2000)
0.30	550	0	0	640	1120	28	Cl <sup>-</sup>	2.6E-09	9.7	2.68E-08	Leng et al. (2000)
0.32	425	0	0	750	1130	14	Cl <sup>-</sup>	1.1E-08 <sup>6</sup>	10.0	1.10E-07	Truc et al. (2000)
0.34	500	0	0	640	1150	28	Cl <sup>-</sup>	5.4E-09	10.3	5.24E-08	Leng et al. (2000)
0.40	380	0	0	771	1177	28	Cl <sup>-</sup>	9.4E-09 <sup>4</sup>	11.2	8.39E-08	Castellote et al. (2001a)
0.40	382	0	0	679	967	50	NO <sub>2</sub> <sup>-</sup>	4.5E-08	11.2	4.02E-07	Liang et al. (2003)
0.40	382	0	0	679	967	100	NO <sub>2</sub> <sup>-</sup>	2.8E-08	11.2	2.50E-07	Liang et al. (2003)
0.40	382	0	0	679	967	270	NO <sub>2</sub> <sup>-</sup>	1.6E-08	11.2	1.43E-07	Liang et al. (2003)
0.50	300	0	0	UA	UA	90	Cl <sup>-</sup>	5.0E-08	12.7	3.94E-07	Stanish and Thomas (2003)
0.55	550	0	0	708	1062	14	Cl <sup>-</sup>	2.7E-08 <sup>6</sup>	13.4	2.01E-07	Truc et al. (2000)
0.26	480	120 <sup>5</sup>	0	620	1100	28	Cl <sup>-</sup>	2.2E-09	9.0	2.44E-08	Leng et al. (2000)
0.30	495	55 <sup>5</sup>	0	640	1120	28	Cl <sup>-</sup>	3.8E-09	9.7	3.92E-08	Leng et al. (2000)
0.30	440	110 <sup>5</sup>	0	640	1120	28	Cl <sup>-</sup>	2.3E-09	9.7	2.37E-08	Leng et al. (2000)
0.30	385	165 <sup>5</sup>	0	640	1120	28	Cl <sup>-</sup>	3.6E-09	9.7	3.71E-08	Leng et al. (2000)
0.30	330	220 <sup>5</sup>	0	640	1120	28	Cl <sup>-</sup>	3.2E-09	9.7	3.30E-08	Leng et al. (2000)
0.34	400	100 <sup>5</sup>	0	640	1150	28	Cl <sup>-</sup>	3.1E-09	10.3	3.01E-08	Leng et al. (2000)
0.40	310	78 <sup>5</sup>	0	674	986	180	NO <sub>2</sub> <sup>-</sup>	6.4E-09	11.2	5.71E-08	Liang et al. (2003)
0.5	225	75 <sup>2</sup>	0	UA	UA	90	Cl <sup>-</sup>	1.1E-08 <sup>3</sup>	12.7	8.66E-08	Stanish and Thomas (2003)
0.5	132	168 <sup>2</sup>	0	UA	UA	90	Cl <sup>-</sup>	1.0E-08 <sup>3</sup>	12.7	7.87E-08	Stanish and Thomas (2003)

**Table 6-9. Saturated effective diffusion coefficients of concretes (contains cement, fine and coarse aggregate, and water) - continued**

WCR	Cement (kg/m <sup>3</sup> )	Fly Ash (kg/m <sup>3</sup> )	BFS (kg/m <sup>3</sup> )	Sand (kg/m <sup>3</sup> )	Aggregate (kg/m <sup>3</sup> )	Cure Time (days)	Species	Intrinsic Diffusion Coefficient, $D_i$ (cm <sup>2</sup> /s)	Assumed Porosity, $\eta^1$ (%)	Effective Diffusion Coefficient, $D_e = D_i/\eta$ (cm <sup>2</sup> /s)	Source
0.26	420	0	180	620	1100	28	Cl <sup>-</sup>	1.3E-09	9.0	1.44E-08	Leng et al. (2000)
0.30	495	0	55	640	1120	28	Cl <sup>-</sup>	4.2E-09	9.7	4.33E-08	Leng et al. (2000)
0.30	440	0	110	640	1120	28	Cl <sup>-</sup>	2.3E-09	9.7	2.37E-08	Leng et al. (2000)
0.30	385	0	165	640	1120	28	Cl <sup>-</sup>	1.5E-09	9.7	1.55E-08	Leng et al. (2000)
0.30	330	0	220	640	1120	28	Cl <sup>-</sup>	1.6E-09	9.7	1.65E-08	Leng et al. (2000)
0.30	275	0	275	640	1120	28	Cl <sup>-</sup>	1.4E-09	9.7	1.44E-08	Leng et al. (2000)
0.34	350	0	150	640	1150	28	Cl <sup>-</sup>	2.8E-09	10.3	2.72E-08	Leng et al. (2000)

<sup>1</sup>  $\eta = (15.208 \times WCR) + 5.0941$

<sup>2</sup> Class C fly ash

<sup>3</sup> Average of four measurements taken over the following durations: 90 to 180 days; 90 to 270 days; 90 to 455 days; 90 to 1550 days

<sup>4</sup> Average of four measurements: two obtained with natural diffusion tests and two with migration tests

<sup>5</sup> Class F fly ash

<sup>6</sup> Average of four measurements

WCR = water-cementitious material ratio; BFS = blast furnace slag; UA = unknown amount; Cl<sup>-</sup> = chloride; NO<sub>2</sub><sup>-</sup> = nitrite

**Table 6-10. Saturated effective diffusion coefficients of mortars (contains cement, fine aggregate, and water)**

WCR	Cement	SF	Sand	Cure Time (days)	Species	Intrinsic Diffusion Coefficient, $D_i$ (cm <sup>2</sup> /s)	Porosity, $\eta$ (%)	Effective Diffusion Coefficient, $D_e = D_i/\eta$ (cm <sup>2</sup> /s)	Source
0.25	100 wt % CM	0	50 vol%	90	T3	3.8E-09	7.5 <sup>1</sup>	5.07E-08	Delagrave et al. (1998)
0.45	100 wt % CM	0	50 vol%	90	T3	4.58E-08	12.2 <sup>1</sup>	3.75E-07	Delagrave et al. (1998)
0.25	94 wt % CM	6 wt % CM	50 vol%	90	T3	1.1E-09	4.6 <sup>1</sup>	2.39E-08	Delagrave et al. (1998)
0.45	94 wt % CM	6 wt % CM	50 vol%	90	T3	7.9E-09	11.7 <sup>1</sup>	6.75E-08	Delagrave et al. (1998)

<sup>1</sup> Porosity measured by Delagrave et al. (1998)

WCR = water-cementitious material ratio; SF = silica fume; wt% = weight percent; CM = cementitious materials; vol% = volume percent; T3 = tritiated water

Table 6-11. Saturated effective diffusion coefficients of cementitious pastes (contains cementitious materials and water)

WCR	Cement (wt% of CM)	Fly Ash (wt% of CM)	BFS (wt% of CM)	SF (wt% of CM)	Cure Time (days)	Species	Intrinsic Diffusion Coefficient, $D_i$ (cm <sup>2</sup> /s)	Assumed Porosity, $\eta^1$ (%)	Effective Diffusion Coefficient, $D_e = D_i/\eta$ (cm <sup>2</sup> /s)	Source
0.25	100	0	0	0	90	T3	0.63E-08	8.7 <sup>2</sup>	7.24E-08	Delagrave et al. (1998)
0.25	100	0	0	0	56	T3	-	11.3 <sup>3</sup>	9.12E-08 <sup>3</sup>	Johnston and Wilmot (1992)
0.25	100	0	0	0	56	Cl <sup>-</sup>	-	11.3 <sup>3</sup>	5.18E-08 <sup>3</sup>	Johnston and Wilmot (1992)
0.35	100	0	0	0	56	T3	-	18.1 <sup>3</sup>	8.43E-08 <sup>3</sup>	Johnston and Wilmot (1992)
0.35	100	0	0	0	56	Cl <sup>-</sup>	-	18.1 <sup>3</sup>	7.18E-08 <sup>3</sup>	Johnston and Wilmot (1992)
0.4	100	0	0	0	28	Cl <sup>-</sup>	3.7E-08	19.8	1.87E-07	Castellote et al. (2001b)
0.4	100	0	0	0	28	O <sub>2</sub>	9.3E-08	19.8	4.70E-07	Castellote et al. (2001b)
0.45	100	0	0	0	90	T3	9.83E-08	22.2 <sup>2</sup>	4.43E-07	Delagrave et al. (1998)
0.45	100	0	0	0	28	Cl <sup>-</sup>	1.040E-08	22.9	4.54E-08	Ampadu et al. (1999)
0.45	100	0	0	0	365	Cl <sup>-</sup>	2.586E-08	22.9	1.13E-07	Ampadu et al. (1999)
0.55	100	0	0	0	28	Cl <sup>-</sup>	2.737E-08	29.2	9.37E-08	Ampadu et al. (1999)
0.55	100	0	0	0	365	Cl <sup>-</sup>	3.703E-08	29.2	1.27E-07	Ampadu et al. (1999)
0.65	100	0	0	0	28	Cl <sup>-</sup>	3.166E-08	35.5	8.92E-08	Ampadu et al. (1999)
0.65	100	0	0	0	365	Cl <sup>-</sup>	6.336E-08	35.5	1.78E-07	Ampadu et al. (1999)
0.45	80	20	0	0	28	Cl <sup>-</sup>	2.445E-08	22.9	1.07E-07	Ampadu et al. (1999)
0.45	80	20	0	0	365	Cl <sup>-</sup>	5.073E-09	22.9	2.22E-08	Ampadu et al. (1999)
0.45	60	40	0	0	28	Cl <sup>-</sup>	2.977E-08	22.9	1.30E-07	Ampadu et al. (1999)
0.45	60	40	0	0	365	Cl <sup>-</sup>	4.069E-09	22.9	1.78E-08	Ampadu et al. (1999)
0.55	80	20	0	0	28	Cl <sup>-</sup>	3.731E-08	29.2	1.28E-07	Ampadu et al. (1999)
0.55	80	20	0	0	365	Cl <sup>-</sup>	6.462E-09	29.2	2.21E-08	Ampadu et al. (1999)
0.55	60	40	0	0	28	Cl <sup>-</sup>	4.861E-08	29.2	1.66E-07	Ampadu et al. (1999)
0.55	60	40	0	0	365	Cl <sup>-</sup>	3.695E-09	29.2	1.27E-08	Ampadu et al. (1999)
0.65	80	20	0	0	28	Cl <sup>-</sup>	4.812E-08	35.5	1.36E-07	Ampadu et al. (1999)
0.65	80	20	0	0	365	Cl <sup>-</sup>	1.732E-08	35.5	4.88E-08	Ampadu et al. (1999)
0.65	60	40	0	0	28	Cl <sup>-</sup>	5.848E-08	35.5	1.65E-07	Ampadu et al. (1999)
0.65	60	40	0	0	365	Cl <sup>-</sup>	5.085E-09	35.5	1.43E-08	Ampadu et al. (1999)

**Table 6-11. Saturated effective diffusion coefficients of cementitious pastes (contains cementitious materials and water) - continued**

WCR	Wt% of CM				Cure Time (days)	Species	Intrinsic Diffusion Coefficient, $D_i$ (cm <sup>2</sup> /s)	Assumed Porosity, $\eta^1$ (%)	Effective Diffusion Coefficient, $D_e = D_i/\eta$ (cm <sup>2</sup> /s)	Source
	Cement	Fly Ash	BFS	SF						
0.25	94	0	0	6	90	T3	0.16E-08	4.0 <sup>2</sup>	4.00E-08	Delagrave et al. (1998)
0.25	90	0	0	10	56	T3	-	0.142 <sup>3</sup>	5.92E-08 <sup>3</sup>	Johnston and Wilmot (1992)
0.25	90	0	0	10	56	Cl <sup>-</sup>	-	0.142 <sup>3</sup>	1.53E-08 <sup>3</sup>	Johnston and Wilmot (1992)
0.25	85	0	0	15	56	T3	-	0.130 <sup>3</sup>	4.86E-08 <sup>3</sup>	Johnston and Wilmot (1992)
0.25	85	0	0	15	56	Cl <sup>-</sup>	-	0.130 <sup>3</sup>	2.52E-08 <sup>3</sup>	Johnston and Wilmot (1992)
0.35	90	0	0	10	56	T3	-	0.225 <sup>3</sup>	5.29E-08 <sup>3</sup>	Johnston and Wilmot (1992)
0.35	90	0	0	10	56	Cl <sup>-</sup>	-	0.225 <sup>3</sup>	3.37E-08 <sup>3</sup>	Johnston and Wilmot (1992)
0.35	85	0	0	15	56	T3	-	0.198 <sup>3</sup>	4.64E-08 <sup>3</sup>	Johnston and Wilmot (1992)
0.35	85	0	0	15	56	Cl <sup>-</sup>	-	0.198 <sup>3</sup>	1.58E-08 <sup>3</sup>	Johnston and Wilmot (1992)
0.45	94	0	0	6	90	T3	3.79E-08	18.6 <sup>2</sup>	2.04E-07	Delagrave et al. (1998)

<sup>1</sup>  $\eta = (62.818 \times WCR) - 5.3409$

<sup>2</sup> Porosity measured by Delagrave et al. (1998)

<sup>3</sup> Porosity and Effective Diffusion coefficient determined by Johnston and Wilmot (1992)

WCR = water-cementitious material ratio; BFS = blast furnace slag; SF = silica fume; wt% = weight percent; CM = cementitious materials  
 wt% = weight percent of total; Cl<sup>-</sup> = chloride; T3 = tritiated water

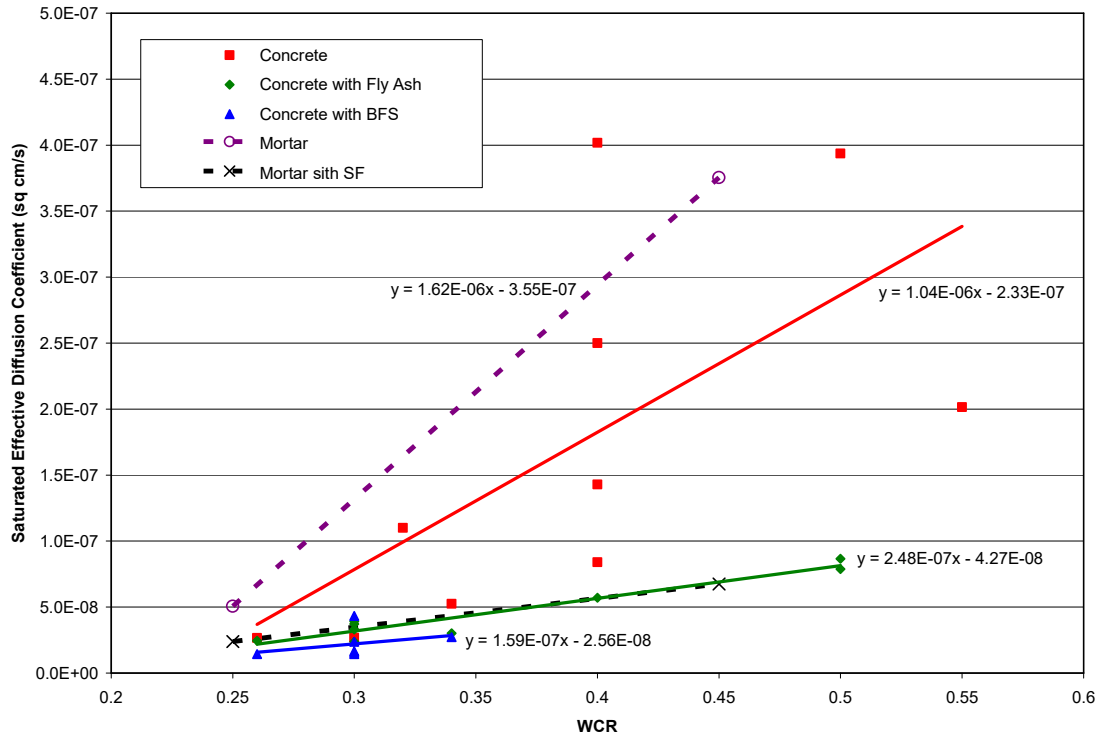


Figure 6-5. Saturated effective diffusion coefficient of concrete and mortar with WCR

## 6.2 INTERNAL LITERATURE REVIEW

### 6.2.1 1993 Physical Properties Measurement Program (Yu et al., 1993)

During 1992 and 1993 a materials characterization program, which included the characterization of E-Area vault concrete, Saltstone vault concrete, and the Saltstone waste form, was conducted and documented by Yu et al. (1993). Testing of these materials by Core Laboratories was conducted to determine their saturated intrinsic permeability, saturated hydraulic conductivity, water retention properties, total porosity, and dry bulk density, among other properties. The following discussion pertains only to the testing of E-Area vault concrete.

A 1-foot by 1-foot by 1-foot block of E-Area vault concrete (it is assumed that this block was associated with the E-Area concrete test wall) was supplied to Core Laboratories. The Core Laboratories drilled ten 1-½ inch diameter samples from the E-Area vault concrete bulk sample and trimmed them to right cylinders approximately 5 centimeters long. These drilled and trimmed samples were utilized for all the testing conducted.

Saturated hydraulic conductivity testing of these cementitious samples was conducted on samples pressure-saturated for a week with tap water. After saturation, the samples were mounted in an epoxy coating to prevent bypass flow. It is assumed that the samples were mounted in a horizontal orientation. Tap water was injected into the sample at a constant upstream pressure of 50 psi, and the flow rate out of the sample was measured until the flow rate essentially obtained steady state. The viscosity and density of the permeant was determined so that both intrinsic permeability and saturated hydraulic conductivity to the permeant could be determined.

Core Laboratories attempted to determine the water retention properties of the cementitious samples, however the methodology utilized was inappropriate for such a determination. They desaturated the samples in humidified air under a pressure of 35 psi. The samples were then completely immersed in tap water and subjected to increasing pressures from 1 to 35 psi. At each pressure increment the samples were allowed to “equilibrate” and a final sample weight was determined. This produced increasing water contents with pressure. Immersion of the samples and the application of increasing pressures simply forced more water into the samples. Such measurements have no relationship to water retention properties. The water retention data reported by the Core Laboratories do not represent the water retention properties of the cementitious materials, therefore those data are not reproduced herein.

The dry bulk density and total porosity of the cementitious samples were determined in conjunction with other tests and are based upon dimensional and weight measurements.

Table 6-12 provides summary saturated intrinsic permeability, saturated hydraulic conductivity, total porosity, and dry bulk density data for the E-Area vault concrete.

**Table 6-12. Summary E-Area Vault concrete properties from Core Laboratories testing (Yu et al., 1993)**

<b>Sample</b>	<b>Dry Bulk Density (g/cm<sup>3</sup>)</b>	<b>Calculated Porosity (%)</b>	<b>Calculated Particle Density (g/cm<sup>3</sup>)</b>	<b>Saturated Intrinsic Permeability (water) (darcy)</b>	<b>Saturated Hydraulic Conductivity (water) (cm/s)</b>	<b>Log Saturated Hydraulic Conductivity (water) (cm/s)</b>
1E	2.12	16.42	2.54	na	na	-
2E	2.10	18.07	2.57	7.44E-10	7.21E-13	-12.14
3E	2.07	na	-	na	na	-
4E	2.15	19.26	2.66	1.23E-09	1.19E-12	-11.93
5E	2.11	na	-	na	na	-
7E	2.11	19.76	2.63	1.26E-09	1.22E-12	-11.91
Average	2.11	18.38	2.59	1.08E-09	1.04E-12	-11.99
Std Dev of Population	0.03	1.48	0.05	2.87E-10	2.79E-13	0.13
Count	6	4	4	3	3	3
Std Dev of Mean	0.010	0.741	0.027	1.66E-10	1.608E-13	0.074

Std Dev = standard deviation; na = not analyzed

In addition to saturated intrinsic permeability, the Core Laboratories reported the unsaturated intrinsic permeability for one sample of E-Area vault concrete at one saturation level as shown in Table 6-13.

**Table 6-13. Unsaturated intrinsic permeability from Core Laboratories testing (Yu et al., 1993)**

<b>Material</b>	<b>Sample</b>	<b>Percent Saturation (%)</b>	<b>Unsaturated Intrinsic Permeability (water) (darcy)</b>
E-Area Vault Concrete	7E	98.7	5.41E-10

**6.2.2 2005 Concrete Porosity, Bulk Density, and Particle Density (Sappington and Phifer, 2005)**

Sappington and Phifer (2005) collected twenty-four concrete rubble samples from three different facilities being demolished at the Savannah River Site (SRS) and evaluated the samples for in-field moisture content and effective porosity. In addition, the data necessary to determine the dry bulk density and particle density of the concrete were also obtained ((Sappington and Phifer, 2005), Appendix C, page C-14). Table 6-14 provides information extracted from Sappington and Phifer (2005) including effective concrete porosity and provides the associated calculated concrete bulk density and concrete particle density. As seen in Table 6-14 the concrete porosity ranged from 0.083 to 0.178 with an average of 0.132; the concrete dry bulk density ranged from 2.11 to 2.38 with an average of 2.26; and the concrete particle density ranged from 2.49 to 2.73 with an average of 2.60.

**Table 6-14. Concrete porosity, bulk density, and particle density (Sappington and Phifer, 2005)**

Sample ID	Sample Location and Type	Sample Effective Porosity <sup>1</sup>	Final Oven Dry Sample Mass (g)	Sample Volume (mL)	Sample Dry Bulk Density <sup>2</sup> (g/cm <sup>3</sup> )	Sample Particle Density <sup>3</sup> (g/cm <sup>3</sup> )
A-01	734-A Wall	0.083	3759.4	1580.3	2.38	2.59
A-02	734-A Wall	0.087	3474.1	1464.8	2.37	2.60
A-03	734-A Wall	0.096	2617.2	1107.6	2.36	2.61
A-04	734-A Wall	0.090	3762.1	1589.5	2.37	2.60
A-05	734-A Wall	0.093	419.6	181.1	2.32	2.56
A-06	734-A Wall	0.086	761.3	320.7	2.37	2.60
A-07	734-A Wall	0.100	332.4	141.1	2.36	2.62
A-08	734-A Wall	0.108	407.4	174.6	2.33	2.62
734-A Average		0.093	-	-	2.36	2.60
734-A Std Dev of Population		0.0082	-	-	0.022	0.020
734-A Count		8	-	-	8	8
734-A Std Dev of Mean		0.0029	-	-	0.0077	0.0071
D-01	701-1D Slab	0.130	2269.4	1002.2	2.26	2.60
D-02	701-1D Slab	0.154	3177.8	1442.7	2.20	2.60
D-03	701-1D Slab	0.154	2336.6	1055.5	2.21	2.62
D-04	701-1D Slab	0.174	2478.6	1134.6	2.18	2.65
D-05	701-1D Slab	0.144	509.7	228.6	2.23	2.60
D-06	701-1D Slab	0.167	512.8	228.3	2.25	2.70
D-07	701-1D Slab	0.124	491.3	216.3	2.27	2.59
701-1D Average		0.150	-	-	2.23	2.62
701-1D Std Dev of Population		0.018	-	-	0.032	0.036
701-1D Count		7	-	-	7	7
701-1D Std Dev of Mean		0.0069	-	-	0.0122	0.0136
D-08	675-T Column <sup>4</sup>	0.159	414.2	188.9	2.19	2.61
TNX-01	675-T Column	0.157	3099.5	1411.5	2.20	2.61
TNX-02	675-T Slab	0.127	2723.5	1241.3	2.19	2.51
TNX-03	675-T Column	0.159	2412.9	1102.2	2.19	2.60
TNX-04	675-T Slab	0.141	2037.5	943.0	2.16	2.52
TNX-05	675-T Column	0.162	401.3	175.5	2.29	2.73
TNX-06	675-T Slab	0.133	487.1	223.5	2.18	2.51
TNX-07	675-T Column	0.178	528.5	246.3	2.15	2.61
TNX-08	675-T Slab	0.154	538.4	255.1	2.11	2.49
675-T Average		0.152	-	-	2.18	2.58
675-T Std Dev of Population		0.0160	-	-	0.048	0.075
675-T Count		9	-	-	9	9
675-T Std Dev of Mean		0.0053	-	-	0.0159	0.0250
Overall Average		0.132	-	-	2.26	2.60
Overall Std Dev of Population		0.0313	-	-	0.084	0.053
Overall Count		24	-	-	24	24
Overall Std Dev of Mean		0.0064	-	-	0.0171	0.0108

Table 6-14 Notes:

- <sup>1</sup> Porosity is expressed as a fraction as provided in Sappington and Phifer (2005) rather than as a percent (%) as expressed in the bulk of this document
- <sup>2</sup> Sample Dry Bulk Density (g/cm<sup>3</sup>) = Final Oven Dry Sample Mass (g) / Sample Vol (mL)
- <sup>3</sup>  $\rho_p = \rho_b / (1 - (\eta/100))$  (Hillel 1982)
- <sup>4</sup> Sample ID D-8 appears to have been a TNX Column Sample  
Std Dev = standard deviation

### 6.2.3 2006 Component-in-Grout (CIG) Grout and Intermediate Level (IL) Vault Controlled Low Strength Material (CLSM) Testing (Dixon and Phifer, 2006)

Dixon and Phifer (2006) documented the determination of hydraulic and physical properties of the old Component-in-Grout (CIG) high flow grout and ILV Controlled Low Strength Material (CLSM). Two field test trenches were created, one each for the placement of grout and CLSM. The trenches were 6 feet wide by 12 feet long with a minimum depth of 4 feet. A total of eight cubic yards of the appropriate mix was poured into each trench. The grout used in the CIG Segments 1 through 8 and for this testing is mix A2000-X-0-0-AB as given in Table 4-1. The CLSM used in the IL Vault and for this testing is mix EXE-X-P-0-X as given in Table 4-1. Cementitious material was collected during each pour in order to prepare mold samples. Some of both the grout and CLSM mold samples were used to determine compressive strength at 7, 14, 28, 56, and 90 days. After the grout and CLSM had aged for a minimum of twenty-eight days, core samples were collected using a wet abrasive coring bit and drill motor. These core samples along with mold samples prepared at the time of placement were submitted to offsite laboratories (i.e., GeoTesting Express, Inc (GTX) and Idaho National Laboratory (INL)) in order to determine the saturated hydraulic conductivity, unsaturated hydraulic conductivity, water retention characteristics, dry bulk density, and porosity.

Table 6-15 through Table 6-21 provide a summary of the data produced. Details concerning the test methods and results can be found in Dixon and Phifer (2006).

**Table 6-15. Old CIG Grout and CLSM compressive strength**

Days Aged	Compressive Strength, psi		
	Old Grout (Segments 1-8)	New Grout <sup>a</sup> (Future Trench)	CLSM
7	1090		-
14	1045	3370	85
28	1960	4680 <sup>b</sup>	110
56	2790	6475 <sup>b</sup>	215
90	2615	7610 <sup>a</sup>	565

Notes: <sup>a</sup> See Section 6.2.4 for discussion of new CIG grout; <sup>b</sup> = average of 2 results

**Table 6-16. Old CIG High-Flow Grout hydraulic and physical properties**

Sample ID	Lab	Porosity <sup>1</sup>	Dry Bulk Density (g/cm <sup>3</sup> )	Particle Density <sup>2</sup> (g/cm <sup>3</sup> )	Volumetric Moisture Content (cm <sup>3</sup> /cm <sup>3</sup> )	Saturation	Saturated Hydraulic Conductivity (cm/s)	Log Saturated Hydraulic Conductivity (cm/s)
GRT004A	INL <sup>3</sup>	0.241	1.82	2.40	0.241	1.000	1.93E-08	-7.71
GRT004B	INL	0.205	1.87	2.35	0.205	1.000	2.60E-08	-7.59
GRT006A	INL	0.236	1.87	2.45	0.236	1.000	8.40E-05	-4.08
					0.231	0.979		
					0.228	0.966		
GRT006B	INL	0.216	1.86	2.37	0.216	1.000	4.80E-05	-4.32
					0.215	0.995		
					0.213	0.986		
					0.209	0.968		
GRT006D	INL	-	1.79	-	-	-	-	
GRT008A	INL	-	1.70	-	-	-	-	
GRT008B	INL	0.233	1.77	2.31	0.233	1.000	1.25E-06	-5.90
					0.229	0.983		
GRT008C	INL	0.213	1.83	2.33	0.213	1.000	1.38E-04	-3.86
GRT001	GTX <sup>4</sup>	0.40 <sup>6</sup>	1.56	2.60	0.40	1.000	2.30E-04	-3.64
GRT002	GTX <sup>4</sup>	0.28 <sup>6</sup>	1.85	2.57	0.28	1.000	4.30E-04	-3.37
GRT003 <sup>5</sup>	GTX <sup>4</sup>	0.23	1.98	2.57	0.23	1.000	1.90E-06	-5.72
Average		0.224	1.79	2.31 <sup>2</sup>	-	-	1.16E-04 <sup>7</sup> (4.5E-05 <sup>8</sup> )	-5.06
Std Dev of Population		0.015	0.097	0.051	-	-	1.50E-04	1.77
Count		6	10	6	-	-	8	8
Std Dev of Mean		0.006	0.031	0.021	-	-	5.31E-05	0.626

Notes to Table 6-16:

- <sup>1</sup> Porosity is expressed as a fraction as provided in Dixon and Phifer (2006) rather than as a percent (%) as expressed in the bulk of this document
- <sup>2</sup>  $\rho_p = \rho_b / (1 - \eta)$  (Hillel 1982)
- <sup>3</sup> INL = Idaho National Laboratory
- <sup>4</sup> GTX = GeoTesting Express, Inc.
- <sup>5</sup> Sample GRT003 is a mold sample; the remainder are core samples. Due to the significant matrix difference as seen in computed tomography (CT) scans, the mold sample (GRT003) has been excluded from the average and standard deviation calculations.
- <sup>6</sup> Based upon the grout water retention data reported in Table 6-17, the porosity of samples GRT001 and GRT002 should have been less than ~0.27; therefore, the porosity and particle density of these samples have been excluded from the average and standard deviation calculations.
- <sup>7</sup> Saturated hydraulic conductivity average (i.e., average of hydraulic conductivities of samples with a saturation of 1.
- <sup>8</sup> Laboratory hydraulic property data for core samples and computed tomography (CT) scans provided by Dixon and Phifer (2006) suggest that the old E-Area CIG grout is composed of both micropores and macropores. Saturated hydraulic conductivity for the 1-inch diameter CIG grout core samples ranged from 1.9E-8 cm/s to 1.4E-4 cm/s and for the 3-inch diameter CIG grout core samples from 2.3E-4 cm/s to 4.3E-4 cm/s (Dixon and Phifer, 2006). Also, as shown in the table the arithmetic averaged saturated hydraulic conductivity is 1.2E-04 cm/s; whereas the harmonic averaged (i.e., log averaged) saturated hydraulic conductivity is 8.8E-06 cm/s. The true saturated hydraulic conductivity should be between these two

bounding values. This variability was attributed to the heterogeneity of the grout and the diameter of the samples analyzed. Because the smaller diameter samples incorporated only a small fraction of the CIG material, they were more likely affected by the variability in pore interconnectedness than the larger (3-inch) samples. This sampling bias was evident in the wide range of measured saturated hydraulic conductivities but was also observed in the CT images. In particular, 1-inch samples with higher saturated hydraulic conductivities showed interconnected pores around poorly cemented aggregate-paste boundaries. These interconnected pores would likely have created preferential flow paths. In contrast, samples with lower saturated hydraulic conductivities contained less observable interconnected porosity in the CT scans (Dixon and Phifer, 2006). Due to this heterogeneity the upscaling methodology described in Section 5.2.2, Saturated Hydraulic Conductivity, for the undisturbed vadose zone soil with a power-averaging exponent of  $p=0.33$  (assuming sample isotropy) was used to estimate the saturated hydraulic conductivity. Based upon this methodology a saturated hydraulic conductivity of  $4.5E-5$  cm/s was calculated for the old E-Area CIG grout. Implicit in the analysis is the assumption that the sample variability is representative of the grout spatial heterogeneity.

Std Dev = standard deviation

Table 6-17. Grout water retention properties as measured by GeoTesting Express, Inc.

Sample ID	Potential (cm)					
	-102.07 (-0.1 bars)	-510.35 (-0.5 bars)	-1,020.7 (-1.0 bars)	-2,041.4 (-2.0 bars)	-5,103.5 (-5.0 bars)	-15,310.5 (-15.0 bars)
	Volumetric Water Content (cm <sup>3</sup> /cm <sup>3</sup> )					
GRT001	0.211	0.207	0.203	0.196	0.195	0.190
GRT001	0.223	0.215	0.210	0.207	0.205	0.200
GRT002	0.220	0.217	0.214	0.212	0.211	0.207
GRT002	0.222	0.216	0.212	0.210	0.208	0.200
GRT003	0.253	0.249	0.245	0.237	0.229	0.218
GRT003	0.238	0.234	0.229	0.220	0.215	0.203

Table 6-18. Grout water retention properties as measured by Idaho National Laboratory

Sample ID					
GRT004		GRT006		GRT008	
Potential (cm)	Volumetric Water Content (cm <sup>3</sup> /cm <sup>3</sup> )	Potential (cm)	Volumetric Water Content (cm <sup>3</sup> /cm <sup>3</sup> )	Potential (cm)	Volumetric Water Content (cm <sup>3</sup> /cm <sup>3</sup> )
0	0.223	0	0.226	0	0.223
-47,200	0.161	-11.5	0.217	-3,220	0.208
-88,400	0.151	-13.2	0.215	-849,020	0.012
-132,000	0.142	-15.7	0.213		
-849,020	0.018	-31.4	0.209		
		-3,220	0.217		
		-356,000	0.096		
		-849,020	0.019		

**Table 6-19. CLSM hydraulic and physical properties**

Sample ID	Lab	Porosity <sup>1</sup>	Dry Bulk Density (g/cm <sup>3</sup> )	Particle Density <sup>2</sup> (g/cm <sup>3</sup> )	Volumetric Moisture Content (cm <sup>3</sup> /cm <sup>3</sup> )	Saturation	Saturated Hydraulic Conductivity (cm/s)	Log Saturated Hydraulic Conductivity (cm/s)
CLSM005	INL <sup>3</sup>	na	1.73		na	-	na	
CLSM005A	INL	na	1.74		na	-	na	
CLSM005B	INL	na	1.81		na	-	na	
CLSM005E	INL	0.340	-	2.67 <sup>6</sup>	0.340	1.00	3.42E-06	-5.47
			-		0.301	0.89		
			-		0.245	0.72		
CLSM005F	INL	0.335	-	2.65 <sup>6</sup>	0.335	1.00	1.40E-06	-5.85
			-		0.292	0.87		
			-		0.200	0.60		
CLSM001 <sup>5</sup>	GTX <sup>4</sup>	0.31	1.85	2.68	0.310	1.00	1.90E-06	-5.72
Average		0.328	1.78	2.65 <sup>2</sup>	-	-	2.24E-06 <sup>7</sup>	-5.62
Std Dev of Population		0.02	0.06	0.02	-	-	1.05E-06 <sup>7</sup>	0.20
Count		3	4	3	-	-	3 <sup>7</sup>	3
Std Dev of Mean		0.009	0.029	0.010	-	-	6.07E-07 <sup>7</sup>	0.114

Notes to Table 6-19:

<sup>1</sup> Porosity is expressed as a fraction as provided in Dixon and Phifer (2006) rather than as a percent (%) as expressed in the bulk of this document

<sup>2</sup>  $\rho_p = \rho_b / (1 - \eta)$  (Hillel 1982)

<sup>3</sup> Idaho National Laboratory

<sup>4</sup> GeoTesting Express, Inc.

<sup>5</sup> Sample CLSM001 is a mold sample; the remainder are core samples. The mold sample is considered similar enough to the core samples to include in the average and standard deviations.

<sup>6</sup> The particle densities for samples CLSM005E and CLSM005F were determined using the average dry bulk density of samples CLSM005, CLSM005A, and CLSM005B.

<sup>7</sup> Saturated hydraulic conductivity average (i.e., average of hydraulic conductivities of samples with a saturation of 1, and standard deviation of population, count, and standard deviation of mean of the saturated hydraulic conductivity values.

Std Dev = standard deviation

**Table 6-20. CLSM water retention properties as measured by GeoTesting Express, Inc.**

Sample ID	Potential (cm)					
	-102.07 (0.1 bars)	-510.35 (0.5 bars)	-1,020.7 (1.0 bars)	-2,041.4 (2.0 bars)	-5,103.5 (5.0 bars)	-15,310.5 (15.0 bars)
Volumetric Water Content (cm <sup>3</sup> /cm <sup>3</sup> )						
CLSM-001	0.271	0.248	0.241	0.210	0.194	0.154
CLSM-001	0.280	0.252	0.247	0.207	0.189	0.147

**Table 6-21. CLSM Water Retention Properties as Measured by Idaho National Laboratory**

Sample CLSM005	
Potential (cm)	Volumetric Water Content (cm <sup>3</sup> /cm <sup>3</sup> )
0	0.338
-3,220	0.277
-849,020	0.003

**6.2.4 2007 Cementitious Material Selection for Future Component-in-Grout Waste Disposals (Dixon and Phifer, 2007)**

Dixon and Phifer (2007) present the result of a study undertaken to identify a grout formulation for use in future CIG waste disposals. The previously used high flow CIG grout mix (i.e., “old” CIG grout) was designed primarily to encapsulate and fill between adjacent components. In 2007, a new mix design that satisfied both the hydraulic and placement requirements was tested by Dixon and Phifer (2007) and replaced the old CIG grout. Four mix designs were tested. The mixes were prepared and placed in test trenches and allowed to cure. After 28 eight days core samples were collected from each of the test trenches and submitted to independent testing laboratories to determine porosity, bulk density, saturated hydraulic conductivity and moisture retention characteristics along with VG parameters. The grout containing blast furnace slag, 4000-SCC-FA-Grout (Table 4-1), was selected for further testing based on the results of standard geotechnical testing of the 28-day samples. Additional samples of 4000-SCC-FA-Grout were collected after curing 125 days and submitted for further testing. Dixon and Phifer (2007) recommended grout 4000-SCC-FA-Grout for use in future CIG waste disposals. Hydraulic properties for 4000-SCC-FA-Grout are discussed in section 6.3.3.2. Hydraulic and physical properties and van Genuchten parameters for samples of mix 4000-SCC-FA-GROUT are listed in Table 6-15, Table 6-22, and Table 6-23

**Table 6-22. Hydraulic and physical properties of Mix 4000-SCC-FA-GROUT<sup>1</sup>**

Sample ID	Minimum Curing Period (days) <sup>2</sup>	Porosity <sup>3</sup>	Dry Bulk Density (g/cm <sup>3</sup> )	Particle Density <sup>3</sup> (g/cm <sup>3</sup> )	Saturated Hydraulic Conductivity (cm/s)	Log Saturated Hydraulic Conductivity (cm/s)
GRT025A	28	0.210	1.92	2.43	2.3E-08	-7.64
GRT025B	28	0.245	1.91	2.53	3.6E-08	-7.44
GRT026A	28	0.205	1.93	2.42	1.2E-08	-7.92
GRT026B	28	0.232	1.92	2.49	1.8E-08	-7.74
GRT027A	28	0.205	1.91	2.40	6.5E-08	-7.19
GRT027B	28	0.236	1.93	2.53	4.5E-09	-8.35
GRT030A	125	0.235	1.90	2.49	9.6E-09	-8.02
GRT030B	125	0.233	1.86	2.43	9.7E-09	-8.01
GRT031A	125	0.237	1.90	2.49	9.6E-09	-8.02
GRT031B	125	0.229	1.93	2.50	1.1E-08	-7.96
GRT032A	125	0.234	1.90	2.48	6.7E-09	-8.17
GRT032B	125	0.229	1.92	2.49	7.2E-09	-8.14
Average		0.233	1.90	2.48	9.0E-09	-8.05
Std Dev of Population		0.0033	0.023	0.027	1.7E-09	-0.084
Count		6	6	6	6	6
Std Dev of Mean		0.0013	0.0095	0.011	6.8E-10	0.034

<sup>1</sup> As measured by Mactec Engineering and Consulting, Inc.

<sup>2</sup> Only used samples cured for 125 days were considered representative of long-term property values. Therefore, these samples have been excluded from the average and standard deviation calculations.

<sup>3</sup> Porosity calculated as  $n = ((M_{sat} - M_{dry})/pw) / Vol$

$$\rho_p = \rho_b / (1 - \eta)$$

Source Dixon and Phifer (2007)

**Table 6-23. van Genuchten parameters for Mix 4000-SCC-FA-GROUT**

Mix	$\theta_s$ (cm <sup>3</sup> /cm <sup>3</sup> )	$\theta_s$ (cm <sup>3</sup> /cm <sup>3</sup> )	$\alpha$ (1/cm)	n	m
4000-SCC-FA-GROUT <sup>1</sup>	0.241	0.000	3.3E-06	1.479	0.3239
4000-SCC-FA-GROUT <sup>2</sup>	0.244	0.000	3.3E-06	1.356	0.2625

<sup>1</sup>Sample GRT034A

<sup>2</sup>Sample GRT035A

Source Dixon and Phifer (2007)

### 6.2.5 2013 E-Area Vault Concrete Material Property and Vault Durability/Degradation Projection Recommendations (Phifer, 2014)

Concrete cores were collected from the E-Area LLWF ILV/LAWV concrete test wall in 2010 and submitted to SIMCO Technologies Inc. to evaluate hydraulic and physical properties of the concrete. The E-Area LLWF ILV/LAWV concrete test wall was constructed in 1991 utilizing the same concrete formulation as the LAWV and ILV, mix C-4000-8-S-2-AB, and was placed and cured in the same manner. SIMCO tested concrete samples for bulk physical properties, i.e., porosity, dry bulk density, and effective diffusion

coefficient as well as saturated hydraulic conductivity, and collected water retention data. Table 4-1 shows the formulation for the vault concrete.

Phifer compared these results with those from earlier E-Area Vault concrete testing. The SIMCO results are considered to be the most accurate of the E-Area vault concrete testing to-date because SIMCO is a leader in the field and the test methodology was designed specifically for cementitious materials. Phifer (2014) recommended the nominal property values shown in Table 6-24 for use in future PA and Special Analysis (SA) modeling. Because the SIMCO results essentially represent one measurement per property, an uncertainty cannot be assigned based upon the SIMCO results alone. Multiple E-Area vault concrete results from the Core Laboratory testing, however, are available for saturated hydraulic conductivity, dry bulk density, porosity, and particle density (Table 6-12). Therefore, Phifer (2014) recommended the uncertainty distributions provided in Table 6-25 which are based upon the uncertainty distributions developed for the Core Laboratory results. The standard deviation of the mean was adjusted from the values provided in Table 6-12 for dry bulk density, porosity, and particle density based upon the proportionality of the recommended values to that of the average value in Table 6-12. The uncertainty distributions for the recommended saturated hydraulic conductivity are the same as those provided in Table 6-12.

**Table 6-24, Hydraulic and physical properties of Mix C-4000-8-S-2-AB**

Sample ID	Lab	Porosity <sup>1</sup>	Dry Bulk Density (g/cm <sup>3</sup> )	Particle Density <sup>2</sup> (g/cm <sup>3</sup> )	Hydraulic Conductivity (cm/s)
n/a	SIMCO	0.158	2.54	3.02	8.2E-14 <sup>(4)</sup>

<sup>1</sup> Porosity calculated as  $n = ((M_{sat} - M_{dry})/pw) / Vol$

$$^3 \rho_p = \rho_b / (1 - \eta)$$

Source Dixon and Phifer (2007)

<sup>4</sup> In order to maintain some conservatism, it was recommended that the previously used saturated hydraulic conductivity of 1.0E-12 cm/s continue to be used rather than the results from SIMCO (i.e. 8.2E-14 cm/s).

**Table 6-25. Recommended E-Area Vault Concrete uncertainty distributions**

Uncertainty Distribution Parameter	Saturated Hydraulic Conductivity (cm/s)	Log Saturated Hydraulic Conductivity (cm/s)	Tortuosity <sup>1</sup> (-)	Log Tortuosity <sup>1</sup> (-)	Saturated Effective Diffusion Coefficient (cm <sup>2</sup> /s)	Log Saturated Effective Diffusion Coefficient (cm <sup>2</sup> /s)	Dry Bulk Density (g/cm <sup>3</sup> )	Porosity (-)	Particle Density (g/cm <sup>3</sup> )
Recommended Nominal Value	1.00E-12	-12.00	0.004	-2.40	6.40E-08	-7.19	2.540	0.158	3.02
Distribution Type	-	normal <sup>2</sup>	-	normal <sup>2</sup>	-	normal <sup>2</sup>	normal	normal	normal
Standard Deviation of Mean	-	0.074	-	0.025	-	0.025	0.0125	0.0064	0.0313
Variance of the Mean	-	0.0055	-	0.000635	-	0.000635	0.000157	0.000041	0.000977
Mean Minimum (3 sigma)	-	-12.22	-	-2.47	-	-7.27	2.502	0.139	2.926
Mean Maximum (3 sigma)	-	-11.78	-	-2.32	-	-7.12	2.578	0.177	3.114

<sup>1</sup>  $\tau = D_e \div D_m$  (Assuming a  $D_m$  for a representative species (NaCl) of 1.6E-5 cm<sup>2</sup>/s (Bruins 2003))

<sup>2</sup> Saturated hydraulic conductivity, tortuosity, and effective diffusion coefficient are log normally distributed therefore the log of saturated hydraulic conductivity, tortuosity, and effective diffusion coefficient is normally distributed

Data for the water retention curve was also collected. A constant vapor pressure (CVP) method was used to create the various levels of suction necessary to determine the moisture desorption isotherm for a sample of the E-Area vault concrete. Slices 100mm in diameter by 10 mm of a concrete core were saturated in lime water until a constant mass was achieved. The saturated slices were then placed above a saturated salt solution inside sealed containers. The saturated salt solution produces a constant relative humidity (RH) in the headspace of the sealed container.

The capillary pressure in the slice is equal to the vapor pressure in the sealed chamber which can be determined from relative humidity using the Kelvin equation (54) (Nimmo and Winfield, 2002). Each wafer drains by evaporation until total capillary pressure in the sample is at equilibrium with the vapor pressure in the headspace of the container. At equilibrium, the material is assumed to attain the same total potential as the vapor in the headspace of the container. The salts and associated capillary pressures used in this study are listed in Table 6-26.

$$p_c = -\frac{\rho_l RT}{M_v} \ln(H) \quad (54)$$

where:

$p_c$	capillary pressure
$\rho_l$	density of water
$R$	ideal gas constant
$T$	temperature
$M_v$	molar mass of water
$H$	relative humidity

The method for determining water retention characteristics for individual sediment samples described in Section 5.2.3 was used to determine van Genuchten parameters defining the WRC curve for vault concrete C-4000-8-S-2-AB using data from SIMCO in Table 6-26. The van Genuchten parameters are presented in Table 6-27 and the WRC is shown in Figure 6-6. As stated earlier, SIMCO results are considered to be the most accurate of the E-Area vault concrete testing to-date. Both SIMCO and MACTEC data are plotted in Figure 6-6. MACTEC results appear to be uncharacteristic of drainage curve behavior and are therefore excluded from van Genuchten curve fitting.

**Table 6-26. Salts used in constant vapor pressure method for moisture retention characteristics and resulting saturation of vault concrete sample. (Phifer, 2014)**

Salt	RH	h (Pa) <sup>1</sup>	h (cmH <sub>2</sub> O) <sup>2</sup>	Sample Saturation
MgCl*6H <sub>2</sub> O	0.33	151580838	1.55E+06	0.55
n/a <sup>3</sup>	0.5	94769886	9.66E+05	0.65
NaCl	0.75	39333056	4.01E+05	0.89
KCl	0.85	22220245	2.27E+05	0.86
KNO <sub>3</sub>	0.92	11400271	1.16E+05	0.90

<sup>1</sup> Calculated using equation 54

<sup>2</sup> 1 Pa = 1.02e-2 cm H<sub>2</sub>O

<sup>3</sup> sample equilibrated in environmental chamber

**Table 6-27. van Genuchten parameters for Mix C-4000-8-S-2-AB**

Mix	$\theta_s$ (cm <sup>3</sup> /cm <sup>3</sup> )	$\theta_r$ (cm <sup>3</sup> /cm <sup>3</sup> )	$\alpha$ (1/cm)	n	m
C-4000-8-S-2-AB	0.158000	0.000000	3.701E-06	1.305542	0.234034

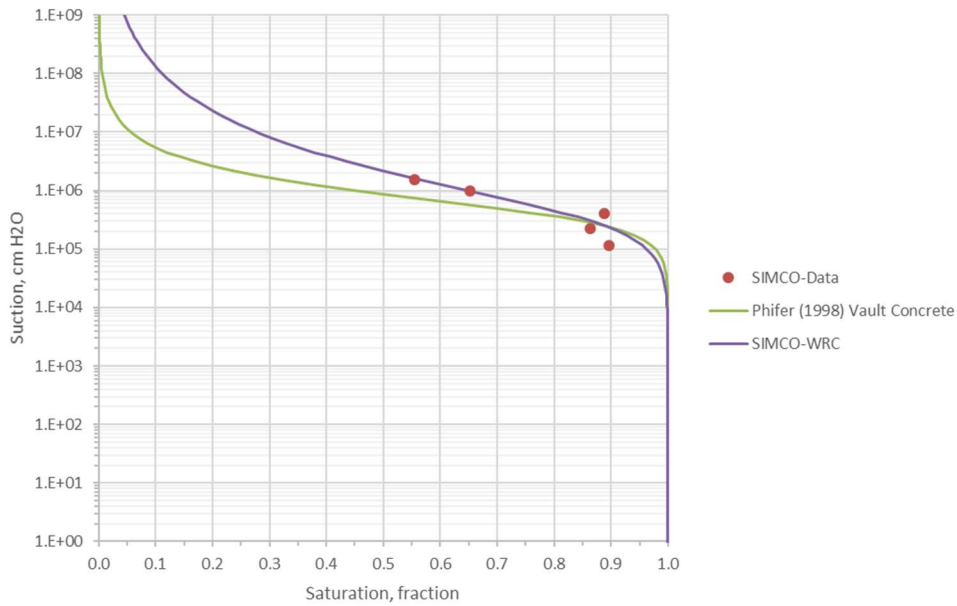


**Figure 6-6. Water retention curve for Mix C-4000-8-S-2-AB based on SIMCO data.**

### 6.3 E-AREA CEMENTITIOUS MATERIAL PROPERTY REPRESENTATIONS

Five cementitious materials are used to represent the various cementitious barriers present in disposal of solid low-level radioactive waste as described in Section 4.4, E-Area LLWF Disposal Unit Types. These five materials are identified as old E-Area CIG grout, new E-Area CIG Grout, E-Area CLSM, E-Area CIG Concrete Mat, and E-Area Vault Concrete. This section of the report presents recommended property values for the five cementitious materials used in the disposal of solid low-level waste. As outlined within Chapter 3.0, Approach to Data Selection, the property values assigned to the various E-Area cementitious materials are based upon the following in order of priority:

- Site-specific field data
- Site-specific laboratory data
- Similarity to material with site-specific laboratory data
- Literature data

There are limited site-specific field and laboratory data for most of the E-Area cementitious materials as outlined within Section 6.2, Internal Literature Review. Literature data for generic cementitious materials are provided within Section 6.1, External Literature Review. When available the site-specific field and laboratory data provided within Section 6.2 are utilized to provide material property representations for both the material tested and similar materials. When site-specific laboratory data are not available, the generic literature data provided in Section 6.1 are utilized to provide material property representations.

Site specific data for old E-Area CIG Grout used in trenches 1-8 are the same as used in Phifer et al. (2006). These data are found in a 2006 study (Dixon and Phifer 2006) which is described in Section 6.2.3 of this report (see Table 6-16). A semi-empirical approach was selected to generate WRCs using surrogate materials to represent the micro- and macro-porosity drainage behavior of this grout material. The composite WRC is a blend of these two materials but does not adhere to a van Genuchten formulation. Additional details are provided in Section 6.3.3.1.

Site specific data for the new E-Area CIG grout formulation are available from a 2007 study (Dixon and Phifer 2007) published after the original 2006 data package (Phifer 2006). This study is described in section 6.2.4. WRCs based on a van Genuchten formulation were fitted to selected available data sources where physical properties were employed to establish the saturated water content value.

Site specific data for ILV CLSM backfill is the same as used in Phifer et al. (2006). This study is described in section 6.2.3. The tabulated values for the WRCs have been replaced with a van Genuchten formulation. WRCs based on a van Genuchten formulation were fitted to selected available data sources where physical properties were employed to establish the saturated water content value.

No physical or hydraulic data are available for E-Area CIG concrete mats. Therefore, properties for this material have been assumed to be the same as the new E-Area CIG Grout as discussed in Section 6.3.3.4.

Site specific data for the vault concrete are available from a 2010 study (Phifer 2013). This study is described in section 6.2.5. WRCs based on a van Genuchten formulation were fitted to selected available data sources where physical properties were employed to establish the saturated water content value.

### **6.3.1 Porosity, Bulk Density, and Particle Density**

Site-specific porosity and bulk density laboratory data are available for the old and new E-Area CIG grout, E-Area CLSM, and E-Area vault concrete (i.e., LAWV and ILV). Table 6-28 provides the porosity, bulk density, and calculated particle density data for each of the cementitious materials. Typically, average values were used.

Site-specific laboratory data are not available for the E-Area CIG reinforced concrete mats. The porosity, bulk density, and particle density of the E-Area CIG concrete mats have been assumed to be the same as the new E-Area CIG Grout as both materials are placed with standard field construction practices (i.e., minimal consolidation and curing requirements).

**Table 6-28. Recommended material properties for cementitious materials in the various E-Area LLWF Disposal Unit Types**

Property	Material				
	CIG Grout		CLSM (C3)	Concrete Mat (C4)	Vault Concrete (C5)
	Old (C1)	New (C2)			
$K_{sat}$ , cm/sec	4.5E-5	2.6E-08	2.2E-06	2.6E-08	1.0E-12
Porosity, $\phi$	0.224	0.233	0.328	0.233	0.158
Dry bulk density, gm/cm <sup>3</sup>	1.79	1.90	1.78	1.90	2.54
Particle Density, gm/cm <sup>3</sup>	2.31	2.48	2.65	2.48	3.02
$\theta_s$	WRC calculated from combination of 2 materials, see section 6.3.3.1	0.233000	0.328000	0.233000	0.158000
$\theta_r$		0.000000	0.028399	0.000000	0.000000
$\alpha$		7.555E-06	2.867E-03	7.555E-06	3.701E-06
n		1.191467	1.500000	1.191467	1.305542
m		0.160698	0.333333	0.160698	0.234034
Saturated Effective Diffusion Coefficient $D_e$ , cm <sup>2</sup> /s	1.9E-6	8.0E-07	4.0E-06	8.0E-07	6.4E-08

### 6.3.2 Saturated Hydraulic Conductivity

Site-specific saturated hydraulic conductivity laboratory data are available for the old and new E-Area CIG grout, E-Area CLSM, and E-Area vault concrete (i.e., LAWV and ILV). Table 6-28 provides the saturated hydraulic conductivity laboratory data for each of these materials.

Site-specific laboratory data are not available for, the E-Area CIG concrete mats. As with porosity, dry bulk density, and particle density (Section 6.3.1), the saturated hydraulic conductivity of the E-Area CIG concrete mats (Table 4-1) has been assumed to be the same as that of the new E-Area CIG grout (i.e.,  $2.6E-08$  cm/s). This is considered reasonable for the reasons stated previously.

### 6.3.3 Water Retention Curves (Suction Head, Saturation, and Relative Permeability)

Site specific water retention curves are available for old and new CIG grout, CLSM and vault concrete. The water retention curve for concrete mats is based on the new CIG grout.

#### 6.3.3.1 Old E-Area CIG Grout

Laboratory hydraulic property data for core samples and computed tomography (CT) scans provided by Dixon and Phifer (2006) suggest that the old E-Area CIG grout is composed of both micropores and macropores. Saturated hydraulic conductivity for the 1-inch diameter CIG grout core samples ranged from  $1.9E-8$  cm/s to  $1.4E-4$  cm/s and for the 3-inch diameter CIG grout core samples from  $2.3E-4$  cm/s to  $4.3E-4$  cm/s (see Table 6-16). This variability was attributed to the heterogeneity of the grout and the diameter of the samples analyzed. Because the smaller diameter samples incorporated only a small fraction of the CIG material, they were more likely affected by the variability in pore interconnectedness than the larger (3-inch) samples. This sampling bias was evident in the wide range of measured saturated hydraulic conductivities but was also observed in the CT images. 1-inch samples with higher saturated hydraulic conductivities showed interconnected pores around poorly cemented aggregate-paste boundaries. These interconnected pores would likely have created preferential flow paths. In contrast, samples with lower saturated hydraulic conductivities contained less observable interconnected porosity in the CT scans (Dixon and Phifer, 2006).

Based on laboratory data and CT scans, the old E-Area CIG grout was conceptualized as consisting of two components with different porosities and drainage behaviors. The two components consisted of:

1. A predominantly intact concrete with fine pore structure, which would drain slowly, and
2. A smaller amount of material with bigger pores and preferential flow paths, which would drain easily and produce a higher saturated conductivity.

A semi-empirical approach was selected to generate characteristic curves for the old E-Area CIG grout material. Specifically, surrogate materials were used to represent the drainage behavior of the micro- and macro-porosity in the CIG grout conceptual model. The Hanford Concrete (Table 6-5) was used to represent the micro-porosity in old CIG grout and macro-porosity is represented by gravel (Table 5-9).

These two surrogates were proportioned through a visual trial-and-error process to produce properties that mimicked the water retention data for old CIG grout. A combination of 85% Hanford concrete and 15% gravel appeared to best fit the laboratory data.

Similarly, saturated hydraulic conductivity for the hypothetical composite material (i.e., old E-Area CIG grout) was calculated based on the blend of 85% low-quality concrete, 15% coarse material, and an upscaling power-average exponent of  $p=0.33$ . The resulting saturated hydraulic conductivity of  $3.8E-5$  cm/sec and a porosity of 0.24 (or 24%) for the composite material are similar to  $4.5E-5$  cm/s and 0.224 (22.4%) based on actual sample data statistics from Table 6-16, respectively. The comparison suggests that the surrogate materials selected for grout micro- and macro-porosity, and their proportions, are reasonable.

Saturation values for the CIG material were calculated by:

$$S_{CIG} = \frac{(0.85 * S_C * \phi_C) + (0.15 * S_G * \phi_G)}{\phi_{CIG}} \quad (55)$$

where  $S$  = saturation,  $n$  = porosity, CIG = CIG grout, C = concrete, and G = gravel.

Unsaturated hydraulic conductivity was calculated by:

$$K_{unsat-CIG} = [0.85 * (K_{unsat-C})^p + 0.15 * (K_{unsat-G}^p)]^{1/p} \quad (56)$$

where  $K_{unsat}$  = unsaturated hydraulic conductivity,  $p$  = power-averaging exponent of 0.33, CIG = CIG grout, C = concrete, and CGM = coarse grained material.

Relative permeability ( $K_r$ ) for the CIG grout was calculated by:

$$K_{r-CIG} = \frac{K_{unsat-CIG}}{K_{sat-CIG}} \quad (57)$$

where  $K_{sat-CIG} = 3.8E-5$  cm/sec.

Figure 6-7 shows suction head and relative permeability versus saturation curves for the concrete, the coarse-grained material, and the resulting blend (i.e., the old E-Area CIG grout). As seen, the composite grout behaves similar to the gravel at low suction, but more like the fine-grained material at high suction. This behavior is consistent with the concept of macro-pores draining under low suction while micro-pores remain saturated until much higher suction is applied.

Figure 6-8 shows the effect of suction on relative hydraulic conductivity for old CIG grout based. Large diameter pores drain first as suction increases leaving pores with decreasing diameter saturated to transport water. As the size of saturated pores decreases relative

hydraulic conductivity decreases. The rapid increase in suction during drainage shown in Figure 6-7 results in the rapid decrease in relative hydraulic conductivity in Figure 6-8. After large pores associated with gravel drain small pores in the concrete control drainage resulting in a migration of the  $K_{rel}$  curve from the gravel curve to the concrete curve.

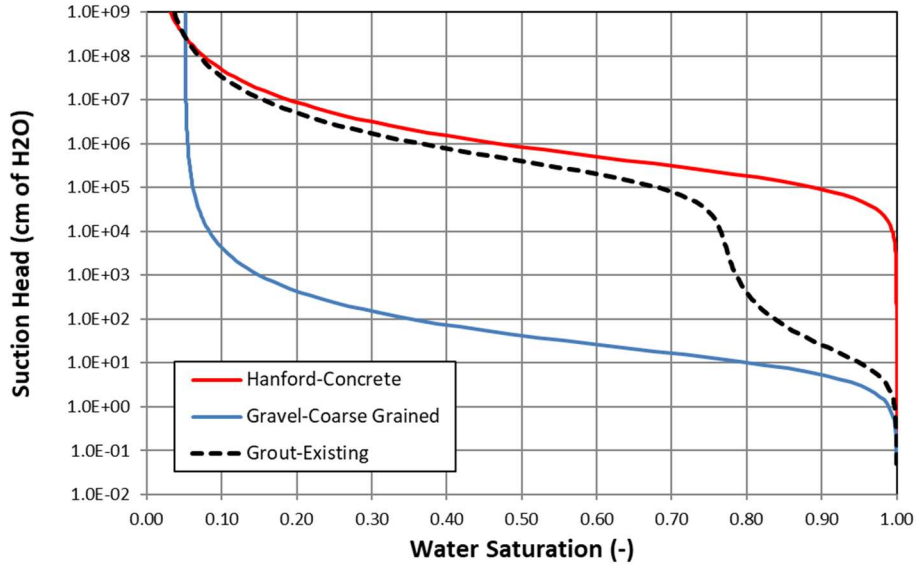


Figure 6-7. Old E-Area CIG Grout characteristic curves

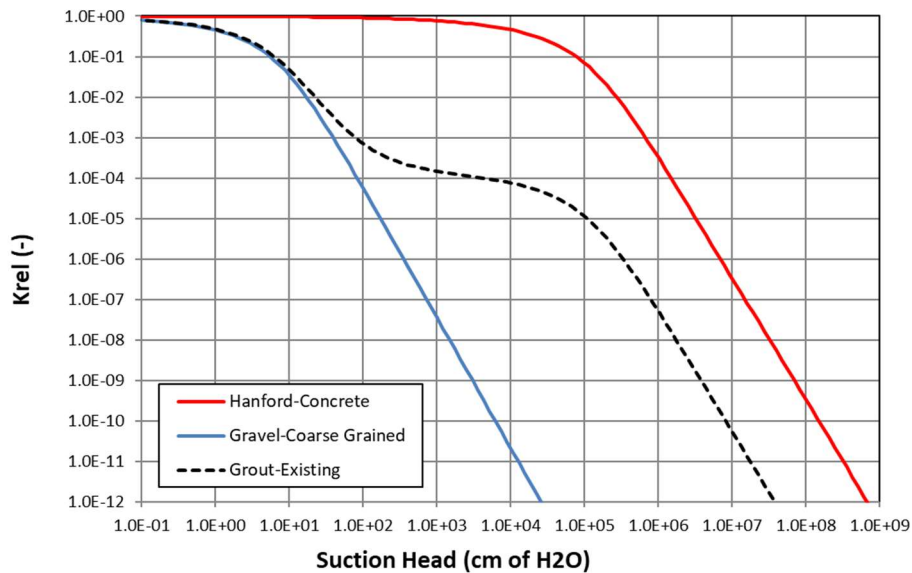
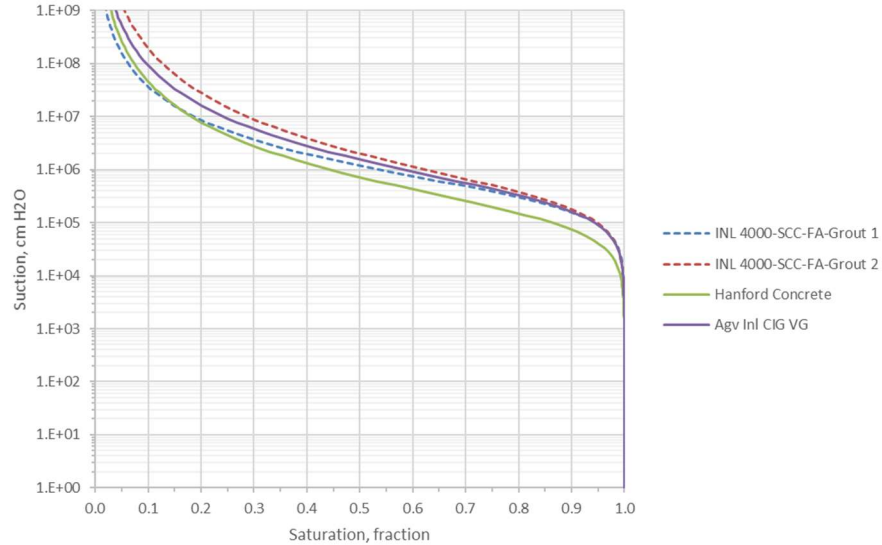


Figure 6-8. Relative hydraulic conductivity curve for Old E-Area CIG grout

**6.3.3.2 New E-Area CIG Grout**

Results from the Dixon and Phifer (2007) study of grouts for future CIG disposal were used to develop the water retention properties for the new CIG grout listed in Table 6-28. The WRCs for samples in Table 6-23 were combined using the method described in Section 5.2.3 for combining WRCs for individual soil samples into a curve for an equivalent representative soil using equation 17. Figure 6-9 shows the recommended WRC for new CIG grout and compares it to the WRC for future CIG grout (Hanford concrete) used in Phifer et al. (2006). Figure 6-10 compares the recommended  $K_{rel}$  curve for new CIG grout to the  $K_{rel}$  for future CIG grout (Hanford concrete) used in Phifer et al. (2006).



**Figure 6-9. Water retention curve for new CIG grout**

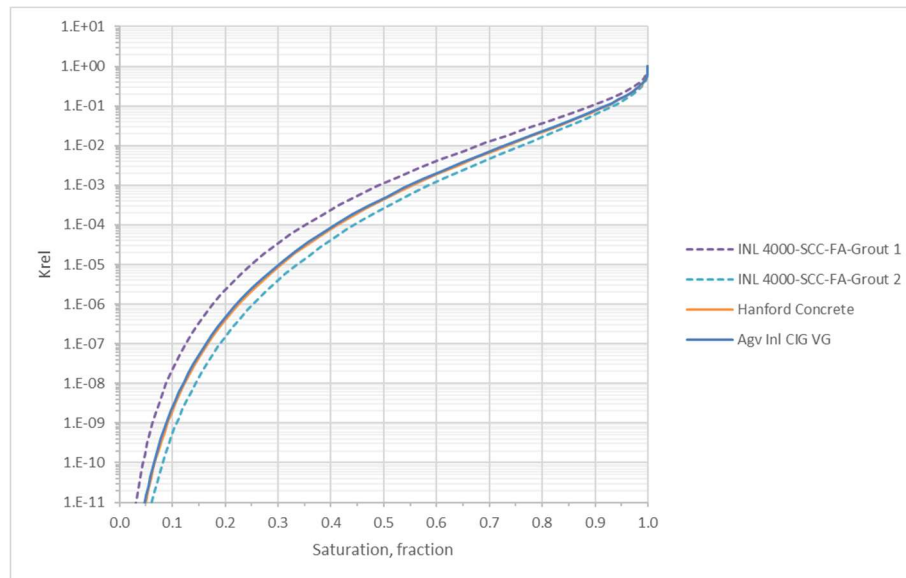


**Figure 6-10. Relative hydraulic conductivity curve for New CIG grout**

### 6.3.3.3 E-Area CLSM

Table 6-19 provides the site-specific saturated and unsaturated hydraulic conductivity laboratory data and Table 6-20 and Table 6-21 provide the water retention laboratory data for the E-Area CLSM from which characteristic curves were derived. These laboratory measurements of hydraulic conductivity (average of 2.2E-06 cm/s) and porosity (average of 32.8%) along with computed tomography (CT) scans indicate that the CLSM has significant interconnected porosity, poor cementation at the aggregate-paste boundaries and heterogeneity (Dixon and Phifer, 2006). Based on these attributes, the CLSM was conceptually viewed as having soil-like properties. Characteristic curves for the CLSM were generated using RETC software, which is designed for soils, and matching the available water retention and relative permeability data. The van Genuchten parameters for CLSM are provided in Table 6-28, and Figure 6-12 show the resulting characteristic curves (i.e., suction head and relative permeability versus saturation, respectively) for the E-Area CLSM. For CLSM not only were there WRC data, but also relative permeability (Krel) data was available from INL testing. In the first step of creating a new representation of CLSM behavior the three data sample sets (i.e., for CLSM1A, CLSM1B, and CLSM5) were each fitted to individual WRCs. In the second step these three individual WRCs were fitted to one composite vG WRC (i.e., where data weighting was employed). The resulting vG WRC and corresponding Krel curve are shown in Figures x and y, respectively (i.e., dashed cyan curves). In the third and final step Krel data (i.e., CLSM5E and CLSM5F) were incorporated into the fitting process where only the shape factors were changed. Specifically, the resulting shift in the “n” shape parameter yielded:

- 1.234808 for the “WRC data fitted only” case and
- 1.500000 for the “WRC and Krel data fitted” case.

where the constraint of  $m=1-1/n$  was maintained throughout. The updated WRC and Krel curves are shown in Figures x and y, respectively (i.e., as solid black lines).

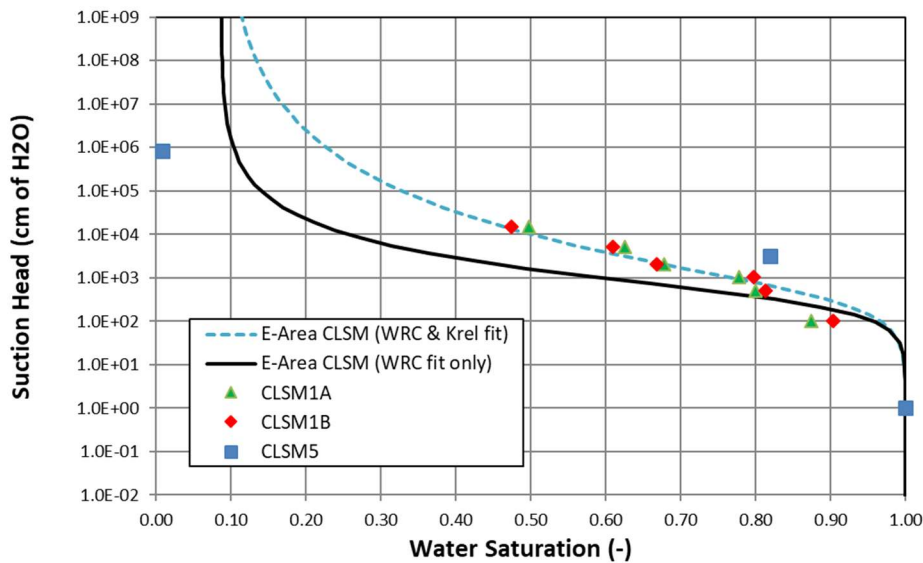
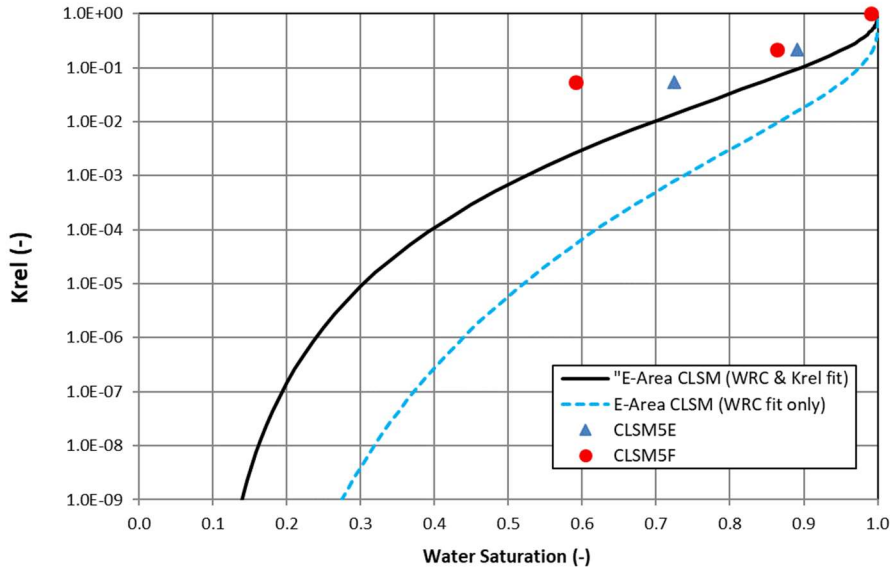


Figure 6-11. Water retention curve and data for E-Area CLSM



**Figure 6-12. Relative hydraulic conductivity curve for E-Area CLSM**

**6.3.3.4 E-Area CIG Concrete Mats**

Site-specific unsaturated hydraulic conductivity and water retention laboratory data are not available for the E-Area CIG concrete mats. Characteristic curves for the concrete mats will be based upon the new CIG grout described in Section 6.3.3.2. Table 6-28 lists the van Genuchten parameters assigned for concrete mats.

**6.3.3.5 E-Area Vault Concrete**

Site-specific data for evaluating the WRC for vault concrete is summarized in Section 6.2.5. Table 6-28 lists the recommended van Genuchten parameters describing the WRC for vault concrete. Figure 6-6 shows the WRC based on the recommended van Genuchten parameters and compares it this the WRC recommended in Phifer (2014). The parameters in Table 6-28 are preferred because they are based on site-specific samples.

**6.3.4 Saturated Effective Diffusivity**

The new E-Area CIG Grout, the E-Area CIG concrete mats, and the E-Area vault concrete (i.e., LAWV and ILV) are considered fairly typical cementitious materials for which the saturated effective diffusivity coefficient can be reasonably derived from literature values presented in Section 6.1.4.

As concluded in Section 6.1.4, the saturated effective diffusion coefficients of typical cementitious materials range from approximately 1.0E-08 to 5.0E-07 cm<sup>2</sup>/s (see Table 6-9, Table 6-10, and Table 6-11). This is a relatively narrow range at just over one order of magnitude, particularly in comparison to the range of saturated hydraulic conductivities for cementitious materials. These data clearly show that the effective diffusion coefficient decreases with decreasing WCR and with the addition of fly ash, blast furnace slag, and silica fume. Based upon this information the three categories of cementitious materials outlined in Table 6-29 will be established in order to assign appropriate saturated effective diffusivity coefficients to each of these E-Area cementitious materials. Table 6-29 provides the resulting

saturated effective diffusivity coefficient assignments for each of these materials along with its justification.

While the old E-Area CIG grout and E-Area CLSM are cementitious materials, it is not considered appropriate to assign these materials saturated effective diffusivity coefficients based strictly upon the cementitious material literature for the following reasons:

- As outlined in Sections 6.3.2 and 6.3.3, the old E-Area CIG grout porosity consists of a small fraction of macropores (~15% of material volume characterized as containing macropores) with a high hydraulic conductivity that results in rapid drainage and a larger fraction of micropores (~85% of material volume characterized as containing micropores) with a relatively low hydraulic conductivity that drain slowly. Therefore, in terms of a saturated effective diffusion coefficient, this E-Area CIG grout probably behaves more like a combination of ~15% sand containing macropores and ~85% cementitious material containing micropore than solely a cementitious material.
- As outlined in Section 6.3.2, the E-Area CLSM has a saturated hydraulic conductivity (average of 2.2E-06 cm/s) like that of the clay (>50% mud) discussed in Section 5.2.2 and Table 5-20 (2.0E-06 cm/s). Additionally, as outlined in Section 6.3.3.3, E-Area CLSM has significant interconnected porosity, poor cementation at the aggregate-paste boundaries and heterogeneity, which make the CLSM appear to have soil-like properties. Finally, the fly ash used in the CLSM is a relatively fine-grained material. Therefore, in terms of a saturated effective diffusion coefficient, the E-Area CLSM probably behaves more like a clayey soil than a cementitious material.

Based upon this reasoning, the saturated effective diffusion coefficient for the old E-Area CIG grout will be calculated as though it consists of 15% sand with a  $D_e$  of 8.0E-06 cm<sup>2</sup>/s (see Section 5.2.5 and Table 5-13) and 85% cementitious material with a  $D_e$  of 8.0E-07 cm<sup>2</sup>/s (see Table 6-29 for the low quality concrete  $D_e$ ). This results in a  $D_e$  of 1.9E-06 cm<sup>2</sup>/s for the old E-Area CIG grout as shown below:

$$D_e = (0.85 \times 8.0E - 07 \text{ cm}^2/\text{s}) + (0.15 \times 8.0E - 06) = 1.9E - 06 \text{ cm}^2/\text{s}$$

Additionally, based upon this reasoning, E-Area CLSM will be assigned the same saturated effective diffusion coefficient as clay (>50% mud), which is 4.0E-06 cm<sup>2</sup>/s (see Section 5.2.5 and Table 5-13).

Table 6-30 lists the saturated effective diffusion coefficients assigned to each of the E-Area cementitious materials.

**Table 6-29. Cementitious material categories for assignment of representative saturated effective diffusion coefficient**

<b>Cementitious Material Category</b>	<b>Description</b>	<b>Representative Saturated Effective Diffusion Coefficient (cm<sup>2</sup>/s)</b>	<b>Justification</b>
Low-Quality Concrete	Does not contain fly ash, blast furnace slag, and/or silica fume; little placement quality control	8.0E-07	Slightly greater than the highest diffusion coefficient of 5.0E-07 cm <sup>2</sup> /s from Table 6-9, Table 6-10, and Table 6-11
Ordinary-Quality Concrete	Low to moderate WCR; does not contain fly ash, blast furnace slag, and/or silica fume; good placement quality control	1.0E-07	Represents the upper two thirds of the diffusion coefficient range of 1.0E-08 to 5.0E-07 cm <sup>2</sup> /s
High-Quality Concrete	Relatively low WCR; contains fly ash, blast furnace slag, and/or silica fume; good placement quality control	5.0E-08	Consistent with Figure 6-5 concretes and mortars containing fly ash, blast furnace slag, and/or silica fume; and 5 times greater than the lower range of diffusion coefficients

**Table 6-30. E-Area saturated effective diffusion coefficient representation summary**

<b>Cementitious Material</b>	<b>Effective Diffusion Coefficient Representation</b>	<b>Reason for Selection</b>
Old E-Area CIG Grout	Blend of Low-Quality Concrete and Sand with $D_e = 1.9E-06 \text{ cm}^2/\text{s}$	Has a moderate WCR, placed with standard field construction practices, and is not built under the same level of quality control as major projects.
New E-Area CIG Grout	Low-Quality Concrete with $D_e = 8.0E-07 \text{ cm}^2/\text{s}$	Will be designed to be a high flow grout and will be placed with minimal consolidation and curing requirements.
E-Area CLSM	Clayey Soil with $D_e = 4.0E-06 \text{ cm}^2/\text{s}$	Behaves more like a clayey soil than a cementitious material.
E-Area CIG Concrete Mats	Low-Quality Concrete with $D_e = 8.0E-07 \text{ cm}^2/\text{s}$	Has a moderate WCR, placed with standard field construction practices, and is not built under the same level of quality control as major projects.
E-Area Vault Concrete (i.e., LAWV and ILV)	High-Quality Concrete as measured by SIMCO with $D_e = 6.4E-08 \text{ cm}^2/\text{s}$	Has a fairly low WCR, BFS and fly ash, and was built under strict project placement and curing requirements (see Table 4-1 and Table 4-2)

### 6.3.5 E-Area Cementitious Material Nominal Property Summary

Table 6-28 provides a summary of the recommended nominal cementitious material hydraulic properties for use in modeling flow associated with various E-Area disposal units (see Sections 6.3.1 through 6.3.4 for development of the nominal values).

## 6.4 E-AREA CEMENTITIOUS MATERIAL UNCERTAINTY REPRESENTATION

Uncertainty has been assigned to porosity, bulk density, particle density, saturated hydraulic conductivity, and saturated effective diffusion coefficients for each of the E-Area cementitious materials. As outlined within Section 3.0 the uncertainty assigned to the hydraulic properties of the various cementitious materials is based upon the following in order of priority:

- Site-specific field data,
- Site-specific laboratory data,
- Similarity to material with site-specific laboratory data, and
- Literature data.

There are no site-specific field data for any of the E-Area cementitious materials. There are limited site-specific laboratory data for most of the E-Area cementitious materials as outlined within Section 6.2. Literature data for generic cementitious materials are provided within Section 6.1. When available, the site-specific laboratory data provided within Section 6.2 are utilized to provide a representation of material property uncertainty for both the material tested and similar materials. When site-specific laboratory data are not available, the generic

literature data provided in Section 6.1 are utilized to provide a representation of material property uncertainty.

#### **6.4.1 Porosity, Bulk Density, and Particle Density Uncertainty**

Uncertainty statistics are provided for E-Area cementitious materials based on laboratory data for the site-specific materials. Uncertainty statistics for generic categories of high, ordinary and low-quality concrete have also been assigned based on data for similar site-specific concretes. These generic categories are included to provide a ready source of property values and statistics for modeling any potential future cementitious materials employed in E-Area where site-specific data may be lacking.

##### ***6.4.1.1 E-Area Cementitious Materials***

Site-specific laboratory data are available for the old and new E-Area CIG grout, E-Area CLSM, and E-Area vault concrete (i.e., LAWV and ILV), in order to establish the uncertainty associated with the representative nominal values of porosity, dry bulk density, and particle density.

Site-specific laboratory data for the porosity, bulk density, and particle density of the E-Area CIG concrete mats are not available. This material has been assumed to be the same as the new E-Area CIG Grout as both materials are placed with standard field construction practices (i.e., minimal consolidation and curing requirements). Therefore, representation of material property uncertainty for this concrete will be based upon new CIG grout values.

Table 6-31 provides the porosity, bulk density, and particle density nominal values and the standard deviation of the mean for each of the materials along with the source of these data.

##### ***6.4.1.2 High Quality Concrete***

The high-quality concrete category will be assigned the standard deviation of the population determined for the E-Area vault concrete (Table 6-12) as its standard deviation of the mean. This is considered reasonable for two reasons. First, the E-Area vault concrete is a high-quality concrete. Second, the standard deviation of the population was used because there are currently no data associated with these concretes.

##### ***6.4.1.3 Ordinary Quality Concrete***

The ordinary quality concrete category will be assigned the standard deviation of the population associated with the 675-T concrete from Table 6-14 as its standard deviation of the mean. This is considered reasonable for two reasons. First, the 675-T concrete represents material used in typical building construction. Second, the standard deviation of the population was used because there are currently no data associated with these concretes.

##### ***6.4.1.4 Low Quality Concrete***

The low-quality concrete classification was assigned a standard deviation of the mean twice that of the ordinary quality concrete, due to the assumption that poorer workmanship and quality control are associated with this classification than the ordinary concrete. Table 6-32 provides a summary of the assigned standard deviation of mean for low quality, ordinary quality, or high-quality concretes. The resulting summary of uncertainty statistics are provided for effective porosity, dry bulk density, and particle density in Table 6-33, Table 6-34, and Table 6-35, respectively.

**Table 6-31. Site-Specific porosity, bulk density, and particle density nominal value and standard deviation of mean**

<b>Cementitious Material</b>	<b>Effective Porosity Nominal Value (%)</b>	<b>Effective Porosity Standard Deviation of Mean (%)</b>	<b>Dry Bulk Density Value (g/cm<sup>3</sup>)</b>	<b>Dry Bulk Density Standard Deviation of Mean (g/cm<sup>3</sup>)</b>	<b>Particle Density Value (g/cm<sup>3</sup>)</b>	<b>Particle Density Standard Deviation of Mean (g/cm<sup>3</sup>)</b>	<b>Source of Porosity and Dry Bulk Density Value</b>
Old E-Area CIG Grout	22.4	0.59	1.79	0.031	2.31	0.021	Table 6-16
New E-Area CIG Grout	23.3	0.13	1.90	0.0095	2.48	0.011	Table 6-22 <sup>1</sup>
E-Area CLSM	32.8	0.93	1.78	0.029	2.65	0.010	Table 6-19
E-Area Vault Concrete	15.8	0.64	2.54	0.013	3.02	0.0314	Table 6-12

<sup>1</sup>New CIG grout nominal values and standard deviations based on data from samples cured for 125 days as representing longer term properties.

**Table 6-32. Low, Ordinary, and High-Quality Concrete assigned standard deviation of mean for effective porosity, dry bulk density, and particle density**

<b>Concrete Material Classification</b>	<b>Assigned Effective Porosity Standard Deviation of the Mean (%)</b>	<b>Assigned Dry Bulk Density Standard Deviation of the Mean (g/cm<sup>3</sup>)</b>	<b>Assigned Particle Density Standard Deviation of the Mean (g/cm<sup>3</sup>)</b>
High-quality concrete	1.5	0.026	0.054
Ordinary-quality concrete	1.6	0.048	0.075
Low-quality concrete	3.2	0.096	0.15

**Table 6-33. E-Area cementitious material uncertainty summary statistics for effective porosity (%)**

<b>Material</b>	<b>Distribution Type</b>	<b>Value (%)</b>	<b>Count</b>	<b>Standard Deviation of the Mean</b>	<b>Variance of the Mean</b>	<b>Mean Minimum (3 sigma)</b>	<b>Mean Maximum (3 sigma)</b>
Old E-Area CIG Grout (Segments 1 - 8 only)	Normal	22.4	6	0.59	0.36	20.6	24.2
New E-Area CIG Grout (i.e., Segments beyond Segment 8)	Normal	23.3	6	0.13	0.02	22.9	23.7
E-Area CLSM	Normal	32.8	3	0.93	0.81	30.1	35.5
E-Area CIG Concrete Mats <sup>1</sup>	Normal	23.3	-	0.13	0.02	22.9	23.7
E-Area Vault Concrete	Normal	15.8	4	0.64	0.0041	13.9	17.7

<sup>1</sup> No data are available on E-Area CIG concrete mats. Therefore, bulk properties for this material have been assumed to be the same as new E-Area CIG grout.

**Table 6-34. E-Area cementitious material uncertainty summary statistics for dry bulk density (g/cm<sup>3</sup>)**

<b>Material</b>	<b>Distribution Type</b>	<b>Value (g/cm<sup>3</sup>)</b>	<b>Count</b>	<b>Standard Deviation of the Mean</b>	<b>Variance of the Mean</b>	<b>Mean Minimum (3 sigma)</b>	<b>Mean Maximum (3 sigma)</b>
Old E-Area CIG Grout (Segments 1 - 8 only)	Normal	1.79	10	0.031	9.61E-04	1.70	1.88
New E-Area CIG Grout (i.e., Segments beyond Segment 8)	Normal	1.90	6	0.0095	9.6E-05	1.87	1.93
E-Area CLSM	Normal	1.78	4	0.029	8.41E-04	1.69	1.87
E-Area CIG Concrete Mats	Normal	1.90	-	0.0095	1.00E-02	1.76	2.36
E-Area Vault Concrete	Normal	2.54	6	0.013	1.57E-04	2.50	2.58

**Table 6-35. E-Area cementitious material uncertainty summary statistics for particle density (g/cm<sup>3</sup>)**

<b>Material</b>	<b>Distribution Type</b>	<b>Value (g/cm<sup>3</sup>)</b>	<b>Count</b>	<b>Standard Deviation of the Mean</b>	<b>Variance of the Mean</b>	<b>Mean Minimum (3 sigma)</b>	<b>Mean Maximum (3 sigma)</b>
Old E-Area CIG Grout (Segments 1 - 8 only)	Normal	2.31	6	0.021	4.41E-04	2.25	2.37
New E-Area CIG Grout (i.e., Segments beyond Segment 8)	Normal	2.48	6	0.011	1.03E-4	2.45	2.51
E-Area CLSM	Normal	2.65	3	0.010	1.00E-04	2.62	2.68
E-Area CIG Concrete Mats	Normal	2.48	-	0.011	2.25E-02	2.16	3.06
E-Area Vault Concrete	Normal	3.02	4	0.031	9.87E-04	2.93	3.11

## **6.4.2 Saturated Hydraulic Conductivity Uncertainty**

Typically, the saturated hydraulic conductivity of porous material is considered log normally distributed, which means the log of saturated hydraulic conductivity is normally distributed. Therefore, the uncertainty associated with the saturated hydraulic conductivity of the cementitious materials will be expressed logarithmically.

Uncertainty statistics are provided for E-Area cementitious materials based on laboratory data for the site-specific materials. Uncertainty statistics for generic categories of high, ordinary and low-quality concrete have also been assigned based on data for similar site-specific concretes. These generic categories are included to provide a ready source of property values and statistics for modeling any potential future cementitious materials employed in E-Area where site-specific data may be lacking.

### ***6.4.2.1 E-Area Cementitious Materials***

Site-specific laboratory data are available for the old and new E-Area CIG grout, E-Area CLSM, and E-Area vault concrete (i.e., LAWV and ILV) in order to establish the uncertainty associated with the representative nominal values of saturated hydraulic conductivity. Table 6-36 provides the site-specific saturated hydraulic conductivity nominal value (from Table 6-28) and standard deviation of mean for each of these materials in log space along with the source of these data.

Site-specific laboratory data for the saturated hydraulic conductivity of E-Area CIG concrete mats are not available. Therefore, this material has been assumed to be the same as the new E-Area CIG Grout as both materials are placed with standard field construction practices (i.e., minimal consolidation and curing requirements). Therefore, representation of material property uncertainty for this concrete will be based upon new CIG grout values.

### ***6.4.2.2 High-Quality Concrete***

The log standard deviation of the mean for the high-quality concrete category will be assigned the E-Area vault concrete log standard deviation of the population (see Table 6-12). This is considered reasonable for two reasons. First the E-Area vault concrete is a high-quality concrete. Second the log standard deviation of the population was used for the log standard deviation of the mean because there are currently no data associated with these concretes.

### ***6.4.2.3 Low-Quality Concrete***

The log standard deviation of the mean for the low-quality concrete category will be assigned the old E-Area CIG grout log standard deviation of the population (see Table 6-16). This is considered reasonable for two reasons. The old E-Area CIG grout had a high WCR and minimal placement and curing requirements. Second the log standard deviation of the population was used for the log standard deviation of the mean because there are currently no data associated with these concretes.

**6.4.2.4 Ordinary Quality Concrete**

The ordinary quality concrete category will be assigned a log standard deviation of the mean that is the average of the high-quality and low-quality concrete categories. Table 6-37 provides a summary of the log standard deviation of the mean assigned to the low, ordinary, and high-quality concretes. The resulting summary uncertainty statistics are provided for the saturated hydraulic conductivity of these various cementitious materials in Table 6-38.

**Table 6-36. Site-Specific saturated hydraulic conductivity nominal value and standard deviation of mean**

<b>Cementitious Material</b>	<b>Log Nominal Saturated Hydraulic Conductivity Value <sup>1</sup> (cm/s)</b>	<b>Log Saturated Hydraulic Conductivity Standard Deviation of Mean (cm/s)</b>	<b>Source of Standard Deviation of Mean Value</b>
Old E-Area CIG Grout	-5.06 (1.2E-04)	0.63 <sup>2</sup>	Table 6-16
New E-Area CIG Grout	-8.05 (9.0E-09)	0.034	Table 6-22
E-Area CLSM	-5.65 (2.2E-06)	0.11	Table 6-19
E-Area Vault Concrete	-12 (1.0E-12)	0.074	Table 6-12

<sup>1</sup> Saturated hydraulic conductivities from Table 6-28 are provided in parenthesis and the log of the value is shown above it

<sup>2</sup> The log saturated hydraulic conductivity standard deviation of mean associated with the average saturated hydraulic conductivity of 8.75E-06 cm/s is assumed to adequately apply to a saturated hydraulic conductivity of 4.5E-05 cm/s (see Table 6-16)

**Table 6-37. Low, Ordinary, and High-Quality Concrete assigned standard deviation of mean to nominal saturated hydraulic conductivity value**

<b>Concrete Material Classification</b>	<b>Log Nominal Saturated Hydraulic Conductivity (cm/s)</b>	<b>Assigned Log Saturated Hydraulic Conductivity Standard Deviation of the Mean</b>	<b>Source of Nominal and Standard Deviation of Mean Values</b>
High-quality concrete	-12 (1.0E-12)	0.13	E-Area Vault Concrete
Ordinary-quality concrete	-	0.95	Average of high and low-quality concrete
Low-quality concrete	-5.06 (4.5E-05)	1.77	Old E-Area CIG Grout

**Table 6-38. E-Area cementitious material uncertainty summary statistics for saturated hydraulic conductivity**

<b>Material</b>	<b>Distribution Type</b>	<b>Log Nominal Value <sup>1</sup> (cm/s)</b>	<b>Count</b>	<b>Log Standard Deviation of the Mean</b>	<b>Log Variance of the Mean</b>	<b>Log Mean Minimum (3 sigma)</b>	<b>Log Mean Maximum (3 sigma)</b>
Old E-Area CIG Grout (Segments 1 - 8 only)	Normal <sup>2</sup>	-5.06 (4.5E-05)	8	0.63	3.92E-01	-6.228	-2.472
New E-Area CIG Grout (i.e., Segments beyond Segment 8)	Normal	-8.05 (9.0E-09)	6	0.034	1.0E-03	-8.157	-7.950
E-Area CLSM	Normal	-5.62 (2.2E-06)	3	0.11	1.30E-04	-6.002	-5.318
E-Area CIG Concrete Mats	Normal	-8.05 (9.0E-09)	-	0.034	3.92E-01	-9.878	-6.122
E-Area Vault Concrete	Normal	-12 (1.0E-12)	3	0.074	5.48E-03	-12.222	-11.778

<sup>1</sup> Saturated hydraulic conductivities from Table 6-28 are provided in parenthesis and the log of the value is shown above it

<sup>2</sup> Saturated hydraulic conductivity is log normally distributed therefore the log of saturated hydraulic conductivity is normally distributed

### 6.4.3 Saturated Effective Diffusion Coefficient Uncertainty

The new E-Area CIG Grout, E-Area CIG concrete mats and E-Area vault concrete (i.e., LAWV and ILV) are considered fairly typical cementitious materials for which the log saturated effective diffusion coefficient standard deviation of the mean can be reasonably derived from that of the associated log saturated hydraulic conductivity standard deviation of the mean. This is considered reasonable, because both the saturated hydraulic conductivity and saturated effective diffusion coefficient of cementitious materials are dependent upon the pore structure characteristics (i.e., porosity, pore size distribution, connectivity of pores, and extent of separation and microcracking at aggregate-paste interfaces) as outlined in Sections 6.1.2 and 6.1.4. As outlined in Section 6.1.2 the typical range of concrete saturated hydraulic conductivity is from  $1.0\text{E-}13$  to  $1.0\text{E-}08$  cm/s (i.e., 5 orders of magnitude), whereas that of concrete saturated effective diffusion coefficient is from  $1.0\text{E-}08$  to  $5.0\text{E-}07$  cm<sup>2</sup>/s (i.e., 1.7 orders of magnitude) as outlined in Section 6.1.4. Based upon these ranges and the link between conductivity and diffusivity, the log saturated effective diffusion coefficient standard deviation of the mean for these materials will be assigned that of their respective log saturated hydraulic conductivity standard deviation of the mean modified by the factor 1.7/5. Table 6-39 provides the calculated log saturated effective diffusion coefficient standard deviation of the mean for these materials.

In terms of saturated effective diffusion coefficient, the old E-Area CIG grout probably behaves more like a combination of ~15% sand containing macropores and ~85% cementitious material containing micropore than solely a cementitious material and the E-Area CLSM probably behaves more like a clayey soil than a cementitious material as outlined within Section 6.3.4. The old E-Area CIG grout has been assigned a saturated effective diffusion coefficient of  $1.9\text{E-}06$  cm<sup>2</sup>/s, and the E-Area CLSM has been assigned  $4.0\text{E-}06$  cm<sup>2</sup>/s (see Table 6-28, Table 4-1). These diffusion coefficients are similar to that of the clay soil ( $4.1\text{E-}06$  cm<sup>2</sup>/s) outlined in Section 5.2.5. Therefore, the old E-Area CIG grout and E-Area CLSM will be assigned the same log saturated effective diffusion coefficient standard deviation of the mean as that of the clay soil in Table 5-19 of Section 5.7 (i.e., 0.053).

The resulting summary uncertainty statistics are provided for the saturated effective diffusion coefficient of these various cementitious materials in Table 6-40.

**Table 6-39. Log saturated effective diffusion coefficient standard deviation for concretes**

<b>Material</b>	<b>Log Saturated Hydraulic Conductivity Standard Deviation of the Mean</b>	<b>Log Saturated Effective Diffusion Coefficient Standard Deviation of the Mean<sup>1</sup></b>
New E-Area CIG Grout (i.e., Segment 9 and future)	0.63	0.21
E-Area CIG Concrete Mats	0.63	0.21
E-Area Vault Concrete	0.074	0.025

<sup>1</sup> Log Saturated Effective Diffusion Coefficient Standard Deviation of the Mean =  $(1.7/5) \times$  Log Saturated Hydraulic Conductivity Standard Deviation of the Mean

**Table 6-40. E-Area cementitious material uncertainty summary statistics for saturated effective diffusion coefficient**

<b>Material</b>	<b>Distribution Type</b>	<b>Log Nominal Value<sup>1</sup> (cm<sup>2</sup>/s)</b>	<b>Count</b>	<b>Log Standard Deviation of the Mean</b>	<b>Log Variance of the Mean</b>	<b>Log Mean Minimum (3 sigma)</b>	<b>Log Mean Maximum (3 sigma)</b>
Old E-Area CIG Grout (Segments 1 - 8 only)	Normal <sup>2</sup>	-5.72 (1.9E-06)	-	0.053	2.81E-03	-5.88	-5.56
New E-Area CIG Grout (i.e., Segments beyond Segment 8)	Normal	-6.10 (8.0E-07)	-	0.21	4.54E-02	-6.74	-5.46
E-Area CLSM	Normal	-5.40 (4.0E-06)	-	0.053	2.81E-03	-5.56	-5.24
E-Area CIG Concrete Mats	Normal	-6.10 (8.0E-07)	-	0.21	4.54E-02	-6.74	-5.46
E-Area Vault Concrete	Normal	-7.19 (6.4E-08)	-	0.025	6.25E-04	-7.38	-7.22

<sup>1</sup> Saturated effective diffusion coefficients from Table 6-28 are provided in parenthesis and the log of the value is shown above it

<sup>2</sup> Saturated effective diffusion coefficients are log normally distributed; therefore, the log of the saturated effective diffusion coefficients are normally distributed

## 6.5 E-AREA CRACKED CONCRETE REPRESENTATION

Degradation of the E-Area vaults (i.e., LAWV and ILV) is based upon the results of structural modeling that provides information on the concrete cracking and structural failure associated with each vault (Carey 2006)(Peregoy, 2006b). The primary impact of concrete cracking is the increase in saturated hydraulic conductivity and the subsequent increase in saturated water flux.

The following discussion on the simulation of the degradation of grout and concrete and its' impact on hydraulic properties is reproduced from a analysis performed by Flach (2017)

Cementitious and other engineered porous materials encountered in waste disposals may degrade over time due to one or more mechanisms. Physical degradation may take the form of cracking (fracturing) and/or altered (e.g. increased) porosity, depending on the material and underlying degradation mechanism. In most cases, the hydraulic properties of degrading materials are expected to evolve due to physical changes occurring over roughly the pore to decimeter scale, which is conducive to calculating equivalent or *effective* material properties.

The exact morphology of a degrading material in its end-state may or may not be known. In the latter case, the fully-degraded condition can be assumed to be similar to a more-permeable material in the surrounding environment, such as backfill soil. Then the fully-degraded waste form or barrier material is hydraulically neutral with respect to its surroundings, constituting neither a barrier to nor conduit for moisture flow and solute transport.

Unless the degradation mechanism is abrupt, a gradual transition between the intact initial and fully-degraded final states is desired. Linear interpolation through time is one method for smoothly blending hydraulic properties between those of an intact matrix and those of a soil or other surrogate for the end-state.

Letting  $f$  and  $F$  represent the fractions of the final (e.g. soil) and initial (intact matrix) states, respectively, the component fractions satisfy the equation:

$$f + F = 1 \quad (58)$$

The soil fraction  $f$ , which can also be interpreted as a degradation fraction, varies between 0 and 1 according to the piecewise linear function:

$$f(t) = \max \left[ 0, \min \left( 1, \frac{t - t_1}{t_2 - t_1} \right) \right] \quad (59)$$

where  $t_1$  and  $t_2$  are the degradation start and end times, respectively. The composite porosity [ $\text{cm}^3$  void /  $\text{cm}^3$  total] is

$$n = fn_s + Fn_m \quad (60)$$

where  $n_s$  and  $n_m$  are the porosities of the soil and matrix, respectively. Using the same subscripting convention and weighting scheme, the effective saturated hydraulic conductivity [cm/s] of the composited material is:

$$K = fK_s + FK_m \quad (61)$$

For an anisotropic material,  $K$  may represent either horizontal or vertical conductivity. Equation (61) is an arithmetic average consistent with parallel flow through the binary constituents (Freeze and Cherry (1979) Equation [2.32]). Alternative, non-linear, weighting/averaging schemes may be justified depending on the structure of composite material. For example, harmonic averaging would be appropriate for perpendicular flow through the constituents (Freeze and Cherry (1979) Equation [2.31]) and geometric averaging produces the effective conductivity of an isotropic, two-dimensional, medium with log-normally distributed  $K$  (Gelhar (1993), Equation [4.1.58]). Equation (61) can be generalized as (Ababou and Wood, 1990);

$$K = [fK_s^p + FK_m^p]^{1/p} \quad (62)$$

where  $-1 \leq p \leq 1$  and special cases include:

arithmetic	$p = 1$
geometric	$p \rightarrow 0$
harmonic	$p = -1$

Non-integer values of  $p$  are permissible; see Phifer et al. (2006), Section 5.2.2.2 for several examples. Arithmetic averaging produces the largest  $K$  for a given  $f$  and is adopted for the remainder of this discussion as a conservative-tending assumption and to be consistent with recent Savannah River Performance Assessment examples.

Continuing with the remaining material properties, the saturation [cm<sup>3</sup> liquid /cm<sup>3</sup> void] function of the composited material is:

$$S(\psi) = \frac{fn_s S_s(\psi) + Fn_m S_m(\psi)}{n} \quad (63)$$

where  $\psi$  is suction (negative pressure) head [cm]. The relative permeability [-] function becomes:

$$k_r(\psi) = \frac{fk_{rs}[S(\psi)]K_s + Fk_{rm}[S(\psi)]K_m}{k_r(\psi)K} \quad (64)$$

The unsaturated conductivity [cm/s] of the composited material is

$$K_u = k_r(\psi)K \quad (65)$$

The water retention curve for the composited material represented by Equation (63) is presented with suction head as the independent variable, the usual convention. However, the relative permeability curve is also presented in Equation (64) as a direct function of suction head, rather than the usual choice of saturation, to more clearly illustrate how unsaturated conductivity defined by  $k_r(\psi)K$  varies with the primary flow variable, pressure head ( $-\psi$ ). That is, rather than viewing unsaturated conductivity variation for the composited material through the separate functions  $k_r(S)$  and  $S(\psi)$ , the confounding intermediate variable  $S$  is eliminated between the water retention and conventional relative permeability curves to achieve the single characteristic curve  $k_r(\psi)$ .

The blending process is most conveniently conducted using analytic expressions for the water retention and relative permeability curves of the intact and soil materials, as opposed to tabular data that may not share the same suction head values ( $\psi_i$ ). The van Genuchten (1980) / Mualem (1976) functions are a popular choice for analytic characteristic curves. The water retention function is:

$$S_e = \frac{S - S_r}{1 - S_r} = \frac{\theta - \theta_r}{\theta_s - \theta_r} = \left[ \frac{1}{1 + (\alpha\psi)^n} \right]^m \quad (66)$$

where  $\theta$  is water content [ $\text{cm}^3$  liquid /  $\text{cm}^3$  total], the subscripts  $e$ ,  $r$ , and  $s$  refer to effective, residual, and saturated conditions, respectively. The model parameters are  $S_r$  (or  $\theta_s$  and  $\theta_r$ ),  $\alpha$ ,  $n$ , and  $m$ . The relative permeability function is given by:

$$k_r = S_e^{1/2} \left[ 1 - (1 - S_e^{1/m})^m \right]^2 \quad (67)$$

For the Mualem (1976) conductivity model:

$$m = 1 - 1/n \quad (68)$$

leaving  $S_r$ ,  $\alpha$ , and  $n$  as the independent model parameters.

Figure 6-13 reproduced from Jordan and Flach (2013) illustrates example transitions from intact cementitious materials to fully-degraded conditions resembling those of soils. At intermediate blending fractions ( $0 < f < 1$ ) the hydraulic conductivity functions are observed to have a characteristic double-hump or two-tiered nature.

Transitioning completely to a soil is conceptually most clearly consistent with a degradation mechanism where porosity and pore size increase but internal stresses are not present that

would produce a fractured medium. An example mechanism is decalcification of a concrete or grout. Linear blending of properties is consistent with the concept of parallel flow through distinct intact and fully-degraded regions that vary in proportion, and results in the intermediate conductivity variations that are two-tiered (Figure 6-13). In this manner, the partially-degraded cementitious materials resemble a soil with a bimodal pore size distribution, that is, having both micro- and macro-porosity (Durner (1994), Šimůnek et al. (2003), Priesack and Durner (2006)). As discussed earlier, alternative (non-linear) weighting schemes are possible, but lacking a specific physical driver, are rejected here in favor of simple linear averaging.

For degradation resulting in an increasingly fractured medium, several alternative representations of degraded conditions could be adopted as shown in reproduced from Altman et al. (1996) Altman et al. (1996). The blending process described above falls under the “Equivalent Matrix and Fracture Continuum” representation depicted in Figure 6-14, or *Equivalent Continuum Model* (ECM) in short. The ECM is most appropriate for steady-state flow conditions and smaller scale fractures, such that local equilibrium is achieved between fractures and matrix. The former conditions are generally expected for cementitious materials degrading by chemical attack and lying several feet below the ground surface.

Within the ECM framework, blending approaches other than a 100% transition to soil could be adopted following Peters and Klavetter (1988) among others Šimůnek et al. (2003). Pruess (1998) notes that

“Recent theoretical and experimental work suggests that relative permeability and capillary pressure behavior of fractures is similar to that of highly permeable media with intergranular porosity (Pruess (1998); Firoozabadi and Hauge, 1990; Persoff and Pruess, 1995). Accordingly, we used the customary van Genuchten correlations, with parameters chosen as for coarse sands”.

Thus high-permeability granular materials such as coarse sands or gravels are reasonable surrogates for natural fractures with rough surfaces and/or infilled with granular material.

Figure 6-15 modified from Jordan and Flach (2013) shows the results of compositing an intact concrete first with the “Gravel” and then alternatively with the “Sand” materials from Phifer et al. (2006). while preserving the saturated conductivity of Lower Vadose Zone (LVZ) soil. The LVZ soil curve is included in the figure as a point of reference. “Sand” is shorthand for sandy native sediments at the Savannah River Site, which contain up to 25% fines under the chosen classification. Thus the “Sand” material from Phifer et al. (2006) has a lower saturated conductivity than a clean coarse-grained sand, and could be questioned as a surrogate for high-permeability fractures. Nonetheless both materials have a higher saturated conductivity than Backfill, and the volume fraction ( $b$ ) of higher-permeability material needed to achieve the same saturated hydraulic conductivity as Backfill for the fully-degraded concrete is less than 100%. The specific fractions of Gravel or Sand used in Figure 6-15 are 0.06% and 32.5%, respectively. Considering the tiny fraction of total volume occupied by fractures, Gravel is viewed as the more appropriate surrogate material for fractures. Blending with Gravel produces a more pronounced two-tiered curve, which is consistent with the ease with which fractures are dewatered through tension in the adjoining

matrix (Wang and Narasimhan, 1985). Blending to 100% LVZ soil is observed to produce higher unsaturated conductivities within the suction head range  $-\infty < \psi < 1500$  cm typical of Savannah River Site applications than blending with the two higher permeability materials. In this sense, a choice of LVZ (or Backfill) soil would be a conservative-tending assumption for the end-state surrogate.

Another ECM approach is to match the saturated conductivity of a concrete-gravel blend to that of a fractured medium with specified attributes, principally fracture aperture  $b$  and spacing  $B$ . For this exercise, gravel from Phifer et al. (2006) (2006) is again considered to be a reasonable surrogate for fractures. The saturated conductivity of a saturated fracture is (e.g. Wang and Narasimhan (1985):

$$K_f = \frac{\rho g b^2}{12\eta} \quad (69)$$

where  $\rho$  is liquid density [ $\text{kg/m}^3$ ],  $g$  is gravitational acceleration [ $\text{m/s}^2$ ],  $b$  is fracture aperture [ $\text{m}$ ], and  $\eta$  is liquid viscosity [ $\text{kg/m}\cdot\text{s}$ ]. The effective conductivity of the fractured porous matrix is:

$$K = \frac{bK_f + BK_m}{b + B} \approx \frac{b}{b + B} K_f = fK_f \quad (70)$$

where  $f = b/(b + B)$  in Equation (4) and the contribution of the low-permeability matrix is then assumed to be negligible. As an example, the effective saturated conductivity of a low-permeability porous medium with 5 mil (0.127 mm) fractures spaced at 1 cm is 1.65E-02 cm/s. The fraction of gravel required to produce this same saturated conductivity is 10.7% using Equation (61). Unsaturated conductivity for this concrete-gravel blend, which is representative of a severely damaged concrete, is shown in Figure 6-16 modified from Jordan and Flach (2013) Jordan and Flach (2013). The LVZ soil curve also shown as a point of reference to preceding figures.

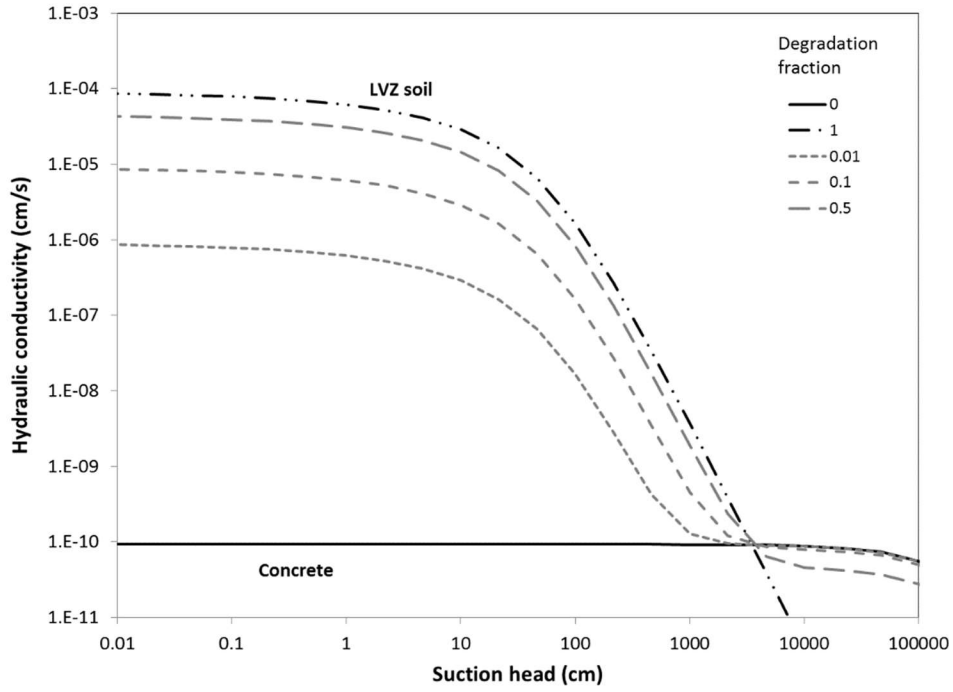
Or and Tuller (2000) present a direct method for defining fracture hydraulic properties based on an idealized fracture geometry. These derived fracture properties can be used instead of properties from a surrogate granular material in an ECM model. Following Flach et al. (2009, Section 3.7), Figure 6-17 from Jordan and Flach (2013) presents example ECM curves for two conditions: a) 5 mil (0.127 mm) fractures spaced at 1 cm (as considered in Figure 6-16), and b) 50 mil (1.27 mm) fractures spaced at 10 cm. Within the suction head range  $50 < \psi < 1500+$  cm, conductivities based on Or and Tuller (2000) are lower than both the concrete-gravel blend and LVZ soil. Thus, selecting a granular material to represent a degraded state in the form of fractures is a conservative-tending assumption compared to Or and Tuller (2000).

Flach et al. (2015) used an *outflow extraction method* to estimate the unsaturated hydraulic conductivity of a fractured grout and compared their experimental results to LVZ and

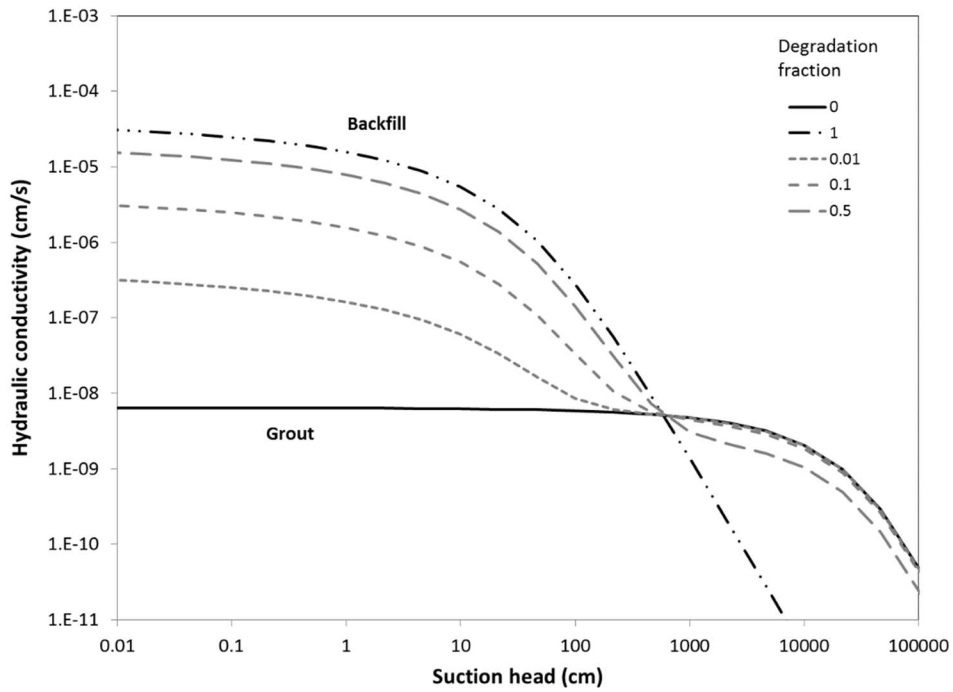
Backfill materials. Similar to Figure 6-17, the hydraulic conductivity of the fractured specimens was estimated to be lower than that of the soil materials for  $100 < \psi < 1000$  cm (see Figure 5 in Flach et al. (2015)). The authors concluded that:

“With respect to PA applications, comparisons of the unsaturated conductivity for the micro-fractured grout samples suggests that soils may serve as conservative surrogates for damaged cementitious materials, assuming that higher conductivity at higher tension heads is conservative for facility performance.”

Figure 6-13, Figure 6-15, Figure 6-16, Figure 6-17 illustrate example applications of the general concept defined by Equations (60) through (65) for smoothly evolving material properties, and are not intended to be limiting. For example, Section 6.3.3.1 uses non-linear weighting per Equation (56) with  $p = 0.33$  for a Components-In-Grout material.



(a)



(b)

Figure 6-13. Example transitions of intact cementitious materials from intact to fully-degraded conditions represented by soils: (a) concrete and (b) grout

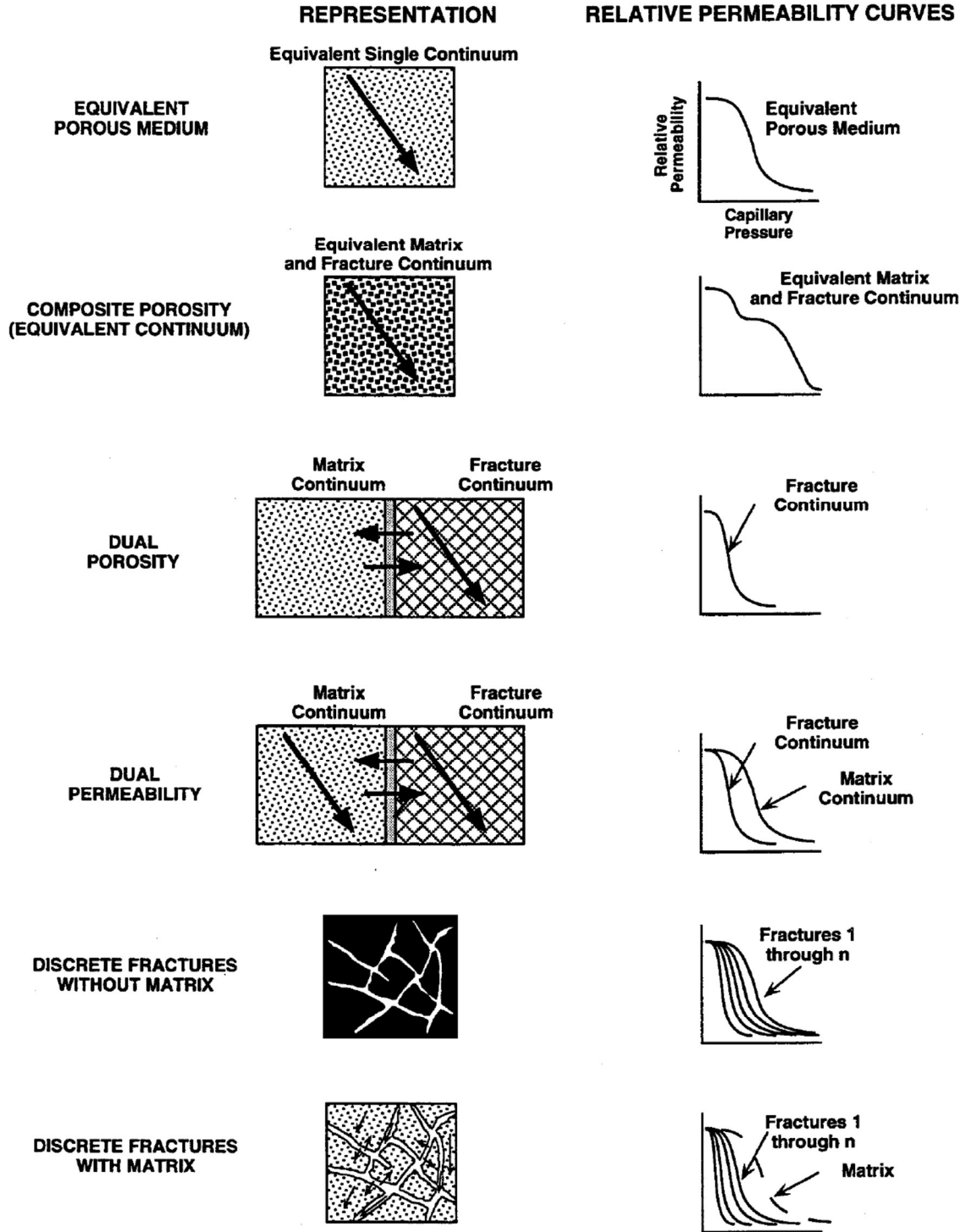


Figure 6-14. Alternative representations of a fractured medium; reproduced from Altman et al. (1996), Figure 2-2

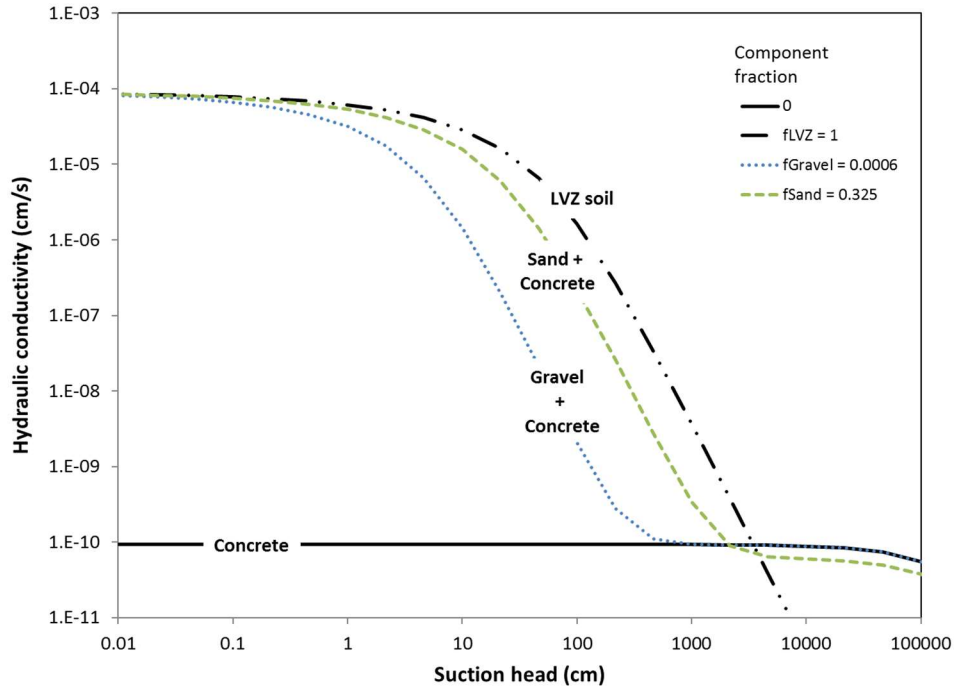


Figure 6-15. Alternative surrogate soils for blending to fully-degraded conditions

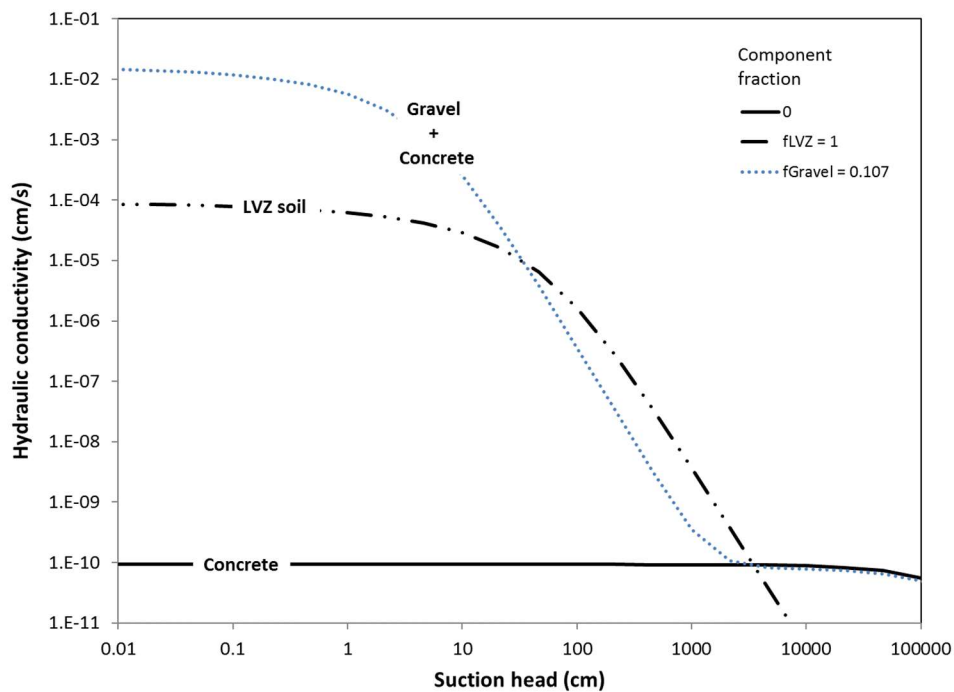
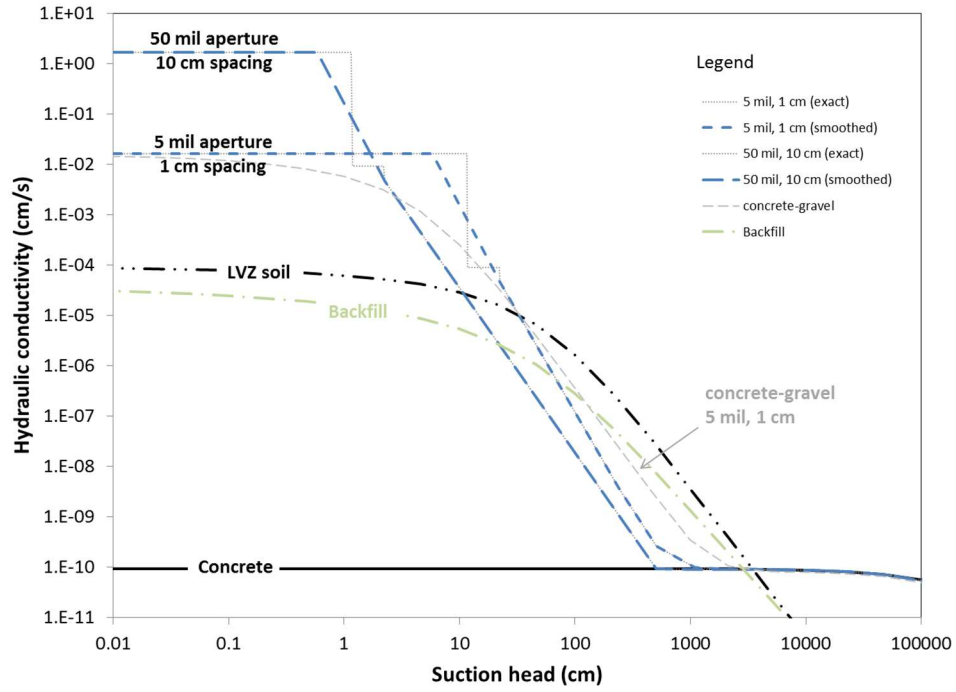


Figure 6-16. Partial blending (10.7%) to gravel representing degradation to 5 mil fractures spaced at 1 cm



**Figure 6-17. Degradation to selected fractured conditions using fracture properties based on Or and Tuller (2000)**

## 7.0 WASTE ZONE REPRESENTATION

The waste forms within the E-Area Low-Level Waste Facility (LLWF) are extremely varied and have undergone little quantitative characterization. Therefore, gross assumptions based upon qualitative information must be made relative to the hydraulic properties of the waste zones within the E-Area LLWF disposal units. The following discussion provides the available qualitative information regarding the various E-Area LLWF disposal units.

### 7.1 SLIT TRENCH WASTE ZONE REPRESENTATION

A description of the Slit Trenches is provided in Section 4.4.1. As described in Section 4.4.1, Slit Trenches are filled with either bulk waste or stacks of containerized (typically B-25 box) waste. Slit Trenches are nominally excavated in segments along a row that is 20 feet deep, 20 feet wide, and 650 feet long although wider, shallower and deeper trench segments have been used within the footprint of a Slit Trench unit. Waste disposed within Slit Trenches consists of soil, debris, rubble, wood, and job control waste. The waste may be disposed as bulk waste or contained within B-25 boxes, B-12 boxes, 55-gallon drums, SeaLand containers, and other metal containers. Bulk waste is generally dumped on one end of the trench and pushed into the trench by a bulldozer along with soil backfill to produce an approximately 16-foot waste layer thickness. Containers are placed with a crane and surrounded with bulk waste and/or soil backfill to make a 16-foot waste layer. A minimum 4-foot operational soil cover is placed above the filled waste zone in the trench. Additional clean soil is added as needed to provide positive drainage off the trench. The only compaction of the waste layer is that of bulldozers running over the top of the trench when placing the 4+ feet clean soil cover.

It is anticipated that dynamic compaction of the Slit and Engineered Trenches will be performed at the end of the 100-year institutional control period. An analysis of historical data in the Waste Inventory Tracking System (WITS) by Sink (2010) indicates that from 1995 to 2010 approximately 67% of all the waste disposed of in Slit Trenches was bulk waste and 33% percent of the waste disposed in Slit Trenches was in stacks of containerized (typically B-25 box) waste. Based on the analysis by Sink (2010) a hybrid Slit Trench waste representation was developed by Phifer (2010) to address uncertainties in porosity and bulk density of the actual disposed waste both before and after dynamic compaction.

The Slit Trench waste zone representation is shown in Figure 7-2 (a) prior to dynamic compaction and after dynamic compaction at the end of the 100-year institutional control period in Figure 7-3 (a).

#### 7.1.1 Bulk Waste Disposal Slit Trench

Bulk waste, typically consisting of rubble and debris, is frequently delivered by roll-off pan and bull-dozed into the end of a Slit Trench segment (see figure 4-10). Following these actions, clean soil is bulldozed over the emplaced bulk waste to prevent spread of contamination. Thus, the waste zone contains significant amounts of clean backfill soil mixed with contaminated rubble and debris. Clean soil is then emplaced to cap the waste layer with the required 4 feet of operational soil cover (OSC1) to bring the trench up to grade. Finally,

more soil is added as needed for positive drainage away from the trench. Based on the significant amount of uncompacted soil mixed with rubble in the waste layer Phifer (2010) recommended the hydraulic properties of operational soil cover for bulk waste disposals in Slit Trenches. Thus, for bulk waste sections of a slit trench, Table 7-1 shows values for saturated hydraulic conductivity, saturated effective diffusion coefficient, VG parameters, total porosity, dry bulk density, and particle density based on operational soil cover before dynamic compaction (OSC1) and after dynamic compaction (OSC2).

### 7.1.2 Containerized Waste Disposal Slit Trench

Various types of disposal containers are crane-lifted into Slit Trenches. Containers are frequently stacked in disposal campaigns to optimize use of disposal space and fill up the 16-foot thick waste zone. For estimating hydraulic properties, Phifer (2010) assumed a four-high stack of B-25 boxes was representative of a containerized waste section of trench. Once a section of the slit trench is filled with boxes four feet of clean OSC1 is placed over the completed stack of boxes in a single lift using a bulldozer bringing the trench up to grade and filling the voids between the boxes and between the box stack and sidewalls of the trench. Based on this conceptual model, Phifer (2010) recommended properties for containerized waste disposal in slit trenches before and after dynamic compaction, Table 7-1.

#### 7.1.2.1 Containerized Waste Disposal in Slit Trenches Before Dynamic Compaction

A containerized waste section of a Slit Trench is initially comprised of intact impermeable boxes, permeable soil and void space. A way to conceptually represent the hydraulic properties of these diverse components is by a uniform (composite) waste zone material with equivalent hydraulic properties. To that end, each stack of four B-25 boxes with OSC1 cover is represented by 20% by volume OSC1 and 80% by volume B-25 boxes as determined by the overall bulk density of the containerized Slit Trench waste zone,  $\rho_{bcw}$ , in Phifer (2010), particle density, and relationship for volume fraction,  $f_1$  and  $f_2$ , shown in equation 71. Waste zone porosity is derived using equation 25 on page 83. Values for the saturated effective diffusion coefficient and particle density in this uniform material are assumed to be the same as that for bulk waste.

$$\begin{aligned} V &= V_1 + V_2 \\ 1 &= \frac{V_1}{V} + \frac{V_2}{V} = f_1 + f_2 \end{aligned} \quad (71)$$

where:

$V$  = total volume

$V_1$  = volume of OSC1 fill in a slit trench

$V_2$  = volume of containerized slit trench waste in slit trench

A composite WRC was developed for the containerized Slit Trench waste zone before dynamic compaction and is based on the WRC for OSC1 before dynamic compaction and on the WRC for B-25 boxes, equation 72. The WRC for B-25 boxes is a special case where  $S_2$

= 0 at all capillary pressures and  $K_{sat2} = 0$ . The saturation of OSC1 ( $S_l$ ) in equation 72 is calculated using equation 15 on page 67 and the van Genuchten parameters for OSC1.

$$S_{CW} = \frac{f_1 S_1 n_1 + f_2 S_2 n_2}{n} \quad (72)$$

$$\Downarrow$$

$$S_{CW} = \frac{f_1 S_1 n_1}{n}$$

Similarly,  $K_{sat}$  and  $k_{rel}$  for the containerized Slit Trench waste zone are based on a composite of properties for OSC1 before dynamic compaction and WRC for B-25 boxes using the equations 73 and 74 developed in Flach and Whiteside (2016). Figure 7-1 shows the WRCs for the containerized waste zone in a Slit Trench (STETboxesBefore), OSC1 before dynamic compaction, and resulting Slit Trench hybrid waste zone (SThybridBefore).

$$K_{sat} = f_1 K_{sat1} + f_2 K_{sat2} \quad (73)$$

$$k_r = \frac{f_1 k_{r1} K_1 + f_2 k_{r2} K_2}{K_{sat}} \quad (74)$$

$$\Downarrow$$

$$k_r = \frac{f_1 k_{r1} K_{sat1}}{K_{sat}}$$

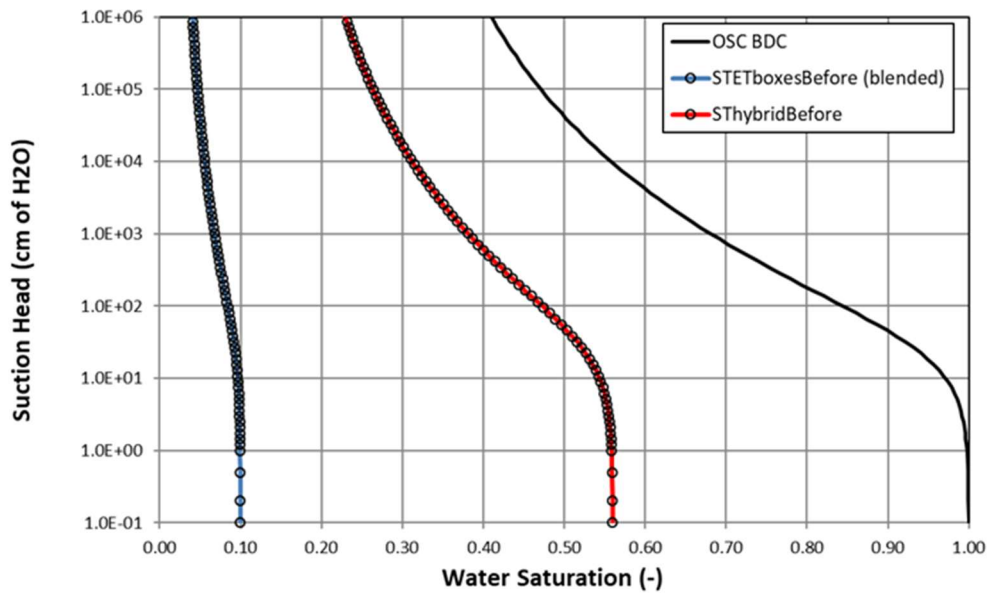


Figure 7-1. Water retention curves for Containerized Slit Trench and Hybrid Slit Trench waste zones before dynamic compaction

### **7.1.2.2 Containerized Waste Disposal in Slit Trenches After Dynamic Compaction**

Phifer (2010) presents waste zone properties for containerized waste disposal in Slit Trenches after dynamic compaction. The values are shown in Table 7-1. Bulk density and porosity for containerized waste disposal in Slit Trenches after dynamic compaction are similar to the values reported for bulk waste disposal in Slit Trenches after dynamic compaction. Therefore, the VG parameters for OSC2 will be used for containerized waste disposal in Slit Trenches after dynamic compaction.

### **7.1.3 Hybrid Slit Trench**

The exact location of bulk waste and containerized waste in individual Slit Trenches is not known and as a result a hybrid waste zone was proposed by Phifer (2010) that represents each trench as a mix of bulk and containerized waste based on the information in WITS and analysis by Sink (2010). The method proposed by Phifer (2010) blends properties for bulk and containerized waste in Slit Trenches based on the historic (1995-2010) fraction of each waste disposed of in the Slit Trenches. The approach for determining properties of the hybrid Slit Trench waste zone are described in the sections below.

#### **7.1.3.1 Hybrid Slit Trench Before Dynamic Compaction**

Equivalent bulk density of the hybrid Slit Trench waste zone prior to dynamic compaction ( $\rho_{bHybridBC}$ ) was calculated from the individual bulk density of bulk and containerized waste using the volume fraction for each waste type as shown in equation 75.

$$\rho_{bHybridBC} = (\rho_{1BC} * f_{1BC}) + (\rho_{2BC} * f_{2BC}) \quad (75)$$

Waste zone porosity is derived using equation 25 on page 83 using the hybrid bulk density. Saturated effective diffusion coefficient and particle density are the same as that for bulk and containerized waste before dynamic compaction.

A composite WRC was developed to represent the hybrid Slit Trench waste zone prior to dynamic compaction using the method described in section 7.1.2.1. Likewise,  $K_{sat}$  and  $k_{rel}$  for the hybrid Slit Trench waste zone during the period before dynamic compaction were also developed using the method described in section 7.1.2.1. Hybrid Slit Trench waste zone properties for the period before dynamic compaction are listed in Table 7-1

#### **7.1.3.2 Hybrid Slit Trench After Dynamic Compaction**

The equivalent thickness for the hybrid Slit Trench waste zone after dynamic compaction ( $b_{HybridAC}$ ) was calculated using the compacted thickness and historic volume fraction of bulk and containerized waste similar to the method to calculate the bulk density of the hybrid waste zone before dynamic compaction in equation 75. Equation 76 is the equation for the equivalent thickness after dynamic compaction of the hybrid slit trench waste zone.

$$b_{HybridAC} = (b_{1AC} * f_1) + (b_{2AC} * f_2) \quad (76)$$

The bulk density of the of the equivalent hybrid Slit Trench waste zone after dynamic compaction ( $\rho_{bHybridAC}$ ) was calculated using  $b_{HybridAC}$  and properties of the bulk and containerized Slit Trench waste zones using equation 77. Waste zone porosity is derived using equation 25 on page 83. Saturated hydraulic conductivity, saturated effective diffusion coefficient, and particle density for the hybrid waste zone are the same as that for bulk and containerized waste after dynamic compaction. Hybrid slit trench waste zone properties for the period before and after dynamic compaction are listed in Table 7-1.

$$\rho_{bHybridAC} = \frac{(\rho_{b1AC} * b_{1AC} * f_1) + (\rho_{b2AC} * b_{2AC} * f_2)}{b_{HybridAC}} \quad (77)$$

Bulk density and porosity for containerized waste disposal in Slit Trenches after dynamic compaction are similar to the values reported for bulk waste disposal in Slit Trenches after dynamic compaction. Therefore, the VG parameters for OSC2 will be used for the hybrid Slit Trench waste zone after dynamic compaction.

**Table 7-1. Waste properties for Slit Trenches and Engineered Trenches before and after dynamic compaction**

Property	Bulk (ST only)		Container (ST & ET)		Hybrid (ST only)	
	Before DC	After DC	Before DC	After DC	Before DC	After DC
Porosity, $n$ , volume fraction	0.457	0.275	0.893	0.317	0.600	0.279
Bulk Density, gm/cm <sup>3</sup>	1.44	1.92	0.282	1.81	1.06	1.91
Particle Density, gm/cm <sup>3</sup>	2.65	2.65	2.65	2.65	2.65	2.65
Saturated Hydraulic Conductivity, $K_s$ , cm/sec	1.2E-04	1.4E-05	2.4E-05	1.4E-05	1.2E-04	1.4E-05
Saturated Effective Diffusion Coefficient, cm <sup>2</sup> /s	5.3E-06	4.0E-06	5.3E-06	4.0E-06	5.3E-06	4.0E-06
Thickness, feet	16.0	12.0	16.0 <sup>1</sup>	2.5	16.0	8.87
Fraction, $f_i$	n/a	n/a	0.195/0.805, (OSC1/B25)	n/a	0.736/0.264, (OSC1/B25)	n/a
$\theta_s$	0.456000	0.275000	The WRC and $k_{rel}$ are calculated using Eq. 72 and 73	0.275000	The WRC and $k_{rel}$ are calculated using Eq. 72 and 73	0.275000
$\theta_r$	0.121330	0.073171		0.073171		0.073171
$\alpha$	0.040416	0.018263		0.018263		0.018263
$n$	1.153656	1.153659		1.153659		1.153659
$m$	0.133191	0.133193		0.133193		0.133193
Source	OSC1	OSC2	Phifer 2010	OSC2	Phifer 2010	OSC2

<sup>1</sup> A stack of four B-25 boxes prior to placement of the operational soil cover is 17.292 feet high and after placement of the operational soil cover, it is assumed to be approximately 16 feet high, due to the collapse of the lid of the top box (Phifer, 2010).

## 7.2 ENGINEERED TRENCH WASTE ZONE REPRESENTATION

A description of the Engineered Trenches is provided in in Section 4.4.2. It is anticipated that dynamic compaction of the Engineered Trenches will be performed at the end of the 100-year institutional control period. The Engineered Trench waste zone representation is shown in Figure 7-2 (b) prior to dynamic compaction, and after dynamic compaction at the end of the 100-year institutional control period in Figure 7-3 (b).

Engineered Trenches are typically 20 feet deep with sloped sides and span the entire width of the Engineered Trench unit footprint. The trench floor consists of compacted soil, and, in some cases, a geotextile filter fabric, and finally topped with approximately 6 inches of a dense grade aggregate (crusher run) for a durable working surface for vehicular traffic. Carbon steel B-25 boxes containing low-level waste are stacked four high in rows (approximately 16 feet high) within the Engineered Trench. Placement of the B-25 boxes continues until the trench is filled with boxes. A minimum 4-foot operational soil cover is placed over the boxes in the trench. More soil is added as necessary and the entire area graded to provide positive drainage off the trench. The only compaction of the waste layer is that of bulldozers running over the top of the trench when placing the 4+ feet of clean soil cover and structural fill.

Dynamic compaction will be employed to achieve waste layer stabilization at or near the end of the 100-year institutional control period when significant corrosion of the containers would have occurred. Such degradation of the containers will improve the efficiency of dynamic compaction to eliminate subsidence potential. Waste containers that can be effectively crushed and compacted at the time of dynamic compaction are termed “crushable” containers, and the balance are considered “non-crushable”.

For B-25 boxes in Engineered Trenches an estimated subsidence/compaction potential of approximately 13.5 feet exists within the 16-foot waste layer thickness, resulting in an ultimate waste layer thickness of approximately 2.5 feet (Phifer and Wilhite, 2001). In addition to B-25 boxes, waste in Engineered Trenches can be contained within B-12 boxes, 55-gallon drums, SeaLand containers, and other metal containers.

The intact waste disposal configuration in Engineered Trenches (i.e., four-high stack of B-25 boxes covered with a 4-foot operational soil cover) is equivalent to the conceptual model of containerized waste disposal in Slit Trenches discussed in section 7.1.2. The same is true of the containerized waste zone following dynamic compaction. Therefore, the properties of the waste zone in Engineered Trenches before and after dynamic compaction have been set equal to those for containerized waste disposal in Slit Trenches, Table 7-1. Figure 7-1 shows the WRC for the zone representing waste disposal in an Engineered Trench (curve representing “ST/ETboxesBefore”).

Table 7-2 is a summary of waste zone material properties for all DU types. Waste zone material properties for CIG Trenches, ILV, LAWV and NRCDA are discussed in Sections 7.3, 7.4, 7.5 and 7.6, respectively.

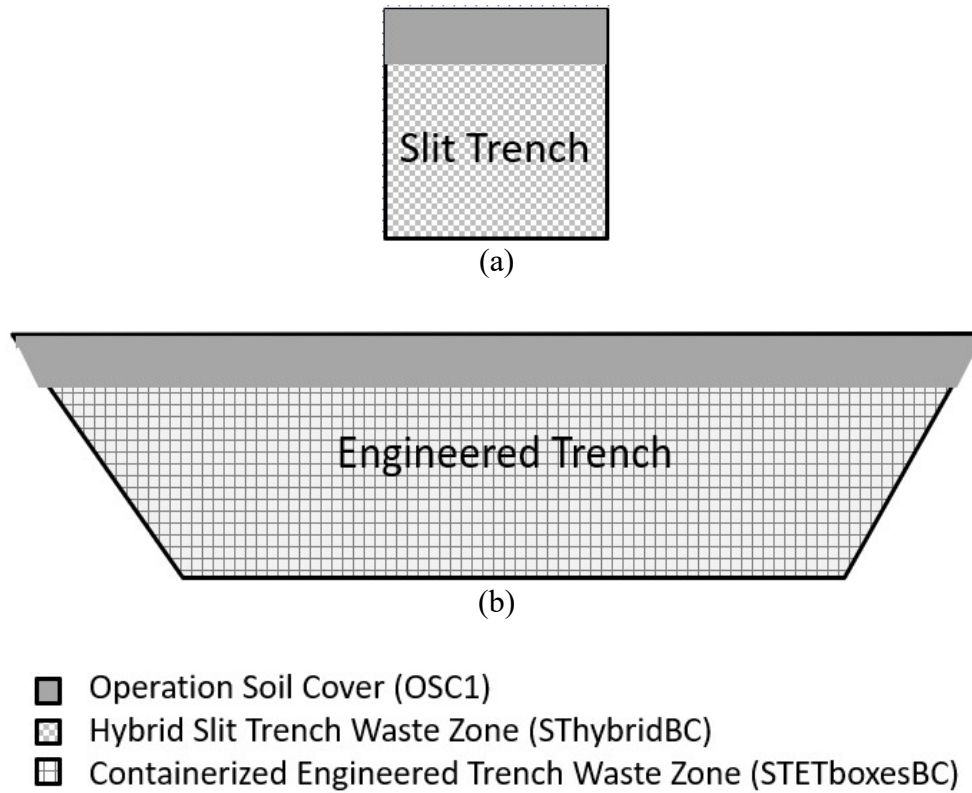


**Figure 7-2. Conceptual model representing hydraulic properties of Slit Trenches and Engineered Trenches before dynamic compaction**

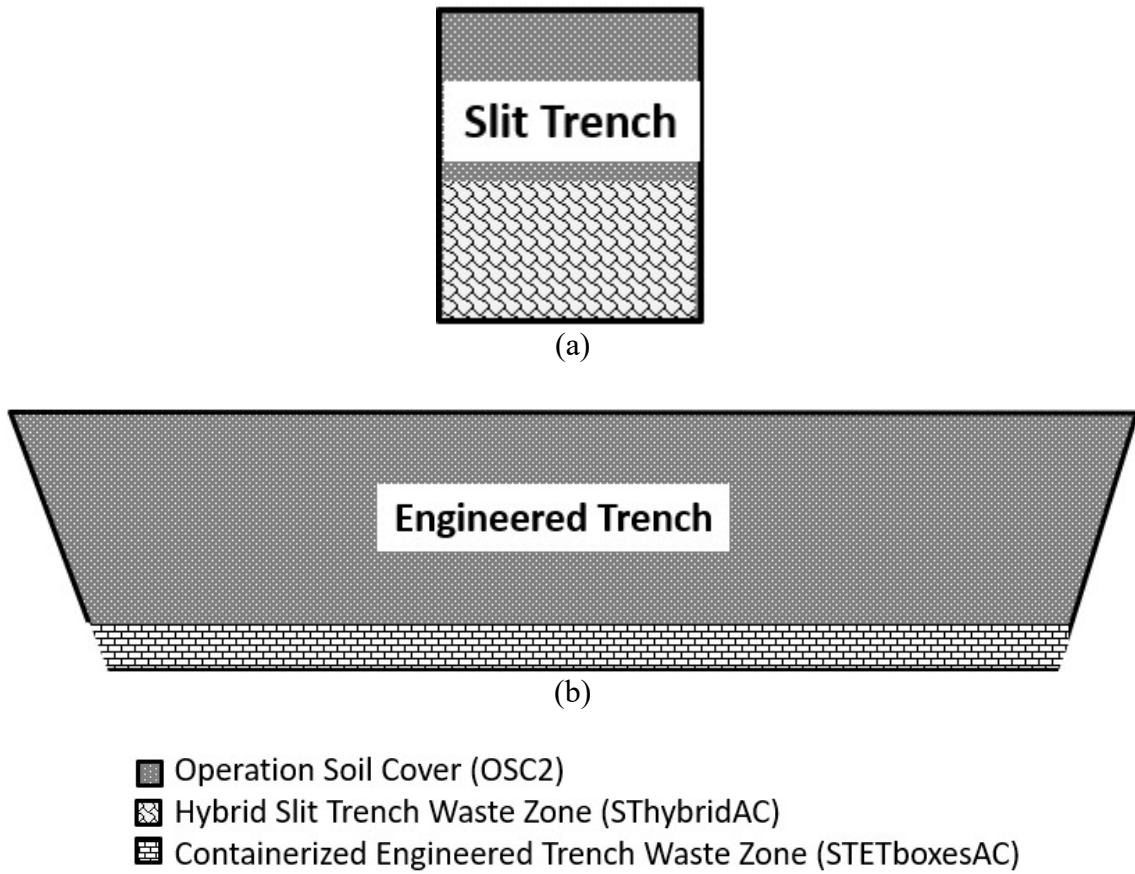


**Figure 7-3. Conceptual model representing hydraulic properties of Slit Trenches and Engineered Trenches after dynamic compaction**

**Table 7-2. Material properties for waste zones in the E-Area LLWF**

Type	Condition	Thickness, ft	Ksat, cm/sec	Porosity, fraction	Bulk Density, gm/cm <sup>3</sup>	Particle Density, gm/cm <sup>3</sup>	Effective Diffusion Coefficient, cm <sup>2</sup> /sec	$\theta_s$	$\theta_r$	$\alpha$	$n$	$m$
Slit Trench	Before Dynamic Compaction	16	8.8E-05	0.600	1.06	2.65	5.3E-06	The WRC and $k_{rel}$ are calculated using Eq. 72 and 74				
	After Dynamic Compaction	8.87	1.4E-05	0.279	1.91	2.65	4.0E-06	0.275000	0.073171	0.018263	1.153659	0.133193
Engineered Trench	Before Dynamic Compaction	16	2.4E-05	0.893	0.282	2.65	5.3E-06	The WRC and $k_{rel}$ are calculated using Eq. 72 and 74				
	After Dynamic Compaction	2.5	1.4E-05	0.317	1.81	2.65	4.0E-06	0.275000	0.073171	0.018263	1.153659	0.133193
CIG Trench Segments	Structurally and Hydraulically Intact	14	1.0E-12	0.456	1.44	2.65	5.3E-06	0.456000	0.121330	0.040416	1.153656	0.133191
	Structurally Intact and Hydraulically Degraded	14	1.2E-04	0.456	1.44	2.65	5.3E-06	0.456000	0.121330	0.040416	1.153656	0.133191
	Structurally and Hydraulically Degraded	7	1.2E-04	0.456	1.44	2.65	5.3E-06	0.456000	0.121330	0.040416	1.153656	0.133191

**Table 7-2. Material properties for waste zones in the E-Area LLWF, continued**

Type	Condition	Thickness, ft	Ksat, cm/sec	Porosity, fraction	Bulk Density, gm/cm <sup>3</sup>	Particle Density, gm/cm <sup>3</sup>	Effective Diffusion Coefficient, cm <sup>2</sup> /sec	$\theta_s$	$\theta_r$	$\alpha$	$n$	$m$
LAWV	Before Collapse	17.3	2.2E-06	0.90 <sup>1</sup>	0.245 <sup>1</sup>	2.45 <sup>1</sup>	4.0E-06	0.328000	0.028399	2.867E-03	1.500000	0.333333
	After Collapse	2.5	1.2E-04	0.456	1.44	2.65	5.3E-06	0.456000	0.121330	0.040416	1.153656	0.133191
ILV	Before Collapse	25.83	1.0E-02	0.736 <sup>1</sup>	0.612 <sup>1</sup>	2.32 <sup>1</sup>	1.6E-05	0.300000	0.021000	0.137676	1.479624	0.324153
	After Collapse	10	1.2E-04	0.456	1.44	2.65	5.3E-06	0.456000	0.121330	0.040416	1.153656	0.133191
Naval Reactor Components	Bolted Containers (generic)	4.1	2.4E-05	0.893	0.282	2.65	5.3E-6	The WRC and $k_{rel}$ are calculated using Eq. 72 and 74				
	Welded Casks Hydraulically Intact (special)	18	5E-15	0.893	0.282	2.65	1E-13	The WRC and $k_{rel}$ are calculated using Eq. 72 and 74				
	Welded Casks Hydraulically Degraded (special)	18	2.4E-05	0.893	0.282	2.65	5.3E-6	The WRC and $k_{rel}$ are calculated using Eq. 72 and 74				

<sup>1</sup> Recommended by Phifer et al. (2006) in order to not overestimate the retardation of radionuclides during transport

<sup>2</sup> Because the welded casks are assumed to be hydraulically intact for 750 years there is essentially no flow and no advective release of contaminants during this period. Thus, the characteristic curves are essentially irrelevant until a leak develops.

### 7.3 COMPONENT-IN-GROUT WASTE ZONE REPRESENTATION

A description of the Component-in-Grout (CIG) Trenches is provided in Section 4.4.3. Structural modeling of the CIG trenches (Peregoy, 2006a) has been conducted to evaluate a CIG Trench design life of 300 years in terms of structural integrity. The structural modeling indicates that the CIG Trench segments can achieve a structural design life of 300 years so long as the interior void spaces of the components are fully grouted, the waste form is otherwise structurally stable (i.e., no voids or robust container design) or the segments are covered with a 20-inch thick reinforced concrete mat. Components disposed within the CIG Trenches consist of large radioactively contaminated equipment along with other containerized waste. The components are mostly made of carbon steel and the type of component with the thinnest walls would most likely be a B-25 box with a 12-gauge (0.1094 inch) wall thickness. Dunn (2002) estimated the time to through-wall pitting of a 12-gauge carbon steel B-25 box buried in soil would be a minimum 40 years. Through-wall pitting of a B-25 box encapsulated within a cementitious grout would take longer than 40 years due to the elevated pH within such an environment. Furthermore, the encapsulating grout would tend to seal any minor openings or joints associated with the components. Therefore, components will be assumed to be hydraulically intact for 40 years. Based upon this information the following three CIG trench waste zone representations will be provided: structurally and hydraulically intact conditions for 40 years; structurally intact but hydraulically degraded conditions from 40 to 300 years; and structurally and hydraulically degraded conditions after 300 years.

#### 7.3.1 CIG Structurally and Hydraulically Intact Conditions

Under structurally and hydraulically intact conditions (prior to 40 years) the CIG Trench waste zone consists of components and containerized waste, which are encapsulated in at least 1-foot of CIG grout. The old CIG grout and future CIG grout are described in Sections 4.5.3 and 6.3. A typical CIG Trench disposal may consist of one or more large radioactively contaminated equipment items surrounded by other containerized waste to optimize the use of disposal space. Prior to disposal, the bottom of the excavated trench segment is filled with grout to a minimum one foot and allowed to cure. The component(s) are then placed on the one-foot base grout layer and grout is then poured around, between, and over the component(s) to completely encapsulate the component(s) with a minimum one-foot layer of grout.

Additional layers of component(s) and grout may be placed on top of previous layers until approximately 16 feet (4.9 m) of trench is filled up with component(s) (approximately a 14-foot waste zone) and grout (approximately 2 feet of grout). The operation is conducted so that a minimum one foot of grout is between the component(s) and the trench bottom and side and so that a minimum one foot of grout is over the top of the upper most component(s). As discussed above, components are typically carbon steel with a minimum 12-gauge (0.1094 inch) wall thickness, in which through-wall pitting should take longer than 40 years (Dunn, 2002), therefore components will be assumed to be hydraulically intact for 40 years. Under these conditions the waste zone will be assumed to consist of an intact container with a saturated hydraulic conductivity of  $1.0E-12$  cm/s (i.e., a low saturated hydraulic conductivity to represent intact carbon steel that is not zero, due to potential model instability

with the use of zero) that is half filled with an air space. Under these conditions, there is essentially no flow and no advective release of contaminants during this period. Thus, the characteristic curves are essentially irrelevant until a leak develops. The waste zone will be assumed to consist of the properties of the E-Area operational soil cover prior to dynamic compaction (see Section 5.4 and Table 5-9), as shown in Figure 7-4 for both old and new CIG grout segments.

### **7.3.2 CIG Structurally Intact but Hydraulically Degraded Conditions**

After 40 years it is assumed that the components within CIG trenches all have through-wall pitting and are no longer hydraulically intact, however based upon the structural modeling the trenches are assumed to remain structurally intact for 300 years (i.e., no subsidence). Under these conditions the waste zone will be assumed to consist of a degraded container with hydraulic properties of the E-Area operational soil cover prior to dynamic compaction (see Section 5.4 and Table 5-9), as shown in Figure 7-4 for both old and new CIG grout segments.

### **7.3.3 CIG Structurally and Hydraulically Degraded Conditions**

The void space within components and the integrity of the components can vary widely. However, the subsidence potential of the 14-foot waste zone has not yet been estimated. If it is assumed that the waste within a trench consists of 3 layers of B-25 boxes, containing waste with the same density as B-25 boxes disposed within the Engineered Trenches (Phifer and Wilhite, 2001), with a total thickness of 14 feet then the subsidence potential of the CIG waste zone would be approximately 10 feet, resulting in a subsided waste zone thickness of 4 feet. This indicates that a significant subsidence potential may exist for the CIG waste zone. However, because the waste zone does not solely consist of low-density waste in B-25 boxes, the subsidence potential will be taken as half the waste zone thickness (i.e., 7 feet). Therefore, the waste zone thickness after subsidence will be taken as 7 feet.

Under structurally and hydraulically degraded conditions (after 300 years) it is assumed that the components and the containerized waste and overlying grout and concrete mat break up and collapse in upon themselves, resulting in the waste zone collapsing to a 7-foot thickness and subsidence of the overlying closure cap soil into the CIG Trench. Due to the significant soil presence within a degraded CIG Trench and the fluffing of the soil as it collapses into the CIG Trench, the CIG Trench waste zone after subsidence will be represented hydraulically by the E-Area operational soil cover prior to dynamic compaction (see Section 5.4 and Table 5-9), as shown in Figure 7-4 for both old and new CIG grout segments.

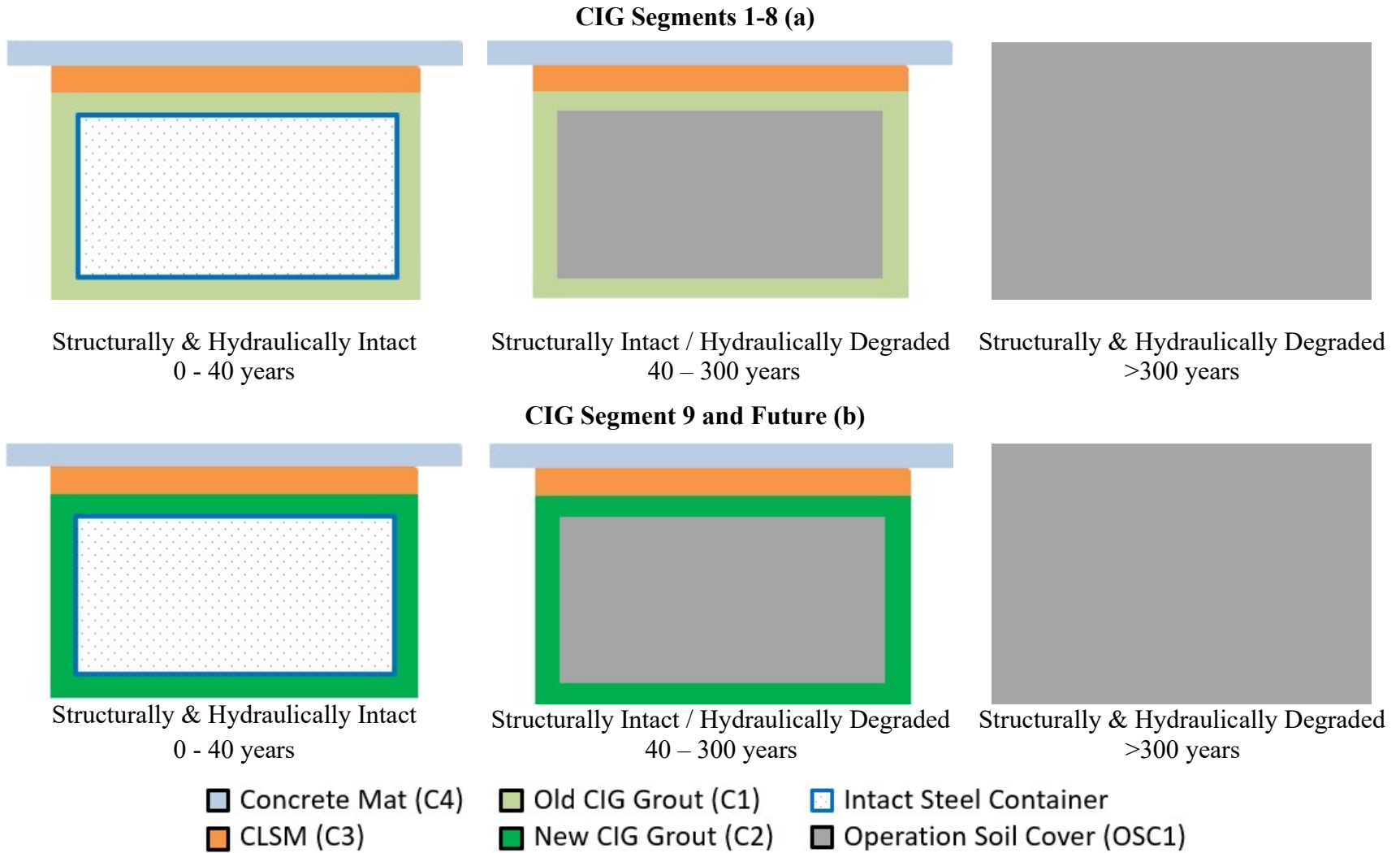


**Figure 7-4. Conceptual model representing hydraulic properties of CIG Trench waste zone from fully intact to degraded condition for (a) Segments 1-8 and (b) Segment 9 and future**

## 7.4 LAW VAULT WASTE ZONE REPRESENTATION

A description of the LAW Vault is provided in Section 4.5.4. Based upon structural modeling which considers vault loadings (both static and seismic) and rebar corrosion, Carey (2006) estimated that the mean time to LAW Vault collapse is 2805 years with a standard deviation of 920 years. The following two LAW Vault waste zone representations will be provided: prior to vault collapse and after vault collapse.

### 7.4.1 Prior to LAW Vault Collapse

Prior to vault collapse, the LAW Vault waste zone will consist of low-activity waste contained within stacked B-25 boxes, B-12 boxes, drums, other metal containers and/or concrete containers. B-25 boxes are stacked four high for a waste thickness of 17.3 feet. The waste within the containers typically has a very low density and significant internal void space. No soil, grout, or any other material will exist between the stacked containers and a significant void space will exist between the top of the container stack and the LAW Vault bridge beams and roof. The bridge beams are a minimum of 20 feet off the floor, while the roof is a minimum 24 feet 6 inches off the floor (see Figure 4-15). Additionally, prior to vault collapse, it is anticipated that significant corrosion of the metal waste containers will occur, resulting in limited self-compaction of the waste zone under its own weight (the waste within the containers typically has a very low density) prior to the time of vault collapse. The PORFLOW code models flow and transport through porous media and cannot represent a significant empty space. Additionally, adjacent materials within a PORFLOW model that have significantly different saturated hydraulic conductivities can create flow convergence problems. Phifer et al. (2006) recommended that the LAW Vault waste zone and vault interior prior to vault collapse will be represented hydraulically by CLSM, Figure 7-5(a), which has a saturated hydraulic conductivity six orders of magnitude greater than the vault concrete enclosing it. This is deemed appropriate as the vault concrete, not the waste zone represented by CLSM, will control the flow of water through the waste zone. Cracking will occur in vault roof, walls and floor before collapse. Cracked zones will be represented hydraulically by gravel as shown in Figure 7-5(b).

### 7.4.2 After LAW Vault Collapse

Jones and Phifer (2006) estimated that the interior of the LAW Vault has a subsidence potential of approximately 21 feet. Upon vault collapse, it is anticipated that the broken bridge beams and roof, along with the overlying closure cap soils, will fall into the vault interior crushing the corroded containers and waste to a nominal 2.5-foot thickness. Due to the significant soil presence within a collapsed LAW Vault and the fluffing of the soil as it collapses into the LAW Vault, the LAW Vault waste zone and vault interior after vault collapse will be represented hydraulically by the E-Area operational soil cover, Figure 7-5(c), prior to dynamic compaction (Section 5.4 and Table 5-20).

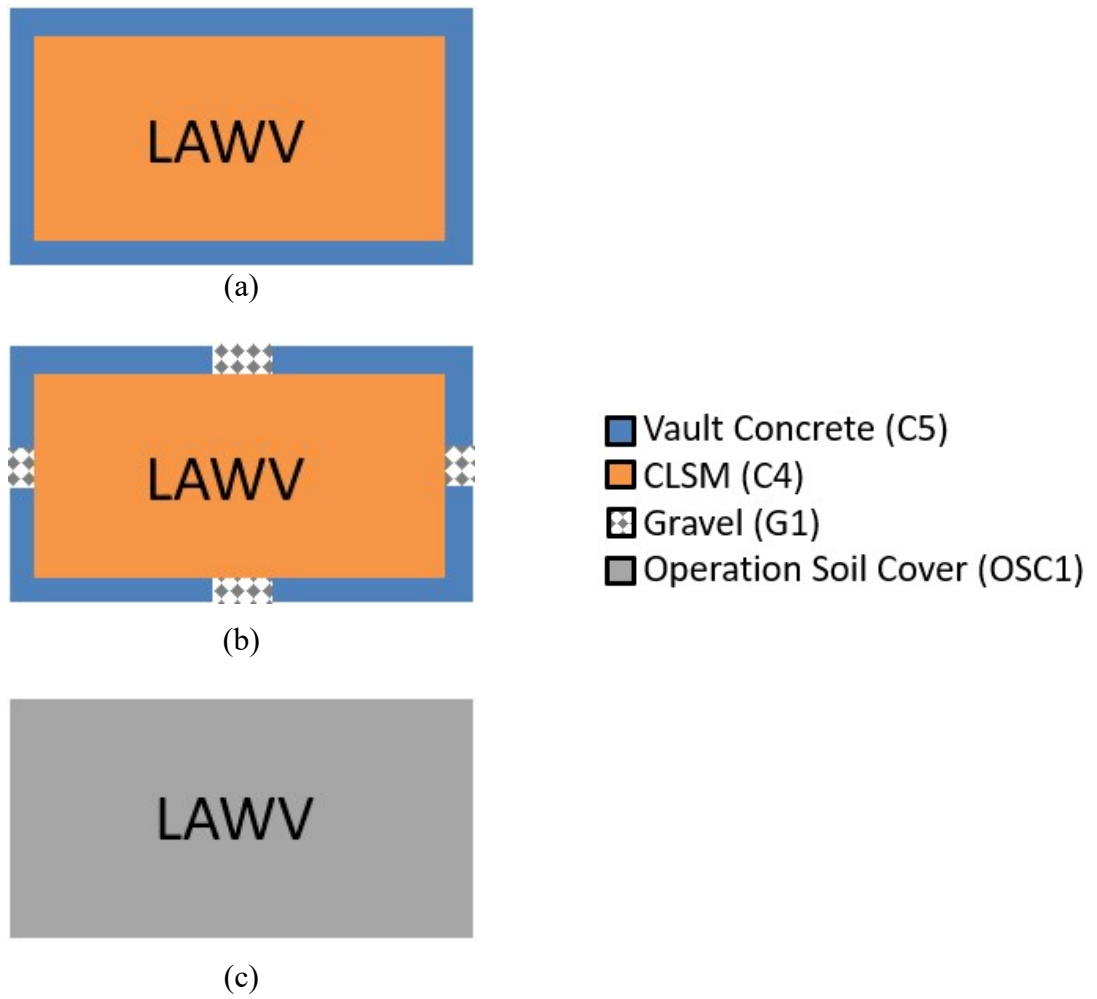


**Figure 7-5. Conceptual model representing hydraulic properties of the Low Activity Waste Vault waste zone in (a) Intact, (b) Cracked, and (c) Collapsed states**

## 7.5 IL VAULT WASTE ZONE REPRESENTATION

A description of the IL Vault is provided in Section 4.4.5. Based upon structural modeling which considers vault loadings (both static and seismic) and rebar corrosion, Peregoy (2006b) has estimated that the mean time to IL Vault collapse is 6703 years with a standard deviation of 1976 years. The following two IL Vault waste zone representations will be provided: prior to vault collapse and after vault collapse.

### 7.5.1 Prior to IL Vault Collapse

Prior to vault collapse, the IL Vault waste zone will include vessels and waste contained within drums, B-12 boxes, B-25 boxes, other metal containers, and concrete containers. The first layer of containers is placed within a cell directly on top of the graded stone leachate collection system. This first layer of waste is encapsulated with the old E-Area CIG grout (see Sections 4.4.5 and 6.3.3.1) and the overlying grout forms the surface for the placement of the next layer of waste. Subsequent layers of containers within a cell are encapsulated with E-Area CLSM (see Sections 4.4.5 and 6.3.3.3). This process is continued until the waste/CLSM zone thickness is 25 feet 10 inches in the ILNT cells and 21 feet 9 inches in the ILT cells. A nominal 1-foot 5-inch final top layer of new E-Area CIG grout is used to provide the surface upon which the final reinforced concrete roof will be placed for the ILNT cells and a nominal 2-foot 6-inch top layer of grout for the ILT cells (see Figure 4-19 and Figure 4-20). Prior to vault collapse (i.e., an estimated 6703 years), it is anticipated that significant corrosion of the metal waste containers will occur, resulting in collapse of individual containers and overlying CLSM and/or grout prior to the time of vault collapse. Over time this will result in a crumbling, fractured waste zone. Phifer et al. (2006) recommended that due to the anticipated crumbling, fractured waste zone, the IL Vault waste zone and vault interior prior to vault collapse will be represented hydraulically by gravel as shown in Figure 7-6(a) (see Section 5.4 and Table 5-20). This material property is deemed appropriate for representing the waste zone. Cracking will occur in vault roof, walls and floor before collapse. Cracked zones will be represented hydraulically by gravel as shown in Figure 7-6(b).

### 7.5.2 After IL Vault Collapse

It is assumed that significant void space exists in most of the containers within the IL Vault. However, the interior subsidence potential of the IL Vault has not yet been estimated. If it is assumed that the waste within a cell consists of 6 layers of B-25 boxes, containing waste with the same density as B-25 boxes disposed within the Engineered Trenches, then the interior subsidence potential of the IL Vault would be approximately 20 feet, resulting in a subsided waste zone thickness of approximately 5 or 6 feet. This indicates that a significant subsidence potential may exist for the IL Vault waste zone. However, because the waste zone does not solely consist of low-density waste in B-25 boxes, the subsided waste zone thickness will be taken as 10 feet (approximately twice that based upon low density waste in B-25 boxes alone).

Upon vault collapse, it is anticipated that the roof, along with the overlying closure cap soils, will fall into the vault interior crushing the crumbling, fractured CLSM/grout, corroded containers and waste to a nominal 10-foot thickness. Due to the significant soil presence within a collapsed IL Vault and the fluffing of the soil as it collapses into the IL Vault, the IL

Vault waste zone and vault interior after vault collapse will be represented hydraulically by the E-Area operational soil cover prior to dynamic compaction as shown in Figure 7-6(c) (see Section 5.4 and Table 5-20).

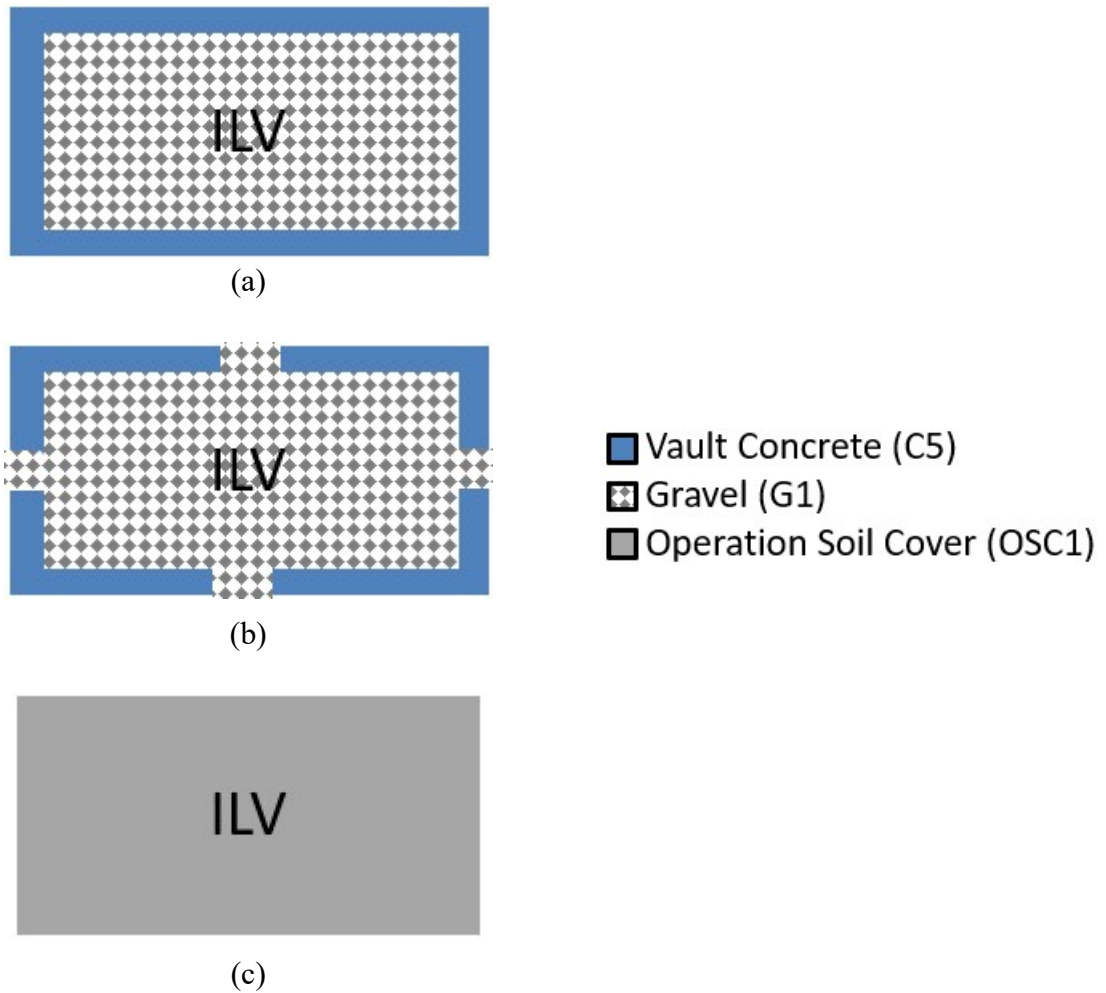


**Figure 7-6. Conceptual model representing hydraulic properties of the Intermediate Level Vault waste zone in (a) Intact, (b) Cracked, and (c) Collapsed states**

## 7.6 NRCDA WASTE ZONE REPRESENTATION

A description of the NRCDA is provided in Section 4.4.6. Hang and Hamm (2019) implemented the vadose zone conceptual model for the NRCDA using PORFLOW. This section summarizes the waste zone representation used for the NRCDA in Hang and Hamm (2019). The NRCDA areas are the at-grade gravel disposal pads, 643-26E and 643-7E. Naval Reactor (NR) waste is comprised of: (1) highly radioactive reactor components consisting of activated corrosion-resistant metal alloy stored within thick carbon-steel casks, and (2) auxiliary equipment contaminated on the surface with Activated Corrosion Products (ACP) (referred to as “crud” by the U.S. Navy) at low levels and stored within thinner-walled bolted containers. The 643-7E disposal pad contains 41 casks and is closed to future receipts. For 643-26E, the current estimates are for a total of 33 heavily shielded, welded casks, and 400+ thinner-walled bolted containers by 2065 (Wohlwend and Butcher, 2018).

### 7.6.1 Welded Cask

Highly radioactive components consisting of activated corrosion-resistant metal alloy are stored within thick carbon-steel welded casks. Based on unclassified information supplied by NR programs (Yu et al., 2002), a representative type of activated metal component is the KAPL core barrel/thermal shield (CB/TS). A schematic of the KAPL CB/TS welded cask is illustrated in Figure 7-7. According to Yu et al. (2002), the activated waste components in the KAPL CB/TS are made of either Inconel or Zircaloy, which are corrosion resistant metal alloys.

During the first 750 years after disposal the welded cask remains hydraulically intact. Under these conditions, there is essentially no flow and no advective release of contaminants. Thus, the characteristic curves are essentially irrelevant until a leak develops. The waste zone will be assumed to consist of the properties of the E-Area Slit & Engineered containerized waste zone before dynamic compaction (see Section 7.1.2.1 and Table 7-1), as shown in Figure 7-9(a) for this intact case. At 750 years, the cask weld is assumed to corrode and develop a leak path for release of contaminants. The waste zone is expected to remain structurally intact during the entire 1,000-year period of performance. For this final period, there is no credit taken for the container and the waste zone is again assumed to consist of the properties of the E-Area Slit & Engineered Trench containerized waste zone before dynamic compaction (see Section 7.1.2.1 and Table 7-1), as shown in Figure 7-9(b).

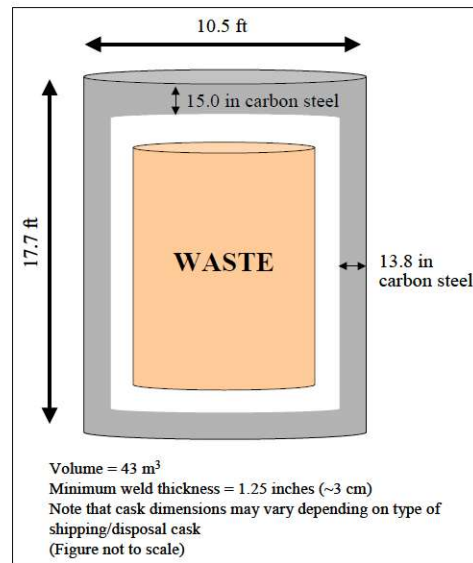


**Figure 7-7. Schematic of KAPL CB/TS welded cask**

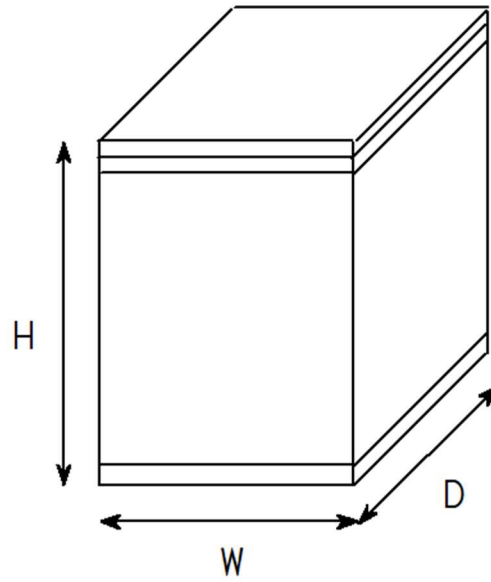
### 7.6.2 Bolted Containers

Auxiliary equipment contaminated with ACP at low levels is stored within thinner-walled bolted containers. Because of the variety of bolted containers received from NR Programs, the large Shear Block disposal container (SBDC) was selected as the representative type of bolted container for the PORFLOW model (BMPC-KAPL 2009a and 2009b). Both large and small versions of SBDC's (8ft<sup>3</sup> and 4ft<sup>3</sup> internal volume, respectively) are being shipped to E-Area by the Navy with approximate external dimensions shown in Figure 7-8. The SBDC was selected because it represents the largest category of bolted containers currently disposed or projected to be shipped to E-Area. Also, assuming this waste configuration conservatively concentrates the inventory from larger bolted containers into the smaller SBDC volume located closer to the water table.

Because of their robust design and generally dense payload (e.g., shear blocks, hold down barrels, closure heads, recirculating pumps, etc.) bolted containers are considered non-crushable during the 1,000-year period of performance. Dynamic compaction is prohibited from occurring over the two NRCDA's at final closure.

There is no credit taken for holdup of contaminants for this generic waste form. Thus, the waste zone is assumed to consist of the properties of the E-Area Slit & Engineered containerized waste zone before dynamic compaction (see Section 7.1.2.1 and Table 7-1), as shown in Figure 7-9(c).

The properties of the NRCDA waste zones (waste, cask) are shown in Table 7-2.



	Large Container <sup>(1)</sup>	Small Container <sup>(2)</sup>
W	24"	19.5"
D	21"	19.5"
H	49"	35"

Figure 7-8. Schematic of a bolted container

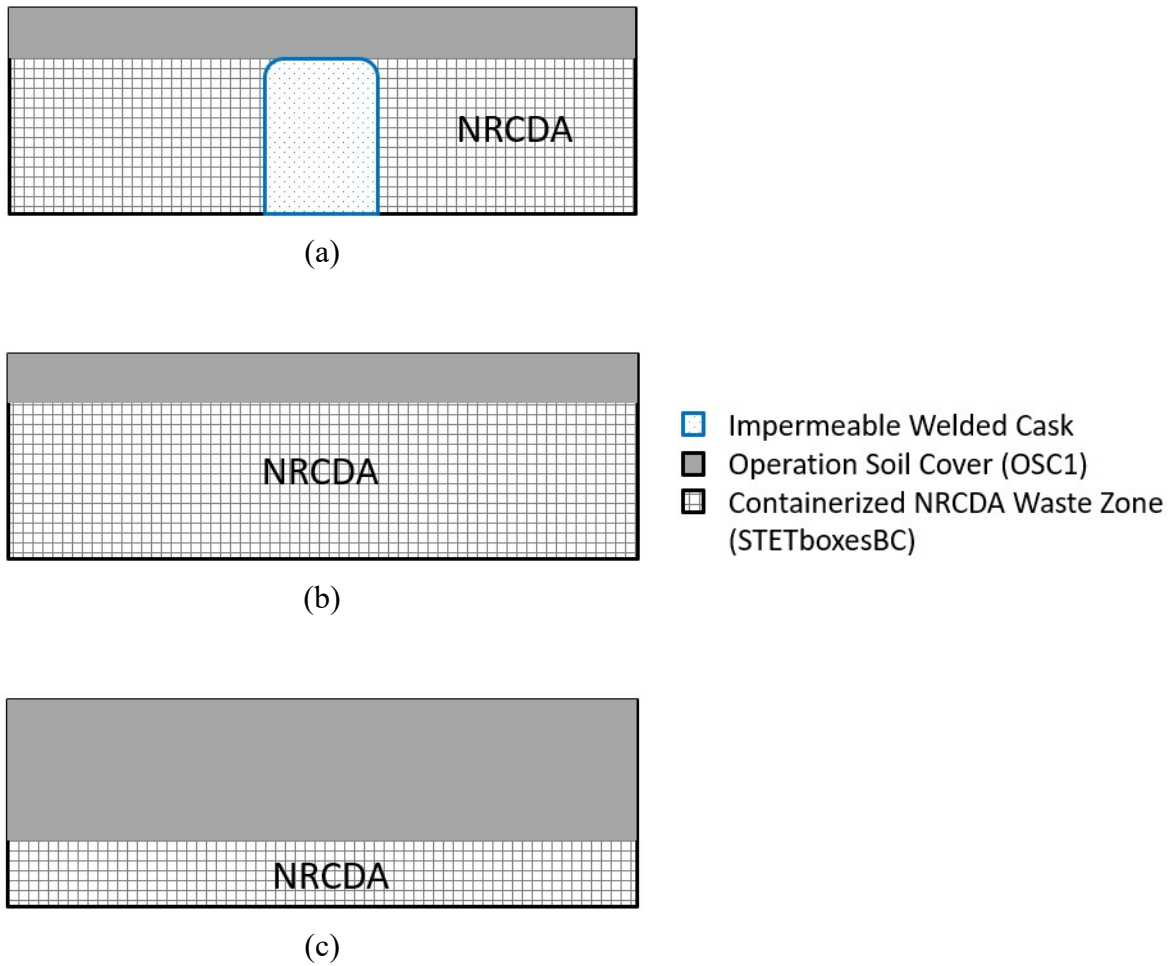


**Figure 7-9. Conceptual model representing hydraulic properties of the Naval Reactor Component Disposal Area waste zone for (a) Intact impermeable welded casks, (b) Hydraulically failed welded casks, and (c) Generic NR containerized waste**

## 8.0 SUMMARY AND RECOMMENDATIONS

### 8.1 SUMMARY

Hydraulic property estimates for soils, cementitious materials and waste zones associated with the E-Area disposal units have been provided to support the E-Area LLWF PA. Nominal or “best estimate” hydraulic property values for use in the deterministic and sensitivity modeling are provided along with representations of the hydraulic property value uncertainty for use in the uncertainty modeling. The hydraulic properties provided for each of the E-Area materials include porosity ( $\eta$ ), dry bulk density ( $\rho_b$ ), particle density ( $\rho_p$ ), saturated hydraulic conductivity ( $K_{sat}$ ), characteristic curves (suction head, saturation, and relative permeability), and effective diffusion coefficient ( $D_e$ ). A representation of the uncertainty associated with each property, except for the characteristic curves, is provided for each material, except for the E-Area waste zones. These nominal parameter values and parameter uncertainty representations for each of the E-Area soils, cementitious materials, and waste zones are based upon the following in order of priority:

- Site-specific field data,
- Site-specific laboratory data,
- Similarity to material with site-specific field or laboratory data, and
- Literature data.

The following tables contained herein provide the nominal parameter values and parameter uncertainty representation for each of the E-Area soils:

- Table 5-20. Summary of recommended soil properties
- Table 5-17. Uncertainty Analysis summary statistics for total porosity, dry bulk density, and particle density
- Table 5-18. Uncertainty analysis summary statistics for saturated hydraulic conductivity
- Table 5-19. Uncertainty analysis summary statistics for saturated effective diffusion coefficient

The following tables contained herein provide the nominal parameter values and parameter uncertainty representation for each of the E-Area cementitious materials:

- Table 6-28. Recommended material properties for cementitious materials in the various E-Area LLWF Disposal Unit Types
- Table 6-33. E-Area cementitious material uncertainty summary statistics for effective porosity (%)
- Table 6-34. E-Area cementitious material uncertainty summary statistics for dry bulk density ( $\text{g}/\text{cm}^3$ )
- Table 6-35. E-Area cementitious material uncertainty summary statistics for particle density ( $\text{g}/\text{cm}^3$ )
- Table 6-38. E-Area cementitious material uncertainty summary statistics for saturated hydraulic conductivity
- Table 6-40. E-Area cementitious material uncertainty summary statistics for saturated effective diffusion coefficient

Table 7-2 provides the recommended waste zone representation for each of the E-Area disposal units. An explicit uncertainty representation for the E-Area disposal unit waste zones is not provided due to the lack of data from which to derive such a representation.

## 8.2 RECOMMENDATIONS

Much of the nominal hydraulic property values and uncertainty representations provided herein are based upon similarity to other materials for which site-specific field or laboratory data is available or are based upon literature data. This reliance upon similarity and literature data increases the uncertainty associated with such representations compared to direct measurement. Therefore, additional work should be considered in order to better define the hydraulic property values and uncertainty representations associated with the E-Area soils, cementitious materials, and waste zones. Such additional work should be based upon the importance of the material and/or property to the results of the deterministic and uncertainty modeling. The relative importance of the various materials and properties should be established through a process of sensitivity modeling. The materials and properties that most affect the results of the deterministic, sensitivity, and uncertainty modeling should receive priority for further field and laboratory testing. The remaining materials and properties should receive a lower priority or even be eliminated for further testing. Prioritization should also consider that no site-specific hydraulic property measurements have been obtained for the following existing E-Area materials:

- E-Area operational soil cover (both before and after dynamic compaction)
- IL Vault permeable backfill
- E-Area CIG concrete mats
- E-Area disposal unit waste zone

Additionally further investigations into the generation of characteristic curves based upon water retention and/or unsaturated hydraulic conductivity data and curve fitting codes such as RETC (USDA, 1998) for both soils and cementitious materials is recommended to ensure that recent advances in modeling water retention and unsaturated hydraulic conductivity are appropriately taken into consideration.

## 9.0 REFERENCES

- Aadland, R. K., Gellici, J. A., and Thayer, P. A. (1995). "Hydrogeologic Framework of West-Central South Carolina," Rep. No. 5. South Carolina Department of Natural Resources, Columbia, South Carolina.
- Aadland, R. K., Harris, M. K., Lewis, C. M., Gaughan, T. F., and Westbrook, T. M. (1991). "Hydrostratigraphy of the General Separations Area, Savannah River Site (SRS), South Carolina," Rep. No. WSRC-RP-91-13. Westinghouse Savannah River Company, Aiken, SC 29808.
- AASHTO (T 259-02). Standard Method of Test for Resistance of Concrete to Chloride Ion Penetration. American Association of State Highway and Transportation Officials, Washington, D.C. .
- AASHTO (T 277-05). Standard Method of Test for Electrical Indication of Concrete's Ability to Resist Chloride Ion Penetration. American Association of State Highway and Transportation Officials, Washington, D.C. .
- Ababou, R., and Wood, E. F. (1990). Comment on "Effective groundwater model parameter values: influence of spatial variability of hydraulic conductivity, leakance, and recharge" by J. J. Gomez-Hernandez and S. M. Gorelick. *Water Resources Research* **26**, 1843-1846.
- ACI (201.2R-01). Guide to Durable Concrete. American Concrete Institute, Farmington Hills, Michigan.
- ACI (232.2R-03). Use of Fly Ash in Concrete. American Concrete Institute, Farmington Hills, Michigan.
- ACI (233R-03). Slag Cement in Concrete and Mortar. American Concrete Institute, Farmington Hills, Michigan.
- ACI (234R-96). Guide for the Use of Silica Fume in Concrete. American Concrete Institute, Farmington Hills, Michigan.
- Altman, S. J., Arnold, B. W., Barnard, R. W., Barr, G. E., Ho, C. K., McKenna, S. A., and Eaton, R. R. (1996). "Flow Calculations for Yucca Mountain Groundwater Travel Time (GWTT 95)," Rep. No. Sandia Report SAND96-0819. Sandial National Laboratory.
- Ampadu, K. O., Torii, K., and Kawamura, M. (1999). Beneficial effect of fly ash on chloride diffusivity of hardened cement paste. *Cement & Concrete Research* **29**, 585-590.
- Anderson, M. P. (1991). Comment on "Universal scaling of hydraulic conductivities and dispersivities in geologic media" by S. P. Neuman. *Water Resources Research* **27**, 1381-1384.
- Anderson, M. P. (1997). Characterization of geological heterogeneity. In "Subsurface flow and transport: a stochastic approach" (G. Dagan and S. P. Neuman, eds.), pp. 241. Cambridge University Press.
- ANS (ANSI/ANS-16.1-2003). Measurement of the Leachability of Solidified Low-Level Radioactive Wastes by a Short-Term Test Procedure. American Nuclear Society, La Grange Park, Illinois.
- ASTM (6527-00). Standard Test Method for Determining Unsaturated and Saturated Hydraulic Conductivity in Porous Media by Steady-State Centrifugation ASTM International, West Conshohocken, PA.

- ASTM (C 642 – 97). Standard Test Method for Density, Absorption, and Voids in Hardened Concrete. West Conshohocken, PA.
- ASTM (C 1202-05). Standard Test Method for Electrical Indication of Concrete's Ability to Resist Chloride Ion Penetration. ASTM International, West Conshohocken, PA.
- ASTM (C 1308-95). Standard Test Method for Accelerated Leach Test for Diffusive Releases from Solidified Waste and a Computer Program to Model Diffusive, Fractional Leaching from Cylindrical Waste Forms. ASTM International West Conshohocken, PA.
- ASTM (C 1556-04). Standard Test Method for Determining the Apparent Chloride Diffusion Coefficient of Cementitious Mixtures by Bulk Diffusion. ASTM International, West Conshohocken, PA.
- ASTM (D 4404-84). Standard Test Method for Determination of Pore Volume and Pore Volume Distribution of Soil and Rock by Mercury Intrusion Porosimetry. ASTM International, West Conshohocken.
- ASTM (D 5084-10). Standard Test Methods for Measurement of Hydraulic Conductivity of Saturated Porous Materials Using a Flexible Wall Permeameter. West Conshohocken, PA.
- Atkinson, A., Nickerston, A. K., and Valentine, T. M. (1984). The Mechanism of Leaching from Some Cement-Based Nuclear Wasteforms. *Radioactive Waste Management and the Nuclear Fuel Cycle* **4**, 357-378.
- Bagwell, L., and Bennett, P. (2017). "Elevation of Water Table and Various Stratigraphic Surfaces beneath E Area Low Level Waste Disposal Facility," Rep. No. SRNL-STI-2017-00301, Rev. 0. Savannah River National Laboratory, Aiken, SC.
- Baroghel-Bouny, V., Mainguy, M., Lassabatere, T., and Coussy, O. (1999). Characterization and identification of equilibrium and transfer moisture properties for ordinary and high-performance cementitious materials. *Cement and Concrete Research* **29**, 1225-1238.
- Basheer, P. A. M. (2001). Chapter 16 Permeation Analysis. In "Handbook of Analytical Techniques in Concrete Science and Technology Principles, Techniques, and Applications" (V. A. Ramachandran and J. J. Beaudoin, eds.), pp. 658-737. Noyes Publications, Park Ridge, New Jersey.
- Bear, J. (1972). "Dynamics of Fluids in Porous Media," Dover Publications, New York
- Beaudoin, J. J., and Marchand, J. (2001). Chapter 14 Pore Structure. In "Handbook of Analytical Techniques in Concrete Science and Technology Principles, Techniques, and Applications" (V. A. Ramachandran and J. J. Beaudoin, eds.), pp. 528-628. Noyes Publications, Park Ridge, New Jersey.
- Bechtel-SAIC (2005). "Saturated Zone Flow and Transport Model Abstraction," Rep. No. MDL-NBS-HS-000021, Rev. 3. Bechtel SAIC Company, LLC, Las Vegas, NV.
- Boudreau, B. P. (1996). The Diffusive Tortuosity of Fine-grained Unlithified Sediments. *Geochimica et Cosmochimica Acta* **60**, 3139-3142.
- Boving, T. B., and Grathwohl, P. (2001). Tracer Diffusion Coefficients in Sedimentary Rocks: Correlation to Porosity and Hydraulic Conductivity *Journal of Contaminant Hydrology* **53**, 85-100.
- Brannan, J. R., and Haselow, J. S. (1993). Compound random field models of multiple scale hydraulic conductivity *Water Resources Research* **29**, 365-372.

- Bruins, H. R. (2003). Coefficients of Diffusion in Liquids. *In* "International Critical Tables of Numerical Data, Physics, Chemistry, and Technology" (E. W. Washburn, ed.), pp. 3414. Knovel, Norwich, New York
- Carey, S. (2006). "Low Activity Waste (LAW) Vault Structural Degradation Prediction," Rep. No. T-CLE-E-00018, Rev. 1. Washington Savannah River Company, Aiken, South Carolina.
- Castellote, M., Alonso, C., Andrade, C., Chadbourn, G. A., and Page, C. L. (2001a). Oxygen and chloride diffusion in cement pastes as a validation of chloride diffusion coefficients obtained by steady-state migration tests. *Cement and Concrete Research* **31**, 621-625.
- Castellote, M., Andrade, C., and Alonso, C. (2001b). Measurement of the steady and non-steady-state chloride diffusion coefficients in a migration test by means of monitoring the conductivity in the anolyte chamber comparison with natural diffusion tests. *Cement & Concrete Research* **31**, 1411-1420.
- Clifton, J. R., and Knab, L. I. (1989). "Service Life of Concrete." Office of Nuclear Regulatory Research, Division of Engineering, Washington, DC.
- Colquhoun, D. J., Woollen, I. D., Nieuwenhuise, D. S. V., Padgett, G. G., Oldham, R. W., Boylan, D. C., Bishop, J. W., and Howell, P. D. (1983). "Surface and Subsurface Stratigraphy, Structure and Aquifers of the South Carolina Coastal Plain," Rep. No. ISBN 0-9613154-0-7. South Carolina Health and Environmental Control.
- Dagan, G., and Neuman, S. P. (1997). "Subsurface flow and transport: a stochastic approach," Cambridge University Press.
- Delagrave, A., Marchand, J., and Pigeon, M. (1998). Influence of Microstructure on the Tritiated Water Diffusivity of Mortars. *Advanced Cement Based Materials* **7**, 60-65.
- Dennehy, K. F., Prowell, D. C., and McMahon, P. B. (1989). "Reconnaissance Hydrogeologic Investigation of the Defense Waste Processing Facility and Vicinity, Savannah River Plant, South Carolina,," Rep. No. 88-4221. U. S. Geological Survey
- Desbarats, A. J. (1992). Spatial averaging of hydraulic conductivity in three-dimensional heterogenous porous media. *Mathematical Geology* **24**, 249-267.
- Dixon, K. L., and Phifer, M. A. (2006). "Hydraulic and Physical Properties of Cementitious Materials Used at the Component-in-Grout Waste Trenches and the Intermediate Level Vault," Rep. No. WSRC-STI-2006-00199 Rev.0. Savannah River National Laboratory, Aiken, SC.
- Dixon, K. L., and Phifer, M. A. (2007). "Cementitious Material Selection for Future Component-In-Grout Waste Disposals," Rep. No. WSRC-STI-2007-00207, Rev. 0. Savannah River National Laboratory, Aiken, SC.
- Dixon, K. L., and Phifer, M. A. (2008). "Hydraulic and Physical Properties of MCU Saltstone," Rep. No. WSRC-STI-2007-00649, Rev. 0. Savannah River National Laboratory, Aiken, SC.
- Dunn, K. A. (2002). "B-25 Corrosion Evaluation Summary Report (U)," Rep. No. WSRC-TR-2001-00587. Westinghouse Savannah River Company, Aiken, South Carolina.
- Durner, W. (1994). Hydraulic conductivity estimation for soils with heterogeneous pore structure. *Water Resources Research* **30**, 211-223.
- Dutro, J., J. T. , Dietrich, R. V., and Foose, R. M. (1989). "AGI Data Sheets for Geology in the Field, Laboratory, and Office," American Geological Institute Alexandria, Virginia.

- Dykhuizen, R. C., and Casey, W. H. (1989). An Analysis of Solute Diffusion in Rocks *Geochimica et Cosmochimica Acta* **53**, 2797-2805.
- Efron, B. (1982). The jackknife, the bootstrap and other resampling plans. In "CBMS-NSF Regional Conference Series in Applied Mathematics". Number 38 Society for Industrial and Applied Mathematics Philadelphia, Pennsylvania,.
- Fallow, W. C., and Price, V. (1995). Stratigraphy of the Savannah River Site and Vicinity. *Southeastern Geology* **35**, 21-58.
- Fallow, W. C., Price, V., and Thayer, P. A. (1990). Stratigraphy of the Savannah River Site, South Carolina. In "Second Bald Head Island Conference on Coastal Plain Geology" (V. A. Zullo, W. B. Harris and V. Price, eds.). University of North Carolina at Wilmington, Bald Head Island, NC.
- Faure, G. (1991). "Principles and Applications of Inorganic Geochemistry," MacMillan Publishing, New York, New York.
- Feehley, C. E., Zheng, C., and Molz, F. J. (2000). A dual-domain mass transfer approach for modeling solute transport in heterogenous aquifers: Application to the Macrodispersion Experiment (MADE) site. *Water Resources Research* **36**, 2501-2515.
- Fetter, C. W. (1993). "Contaminant Hydrogeology," Macmillan Publishing Company, New York.
- Flach, G., Dixon, K. L., and Nichols, R. L. (2015). Characterization of Unsaturated Hydraulic Conductivity in Fractured Media Using the Multistep Outflow Method – 15461, March 15 – 19, 2015. In "WM2015 Conference", Phoenix, Arizona, USA.
- Flach, G. P. (2012). Effective Porosity Implies Effective Bulk Density in Sorbing Solute Transport. *Ground Water* **50**, 657-658.
- Flach, G. P. (2017). "Method for Modeling the Gradual Physical Degradation of a Porous Material," Rep. No. SRNL-STI-2017-00525. Savannah River National Laboratory, Aiken, SC.
- Flach, G. P. (2019). "Updated Groundwater Flow Simulations of the Savannah River Site General Separations Area," Rep. No. SRNL-STI-2018-00643, Rev. 0. Savannah River National Laboratory, Aiken, SC.
- Flach, G. P., Collard, L. B., Phifer, M. A., Crapse, K. P., Dixon, K. L., Koffman, L. D., and Wilhite, E. L. (2005a). "Preliminary Closure Analysis for Slit Trenches #1 and #2." Westinghouse Savannah River Company, Aiken, South Carolina.
- Flach, G. P., Crisman, S. A., and III, F. J. M. (2004). Comparison of single-domain and dual-domain subsurface transport models. *Ground Water* **42**, 815-828.
- Flach, G. P., and Harris, M. K. (1996). "Integrated Hydrogeological Modeling of the General Separations Area, Volume 2, Groundwater Flow Model (U)," Rep. No. WSRC-TR-96-0399, Rev. 1. Washington Savannah River Company, Aiken, SC.
- Flach, G. P., Harris, M. K., Hiergesell, R. A., Smits, A. D., and Hawkins, K. L. (1999). "Regional Groundwater Flow Model for C, K, L, and P Reactor Areas, Savannah River Site, Aiken, South Carolina (U)," Rep. No. WSRC-TR-99-00248, Rev. 0. Westinghouse Savannah River Company, Aiken, SC.
- Flach, G. P., Harris, M. K., Smits, A. D., and Syms, F. H. (2005b). Modeling Aquifer Heterogeneity Using Cone Penetration Testing Data and Stochastic Upscaling Methods. *Environmental Geosciences* **12**, 1-50.

- Flach, G. P., and Whiteside, T. S. (2016). "Interpretation of Vadose Zone Monitoring System Data near Engineered Trench 1," Rep. No. SRNL-STI-2016-00546. Savannah River National Laboratory, Aiken, SC.
- Flint, F. a. (2002a). SSSA Method 2.2.3.1 in SSSA Book Series: 5, Methods of Soil Analysis, Part 4-Physical Methods. *In* "Particle Density-Calculation from Porosity and Bulk Density" (J. H. Dane and G. C. Topp, eds.). Soil Science Society of America, Inc. , Madison, Wisconsin.
- Flint, F. a. (2002b). SSSA Method 2.3.2.2 in SSSA Book Series: 5, Methods of Soil Analysis, Part 4-Physical Methods. *In* "Total Porosity-Gravimetric Method with Water Saturation" (D. J. H. and G. C. Topp, eds.). Soil Science Society of America, Inc. , Madison, Wisconsin.
- Fredlund, D. G., and H.Rahardjo (1993). "Soil Mechanics for Unsaturated Soils " John Wiley & Sons, New York, New York.
- Freeze, R. A., and Cherry, J. A. (1979). "Groundwater," Prentice-Hall, Inc. , Englewood Cliffs, New Jersey
- Gelhar, L. W. (1993). "Stochastic subsurface hydrology," Prentice-Hall, Englewood Cliffs, New Jersey.
- Gelhar, L. W. (1997). Perspectives on field-scale application of stochastic subsurface hydrology. *In* "Subsurface flow and transport: a stochastic approach" (G. Dagan and S. P. Neuman, eds.), pp. 241. Cambridge University Press.
- Gelhar, L. W., and Axness, C. L. (1983). Three-dimensional stochastic analysis of macrodispersion in aquifers. *Water Resources Research* **19**, 161-180.
- Greskovich, E. J., Pommersheim, J. M., and R. C. Kenner, J. (1975). Determination of Hindered Diffusivities for Nonadsorbing Pollutants in Muds. *AIChE* **21**, 1022-1024.
- Hang, T., Collard, L. B., and Phifer, M. A. (2005). "Unreviewed Disposal Question Evaluation:Subsidence Study for Non-Crushable Containers in Slit Trenches (U)," Rep. No. WSRC-TR-2005-00104, Rev. 0. Westinghouse Savannah River Company, Aiken, SouthCarolina.
- Hang, T., and Hamm, L. L. (2019). "PORFLOW Implementation of Vadose Zone Conceptual Model for Naval Reactor Component Disposal Area in the E-Area Low Level Waste Facility Performance Assessment," Rep. No. SRNL-STI-2019-00xxx, Revision Draft. Savannah River National Laboratory, Aiken, SC.
- Harvey, C. F., and Gorelick, S. M. (2000). Rate-limited mass transfer of macrodispersion: Which dominates plume evolution at the Macrodispersion Experiment (MADE) site? . *Water Resources Research* **36**, 637-650.
- Helms, S. B. (1966). Hardened Concrete Air Content and Unit Weight. *In* "Significance of Test of Properties of Concrete and Concrete-Making Materials " (R. Mielenz, D. Bloem, L. Gregg, L. Gregg, C. Kesler and W. Price, eds.), pp. 309-325. ASTM International, West Conshohocken, PA.
- Hillel, D. (1982). "Introduction to Soil Physics," Academic Press, Inc., San Diego, CA.
- Jackson, D. G. (2000). "Laboratory Analysis of Shallow Sediment Samples at the 321-M Solvent Storage Tank." Westinghouse Savannah River Company, Aiken, South Carolina.
- Jean, G. A., Yarus, J. M., Flach, G. P., Millings, M. R., Harris, M. K., Chambers, R. L., and Syms, F. H. (2004). Three-dimensional geologic model of southeastern Tertiary coastal-plain sediments, Savannah River Site, South Carolina: An applied

- geostatistical approach for environmental applications. *Environmental Geosciences* **11**, 205-220.
- Johnston, H. M., and Wilmot, D. J. (1992). Sorption and Diffusion Studies in Cementitious Grouts *Waste Management* **12**, 289-297.
- Jones, W. E., and Phifer, M. A. (2006). "E-Area Low Activity Waste Vault Subsidence Potential and Closure Cap Performance," Rep. No. WSRC-TR-2005-00405, Draft. Washington Savannah River Company, Aiken, South Carolina.
- Jones, W. E., Phifer, M. A., and Kukreja, K. (2004). "Unreviewed Disposal Question Evaluation: Components-in-Grout Options for Structural Stability- Component Filling, Component Stability, or Concrete Mat Cover," Rep. No. WSRC-TR-2004-00039. Savannah River Technology Center, Aiken, SC.
- Jordan, J. M., and Flach, G. P. (2013). "Porflow Modeling Supporting the FY13 Saltstone Special Analysis  
" Rep. No. SRNL-STI-2013-00280, Revision 0. Savannah River National Laboratory, Aiken, SC.
- Kaplan, D. I. (2016). "Geochemical Data Package for Performance Assessment Calculations Related to the Savannah River Site," Rep. No. SRNL-STI-2009-00473. Rev. 1. Savannah River National Laboratory, Aiken, South Carolina.
- Kitanidis, P. K. (1997). "Introduction to Geostatistics: Applications to Hydrogeology," Cambridge University Press, Cambridge, United Kingdom.
- Lambe, W. T., and Whitman, R. V. (1969). "Soil Mechanics," John Wiley & Sons, New York.
- Leng, F., Feng, N., and Xinying, L. (2000). An experimental study on the properties of resistance to diffusion of chloride ions of fly ash and blast furnace slag concrete. *Cement & Concrete Research* **30**, 989-992.
- Liang, H., Li, L., Poor, N. D., and Sagues, A. A. (2003). Nitrite diffusivity in calcium nitrite admixed hardened concrete. *Cement & Concrete Research* **33**.
- Logan, W. R., and Euler, G. M. (1989). "Geology and Groundwater Resources of Allendale, Bamberg, and Barnwell Counties and Part of Aiken County, South Carolina," Rep. No. 155. South Carolina Water Resources Commission.
- Lunne, T., Robertson, P. K., and Powell, J. J. M. (1997). "Cone Penetration Testing in Geotechnical Practice," Blackie Academic and Professional, United Kingdom.
- Maerki, M., Wehrli, B., Dinkel, C., and Muller, B. (2004). The Influence of Tortuosity on Molecular Diffusion in Freshwater Sediment of High Porosity *Geochimica et Cosmochimica Acta* **68**, 1519-1528.
- McAllister, C., Beckert, H., Abrams, C., Bilyard, G., Cadwell, K., Friant, S., Glantz, C., Mazaika, R., and Miller, K. (1996). "Survey of Ecological Resources at Selected U.S. Department of Energy Sites," PNNL.
- McDowell-Boyer, L., Yu, A. D., Cook, J. R., Kocher, D. C., Wilhite, E. L., Holmes-Burns, H., and Young, K. E. (2000). "Radiological Performance Assessment for the E-Area Low-Level Waste Facility," Rep. No. WSRC-RP-94-218, Revision 1. Westinghouse Savannah River Company, Aiken, South Carolina.
- Millings, M., Bagwell, L., Amidon, M., and Dixon, K. (2011). "Sediment Properties: E Area Completion Project," Rep. No. SRNL-STI-2011-00095. Savannah River National Laboratory, Aiken, SC.

- Mualem, Y. (1976). A New Model for Predicting the Hydraulic Conductivity of Unsaturated Porous Media. *Water Resources Research* **12**, 513-522.
- Neville, A. M. (1973). "Properties of Concrete," John Wiley and Sons, New York.
- Nichols, R. L., Looney, B. B., Flach, G. P., and Rossabi, J. (2000). "Recommendations for Phase II Vadose Zone Characterization and Monitoring at the E-Area Disposal "Slit" Trenches and Mega-Trench." Westinghouse Savannah River Company, Aiken, South Carolina.
- Nimmo, J. R., Perkins, K. S., and Lewis, A. M. (2002). Steady-State Centrifuge, SSSA Method 3.6.1.1 bin SSSA Book Series: 5. In "Methods of Soil Analysis, Part 4-Physical Methods" (J. H. Dane and G. C. Topp, eds.). Soil Science Society of America, Inc., Madison, Wisconsin.
- Nimmo, J. R., and Winfield, K. A., eds. (2002). "Water Retention and Storage: Miscellaneous Methods." Soil Science Society of America.
- Or, D., and Tuller, M. (2000). Flow in unsaturated fractured porous media: Hydraulic conductivity of rough surfaces. *Water Resources Research* **36**, 1165-1177.
- Peregoy, W. (2006a). "Structural Evaluation of Component-in-Grout Trenches," Rep. No. T-CLC-E-00026, Rev. 0. Washington Savannah River Company, Aiken, South Carolina.
- Peregoy, W. (2006b). "Structural Evaluation of Intermediate Level Waste Storage Vaults for Long-Term Behavior," Rep. No. T-CLC-E-00024, Rev. 0. Washington Savannah River Company, Aiken, South Carolina.
- Perry, R. H., and Green, D. W. (1997). "Perry's Chemical Engineers' Handbook 7th Edition," McGraw-Hill, New York.
- Peters, R. R., and Klavetter, E. A. (1988). A continuum model for water movement in an unsaturated fractured rock mass. *Water Resources Research* **24**, 416-430.
- Phifer, M. A. (2004). "Unreviewed Disposal Question Evaluation: Low Strength Containers with Compressible Waste in Component-In-Grout Trenches, ," Rep. No. WSRC-TR-2004-00475. Westinghouse Savannah River Company, Aiken, South Carolina.
- Phifer, M. A. (2005). "Vault #4 Closure Cap Estimated Infiltration for Years 50,000 to 1,000,000." Westinghouse Savannah River Company, Aiken, South Carolina.
- Phifer, M. A. (2010). Slit Trench Waste Representation (D. A. Crowley, ed.). Savannah River Nuclear Solutions, Savannah River Site, Aiken, SC.
- Phifer, M. A. (2014). "E-Area Vault Concrete Material Property and Vault Durability/Degradation Projection Recommendations," Rep. No. SRNL-STI-2013-00706, Rev. 0. Savannah River National Laboratory, Aiken, SC.
- Phifer, M. A., Crapse, K. P., Millings, M. R., Serrato, M. G. (2009). "Closure Plan for the E-Area Low-Level Waste Facility", SRNL-RP-2009-00075, Revision 0. Savannah River National Laboratory, Aiken, SC.
- Phifer, M. A., Millings, M. R., and Flach, G. P. (2006). "Hydraulic Property Data Package for the E-Area and Z-Area Soils, Cementitious Materials, and Waste Zones," Rep. No. WSRC-STI-2006-00198 Rev. 0. Washington Savannah River Company, Aiken, SC.
- Phifer, M. A., Sappington, F. C., and Jones, W. E., 2000, "DCB-8C Step and Constant Rate Pump Tests D-Area Unconfined Aquifer Hydraulic Parameter Estimation," SRT-EST-2000-00226, Westinghouse Savannah River Company, Aiken 20808.

- Phifer, M. A., and Wilhite, E. L. (2001). "Waste Subsidence Potential Versus Supercompaction," Rep. No. WSRC-RP-2001-00613. Westinghouse Savannah River Company, Aiken, South Carolina.
- Popovics, S. (1992). "Concrete Materials Properties, Specifications and Testing," 2nd/Ed. Noyes Publications, Park Ridge, New Jersey.
- Priesack, E., and Durner, W. (2006). Closed-Form Expression for the Multi-Modal Unsaturated Conductivity Function. *Vadose Zone Journal* **5**, 121-124.
- Pruess, K. (1998). On water seepage and fast preferential flow in heterogeneous, unsaturated rock fractures. *Journal of Contaminant Hydrology* **30**, 333-362.
- Robinson, R. A., and Stokes, R. H. (1955). "Electrolyte Solutions: The Measurement and Interpretation of Conductance, Chemical Potential and Diffusion in Solutions of Simple Electrolytes " Academic Press, New York, New York.
- Rockhold, M. L., Fayer, M. J., and Heller, P. R. (1993). "Physical and Hydraulic Properties of Sediments and Engineered Materials Associated with Grouted Double-Shell Tank Waste Disposal at Hanford." Pacific National Laboratory, Richland, WA.
- Sanchez-Vila, X., Giradi, J. P., and Carrera, J. (1995). A synthesis of approaches to upscaling of hydraulic conductivities. *Water Resources Research* **31**, 867-882.
- Sappington, F. C., and Phifer, M. A. (2005). "Moisture Content and Porosity of Concrete Rubble Study." Westinghouse Savannah River Company Aiken, South Carolina.
- Sarris, T. S., and Paleologos, E. K. (2004). Numerical investigation of the anisotropic hydraulic conductivity behavior in heterogenous porous media. *Journal of Stochastic Environmental Research & Risk Assessment* **18**, 188-197.
- Savage, B. A., and Janssen, D. J. (1997a). Soil Physics Principles Validated for Use in Predicting Unsaturated Moisture Movement in Portland Cement Concrete. *ACI Materials Journal* **94**, 63-70.
- Savage, B. M., and Janssen, D. J. (1997b). Soil Physics Principles Validated for Use in Predicting Unsaturated Moisture Movement in Portland Cement Concrete. *ACI Materials Journal* **94**, 63-70.
- Seitz, R. R., and Walton, J. C. (1993). "Modeling approaches for Concrete Barriers Used in Low-Level Waste Disposal." U.S. Nuclear Regulatory Commission, Office of Nuclear Regulatory Research, Washington, DC.
- Šimůnek, J., Jarvis, N. J., Genuchten, M. T. v., and Gärdenäs, A. (2003). Review and comparison of models for describing non-equilibrium and preferential flow and transport in the vadose zone. *Journal of Hydrology* **272**.
- Sinclair, A. J. (1976). "Applications of Probability Graphs in Mineral Exploration " The Association of Exploration Geochemists, Vancouver, BC.
- Sink, D. (2010). Percentage Waste Volumes in Slit Trenches. (T. Butcher, ed.). Savannah River Nuclear Solutions, Savannah River Site, Aiken, SC.
- Siple, G. E. (1967). Geology and Ground Water of the Savannah River Plant and Vicinity, South Carolina. In "Water Supply Paper" (U. G. Survey, ed.), pp. 113.
- Snyder, K. A. (2003). "Condition Assessment of Concrete Nuclear Structures Considered for Entombment." National Institute of Standards and Technology.
- Soroushian, P., and Alhozaimy, A. (1995). "Fly Ash Effects on Mortar Permeability in Concrete and Grout in Nuclear and Hazardous Waste Disposal," American Concrete Institute, Detroit, Michigan.

- Stanish, K., and Thomas, M. (2003). The use of bulk diffusion tests to establish time-dependent concrete chloride diffusion coefficients. *Cement & Concrete Research* **33**, 55-62.
- Swingle, R. F., and Phifer, M. A. (2006). "Unreviewed Disposal Question Evaluation: Increased Disposal Volume in Slit and Engineered Trenches (U)," Rep. No. WSTC-TR-2006-00186, Rev. 0. Washington Savannah River Company, Aiken, South Carolina.
- Syms, F. H., Lewis, M. R., and Temples, T. J. (2001). "Calibration of the Piezocone Penetrometer Test for Predicting Soil Character." Westinghouse Savannah River Company, Aiken, South Carolina.
- Thibodeau, L. J. (1979). "Chemodynamics: Environmental Movement of Chemicals in Air, Water and Soil," Wiley-Interscience, New York.
- Truc, O., Ollivier, J. P., and Carcasses, M. (2000). A new way for determining the chloride diffusion coefficient in concrete from steady state migration test *Cement & Concrete Research* **30**, 217-226.
- USACE (1970). "Engineering and Design Laboratory Soils Testing ". U.S Army Corps of Engineers, Washington, DC.
- USACE (1992). Handbook for Concrete and Cement. In "Test Method for Water Permeability of Concrete Using Triaxial Cell". United States Army Corps of Engineers, Vicksburg, Mississippi.
- USDA (1998). RETC for Windows, 1998. U.S. Salinity Laboratory, U.S. Department of Agriculture (USDA).
- USGS (1987). Digital Line Graphs from 1:24,000 Scale Maps. United States Geological Survey.
- van Genuchten, M. T. (1980). A Closed-form Equation for Predicting the Hydraulic Conductivity of Unsaturated Soils. *Soil Science Society of America Journal* **44**, 892-898.
- Verbeck, G. (1966). Hardened Concrete Pore Structure. In "Significance of Test of Properties of Concrete and Concrete-Making Materials" (R. Mielenz, D. Bloem, L. Gregg, L. Gregg, C. Kesler and W. Price, eds.), pp. 211-219. ASTM International, West Conshohocken, PA.
- Walpole, R. E., and Meyers, R. H. (1978). "Probability and Statistics for Engineers and Scientists " MacMillan Publishing New York, New York.
- Walton, J. C., Plansky, L. E., and Smith, R. W. (1990). "Models for Estimation of Service Life of Concrete Barriers in Low-Level Radioactive Waste Disposal ". Office of Nuclear Regulatory Research, Office of Nuclear Regulatory Research, Washington D.C. .
- Wang, J. S. Y., and Narasimhan, T. N. (1985). Hydrologic Mechanisms Governing Fluid Flow in a Partially Saturated, Fractured, Porous Medium. *Water Resources Research* **21**, 1861-1874.
- Webb, E. K., and Anderson, M. P. (1996). Simulation of preferential flow in three-dimensional heterogenous conductivity fields with realistic internal architecture. *Water Resources Research* **32**, 533-546.
- WHC (1993). "Performance Assessment of Grouted Double-Shell Tank Waste Disposal at Hanford." Westinghouse Hanford Company, Richland, Washington.

- Wohlwend, J. L., and Butcher, B. T. (2018). "Proposed NRCDA Groundwater Pathway Conceptual Model," Rep. No. SRNL-STI-2018-00633, Revision 0. Savannah River National Laboratory, Aiken, SC.
- WSRC (1994). "Finishing and Delivery of Concrete," Rep. No. Specification C-SPS-G-00041, Aiken, SC.
- WSRC (2004). "Furnishing and Delivery of Concrete, GS, PS, and SS." Westinghouse Savannah River Company, Aiken, South Carolina.
- WSRC (2006). "Furnishing and Delivery of Concrete, GS, PS, and SS." Westinghouse Savannah River Company, Aiken, South Carolina.
- WSRC (2008). "E-Area Low Level Waste Facility DOE 435.1 Performance Assessment", WSRC-STI-2007-00306, Revision 0, Washington Savannah River Company, Aiken, SC.
- Wyatt, D. E., and Harris, M. K. (2004). Overview of the History and Geology of the Savannah River Site. *Environmental Geosciences* **11**, 181-190.
- Yu, A. D., Langton, C. A., and Serrato, M. G. (1993). "Physical Properties Measurement Program ". Westinghouse Savannah River Company, Aiken, South Carolina.
- Yu, A. D., McDowell-Boyer, L. M., Cook, J. R., and Young, K. E. (2002). "Special Analysis: Naval Reactor Waste Disposal Pad (U)," Rep. No. WSRC-RP-2001-00948, Revision 2. Washington Savannah River Company, Aiken, SC.
- Zhang, D. (2002). "Stochastic methods for flow in porous media: coping with uncertainties " Academic Press, San Diego, California.

This page intentionally left blank.

Distribution:

[alex.cozzi@srnl.doe.gov](mailto:alex.cozzi@srnl.doe.gov)  
[david.crowley@srnl.doe.gov](mailto:david.crowley@srnl.doe.gov)  
[a.fellinger@srnl.doe.gov](mailto:a.fellinger@srnl.doe.gov)  
[samuel.fink@srnl.doe.gov](mailto:samuel.fink@srnl.doe.gov)  
[erich.hansen@srnl.doe.gov](mailto:erich.hansen@srnl.doe.gov)  
[connie.herman@srnl.doe.gov](mailto:connie.herman@srnl.doe.gov)  
[dennis.jackson@srnl.doe.gov](mailto:dennis.jackson@srnl.doe.gov)  
[brady.lee@srnl.doe.gov](mailto:brady.lee@srnl.doe.gov)  
[patricia.lee@srnl.doe.gov](mailto:patricia.lee@srnl.doe.gov)  
[Joseph.Manna@srnl.doe.gov](mailto:Joseph.Manna@srnl.doe.gov)  
[john.mayer@srnl.doe.gov](mailto:john.mayer@srnl.doe.gov)  
[daniel.mccabe@srnl.doe.gov](mailto:daniel.mccabe@srnl.doe.gov)  
[Gregg.Morgan@srnl.doe.gov](mailto:Gregg.Morgan@srnl.doe.gov)  
[frank.pennebaker@srnl.doe.gov](mailto:frank.pennebaker@srnl.doe.gov)  
[Amy.Ramsey@srnl.doe.gov](mailto:Amy.Ramsey@srnl.doe.gov)  
[William.Ramsey@SRNL.DOE.gov](mailto:William.Ramsey@SRNL.DOE.gov)  
[michael.stone@srnl.doe.gov](mailto:michael.stone@srnl.doe.gov)  
[Boyd.Wiedenman@srnl.doe.gov](mailto:Boyd.Wiedenman@srnl.doe.gov)  
Records Administration (EDWS)

[sebastian.aleman@srnl.doe.gov](mailto:sebastian.aleman@srnl.doe.gov)  
[paul.andrews@srs.gov](mailto:paul.andrews@srs.gov)  
[dan.burns@srs.gov](mailto:dan.burns@srs.gov)  
[tom.butcher@srnl.doe.gov](mailto:tom.butcher@srnl.doe.gov)  
[kerri.crawford@srs.gov](mailto:kerri.crawford@srs.gov)  
[Thomas.Danielson@srnl.doe.gov](mailto:Thomas.Danielson@srnl.doe.gov)  
[kenneth.dixon@srnl.doe.gov](mailto:kenneth.dixon@srnl.doe.gov)  
[James.Dyer@srnl.doe.gov](mailto:James.Dyer@srnl.doe.gov)  
[peter.fairchild@srs.gov](mailto:peter.fairchild@srs.gov)  
[gregory.flach@srs.gov](mailto:gregory.flach@srs.gov)  
[luther.hamm@srnl.doe.gov](mailto:luther.hamm@srnl.doe.gov)  
[thong.hang@srnl.doe.gov](mailto:thong.hang@srnl.doe.gov)  
[tim.jannik@srnl.doe.gov](mailto:tim.jannik@srnl.doe.gov)  
[daniel.kaplan@srnl.doe.gov](mailto:daniel.kaplan@srnl.doe.gov)  
[steven.mentrup@srs.gov](mailto:steven.mentrup@srs.gov)  
[verne.mooneyhan@srs.gov](mailto:verne.mooneyhan@srs.gov)  
[ralph.nichols@srnl.doe.gov](mailto:ralph.nichols@srnl.doe.gov)  
[Virginia.Rigsby@srs.gov](mailto:Virginia.Rigsby@srs.gov)  
[Jansen.Simmons@srs.gov](mailto:Jansen.Simmons@srs.gov)  
[Frank.Smith@srnl.doe.gov](mailto:Frank.Smith@srnl.doe.gov)  
[Brooke.Stagich@srnl.doe.gov](mailto:Brooke.Stagich@srnl.doe.gov)  
[Ira.Stewart@srs.gov](mailto:Ira.Stewart@srs.gov)  
[Tad.Whiteside@srnl.doe.gov](mailto:Tad.Whiteside@srnl.doe.gov)  
[Jennifer.Wohlwend@srnl.doe.gov](mailto:Jennifer.Wohlwend@srnl.doe.gov)